Fraunhofer ISE

UNI FREIBURG

THERMAL MANAGEMENT OF PVT COLLECTORS

Development and modelling of highly efficient glazed, flat plate PVT collectors with low-emissivity coatings and overheating protection

Dissertation zur Erlangung des Doktorgrades der
Technischen Fakultät der Albert-Ludwigs-Universität Freiburg im Breisgau

vorgelegt von

Manuel Lämmle

angefertigt am Fraunhofer-Institut für Solare Energiesysteme (ISE)

Datum der Einreichung: 04. Juni 2018

Datum der Verteidigung: 17. August 2018

Referent: Prof. Dr. rer. nat. Hans-Martin Henning

Korreferent: Prof. Dipl.-Ing. Andreas Wagner

Abstract

Climate change is one of the biggest environmental, technological, economic, and social challenges of our time. The global energy system needs to be transformed to renewable energy sources to cut greenhouse gas emissions to a tolerable level. In this context, hybrid photovoltaic-thermal collectors (PVT collectors) are a promising technology that combines the solar generation of both electricity and heat in a single component. By transferring heat from photovoltaic cells to a heat transfer fluid, PVT collectors achieve an efficient utilization of the solar resource and a better use of available surface areas.

This PhD thesis focusses on the development and modelling of highly efficient glazed PVT collectors with an optimized overall system performance. A combination of experimental and numerical methods is applied at both the collector and system level, allowing a multifaceted analysis and optimization of the PVT technology. The research topics are embedded in the thematic framework of "thermal management", which aims to balance the diverging requirements of photovoltaics and solar thermal by controlling energy flows and adjusting the collector temperature to the desired level.

Firstly, this concerns the optimization of the thermal efficiency of PVT collectors by the application of spectrally selective low-emissivity (low-e) coatings, which are transparent for solar irradiance and feature a low emittance for infrared radiation. A glazed PVT collector with low-emissivity coating is built and tested, and its performance is compared to a collector of identical design yet without low-e coating. Due to a reduction of radiative heat losses, the low-e coating improves the thermal efficiency by 60 $\%_{rel}$ and reduces the overall heat losses by 82 $\%_{rel}$ at typical operating conditions. Owing to a slightly higher optical reflectance, a small drop of the electrical efficiency of 3 $\%_{rel}$ has to be accepted. Nonetheless, low-e coatings can be considered an enabling technology allowing a significant improvement of the overall efficiency of PVT collectors.

Secondly, the annual collector performance is evaluated in the system context by means of assessing electrical and thermal energy yields of typical PVT systems. PVT collectors with low-e are applicable for a wide range of temperatures and they achieve highest primary energy yields in all analyzed applications. Due to the central importance of operating temperatures, the characteristic temperature is defined as a new indicator, which shows a strong correlation with electrical and thermal yields. It is therefore suitable for selecting an apt PVT technology for a given system, pre-assessing yields, and for discussing the capability of PVT technologies in general.

Thirdly, new overheating concepts are specifically designed for PVT collectors with low-e, as low heat losses lead to higher stagnation temperatures and aggravate the issue of overheating. High absorber temperatures negatively affect electrical yields and accelerate ageing and degradation, especially above 120 °C. The state-of-the-art overheating concept of venting the collector is applied for the first time to PVT collectors, achieving a reduction of the stagnation temperatures from 149 °C to 102 °C. The novel switchable film insulation, where an inflatable polymer cushion governs heat losses, renders an unprecedented switching range of U_{Loss} and thus combines the characteristics of a high-performing glazed PVT collector with low-e and the low stagnation temperatures of unglazed collectors.

ZUSAMMENFASSUNG

Der Klimawandel ist eine der größten ökologischen, technologischen, ökonomischen und sozialen Herausforderungen unserer Zeit. Eine schnelle Energiewende mit der globalen Transformation des Energiesystems zu erneuerbaren Energien ist notwendig, um die Treibhausgasemissionen drastisch zu reduzieren und dadurch die Erderwärmung einzudämmen. Hybride photovoltaisch-thermische Kollektoren (PVT-Kollektoren) sind dafür eine vielversprechende Technologie, die die solare Erzeugung von Strom und Wärme in einer einzelnen Komponente vereint. Durch den Transport von Wärme aus den PV-Zellen an ein Wärmeträgerfluid wird die Wärme nutzbar gemacht wird, sodass PVT-Kollektoren höchste Gesamtwirkungsgrade erzielen und eine verbesserte Ausnutzung von solaren Flächen ermöglichen.

Der Fokus dieser Dissertation liegt auf der Entwicklung und Modellierung von hocheffizienten, verglasten PVT-Kollektoren mit optimierten Systemerträgen. Diese Forschungsthemen sind in das methodische Gerüst des "Thermischen Managements" eingebettet. Der Ansatz zielt darauf ab, die divergierenden Anforderungen der Photovoltaik und Solarthermie auszubalancieren, indem die Energieflüsse gesteuert und die Kollektortemperaturen an den momentanen Strom- und Wärmebedarf angepasst werden. Das Zusammenspiel von experimentellen und numerischen Methoden auf Kollektor- und der Systemebene erlaubt dabei eine vielseitige Analyse des Potentials der PVT-Kollektortechnologie.

Erstens betrifft dies die Optimierung der thermischen Leistung von PVT-Kollektoren durch die Anwendung von niedrig-emissiven Low-e-Beschichtungen, die transparent für Solarstrahlung sind, aber einen niedrigen Emissionsgrad für Infrarotstrahlung aufweisen. Die Leistung eines PVT-Kollektors mit Low-e-Beschichtung wird mit einem baugleichen PVT-Kollektor ohne Low-e-Beschichtung verglichen. Bei typischen Betriebsbedingungen verbessert die Low-e-Schicht den thermischen Wirkungsgrad um 60 $\%_{rel}$, indem sie die Wärmeverluste um 82 $\%_{rel}$ reduziert. Aufgrund etwas höherer optischer Reflexionen muss allerdings ein Rückgang der elektrischen Leistung um 3 $\%_{rel}$ akzeptiert werden. Dennoch können Low-e-Beschichtungen als eine Schlüsseltechnologie betrachtet werden, die eine wesentliche Steigerung der Gesamteffizienz von PVT-Kollektoren ermöglicht.

Zweitens werden auf Systemebene jährliche Energieerträge und Gesamtsystemleistungen für typische PVT-Systeme untersucht und mit dem neuen Charakteristischen-Temperatur-Ansatz diskutiert. PVT-Kollektoren mit Low-e-Beschichtung sind für ein breites Betriebstemperaturspektrum geeignet und sie erzielen die höchsten Primärenergieerträge in den untersuchten Anwendungen. Auf Grund der zentralen Bedeutung der mittleren Betriebstemperaturen wird die charakteristische Temperatur T_{char} als neuer Indikator eingeführt, der eine starke Korrelation mit Strom- und Wärmeerträgen aufweist. Dadurch ist T_{char} geeignet, um geeignete PVT-Technologien auszuwählen, Erträge abzuschätzen und im Allgemeinen die Einsatzfähigkeit von PVT-Kollektoren zu diskutieren.

Drittens werden neue Überhitzungsschutzkonzepte speziell für thermisch-optimierte PVT-Kollektoren entwickelt. Die niedrigen Wärmeverluste durch die Low-e-Beschichtung führen zu höheren Stagnationstemperaturen und vergrößern die Überhitzungsproblematik. Hohe Absorbertemperaturen insbesondere oberhalb 120 °C beschleunigen Alterung und Degradation und wirken sich negativ auf die elektrische Leistung aus. Das Überhitzungsschutzkonzept der Kollektorbelüftung durch öffnende Gehäuseklappen wird zum ersten Mal auf PVT-Kollektoren angewendet und erzielt eine Reduktion der Stagnationstemperaturen von 149 °C auf 102 °C. Die innovative schaltbare Foliendämmung, bei der ein aufblasbares Polymerkissen die Wärmeverluste reguliert, liefert einen bisher unerreicht großen Schaltbereich von U_{Loss}. Dadurch vereint der Folienüberhitzungsschutz die hohe Leistung eines abgedeckten PVT-Kollektors mit Low-e-Beschichtung mit den unkritischen Stagnationstemperaturen von unverglasten Kollektoren.

TABLE OF CONTENTS

1 INTRODUCTION

1.1 Motivation and background

Climate change is one of the biggest environmental, technological, economic, and social challenges of our time. In the 21st conference of the parties in Paris 2015, the global leaders agreed on "holding the increase in the global average temperature to well below 2 °C above pre-industrial levels […] recognizing that this would significantly reduce the risks and impacts of climate change" (UNFCCC 2015). The main drivers of climate change are anthropogenic greenhouse gas emissions, especially carbon dioxide. The atmospheric concentration of greenhouse gases has increased significantly compared to pre-industrial levels, which causes an ongoing rise of global surface temperatures owing to a radiative imbalance of the climate system (IPCC 2014).

Global greenhouse gas emissions need to be drastically cut in order to mitigate the effects of global warming to acceptable levels (UNFCCC 2015). In 2010, the production of heat and electricity accounted for 25 % of global greenhouse gas emissions, mainly in the energy, buildings and industry sector (IPCC 2015). A combination of different technologies is necessary to mitigate these emissions. In the energy supply sector, renewable energy sources such as wind, solar, hydropower, or nuclear power can substitute fossil power plants. In the building sector a reduction of greenhouse gas intensity can be reached by the local usage of renewable energy sources and energy efficiency measures (IPCC 2014).

Hybrid photovoltaic-thermal collectors (PVT collectors) are a promising technology that combines the solar generation of electricity and heat in a single component. Conventional PV modules convert only 10 - 20 % of their incident solar radiation into electricity, while the major share of the solar resource is transformed into unused heat. By contrast, hybrid PVT collectors transfer this heat to a fluid, which circulates behind the PV cells. In this way, PVT collectors produce both electricity and heat on the same area, and thus achieve the potentially highest solar efficiency with a maximum utilization of space.

Due to the energetic benefits of PVT collectors, the IEA technology roadmap on solar heating and cooling recommends to "develop the PVT technology to make it commercially viable" (IEA 2012). In recent years, mainly unglazed PVT collector products entered the market. These PVT collectors, however, suffer from a low thermal efficiency compared to conventional flat plate collectors. Consequently, the PVT technology cannot exploit its full potential, and the applications are limited to low temperature systems, e. g. swimming pool heating or in combinations with heat pumps. Accordingly, the Renewable Heating and Cooling platform identified the strategic R&D priority to develop "glazed [PVT] collectors with improved thermal performance and high reliability" (RHC 2012).

1.2 Fundamentals of PVT collectors

At present, PV modules convert 10 – 20 % of the incident solar irradiance into electricity, depending on the employed cell technology (Wirth 2017). The major share of the solar spectrum remains unused and dissipates as excessive heat to the environment. Hybrid photovoltaic-thermal PVT collectors, also known as PV/T or PV-T collectors, make use of this excessive heat by transferring heat from the PV cells to a heat transfer fluid. Thus, the otherwise unused heat of PV modules can be used to provide heat for hot water preparation or space heating of buildings.

By co-generating electricity and heat in a single component, PVT collectors achieve a higher overall efficiency than PV modules. The two forms of energy are harvested at cascading exergy levels: high-grade exergy in the form of electricity and low-grade exergy in the form of heat. Thus, PVT collectors transform the solar resource more efficiently, with a better utilization of available area.

The standard solar spectrum AM1.5 of global irradiance (ASTM 2008) and the corresponding spectral distribution of useful electricity and heat of a PVT collector are shown in Figure 1.1. In contrast to PV modules, which typically operate between wavelengths of 300 nm – 1100 nm, PVT collectors utilize the energy over the entire band of the solar spectrum. Optical losses due to reflections at optical interfaces and thermal losses due to heat losses from collector to ambient have to be considered. In total, the exemplary PVT collector achieves an overall electrical and thermal peak efficiency of $\eta_{el,STC} = 15\%$ and $\eta_{th,0} = 61\%$.

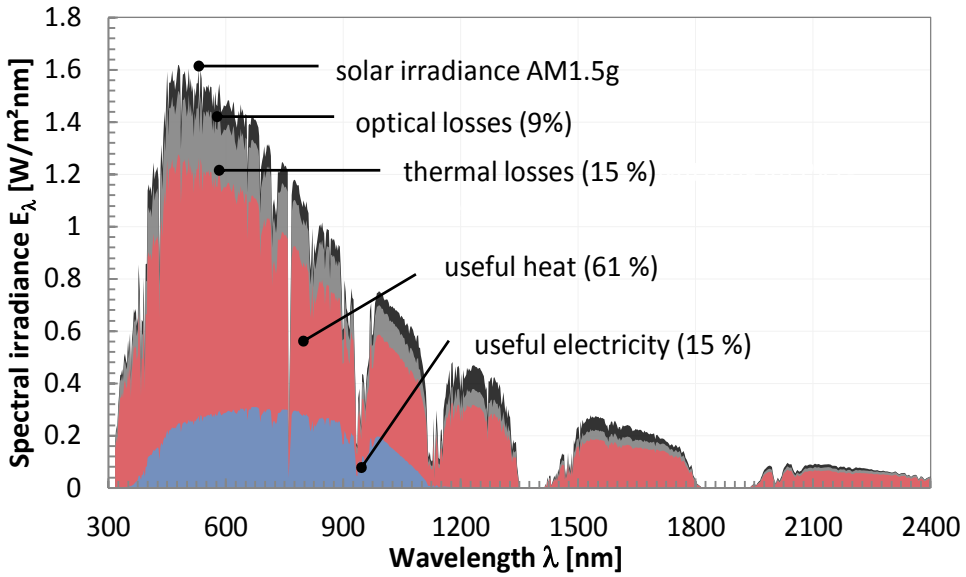

Figure 1.1: Spectral distribution of solar irradiance, optical and thermal losses, and conversion into useful heat and electricity. The indicated numbers are presented for the peak efficiency of an unglazed PVT collector at $T_a = T_m = 25$ °C, $G = 1000$ W/m², and $u_{wind} = 0$ m/s.

Generally speaking, PVT collectors combine the functionality of a conventional PV module and a solar thermal collector in a single component (Figure 1.2). The PV module has the main function of converting solar energy into electricity in PV cells, which are electrically interconnected and protected against environmental influences through a module glass or a backside film. Solar thermal collectors convert solar energy into heat by absorbing solar energy by a typically metallic absorber, and transferring the produced heat to a fluid, which circulates in tubes or channels. At the same time, heat losses should be minimized, for example by the application of a front glazing.

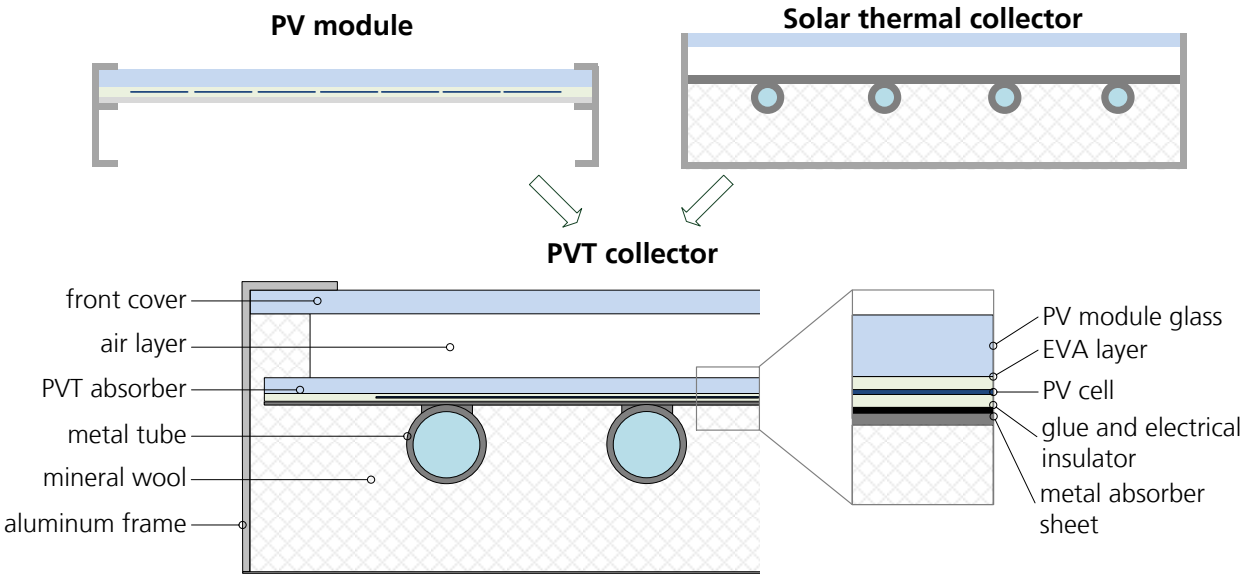

Figure 1.2: Schematic cross section of a PV module (left), solar thermal collector (right), and the combination to a PVT collector (center).

The technical realization of the PVT principle can take many forms, and the possibilities for design and construction are manifold. The PVT absorber, however, forms the common basis for any PVT collector. Therefore, the PVT absorber, which thermally couples the PV cells to the heat transfer fluid, can also be referred to as the heart of the PVT collector. The PV cells are the actual absorbing structure, as the major share of irradiance in PVT collectors is absorbed in the PV cells themselves.[1] One part of the absorbed energy is transformed into electricity; the remaining part of the energy is transformed into heat and has to be transported to the fluid via the PVT absorber. Figure 1.2 shows a schematic cross section of a glazed PVT collector with a glued sheet-and-tube PVT absorber, detailing the individual layers.

According to the irreversible second law of thermodynamics, heat can never pass from a colder to a hotter location. Therefore, the fluid temperature always needs to be lower than the cell temperatures to utilize the excessive heat in the PV cells. As a consequence, the PV cells are the hottest component of a PVT collector. The central issue of PVT collectors lies exactly in the physical coupling of PV cell and fluid temperature.

PV cells operate more efficiently at low temperature as the electrical efficiency in silicone-based PV cell technologies drops by γ = -0.1 $\%_{rel}$ to -0.5 $\%_{rel}$ per Kelvin of increased cell temperature (Skoplaki and Palyvos 2009). The negative temperature coefficient is caused by the decrease of the energy of the semiconductor's band gap with increasing temperature. Hence, the open circuit voltage of PV cells decreases, resulting in a drop of the electrical efficiency (Würfel and Würfel 2008).

[1] There are some so-called hybrid PVT collectors on the market where the PV cells are applied on the inside of the front cover of an otherwise conventional solar thermal collector. These collectors are explicitly excluded from the definition of glazed PVT collectors within this thesis, as the heat absorbed in the PV cells mostly dissipates to the environment and is not utilized.

Solar thermal collectors also operate more efficiently at lower operating temperatures, since the heat losses are proportional to the absorber's surface temperature. However, the operating temperature is determined by the underlying solar thermal system, its required temperature levels, and fluid temperatures that occur in the storage. According to system simulations, solar thermal collectors typically operate at mean fluid temperatures between T_m = 30 °C and 90 °C, which lies above the cell temperatures of PV modules varying between T_{cell} = 10 °C and 60 °C, but there is also an overlap of operating temperatures in the range of 30 °C and 60 °C.

Figure 1.3 compares the efficiency curves of a PV module and a solar thermal collector and shows their typical operating temperatures. Additionally, Figure 1.3 indicates the peak efficiency of the PV module at $\eta_{el,STC}$ = 15 % and the conversion factor of the solar thermal collector at $\eta_{th,0}$ = 80 %.

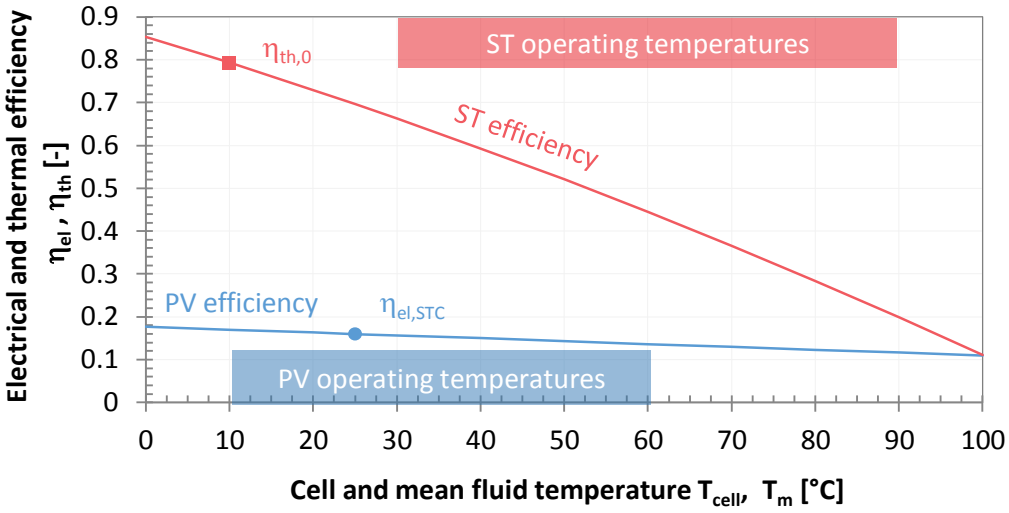

Figure 1.3: Comparison of operating temperature ranges and efficiencies of PV modules and solar thermal (ST) collectors. The efficiency is given for a c-Si PV module and a flat plate collector at typical operating conditions of G = 650 W/m², T_a = 10 °C. The temperatures ranges are obtained from system simulations in chapter 4.6.

As cell and fluid temperatures are coupled, PVT collectors do not operate in the optimum point of either PV or ST operation, but a compromise between thermal and electrical operation is necessary. Using the terminology of combined heat and power plants, PVT collectors can be regarded as solar co-generation, where priority is given to either electricity or heat generation:

- **Electricity priority** implies operating the PVT collector at low temperatures. Thus, low fluid temperatures cool the PV cells and a higher electrical efficiency compared to a PV module without cooling is achieved. However, the solar thermal collector underperforms in this case, as only low operating temperatures are possible.
- **Heat priority** implies operating the PVT collector at higher temperatures close to the operation point of conventional solar thermal collectors. In this case, PVT collectors deliver heat at higher temperatures, which requires a better thermal insulation of the collector, e.g. by applying a front cover or concentrating sunrays. However, in this case the PV operation underperforms due to elevated cell temperatures and a potentially reduced optical efficiency.

The motivation behind the PVT principle of combining PV and solar thermal can be summed up as the more efficient utilization of the solar resource with a better usage of available area, where only a single

"solar co-generation" component delivers both solar heat and solar electricity. However, the central issue arises from coupling cell and fluid temperatures that either the electrical or the thermal operation underperforms compared to the single technologies.

1.3 Classification of PVT collectors

There are different ways to classify PVT collectors (Zondag 2008). A concise classification of PVT collectors is important owing to the existence of multifaceted PVT concepts, each with its individual technological characteristics and its specific technological maturity and research needs. Figure 1.4 shows four categories that can be used to classify PVT collectors. Any PVT collector type can be classified into each of the four categories, while the list is not extensive.

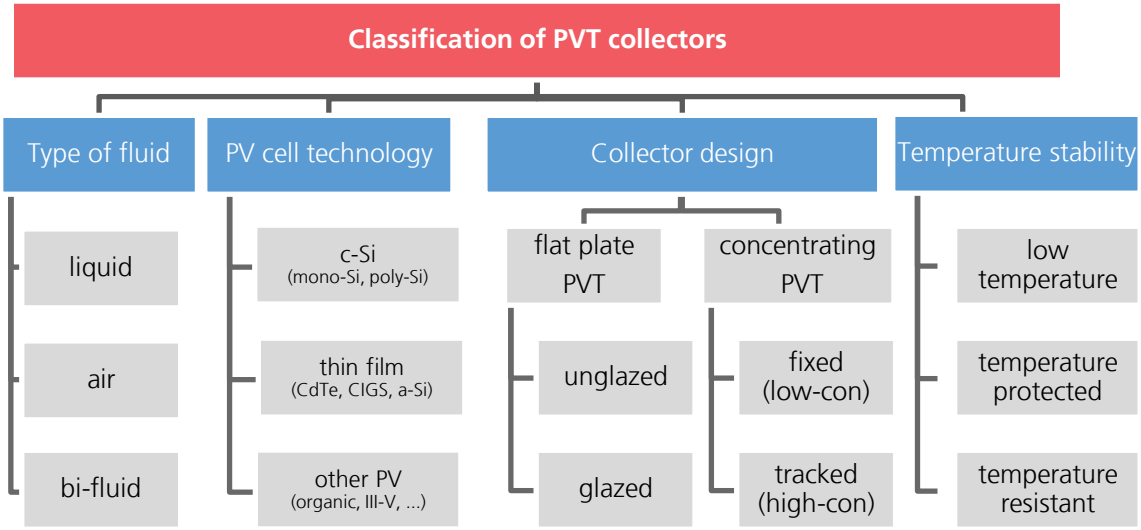

Figure 1.4: Classification of PVT collectors into categories of fluid type, collector design, PV technology, and research needs.

The heat transfer fluid is either liquid (water or a water-glycol mixture) or air. Water has a higher thermal conductivity and heat capacity than air (Zondag 2008), which is why most solar thermal and PVT collectors nowadays are liquid-type collectors. On the other hand, air-type PVT collectors do not suffer from overheating issues, as air can be vented easily. Yet, there are only limited applications for air collectors which are in general still a niche product (Zondag et al. 2006). Furthermore, there has been research on bi-fluid PVT collectors with both air and water as a heat transfer fluid (Assoa et al. 2007; Abu Bakar et al. 2014), but these collectors have more expensive production costs.

In principle, all PV cell technologies can be employed in PVT collectors, but their specific suitability depends on their electrical conversion efficiency, the temperature coefficient of electrical power, and the absorption coefficient of solar energy. Crystalline silicon (c-Si) PV cells have the largest share in PV (Wirth 2017) and PVT applications (Zondag et al. 2006). Monocrystalline silicon (mono-Si) cells reach a higher electrical efficiency and solar absorption than polycrystalline silicon (poly-Si) cells. Thin film PV technologies such as CdTe, CIGS, or amorphous silicon have a lower temperature coefficient than c-Si cells and are therefore considered more suitable for elevated temperatures (Michael et al. 2015). The same applies for organic PV cells, but high reflection of the organic PV stack was found to be an issue. Multi-junction cells (e.g. III-V cells) are used in high concentrating PV applications, where cooling of the PV cells is essential, and hence the application of PVT collectors is especially reasonable.

PVT collectors are also classified according to their design and construction principle into flat plate PVT collectors with the sub-categories unglazed and glazed, and into low or high-concentrating PVT collectors (Figure 1.5). The design has a major influence on heat losses and thus suitable operating temperatures. Unglazed, flat plate PVT collectors are similar in their design to PV modules, but with a heat removal construction attached to the backside and optional thermal insulation. Glazed, flat plate PVT collectors feature an additional front cover spaced to the PV module to reduce convective heat losses. Thus, the design of glazed PVT collectors is more similar to flat plate solar thermal collectors. Concentrating PVT collectors can be carried out from low to high concentration ratios, and either stationary with a fixed tilt angle or tracked along one or two axes (Zondag 2008).

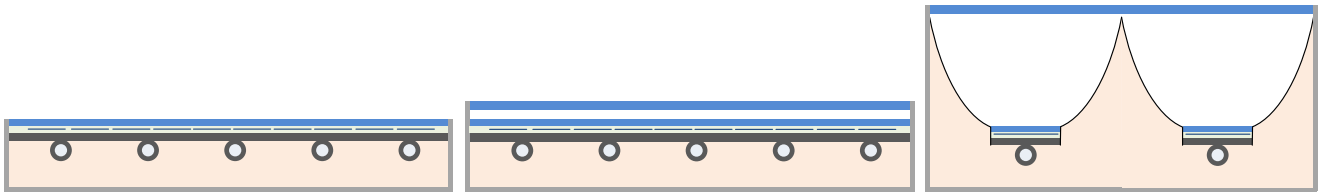

Figure 1.5: Classification of PVT collectors according to their design.

Next to these technical approaches to classify PVT collectors, Fortuin et al. (2014) introduced three categories of PVT collectors following their research needs regarding temperature stability. The "low temperature" concept is inherently temperature resistant due to the occurrence of only uncritical temperatures for which conventional PV modules are designed. This is achieved by a low level of thermal insulation, as found in unglazed PVT collectors, for example. PVT collectors of the "temperature protect" category have lower thermal losses due to a higher level of thermal insulation and the temperatures theoretically would exceed critical levels. To avoid damage, the PVT collector is protected against excessive temperatures through an overheating protection, which is activated either passively or actively. Thus, the temperature protected PVT collectors achieve a high efficiency during normal operation, but are protected against excessive temperatures, so that standard PV module materials can be used. "Temperature resistant" PVT collectors are also well insulated, but use non-standard, high-temperature stable materials and a temperature-resistant design of the PVT laminate, so that the materials employed in the PVT absorber withstand high collector temperatures.

The focus of this PhD thesis is placed on liquid-type, glazed, flat plate PVT collectors with c-Si PV cells. Crystalline silicone (c-Si) PV cells were found to be the favorable PV technology as they are the most prominent PV cell technology, feature a high level of reliability and a high solar absorption coefficient, which outweighs the relatively high temperature coefficient (Wendker et al. 2012). Liquid-type and glazed PVT collectors aim at substituting conventional solar thermal collectors given the similar solar thermal systems and corresponding temperature range. Zondag et al. (2006) expect these types of PVT collectors to potentially address the largest market. To overcome the challenge of temperature stability, the research focus is placed on temperature protected PVT collectors with overheating protection.

1.4 Current state of PVT technology and research topics

The beginning of research on PVT collectors dates back to the early 1960s. In recent years, the concept of PVT collectors has gained renewed interest by stakeholders in research, industry, and end customers.

The recent interest might be caused by the drop in PV module prices, which makes the application of PV in PVT collectors more profitable. Moreover, legal regulations such as the Energy Performance of Buildings Directive (EPBD) in the European Union came into force (EPA 2010). These regulations require a certain amount of its consumed energy to be produced on-site or in proximity of the building. PVT collectors are a technological option with a high overall efficiency and high primary energy yields, and manufactures want to offer such a product to their end customers.

Excellent reviews on PVT collectors were published by Charalambous et al. (2007), Zondag (2008), Chow (2010), and Aste et al. (2014). A mere summary of these reviews is omitted to avoid lengthiness and repetition. Instead, the interested reader is referred to the mentioned reviews to gain a comprehensive understanding of the PVT collector technology and recent progress of research and development. The literature overview in the following section is therefore limited to a short summary of recent developments relevant for this thesis. A stronger focus is placed on the current state of technology, market situation, and research needs.

1.4.1 Unglazed PVT collectors

Adam et al. (2014b) and Zenhäusern et al. (2017) carried out market surveys on PVT collectors and PVT systems. Both studies conclude that most PVT products available on the market are unglazed PVT collectors, which clearly dominate the European PVT market. This can be attributed to their high electrical efficiency, technological maturity and the intrinsic temperature stability.

The construction of unglazed PVT collectors is technologically rather simple and consists of a PV module coupled to a heat exchanger on the module's backside. Unglazed PVT collectors are optimized towards a high electrical efficiency, which is achieved by a high optical efficiency without additional front cover or concentrating devices. Moreover, the operation at low fluid temperatures can enhance the electrical efficiency by cooling the PV cells.

Thermal insulation in unglazed PVT collectors can only be applied at the back side of the collector, resulting in relatively high heat losses due to convection and radiation, which lowers the thermal efficiency (Aste et al. 2014). On account of the high heat losses, stagnation temperatures remain below 100 °C, which is uncritical for most employed PV materials. Therefore, unglazed PVT collectors can be considered relatively reliable and they have the highest technology readiness level of all PVT designs (Zondag et al. 2006). However, the application of unglazed PVT collectors is restricted to low temperature systems.

Unglazed PVT collectors still have a need for research on the optimization of the internal heat transfer, which is especially important in unglazed PVT collectors due to their high heat losses. With a poor thermal contact, heat absorbed in the PV cells is more likely to dissipate to the environment, which results in a low collector efficiency factor F'. Special integrated PVT absorber designs are a possible approach to increase the internal heat transfer (Zondag et al. 2006).

Secondly, the synergetic integration of unglazed PVT collectors in low temperature systems is an important research topic. In the European climate, unglazed PVT collectors are mostly applied for pool heating, pre-heating of hot water in multi-family homes (Rommel et al. 2015), or in heat pump systems. In the latter systems, PVT collectors can be used to regenerate the ground source (Bertram et al. 2012; Zenhäusern et al. 2017), but also directly coupled to the evaporator of the heat pump (Adam et al.

2014a; Schmidt et al. 2017). In this kind of integration, fluid temperatures often fall below ambient temperatures, so that unglazed PVT collectors function as a heat exchanger to harvest ambient energy.

1.4.2 Glazed PVT collectors

Currently, there are only few glazed PVT collectors commercially available (Adam et al. 2014b; Zenhäusern et al. 2017). This may be due to the higher level of product complexity resulting from higher temperatures, which requires an adapted collector design or the usage of non-standard materials which also entails higher costs for the development and production of the PVT absorber (Zenhäusern et al. 2017).

One of the first commercial, glazed PVT collectors was developed at the Dutch research energy center ECN in the research group around Zondag and van Helden (Zondag et al. 2004). This collector was later marketed by a spin-off under the product name PVTWINS. The construction of the PVT collector involved a specifically designed poly-crystalline PV module, which was bonded with a thin glue layer to a copper absorber with laser-welded copper tubes. The research at ECN contributed greatly to the current state of knowledge of PVT collectors.

In a previous PhD thesis at Fraunhofer ISE, Dupeyrat (2011a) developed a novel glazed PVT collector concept. The key improvement concerns the optimization of the internal heat transfer from PV cells to the fluid by laminating the PV cells directly on a one-side-flat aluminum roll-bond absorber with an efficient hydraulic FracTherm® design (Hermann 2005). Moreover, Dupeyrat improved the optical efficiency by substituting the glass sheet of the transparent module glazing of the PVT absorber with a thin FEP film. This is possible because the front glass cover serves as sufficient mechanical protection, and hence the second glass sheet is obsolete. A better match of the refractive indices of air, FEP, EVA, and the PV cells reduces reflections and thus increases the optical performance.

The application of optical coatings is a promising measure to optimize the optical performance. Santbergen et al. (2010) analyzed the influence of anti-reflective (AR) coatings and low-emissivity (low-e) coatings on the performance and yields. Both the electrical and thermal performance benefit from an AR coating on the front glazing and on the surface of the PVT absorber. Low-e coatings improve the thermal efficiency by reducing radiative heat losses. However, the higher reflectance of the coatings also reduces the electrical efficiency.

The application of highly-transparent low-e coatings in PVT collectors was demonstrated experimentally by Wendker et al. (2012) within the joint research project "PVTmax" of Fraunhofer ISE and Solvis. The developed PVT collector utilizes a silver-based low-e coating, which was specifically optimized for PVT collectors. Thus, the collectors achieves a high thermal efficiency, whereas the electrical performance is hardly affected. More recently, Matuska et al. (2015) also developed a glazed PVT prototype with low-e coating and argon filling. Instead of standard EVA, their PVT laminate is encapsulated by a polysiloxane gel, which is deemed stable up to temperatures of 250 °C.

Yet, low-e coatings aggravate the issue of overheating further, as lower heat loss rates lead to higher stagnation temperatures. Therefore, the application of low-e coatings also must involve an adapted collector design that guarantees temperature stability.

The research needs of glazed PVT collectors mainly concern the temperature stability, the optimization of the overall performance, and integration of the PVT collectors into suitable solar thermal systems. Chapter 2.1 will provide a more detailed overview of the research needs.

1.4.3 Concentrating PVT collectors

There are some commercial products of concentrating PVT collectors available. The available products include amongst others a stationary, low-concentrating PVT collector by the Dutch company Solarus, a line focusing, tracked parabolic through PVT collector by the Swedish company Absolicon, and a point concentrating PVT tower collector by the Swiss company AirlightEnergy and IBM research.

The motivation for concentrating PVT collectors is to reduce the active PV area. Thus, the potentially more expensive materials of or cells, encapsulation, etc. are substituted by cheaper reflectors. Additionally, the thermal efficiency benefits from smaller PV areas, as radiative heat losses decrease with smaller hot surfaces. In tracked PVT collectors, intentionally defocusing the collector and turning the PVT absorber away from the sun can avoid overheating.

However, the optical efficiency of concentrating PVT collectors falls below that of flat plate PVT collectors, due to higher optical losses. Furthermore, additional costs arise from the elaborate tracking system, which may not be offset by the lower material costs.

Recent research on concentrating PVT collectors concerns the application of diffuse reflectors to unglazed PVT collectors to increase efficiency while maintaining temperature stability (Tripanagnostopoulos 2007). A more homogenous distribution of the irradiance in the PV cells was achieved by a flux homogenizer (Helmers et al. 2013) or by an adapted geometry of a CPC concentrator (Proell et al. 2016). A different approach uses Nano fluids to split the solar rays according to their wavelength. Thus, the PV cells and the thermal absorber are separated with decoupled temperature levels of the PV cells and the fluid (Mojiri et al. 2013).

1.4.4 Comparison of state of the art efficiency

To assess the current state of the electrical and thermal performance of current PVT products, the following "best of market" products are selected and compared, which can be considered the highest performing PVT collector of their class.

- The unglazed PVT collector by MeyerBurger (CH) features a high electrical efficiency and a good thermal contact between PV cells and the fluid. The collector comes without thermal insulation of the back side resulting in high heat losses at elevated fluid temperatures and higher wind speeds.
- The glazed PVT collector "Ecomesh" by EndeF (ES) features poly-crystalline PV cells and a transparent front cover, which reduces heat losses compared to unglazed PVT collectors. However, the PVT absorber has a high emittance so that heat losses are still considerably higher than in solar thermal collectors.
- The low-concentrating PVT collector by Solarus (NL) is a stationary, non-tracked PVT collector with a concentration ratio of C = 1.75. The collector employs bi-facial PV cells, which absorb both direct solar irradiance and the reflected irradiance from aluminum reflectors. As the collector is not tracked, the acceptance angle is limited with high optical losses at high angles of incidence.

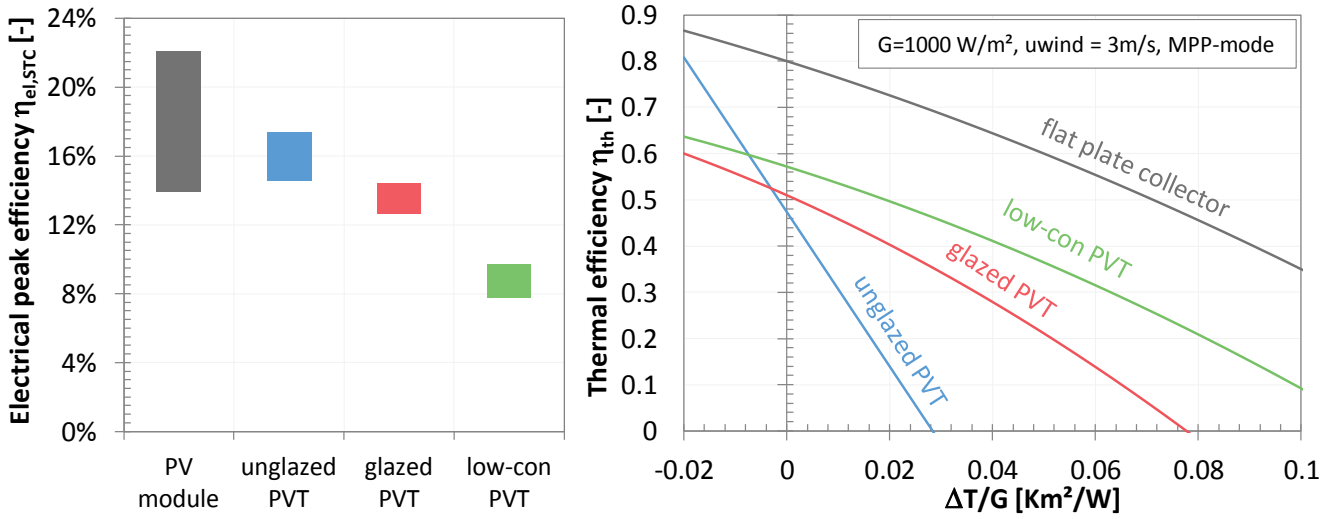

Figure 1.6: Comparison of the electrical and thermal efficiency of best of market unglazed, glazed, and low-concentrating PVT collectors. Efficiency related to aperture area.

The electrical peak efficiency under standard test conditions (STC) ranges between $\eta_{el,STC}$ = 9.7 % of the low-con PVT collector up to $\eta_{el,STC}$ = 17.4 % of the unglazed PVT collector. By comparison, the efficiency of PV modules varies between $\eta_{el,STC}$ = 13.9 % of thin film PV modules and $\eta_{el,STC}$ = 22.2 % of high-efficiency mono-Si modules (Philipps and Warmuth 2017). The industry average amounts to approximately $\eta_{el,STC}$ = 15.0 % of polycrystalline PV modules.

The low-concentrating PVT collector achieves the highest thermal performance, followed by the glazed and the unglazed PVT collector. The lower thermal performance compared to flat plate collector can be firstly attributed to the simultaneous electricity generation. Secondly, PVT absorbers have a lower absorption and higher emittance compared to spectrally selective, solar thermal absorbers. Moreover, the thermal resistance between PV cells and the fluid is, in most cases, higher than for flat plate collectors.

In general, it can be observed that PVT collectors with a higher electrical efficiency achieve a lower thermal efficiency, and vice versa. This underpins the notion that the design of PVT collectors can be either optimized towards a high electrical or a high thermal efficiency.

2 METHODOLOGY

2.1 Thesis approach

2.1.1 Research topics and objectives

The research topics are derived from the current state of the PVT technology as previously described and are embedded into the greater research strategy to "develop PVT technology to make it commercially viable" (IEA 2012). The research topics with the corresponding objectives and research questions are explained in the following.

Research topic 1): Increase the overall performance of PVT collectors by means of highly transparent low-emissivity coatings

PVT collectors aim at a better utilization of scarce roof areas through the cogeneration of heat and electricity. The optimization of the overall energetic output of these areas is therefore a central objective for the further development of PVT collectors. However, an improvement of either the electrical or the thermal efficiency typically affects the corresponding other efficiency adversely. Depending on the design of the PVT system, the highest overall annual energy yields are achieved by improving the thermal efficiency while reducing the electrical efficiency as little as possible.

Accordingly, Zondag (2008) recommends to improve the thermal efficiency of glazed PVT collectors by increasing the absorbed energy in the PV cells and reducing thermal losses. Also RHC (2012) recommends to "develop glazed PVT collectors with improved thermal performance and high reliability".

Thin film coatings with a low infrared emissivity and a high solar transmittance are a promising measure to reduce thermal losses and still maintain a good optical efficiency. Zondag et al. (2006) identify the development and application of highly transparent low-e coatings in PVT collectors as central research area. Dupeyrat (2011a) comes to the same conclusion and describes "the use and adaptation of transparent low-e coatings specifically developed for PV-T collectors" as the next areas of investigation.

The first research objective therefore concerns the improvement of the overall efficiency of glazed PVT collectors by the application of low-e coatings with the following research questions:

- What is the effect of low-e coatings on the thermal and electrical efficiency?
- Which low-e coatings are suitable for application in PVT collectors?
- How can low-e coatings realize an optimum overall efficiency?

Research topic 2): Assess the yields and benefits of PVT systems, with a focus on PVT collectors with low-e

The performance of PVT collectors has to be regarded within its system context by assessing the collector's energy output, useful energy savings, utilization of the available building surface, and associated costs for the electricity and heat generation. Ultimately, the benefit of PVT collectors arises from evaluating these aspects, which is why the collector development and system integration should be oriented towards creating the maximum benefit on the system level.

Systematic research on the system integration of PVT collectors is scarce. Most papers focus on a certain collector type or on a certain system type, but the general applicability of different PVT technologies remains unclear. Hence, the research strategy described in the PVT roadmap of IEA SHC Task 35 recommends "economic optimisation studies […] taking into account the operation temperature of the PVT" (Zondag et al. 2006).

In this context, the approach of this thesis concerns the systematic assessment of various types of PVT applications with varying collector technologies, especially PVT collectors with low-e coatings. The novel characteristic temperature approach puts the operating temperature of the collector into the focus. Annual energy output of the collector, useful system yields, and the economic feasibility are subject to a detailed analysis.

The second research objective therefore concerns the assessment of electrical and thermal yields in PVT systems with the following research questions:

- Which factors influence the electrical and thermal yields?
- Which PVT technology is suitable for which application, especially concerning PVT collectors with low-e?
- What are the energetic benefits and the economic expenses of PVT systems?

Research topic 3): Demonstrate the application of overheating protection on PVT collectors with low-e coatings

High temperatures of glazed PVT collectors pose a challenge for the employed materials (Zondag et al. 2006) and the application of low-e coatings aggravates the critical issue of overheating further. During regular operation, a high level of insulation is desired to achieve a good thermal efficiency. However, if the storage capacity is expired or during system failures or power outages, the high level of collector insulation increases the risk of overheating, which might lead to temperature-induced ageing or even permanent damage of the collector.

There are two concurring approaches to deal with this issue: either the collector is protected from overheating by adjusting the thermal losses, or inherently temperature resistant materials and construction of the PVT absorber are used (Fortuin et al. 2014). Accordingly, Zondag et al. (2006) recommends to "[find] ways to lower the temperature during stagnation conditions" and "[develop] tools to investigate exactly and reliably the temperatures in all components of PVT absorbers". Furthermore Dupeyrat (2011a) notes, that "it is necessary to look for innovative solutions to avoid the high stagnation temperatures", while maintaining the high thermal efficiency during regular operation.

This thesis will concentrate on the application of overheating protection (OHP). In this way, the PVT collector can employ standard PV components and thus benefit from the low cost level of the PV market.

Moreover, lower cell temperatures have a positive effect on electrical yields and avoid premature degradation and ageing.

The third research objective therefore concerns the demonstration of overheating protection concepts in PVT collectors with the following research questions:

- What are the thermal requirements of the materials employed in PVT collectors?
- How does the overheating protection influence temperatures and yields?
- Which overheating protection concepts are suitable for the application in PVT collectors?

As previously noted, glazed, flat-plate PVT collectors with liquid heat transfer fluid and c-Si cells are in the focus of this thesis. Many of the findings on the application of low-e coatings, the characteristic temperature approach, and overheating protections, are also applicable to other PVT categories such as unglazed and concentrating PVT collectors. These technologies will be used occasionally as a benchmark for comparative purposes, which allows putting the findings into a better context.

2.1.2 Thermal management – an approach focusing on collector temperatures

The thematic framework "thermal management of PVT collector" subsumes the three central research topics by putting the collector temperatures into the focus for the development and optimization of PVT collectors and systems. As the cell and fluid temperatures link the thermal and electrical performance, the collector temperatures are the obvious key to optimize the overall performance and balance or even reconcile the contradictory requirements of photovoltaics and solar thermal collectors.

Thermal management is a widely used term in the electronics and automotive industry and concerns managing the temperature of components through a demand-oriented temperature control. In the electronics sector, thermal management refers to the active or passive cooling to guarantee a safe and reliable operation of electronical equipment such as processors or LEDs (Çengel and Ghajar 2015). For the automotive sector, Mause et al. (2010) aptly define thermal management as the demand-driven and efficient control of the thermal energy flows in the vehicle according to the current state of operation and demand. For instance, combustion engines, batteries, and fuel cells produce waste heat, but also operate at specific optimum temperature levels. A smart control of energy flows is therefore essential to distribute the heat efficiently from the corresponding sources to the sinks.

Norton (2014) analogously applies the term to photovoltaics und refers to the cooling of PV cells. He distinguishes between passive thermal management without using the excessive heat and active thermal management where the excessive heat of PV cells is used. The later concept, of course, corresponds to the principle of PVT collectors.

Within this thesis, thermal management of PVT collectors refers to idea of controlling energy flows and adjusting the collector temperature to the desired level. Hereby, thermal management takes place on three different levels:

1) On the collector level with a focus on low-e coatings

On the collector level, thermal management refers to the engineering and design of the PVT collector to achieve an optimized overall efficiency. This is achieved by managing optical, thermal, and electrical energy flows. Low-e coatings are the investigated approach to achieve thermal management on the collector level.

2) On the system level with a focus on the characteristic temperature T_{char}

On the system level, thermal management refers to the PVT system design. Ultimately, the system determines the occurring operating collector temperatures. Optimization of the PVT yields is therefore achieved by the design of PVT system, dimensioning of components, and selection of an apt PVT collector technology that matches the temperature requirements of the system.

3) During operation with a focus on overheating protection

Thermal management during operation refers to adjusting collector temperatures to desired levels by an overheating protection. Firstly, this approach aims at avoiding excessive material temperatures in the collector and thus preventing ageing. Secondly, the overheating protection can be activated depending on the current demand for electricity and heat, allowing a demand-driven operation of the PVT collector.

2.1.3 Thesis structure

The thesis structure follows the three thematic complexes of low-e coatings, PVT systems and overheating protection. Figure 2.1 depicts the overall structure of the thesis and illustrates the framework, objectives and research questions.

To begin with, chapter 2.2 discusses the methodological approach, which is characterized by a combination of numerical and experimental methods on both the collector and system level. Furthermore, the chapter details the assessment of the PVT performance by standardized efficiency parameters, gross energy yields, and system yields under consideration of primary energy factors.

Chapter 3 is concerned with the modelling and development of glazed PVT collectors with low-e coatings. A detailed numerical model physically describes the optical, electrical, and thermal energy flows inside a PVT collector. Two basically identical PVT collectors, yet one with and one without low-e coatings, are built and tested, demonstrating the applicability of low-e coatings. The experimental results are discussed with the numerical model to understand the effect of low-e coatings on the electrical and thermal efficiency. Moreover, chapter 3 discusses practical aspects for the optimum application of low-e coatings in PVT collectors.

Chapter 4 examines the electrical and thermal yields in PVT systems. For this purpose, a performance model for system simulations is presented and validated with measured field data. With this model, the electrical and thermal yields of different types of PVT collectors are assessed in varying system types. The simulation results are analyzed by means of the novel characteristic temperature approach, which puts the mean operating temperature in the focus of the assessment. Chapter 4 concludes with a techno-

economical assessment of the levelized costs of heat and electricity indicating the economic feasibility of PVT systems.

Chapter 5 discusses the application of overheating protection for PVT collectors to avoid excessive temperatures and increase their reliability. An initial analysis discusses material requirements, fault mechanisms, and the typical temperature distributions occurring in PVT systems. Then, a thorough literature review analyzes existing overheating protection concepts and classifies these according to their physical effect on the absorber temperatures. Three innovative concepts demonstrate the technical feasibility of PVT collectors with overheating protection by means of experimental prototyping. Furthermore, the effect of the overheating protection on temperatures and yields is analyzed for these collectors by annual system simulations.

Finally, the thesis concludes with a summary of the key findings and an outlook on future research topics in chapter 6.

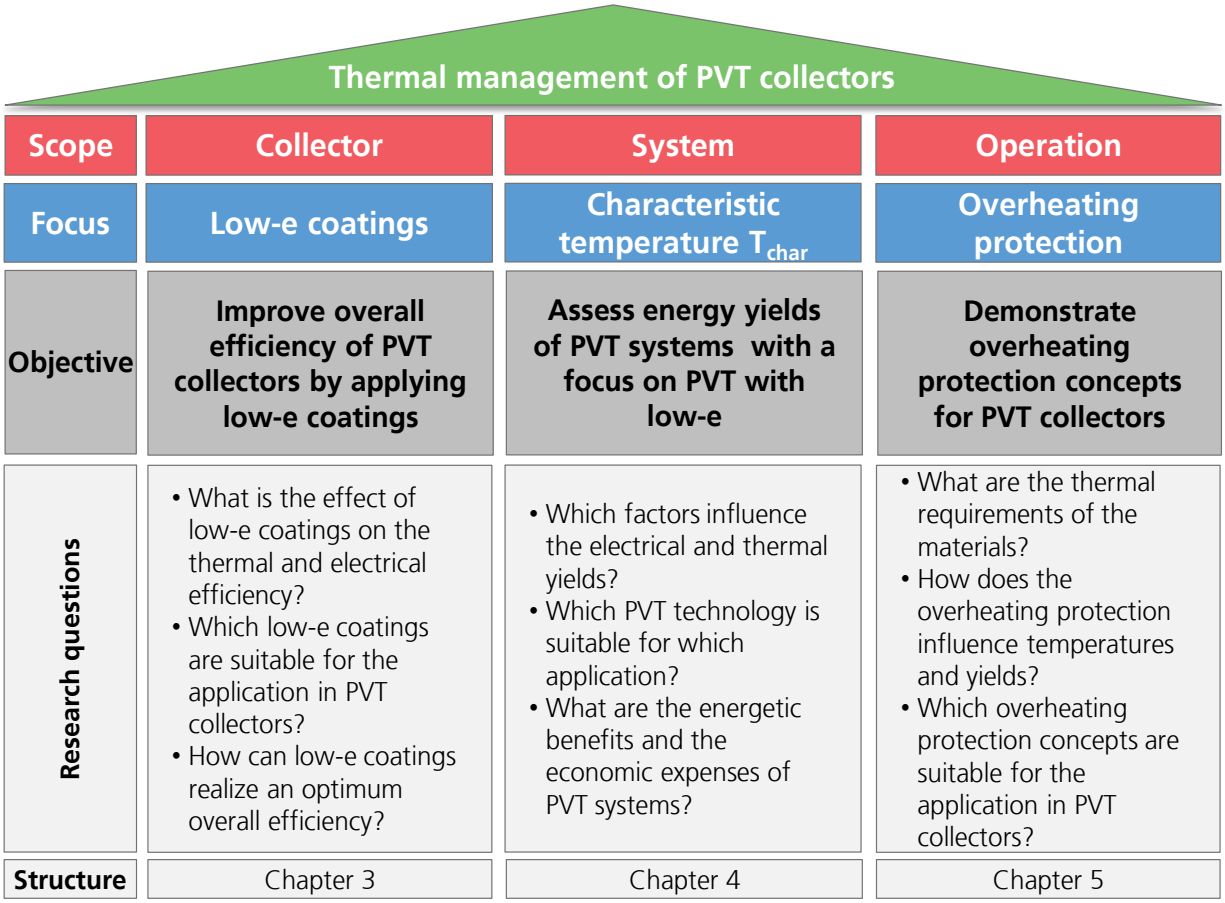

Figure 2.1: Structure and framework of the thesis with underlying research topics, objectives, and questions.

2.2 Methodological approach

This thesis combines experimental and numerical methods on both collector and system level. A well-balanced mixture of simulations and experiments with validated simulation models and experimental demonstrators enables a robust and reliable research methodology and thus a high confidence of the presented results. Figure 2.2 illustrates the interaction of experimental and numerical methods on the collector and system level.

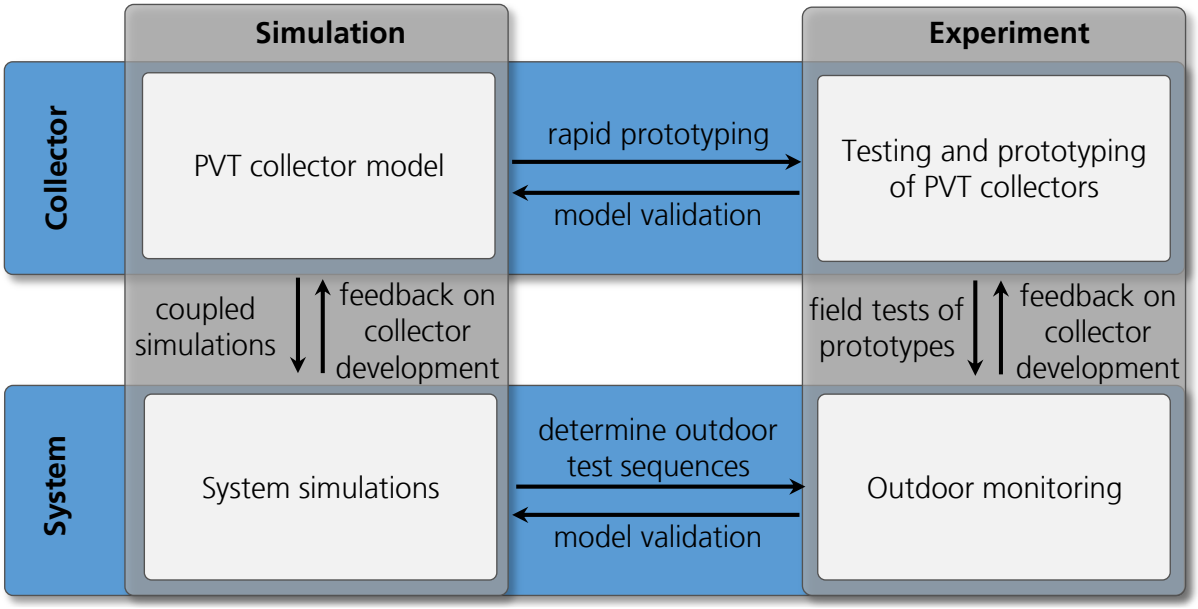

Figure 2.2: Methodological approach combining simulation and experiment on both collector and system level.

Simulation methods allow an in-depth analysis and profound comprehension of the processes and interaction in the collector and system. Furthermore, numerical simulations are suitable for identification of optimization potentials, parameter variation, and rapid prototyping to pre-assess prototypes before construction. Experimental methods, on the other hand, demonstrate the technical feasibility of novel collectors by means of constructing and testing prototypes and functional mock-ups. These experimental results are also used to validate collector and system simulation models.

2.2.1 Simulation approach

Separate simulation models on the collector and system level characterize the applied modelling approach within this thesis.

The PVT collector model describes the physical behavior by numerically describing optical, electrical, and thermal energy flows to study the effect of design parameters on the standardized efficiency parameters. Hence, the PVT collector model can be considered a numerical solar simulator in reference to the test equipment of a solar simulator for the experimental characterization of the collector performance under artificial sunlight.

The PVT system model considers the collector efficiency, weather, user behavior, control, and interaction of electrical and thermal components to assess annual yields and energy savings on the system level. An empirical performance model based on efficiency curves is used to describe the collector behavior. Accordingly, the system model can be regarded as numerical outdoor monitoring or field tests of entire systems.

The collector and system simulations can be coupled by using efficiency parameters from the collector model as input for the system model. Figure 2.3 juxtaposes the PVT collector model and the PVT system model and summarizes their specific objectives, characteristics, and implementation.

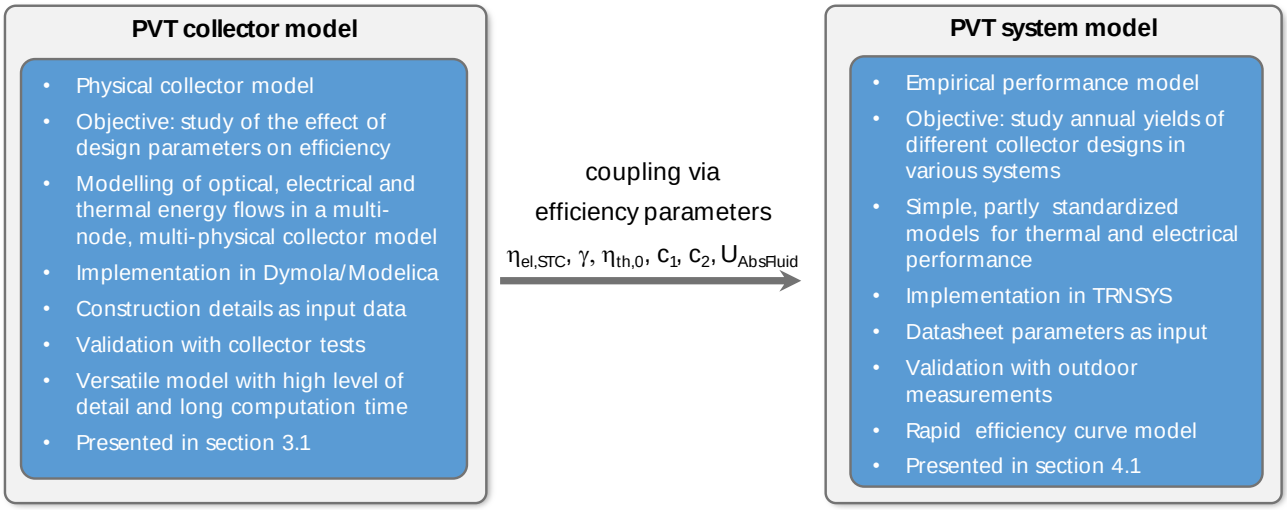

Figure 2.3: Simulation approach with separate performance models for collector and system.

Most research papers on PVT system integration use a single, custom PVT collector model to study effects of design parameters on the collector efficiency and to analyze yields in solar thermal systems (e.g. Zondag et al. (2002a), Chow (2003), Helmers et al. (2012), Bilbao and Sproul (2015), and Haurant et al. (2015)). This contrasts with the less frequently used approach to model collector behavior and system integration with separate models (e.g. Bertram et al. (2012), and Koke and Clement (2016)). However, there are various advantages in separating the collector and system models:

- The collector testing standard ISO 9806 (2013) defines the efficiency parameters as the standard output from collector tests. These well-proven and widely accepted parameters guarantee a consistent and validated simulation interface. Moreover, using interpretable efficiency curve parameters as simulation input instead of a multitude of collector design parameters makes the approach more robust to errors and allows a plausibility check prior to conducting system simulations.
- Only the separate model approach gives the possibility to consistently include commercial products to the system simulations. For these products, only data sheet information is available, but not the exact collector design as required for running collector simulations.
- Using a highly detailed collector model for system simulation leads to time and resource intensive computation of system simulations. The approach based on efficiency curves is generally faster and therefore more suitable for system simulations.
- The separate model approach gives the possibility to implement the models on two different simulation platforms. In the present case, Dymola/Modelica (Modelica 2012) is used for the collector model because of the ease of modelling versatile collector concepts in an object-oriented modelling language. For the system models, TRNSYS (Klein et al. 2015) is used owing to the variety of available component and building libraries, which are essential for system simulations. Likewise, the existing media, electricity, and heat transfer libraries of Modelica are suitable for the multi-physical modelling of the collector component.

Consequently, the approach with two separate models combines the advantages of both collector and system models. It is for these reasons that the separate approach was selected although this requires setting up and validating two separate models.

2.2.2 Experimental approach

Experiments are conducted on different scales from small-scale experiments of functional mock-ups to standardized collector performance characterization and outdoor measurements at real operating conditions.

Small-scale experiments are carried out to characterize optical, electrical, and thermal properties of materials and components. The wavelength dependent optical characteristics, such as transmittance and emissivity, are analyzed by Fourier spectroscopy measurements. Thermal experiments are conducted at the fluid dynamics test rig of Fraunhofer ISE to analyze internal heat transfer phenomena inside the PVT absorber and external heat losses by measuring fluid and surface temperatures as well as the mass flow of hydraulic components. Additionally, thermographic imagery is applied to analyze the surface temperature distribution and measure infrared emissive losses.

The electrical and thermal performance of full-sized PVT collector is characterized at the accredited test labs of Fraunhofer ISE on the basis of standardized measurement procedures. The electrical power at standard testing conditions $P_{el,STC}$ is characterized according to IEC 61853 (2011) at the flasher of Fraunhofer ISE CalLab. The thermal efficiency curves are measured at the Fraunhofer ISE TestLab Solar Thermal Systems according to the current standard ISO 9806 (2013) by measuring the thermal power at varying, standardized operating conditions.

Furthermore, outdoor field tests of the PVT collectors are carried out under real operating conditions. As only one PVT collector of a kind is built, full system monitoring is not possible. Instead, the PVT collectors are mounted on an outdoor rack and a thermostat dictates the inlet collector temperatures as obtained from simulations for typical solar thermal systems. Thus, the PVT collectors operate in the realistic operating conditions of the emulated system behavior while the dynamic collector performance is measured.

An overview of all PVT collectors that were built and tested within this thesis is provided in 0. This comprehensive overview includes collector photos, details on the construction, and test results from performance measurements. The collectors are labeled and numbered to allow a unique cross-referencing and unambiguous allocation of the collectors.

2.2.3 System-oriented collector development

The PVT collector is in continuous interaction with the system, in which it operates. Therefore, it always has to be regarded within the system context. Although this thesis will focus on the component of the PVT collector, it is also clear that the application and system have an important influence on the collector performance, because the system defines the operating environment.

As collectors almost never operate under standardized test conditions in the real system, a sole optimization of the standardized efficiency cannot be expedient. Instead, the specific operating conditions in the system environment should form the basis for optimizing the electrical and thermal performance of PVT collectors. This aspect is especially important for PVT collectors due to the sometimes contradictory requirements of PV and solar thermal operation.

Given the importance of collector-system interaction, this thesis pursues the approach of system-oriented collector development. New methods for the analysis of PVT systems will be presented, which aim at providing a better comprehension of this interaction. For example, the novel characteristic temperature

approach in chapter 4.4 reduces the complexity of the system and its influence on the collector performance on a single temperature. Furthermore, a thermal analysis of the operation fields of PVT collectors is presented in chapter 4.6.

2.2.4 Assessment of PVT collectors on different levels

The performance of PVT collectors can be assessed on different levels:

- Standardized efficiency parameters allow an expert-based comparison of the performance of PVT collectors. Yet, the efficiency parameters do not make an objective statement regarding energy yields and the expected annual performance.
- Gross energy yields can be calculated with the open, Excel-based tool ScenoCalc on the basis of standardized efficiency parameters. The certification body Solar Keymark Network uses this harmonized approach to quantitatively assess the maximum achievable yields if the collector was operated at a constant fluid temperature and at a specific location.
- Assessing the system yields and energy savings by dynamic system simulations is the most detailed approach with the highest level of accuracy of the energy yields. However, the results are only valid for the specific simulation case.

Depending on the desired level of specificity and required accuracy of the energetic evaluation, the level for the assessment of the PVT collector has to be selected. However, it has to be noted that with an increasing level of detail the general validity and universal applicability decrease as well (Figure 2.4).

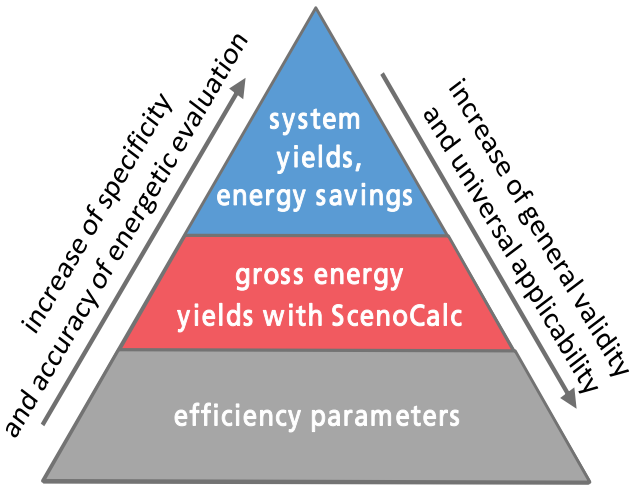

Figure 2.4: Pyramid for the assessment and comparison of PVT collector technologies on different levels.

2.2.4.1 Standard efficiency parameters

Current standards specify the procedure for testing the electrical efficiency of PV modules and the thermal efficiency of solar thermal collectors, but explicit standards for testing the combined efficiency of PVT collectors are not available. Therefore, the standard efficiency parameters from the separate electrical and thermal measurements have to be used.

Electrical efficiency parameters

Terrestrial PV modules are qualified based on standards IEC 61853 (2011) and IEC 61215 (2016). The current-voltage-characteristic of the PV module is measured in natural sunlight, or in pulsed or continuous simulated sunlight under the reference solar spectrum AM1.5 (IEC 60904, 2006). All relevant performance parameters of PV modules can be derived from the I-V curve, such as the open circuit voltage U_{OC}, the short circuit current I_{SC}, and the power in the maximum power point P_{MPP} with the corresponding fill factor FF.

The peak efficiency $\eta_{el,STC}$ is tested based on standard test conditions (STC) at a normal irradiance of G = 1000 W/m², while the temperature of the PV module is maintained at a constant temperature of T_{STC} = 25 °C. The temperature dependence of the PV power γ is obtained by measuring the I-V curve at several module temperatures and a subsequent linear fit. The temperature-dependent electrical efficiency η_{el} is expressed as (Skoplaki and Palyvos 2009):

$$\eta_{el} = \eta_{el,STC}\,(1 - \gamma(T_{cell} - T_{STC})) \tag{2.1}$$

For conventional PV modules, the nominal module operating temperature (NMOT) is measured at the standardized operating conditions of G = 800 W/m², T_a = 20 °C, u_{wind} = 1 m/s, φ_{titlt} = 37°, and operation in maximum power point (IEC 61215-2:2016). These tests, however do not represent typical operation conditions of PVT collectors. On the contrary, the fluid temperatures dictate the governing cell temperature during operation. Therefore, the NOMT alone has a limited significance for PVT collectors.

Thermal efficiency parameters

ISO 9806 (2013) is the current standard for characterizing the performance of solar thermal collectors. It allows to measure the thermal performance in indoor conditions with artificial sun and wind in the solar simulator. Alternatively, ISO 9806 allows outdoor testing under natural weather conditions in steady-state conditions or with the quasi-dynamic method (QDM).

The thermal efficiency curve of solar thermal collectors in its simplest form is reported as (ISO 9806 2013):

$$\eta_{th} = \eta_{th,0} - c_1\frac{(T_m - T_a)}{G} - c_2\frac{(T_m - T_a)^2}{G} \tag{2.2}$$

with the thermal conversion factor $\eta_{th,0}$ and the linear and quadratic heat loss coefficients c_1 and c_2. The temperature difference between mean fluid temperature T_m and ambient temperature T_a divided by the normal irradiance G is often also noted shortly as the reduced temperature $\Delta T/G$.

The efficiency of solar collectors can be described more accurately by taking additional parameters into account. The quasi-dynamic test method also considers the direct and diffuse incidence angle modifiers $K_{\theta b}$ and $K_{\theta d}$, wind speed dependence of thermal losses c_3 and c_6, long wave irradiance characteristics c_4, and thermal capacity effects c_{eff}. The corresponding dynamic, instantaneous heat output is given by (ISO 9806 2013):

$$\begin{aligned}\dot{q}_{coll} = \eta_{th}\cdot G = {} & F'(\tau\alpha)_{en}\cdot K_{\theta b}(\theta)G_b + F'(\tau\alpha)_{en}\cdot K_{\theta d}G_d - c_1(T_m - T_a) - c_2(T_m - T_a)^2 \\ & - c_3 u(T_m - T_a) + c_4(E_L - \sigma T_a^4) - c_{eff}\frac{T_m}{dt} - c_6 uG\end{aligned} \tag{2.3}$$

Depending on the construction of the collector, not all of the parameters c_1 – c_6 have to be evaluated and some may be set to zero. For instance, wind speed and infrared radiative heat exchange have only a minor influence on the efficiency of glazed collectors, which is why c_3, c_4 and c_6 are typically not evaluated. The new standard ISO 9806 (2017) replaced the misleading definition of unglazed collectors by the so-called WISC, which stands for "wind and/or infrared sensitive collectors". For these collectors, it is mandatory to characterize the relevant parameters c_3, c_4, und c_6.

PVT efficiency parameters

The separate electrical and thermal standards disregard the interaction of electrical and thermal operation. However, it is known that the electrical mode of operation – whether operated with or without simultaneous electricity generation – has a significant influence on the thermal performance (Hofmann et al. 2010). Furthermore, the fluid temperatures affect the PV cell temperatures and thus the electrical efficiency through the heat transfer between PV cells and the fluid, which is described by F' or $U_{AbsFluid}$.

A good physical interpretation of the collector parameters can be achieved by converting the standardized efficiency parameters into to temperature-dependent, physical characteristics of the effective transmittance-absorptance product $(\tau\alpha)_{eff}$, the electrical efficiency η_{el}, the internal heat transfer coefficient $U_{AbsFluid}$, and the overall heat loss coefficient U_{Loss}. These derived parameters accurately describe the physical behavior of a PVT collector based on the two-node-model as will be shown in chapter 3.1.

The convention applies throughout this thesis that the thermal performance always indicates the operation with simultaneous electrical operation in MPP mode, if not stated otherwise. Consequently, the thermal performance model implicitly considers the instantaneous electrical operation, so that the generated electrical energy is not explicitly subtracted from Eq. (2.3). Hence, this approach calculates the thermal power independently from the instantaneous electrical power and neglects deviations in the thermal output due to variations of the electrical output. Chapter 4.1 discusses the performance model and the involved uncertainty and errors in more detail.

Thus, the combined overall efficiency of the PVT collector η_{PVT} is given by the sum of the electrical efficiency η_{el} in Eq. (2.1) and the thermal efficiency η_{th} in Eq. (2.3) by:

$$\eta_{PVT} = \eta_{el} + \eta_{th} \tag{2.4}$$

2.2.4.2 Gross energy yields with ScenoCalc

The motivation behind the software tool "ScenoCalc" is the calculation of the energy output of solar collectors to allow a consistent and transparent comparison of solar thermal collector technologies. This Excel-based tool was developed by the Swedish Research Institute RISE and is now provided by the Solar Keymark Network as a free download including reference weather data for the European locations of Athens, Davos, Würzburg, and Stockholm.

ScenoCalc focuses on the collector yields and parameterizes the system integration by the mean fluid temperature T_m. This temperature is assumed constant over the entire year. Moreover, an infinite storage capacity is assumed, so that any heat gain from the collector is also utilized. In this way, the gross energy yields are obtained by evaluating weather conditions and the corresponding collector energy output for

every hour of the year. Thus, the gross energy yields can be interpreted as the maximum achievable collector yield if the collector is operated a constant temperature level.

The current ScenoCalc version v5.01 (SKN 2016) does not support the assessment of electrical yields of PVT collectors. Instead, ScenoCalc v3.10d (SKN 2011) will be used, which features the possibility to simulate both thermal and electrical yields according to the methodology described by Perers et al. (2012). In addition to the thermal efficiency parameters, it requires the input of the electrical peak power P_{STC}, the temperature coefficient γ, and the heat transfer coefficient for the bond between the fluid and PV cells $U_{AbsFluid}$.

Gross energy yields obtained from ScenoCalc also form the basis for evaluating the eligibility of solar thermal collectors for the German market incentive program MAP (Marktanreizprogramm). A weighting function is used to combine the thermal yields $Q_{coll,25\,°C}$ and $Q_{coll,50\,°C}$ at the mean fluid temperatures $T_m = 25$ °C and at $T_m = 50$ °C for the location of Würzburg. Dynamic effects are considered by also including the effective capacity c_{eff}. The MAP weighting function is given by (BAFA 2015):

$$Q_{coll,MAP} = 0.38\, Q_{coll,25\,°C} + 0.71\, Q_{coll,50\,°C} - 1.09\, c_{eff}\, \frac{kWh}{kJ} \tag{2.5}$$

The MAP weighting function does not define weighting factors for the electrical yield and is thus only applicably for thermal collectors. Nonetheless, the weighting factors for the thermal yield in Eq. (2.5) correspond with the annual operation time of the collector at the respective mean fluid temperatures levels of $T_m = 25$ °C and $T_m = 50$ °C. By using normalized weighting factors for the electrical yields, which are derived from the thermal weighting function, and neglecting dynamic loss effects, the MAP-weighted gross electrical yield $E_{PV,MAP}$ is defined as:

$$E_{PV,MAP} = 0.35\, E_{PV,25\,°C} + 0.65\, E_{PV,50\,°C} \tag{2.6}$$

As the MAP weighting function aims at approximating the operating conditions of solar collectors in domestic hot water systems, the weighted gross energy yields represent typical yields for such a system. Therefore $Q_{coll,MAP}$ and $E_{PV,MAP}$ are suitable indicators for comparing the thermal and electrical performance of PVT collectors on a consistent basis.

2.2.4.3 System yields and energy savings

Dynamic system simulations comprise the most detailed and realistic assessment approach and take into account the dynamic interaction of the PVT collector with other system components, control, climate, hydraulics, load profile, and the user behavior. However, the PVT collector is only one factor of many that influences the system yields. Nonetheless, system yields are an essential aspect for comparing and optimizing the performance of PVT collectors. Chapter 4 will focus entirely on collector yields and energy savings within the system context.

2.2.5 Comparing the value of electricity and heat by primary energy factors

The opposing requirements for electricity and heat generation in PVT collectors often require a balance between electrical vs. thermal yields. In certain cases, it is therefore necessary to compare the combined value of the produced electricity and heat and to quantify this value as a single number.

Previous research on PVT collectors discussed different approaches for the comparison of electricity and heat. Coventry (2004) introduces the energy value ratio, which is defined as the ratio of the value of electricity to the value of heat. Comparing several approaches – amongst others energy, exergy, displaced greenhouse gases, and energy costs – the energy value ratio varies between 1 (energy) and 16 (exergy) reaching the conclusion that any particular study needs to define its specific energy value ratio depending on their objective. During the IEA SHC Task 35 on PVT collectors Collins and Zondag (2008) address the same question and recommend the application of primary energy, since it is "the best indicator for the amount of fossil fuel saved, which is the basic goal of any renewable energy system".

Following this guideline, the primary energy yield Q_{PE} is used as parameter throughout this thesis to quantify the combined electrical and thermal yield and is defined as:

$$Q_{PE} = f_{p,el}\, E_{PV} + \frac{f_{p,gas}}{\eta_{boiler}}\, Q_{coll} \tag{2.7}$$

with the primary energy factors for electricity $f_{p,el}$ and gas $f_{p,gas}$, the electrical yield E_{PV}, the thermal yield Q_{coll}, and the efficiency of the reference gas boiler η_{boiler}.

Primary energy factors for electricity and gas have to be defined for this purpose. These factors are set by policy makers for all sources of primary energy and differ between countries and evolve in time. Table 2.1 summarizes the primary energy factors of electricity and gas in Germany for the recent years. The primary energy factor for electricity decreased continuously due to an increased share of renewable electricity in the grid. In fact, the German building directive EnEV even set the electrical primary energy factor to $f_{p,el} = 1.8$ in 2016. Nonetheless, primary energy factors used in this thesis are based on DIN V 18599-1 (2013).

The primary energy yield for solar thermal heat corresponds to the primary energy which is avoided by substituting conventional primary energy carriers. With the primary energy factors $f_{p,el} = 2$ and $f_{p,gas} = 1.1$, and assuming that solar thermal heat replaces heat from a condensing gas boiler with an efficiency of $\eta_{boiler} = 1$ based on the lower heating value, the primary energy yield Q_{PE} is calculated as:

$$Q_{PE} = 2 \cdot E_{PV} + 1.1 \cdot Q_{coll} \tag{2.8}$$

Table 2.1: Comparison of primary energy factors for electricity and gas. Values of DIN V 18599-1:2013-05 are used within this thesis.

	$f_{p,el}$	$f_{p,gas}$	Energy value ratio $f_{p,el}/f_{p,gas}$
DIN EN 15603:2008	3.14	1.36	2.31
DIN V 18599-1:2011-12	2.4	1.1	2.18
DIN V 18599-1:2013-05	2	1.1	1.82
DIN V 18599-1:2016-1	1.8	1.1	1.64

3 DEVELOPMENT AND MODELLING OF PVT COLLECTORS WITH LOW-E COATINGS

The following chapter discusses the application of low-e coatings in glazed PVT collectors to optimize the overall efficiency with the following research questions:

- What is the effect of low-e coatings on thermal and electrical efficiency?
- Which low-e coatings are suitable for the application in PVT collectors?
- How can low-e coatings realize an optimum overall efficiency?

Chapter 3.1 motivates the application of low-e coatings and gives an overview of previous numerical and experimental research on low-e coatings in PVT collectors. Chapter 3.2 presents a numerical model of the PVT collector, which describes the optical, electrical, and thermal energy by physical correlations. With this numerical model, a sensitivity analysis of two key collector parameters, U_{Loss} and $U_{AbsFluid}$, is carried out in chapter 3.3 to study the influence of these parameters on expectable yields. Chapter 3.4 compares the experimental results of two basically identical glazed PVT collectors, yet one with and one without low-e coating. These results are analyzed with the numerical model in chapter 3.5 showing the effect of low-e coatings on the efficiency and gross energy yields. Potentially suitable low-e coatings are screened, characterized, and evaluated in chapter 3.6. Chapter 3.7 discusses application aspects of low-e coatings in glazed, unglazed and concentrating collectors considering the possibility to apply low-e on positions other than the module glass.[2]

3.1 Motivation for the application of low-e coatings

A major reason for the limited success of PVT collectors lies in its relatively low thermal efficiency. In contrast to conventional flat plate collectors with a spectrally selective absorber surface, the surface of the PVT laminate has a high emissivity, which results in high radiative heat losses and thus a reduced thermal efficiency.

Low-emissivity (low-e) coatings are considered a promising option to decrease radiative heat losses (Zondag 2008). Similar to spectrally selective solar thermal absorbers, these coatings feature a low emissivity in the infrared spectrum. At the same time, the coating is transparent in the solar spectrum, so that the incident irradiance can propagate through the coating and is absorbed inside the PV cells. However,

[2] The major findings of the following chapter are also published in the paper titled "Development and modelling of highly-efficient PVT collectors with low-emissivity coatings" (Lämmle et al. 2016a). Chapters 3.2, 3.4, and 3.5 contain in parts literal fragments of the paper. These fragments are not marked as citations to facilitate the legibility for the reader. While acknowledging the co-authors valued contributions, the author claims authorship and responsibility for these sections. An explicit citation of literal fragments is therefore omitted.

the low emissivity comes at the expense of higher reflectance losses reducing both the electrical and optical performance.

A general conflict between the thermal and optical performance can be observed for basically all solar thermal collectors. Most measures to enhance the thermal insulation on the front side also reduce the total transmitted and absorbed energy on the absorber. For example, an additional glazing reduces convective heat losses but adds two optical interfaces and thus higher reflection losses. Concentration of solar irradiance reduces radiative heat losses through a reduction of hot surface area but increases reflectance losses at the mirror. Even so-called transparent insulations, e.g. silica aerogel, reduce the total transmission. Thus, in most cases an enhanced thermal insulation leads to deteriorated optical performance (Duffie and Beckman 2013). Low-e coatings are one option amongst others to decrease thermal losses, but potentially offer a good balance between a good thermal insulation, high optical transmittance and moderate costs.

Nowadays, low-e coatings are primarily used in buildings for anti-condensation and energy efficient glazing with low U-values (Jelle et al. 2015). Architectural glass typically has a relatively high transmittance in the visual range of 0.4 - 0.7 μm. However, for the application in PVT collectors, its low transmittance in the solar spectrum is considered a major drawback since it reduces both electrical and thermal efficiency (Zondag 2008). Cox and Raghuraman (1985) conclude after multiple simulations that low-e coatings require an infrared emissivity of less than 0.25 and solar transmittance of greater than 0.85 to be viably applied in PVT air collectors. Santbergen et al. (2010) numerically investigate different SnO:F low-e coatings for the application in glazed, liquid-type PVT collectors. They show that the thermal efficiency can be improved significantly, yet at the cost of a drop of PV efficiency. Matuska et al. (2015) built a PVT collector with architectural low-e glazing. Due to the low solar transmittance of the low-e coating, a low electrical efficiency η_{el} and a low thermal conversion factor $\eta_{th,0}$ were reached. An optimized low-e coating with good balance between high solar transmittance and low emissivity is therefore essential for a viable application of low-e coatings in PVT collectors.

Figure 3.1 illustrates the qualitative interdependence of the optical parameters of low-e coatings and the electrical and thermal energy yields. The low emissivity ε comes at the expense of a reduced transmittance in both the PV spectrum $\tau_{c\text{-}Si}$ and the solar spectrum $\tau_{AM1.5}$. This affects firstly the electrical efficiency at standard test conditions $\eta_{el,STC}$ and secondly the effective transmittance-absorptance product $(\tau\alpha)_{eff}$. Due to a lower overall heat loss coefficient U_{Loss}, the collector efficiency factor F' increases. Therefore, there is no clear tendency of the effect of low-e on the conversion factor $\eta_{th,0}$, but it depends on the specific balance of optical and thermal design parameters. In any case, low-e coatings reduce the collector heat loss coefficients c_1 and c_2 owing to the lower U_{Loss}.

Due to the reduced electrical efficiency and the increased thermal efficiency, the electrical energy yield decreases while the thermal energy yield increases. Two minor effects need to be considered regarding energy yields: with a lower electrical efficiency $\eta_{el,STC}$, less electricity is produced so that more solar energy is available for the thermal operation. At the same time, a higher thermal efficiency due to lower heat losses results in higher cell temperatures throughout the year, which adds to the reduction of electrical yields.

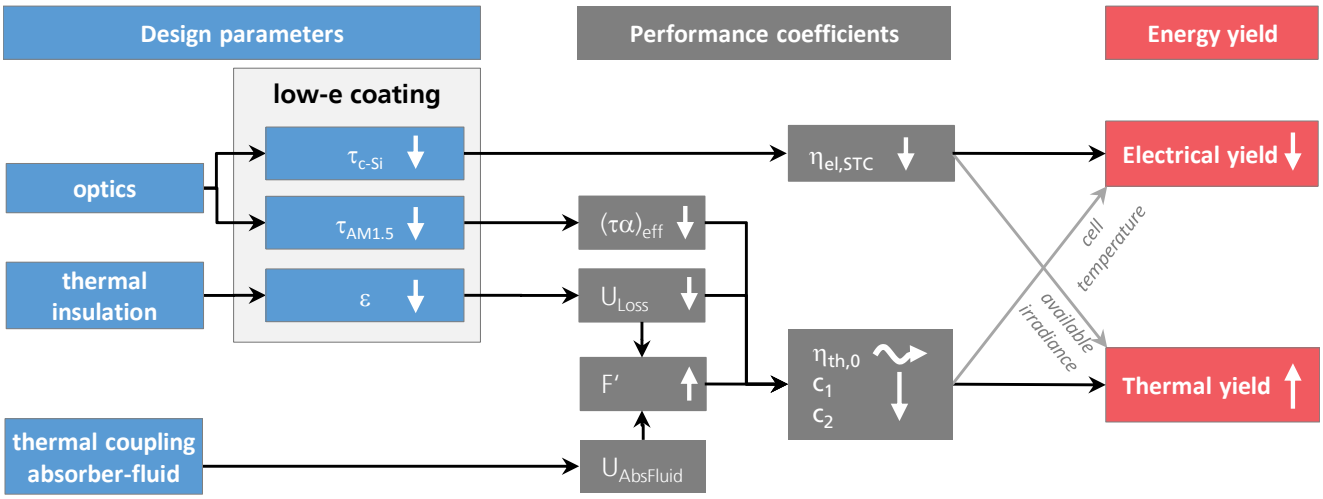

Figure 3.1: Qualitative relationship between the design parameters of a low-e coating and performance coefficients and energy yields.

3.2 Numerical PVT collector model

3.2.1 Introduction

In order to analyze and interpret results, identify optimization potential and perform design studies, a comprehensive PVT collector model is developed. Its main objective is the prediction of the thermal and electrical efficiency for any given set of optical, thermal, electrical, and geometrical input parameters. Thus, the collector model is a powerful tool for the development of new PVT collector concepts and for understanding the interaction of optical, electrical, and thermal energy flows.

In the scientific literature, a multitude of models for solar thermal and PVT collectors can be found, each with a different focus and a different level of detail. Without question, Duffie and Beckman (2013) is considered the standard reference for solar thermal collectors. Matuska and Zmrhal (2009) developed a collector model with an extensive and worthwhile reference for the heat transfer phenomena which occur inside collectors. The first work on modelling PVT collectors was done by Florschuetz (1979) which introduced an internal heat transfer coefficient to couple the PV cell and fluid node. Zondag et al. (2002a) advanced this approach and developed 1D and 2D models by which they studied the influence of the model's level of detail on annual electrical and thermal yields. Chow (2003) also built up on Florschuetz' approach and developed an explicit dynamic collector model with a noteworthy level of detail. Recent work focuses on special modelling topics such as concentrating PVT collectors (Helmers et al. 2012), spatially resolved, fully-wetted absorber (Haurant et al. 2015), a transient PVT collector model implemented into Dymola/Modelica (Greppi 2013), or into an electronic circuit simulating software (Bilbao and Sproul 2015), just to name a few.

All mentioned numerical models share a common structure and thus can be reduced to the basic energy balance of PVT collectors as depicted in Figure 3.2. The incident power $p_{absorber}$ is absorbed in the PV cells, where the energy flow is separated into electricity (p_{el}), useful heat ($\dot{q}_{useful}$) and thermal losses ($\dot{q}_{Loss}$). The electrical efficiency η_{el} is a function of the absorber temperature T_{abs}, which by definition is equal to the cell temperature. Consequently, the two-node collector model describes the energy flows of a PVT col-

lector with four principal parameters: $(\tau\alpha)_{eff}$ on the optical side, U_{Loss} and $U_{AbsFluid}$ on the thermal side, and η_{el} on the electrical side.

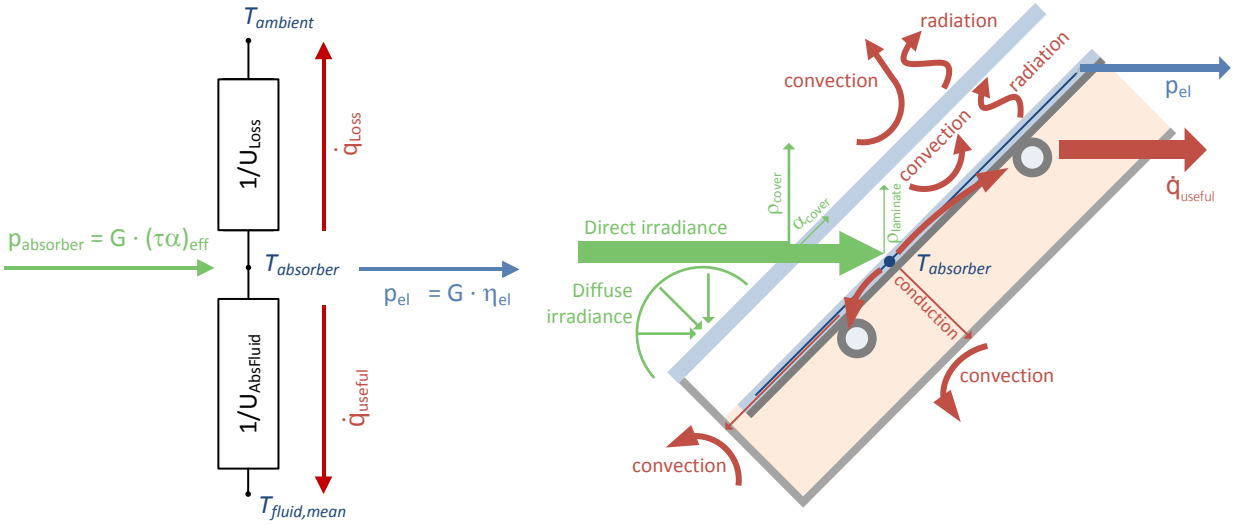

Figure 3.2: Basic energy balance of PVT collectors in form of a two-node collector model (left, adapted from Helmers and Kramer (2013) and corresponding energy flows in a glazed PVT collector (right).

A physically correct description of the PVT collector, however, requires a higher level of detail: for each of the four principal parameters, physical and empirical correlations need to be implemented. These correlations numerically describe the detailed energy flows depending on the optical, electrical, thermal and geometrical properties as depicted exemplarily for a glazed PVT collector in Figure 3.2 (right). Table 3.1 summarizes the four principal parameters and describes experimental and modelling approaches for their characterization.

Table 3.1: Four principal parameters for describing a PVT collector in a two-node model.

Parameter	Energy flow	Experimental approach	Modelling approach
$(\tau\alpha)_{eff}$	Optical	Spectroscopy measurements of transmittance and absorptance of glazing and PVT absorber	Geometric sequence for $(\tau\alpha)_{eff}$
η_{el}	Electrical	PV module power characterization including temperature dependence	Cell-To-Module calculation
U_{Loss}	Thermal	Dark measurement without illumination	Equivalent thermal resistance network
$U_{AbsFluid}$	Thermal	Dark measurement without illumination	Finite element model of a PVT absorber

The focus of the present PVT collector model is placed on the modelling of diverse collector concepts based on the input data of measurable design parameters. The model is mainly used to study the effect of these design parameters on the electrical and thermal efficiencies. In addition, the dynamic behavior and component temperatures are of special interest. For this purpose, the basic two-node collector model is extended to a dynamic multi-node model, which includes thermal capacities for transient conditions and a hydraulic solver.

The multi-physical collector model is implemented into Dymola/Modelica (Modelica 2012), which offers several advantages: the object-oriented modelling language allows easy adaptions and extensions to the model without major modifications to the overall structure. Thus, diverse collector concepts can be modelled in a single, consistent simulation framework. The Modelica fluid property database was found very useful for hydraulic and thermal calculations, especially with regard to temperature dependent material properties. Finally, it is possible to integrate the collector model into existing simulation models of buildings and solar thermal systems.

3.2.2 Optical energy transfer

The total share of solar irradiance which is absorbed by the solar cells under normal incidence is defined as the effective transmittance-absorptance product $(\tau\alpha)_{eff}$. It is obtained from transmittance of the cover τ_{cover}, absorptance of the PVT laminate $\alpha_{laminate}$, and taking into account multiple reflections between cover and PVT laminate. Transmittance and reflectance of the cover are measured in a spectrometer and weighted with the AM1.5 spectrum. The absorptance of the PVT laminate $\alpha_{laminate}$ is derived from the reflectance which is measured in the spectrometer under open circuit conditions. Thereby the active part covered with PV cells has a slightly lower absorptance compared to the inactive part where the underlying layers absorb the major share of irradiance.

Multiple reflections additionally have to be taken into account. The exact geometric sequence for the calculation of $(\tau\alpha)_{eff}$ according to Duffie and Beckman (2013) is given by:

$$(\tau\alpha)_{eff} = \tau_{cover}\alpha_{laminate} \sum_{n=0}^{\infty} [\rho_{cover}(1-\alpha_{laminate})]^n = \frac{\tau_{cover}\alpha_{laminate}}{1-\rho_{cover}(1-\alpha_{laminate})} \quad (3.1)$$

In case that the reflectance of the cover ρ_{cover} is unknown, Duffie and Beckman (2013) suggest a multi-reflection factor of 1.01. According to Dupeyrat et al. (2011a) this factor overestimates multiple reflections for state-of-the-art glazing types and absorbers and they propose the following empirical correlation instead:

$$(\tau\alpha)_{eff} = 0.9542 \cdot \tau\alpha + 0.0427 \quad (3.2)$$

A small share of solar irradiance, typically between α_{cover} = 2 - 4 %, is absorbed in the cover glazing. The major share of this heat dissipates to the environment and cannot be used because of a low heat transfer coefficient between absorber and cover.

The angular dependence of $(\tau\alpha)_{eff}$ is modeled with the b_0 approach for direct irradiance. For non-concentrating flat-plate PVT collectors, the beam incidence angle modifier K_b is symmetrical and can be expressed as:

$$K_b(\theta) = 1 - b_0 \left(\frac{1}{\cos\theta} - 1\right) \quad (3.3)$$

with the collector specific constant b_0 and the incidence angle θ.

Assuming isotropic diffuse sky conditions, the total specific power which is absorbed by the collector is given by:

$$p_{absorber} = (\tau\alpha)_{eff} \cdot (K_b(\theta)G_b + K_d G_d) \quad (3.4)$$

with the direct (beam) irradiance G_b, the incidence angle modifier for diffuse irradiance K_d, and the diffuse irradiance G_d.

For an analysis independent of the total collector area, $p_{absorber}$ is expressed as an area-specific power density, which can be related to either the gross area, aperture area, or absorber area. Yet, it is crucial to explicitly state, to which area the power density is related.

3.2.3 Electricity generation

The PV cells convert the incident solar irradiance G into electrical energy p_{PV} with the instantaneous electrical efficiency η_{el}:

$$p_{PV} = G \cdot \eta_{el} \tag{3.5}$$

The instantaneous electrical efficiency η_{el} is modelled as a function of the cell temperatures. Either diode models or analytical expressions can describe η_{el}. Since PVT collectors are typically operated in the maximum power point (MPP), the explicit current-voltage characteristic is of subordinate interest.

In a series connection of PV cells, as typically found in PV modules, the cell voltages add together while the PV cell with the lowest current determines the overall resulting current. The open circuit voltage U_{OC} is reduced significantly by increased temperatures ($\beta(U_{OC})$ = -0.30 to -0.43 %/K) whereas the short circuit current even increases slightly ($\alpha(I_{SC})$ = +0.02 to +0.09 %/K) (King et al. 1997). A non-uniform temperature distribution of PV cells in a series connection therefore has a negligible influence on the overall electrical module performance, in contrast to the influence of a non-uniform irradiance, e.g. by partially shaded cells. Hence, the mean cell temperature can be used with sufficient accuracy for modeling the temperature dependence of the electrical power on a module level. Experimental observations underline these theoretical considerations. According to Dittmann et al. (2014), a non-uniform temperature distribution "does not affect the electrical performance of the PVT collector".

The general assumption of considering PV operation always and only in its electrical point of maximum, leads to the conclusion that diode models do not offer significant advantages. On the contrary, diode models are more sensitive in their parametrization. Consequently, analytical expressions are used to model the instantaneous efficiency $\eta_{el.}$ The linear temperature dependence is given by the following correlation (Skoplaki and Palyvos 2009):

$$\eta_{el} = \eta_{el,STC}\left(1 - \gamma(T_{abs} - 25\,°C)\right) \tag{3.6}$$

with the rated module efficiency under standard test conditions $\eta_{el,STC}$, the mean absorber temperature T_{abs} and the power temperature coefficient γ.

The electrical efficiency of the PVT collector under standard test conditions $\eta_{el,STC}$ differs from the rated efficiency of the employed PV module owing to the presence of a front cover and potentially inactive aperture area. The optical losses of the front cover can be considered by multiplication with the spectral-response-weighted transmittance of the cover $\tau_{c\text{-}Si}$ and considering multiple reflections. The adaptions due to inactive aperture area are of mere geometrical nature and take into account the different reference areas.

If a custom PV laminate is employed inside the PVT collector, the cell-to-module efficiency can also be calculated according to the methodology described by Haedrich et al. (2014). This approach takes into

account losses due to inactive module area (module border and cell spacing), optical losses in the module glass (losses due to reflection and absorption in the module glass, absorption in the encapsulant, gains due to optical coupling, and backsheet scattering) and connection losses (string and cell interconnection).

3.2.4 Heat losses

Thermal heat transfer mechanisms of PVT collectors do not differ from conventional solar collectors except for the presence of an additional energy sink, namely the PV cells absorbing irradiance and generating electricity. Consequently, the methodology of modelling the overall heat loss coefficient U_{Loss} by the use of thermal networks (Duffie and Beckman 2013) can also be applied for PVT collectors. Overall heat losses are subdivided into losses through the cover to the front U_{Front}, losses through the insulation to the back U_{Back}, and losses through the frame to the edges U_{Edge} (Figure 3.3). The governing area for losses to the front and back is the aperture area; regarding edge losses the lateral frame surface is used.

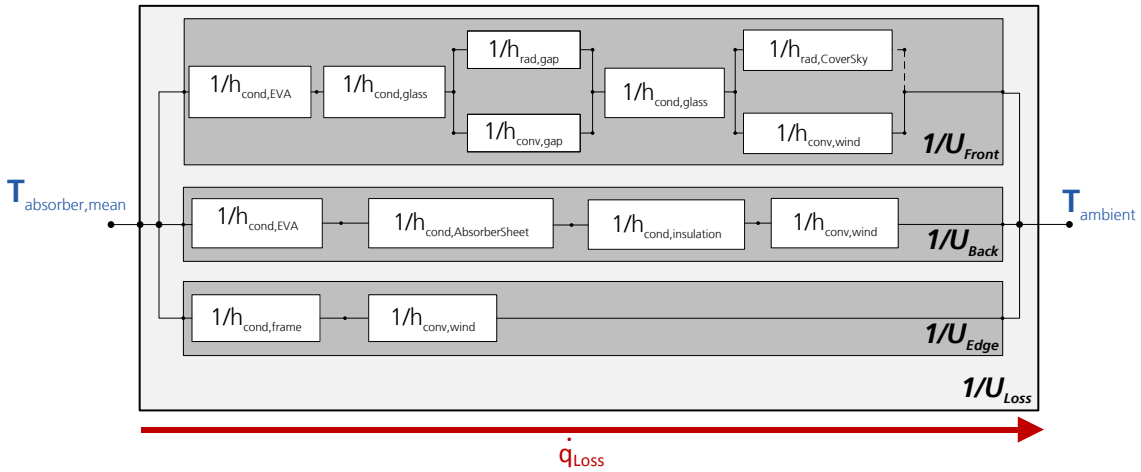

Figure 3.3: Thermal resistance network of the overall collector heat loss coefficient $1/U_{Loss}$ of a glazed PVT collector. The dashed line between $h_{rad,CoverSky}$ and $T_{ambient}$ indicates the differentiation between sky and ambient temperature.

Heat transfer coefficients are calculated based on analytical and physical correlations for the heat loss mechanisms occurring inside the collector, namely conduction, convection, and radiation.

The heat transfer coefficient for conduction in solid materials h_{cond} is given by:

$$h_{cond} = \frac{\lambda(T)}{d} \tag{3.7}$$

with the thermal conductivity λ and the material's thickness d. The thermal conductivity may depend on the material temperature (Ochs et al. 2008) which is why thermal properties as function of temperature are used.

The convective heat transfer coefficient inside the air layer resulting from natural convection of air is given by:

$$h_{conv,gap} = Nu \frac{\lambda_{air}(T)}{d_{gap}} \tag{3.8}$$

with the thermal conductivity of air λ_{air}, the distance between the PVT laminate and the front cover d_{gap}, and the Nusselt number Nu according to Hollands et al. (1976):

$$Nu = 1 + 1.44 \left[1 - \frac{1708}{Ra \cos\phi}\right]^{*} \left(1 - \frac{(sin\, 1.8\phi)^{1.6}\, 1708}{Ra \cos\phi}\right) + \left[\left(\frac{Ra \cos\phi}{5830}\right)^{\frac{1}{3}} - 8\right]^{*} \tag{3.9}$$

The terms [ ]* are only evaluated for positive values. This correlation is valid for inclination angles of $\phi = 0$ - 60° and Rayleigh numbers Ra = 0 - 10^5. Both Ra and λ_{air} are calculated with the temperature-dependent thermodynamic air properties of the Modelica fluid data base.

Regarding wind convection in the collector plane, Matuska and Zmrhal (2009) compare several correlations and observe a variation of the convective heat transfer coefficient $h_{conv,wind}$ in a wide range. Yet, $h_{conv,wind}$ is a sensitive parameter with a strong influence on the overall heat losses. Comparing several correlations in the numerical model, the following empirical correlations by McAdams (1954) give the best agreement between experiment and simulations:

$$h_{conv,wind} = 5.7 + 3.8\, u_{wind} \qquad \text{for } u_{wind} = 0 - 5 \text{ m/s} \tag{3.10}$$

$$h_{conv,wind} = 6.47\, u_{wind}^{0.78} \qquad \text{for } u_{wind} > 5 \text{ m/s} \tag{3.11}$$

In the solar simulator, artificial wind is only applied to the front surface. Hence, wind velocities are set to zero at the back and edge surfaces of the collector for emulating the efficiency curve test procedure.

In glazed PVT collectors, the surfaces standing in radiative exchange are the PVT laminate with the front cover, and the front cover with the sky. Radiative heat exchange between two surfaces is modelled with the temperature-dependent emissivity ε (T) and assuming view factors of unity. Based on these assumptions the radiative heat transfer coefficient h_{rad} can be expressed as (Duffie and Beckman 2013):

$$h_{rad} = \sigma \frac{(T_1^2 + T_2^2)(T_1 + T_2)}{\frac{1}{\varepsilon_1(T_1)} + \frac{1}{\varepsilon_2(T_2)} - 1} \tag{3.12}$$

with the Stefan-Boltzmann constant σ.

The temperature dependence of the surface's emissivity is important for accurately modelling heat losses of PVT collectors, especially with low-e coatings. The emissivity as function of surface temperature T is given by (Duffie and Beckman 2013):

$$\varepsilon(T) = \frac{\int_0^\infty \alpha_\lambda \cdot E_\lambda(T) d\lambda}{\int_0^\infty E_\lambda(T) d\lambda} \tag{3.13}$$

with the monochromatic absorptance α_λ from spectral measurements, and the emissive power of a black body E_λ, i.e. the Planck spectrum for a given surface temperature.

Concerning radiative heat transfer from the front cover to the sky, the sky is treated as a black body with $\varepsilon = 1$ and an equivalent sky temperature T_{sky} is introduced (Swinbank 1963):

$$T_{sky} = 0.0552\, T_a^{1.5} \tag{3.14}$$

The overall heat loss coefficient U_{Loss} results from the iterative solution of the thermal network in Figure 3.3. Therein, the heat transfer coefficients are a function of temperature and consequently U_{Loss} is also temperature dependent. Figure 3.4 shows U_{Loss} of a glazed, non-selective PVT collector and the contribution of the convective and radiative front losses, as well as back and edge losses. For $T_{abs} = T_a$ a small heat loss rate of $\dot{q}_{Loss} = 15.5$ W/m² occurs due to radiative losses to the cold sky. U_{Loss} reaches infinity at this point owing to the singularity of the definition of the U-value:

$$U_{Loss} = \frac{\dot{q}_{Loss}}{T_{abs} - T_a} \tag{3.15}$$

Beyond its minimum at $\Delta T = 22$ K, U_{Loss} grows because of the non-linearity of radiative heat transfer and temperature dependent thermodynamic material properties.

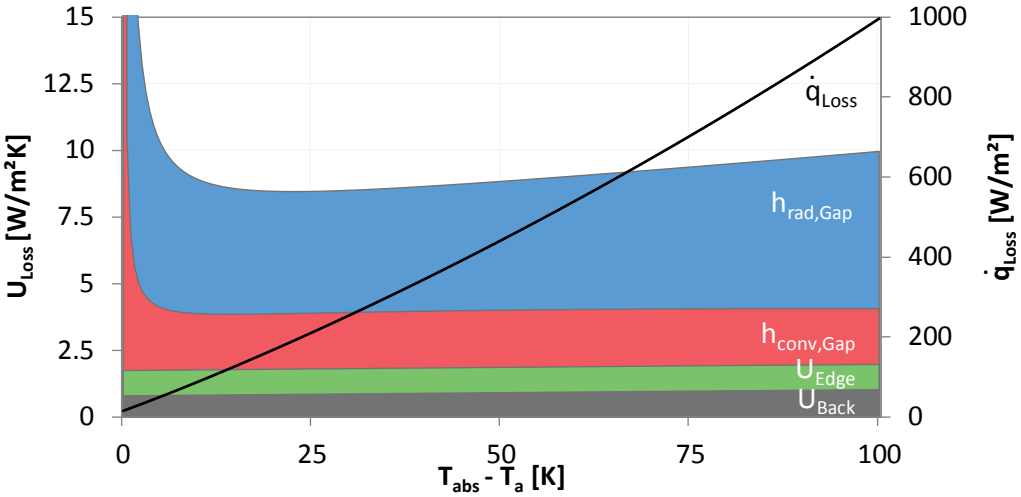

Figure 3.4: Temperature dependence of the overall collector heat loss coefficient U_{Loss} for a glazed PVT collector without low-e coating ("PVT-02") and key design and test parameters $d_{gap} = 25$ mm, $d_{insul,back} = 50$ mm, $\varepsilon_1 = 0.92$, $\varepsilon_2 = 0.92$, $T_a = 25$ °C, $G = 1000$ W/m², $u_{wind} = 3$ m/s.

3.2.5 Thermal coupling of absorber and fluid by $U_{AbsFluid}$

The internal heat transfer coefficient $U_{AbsFluid}$ defines the thermal conductance between the absorber, i.e. the PV cell, and the fluid node. An accurate model of $U_{AbsFluid}$ is essential for a correct solution of the equivalent thermal network.

In the theory of solar thermal collectors, F' is a popular term which is synonymously used for the quality of a specific absorber design. The usage of F' originates from the experimental measurement of the conversion factor $\eta_{th,0}$ at normal incidence and at $\Delta T/G = 0$ Km²/W. At this operating point, the mean fluid temperature equals the ambient temperature, but the absorber temperature is significantly higher and

consequently heat losses from the absorber to ambient occur. In order to compensate for these losses the effective transmittance-absorptance product $(\tau\alpha)_{eff}$ is multiplied with the collector efficiency factor F′:

$$\eta_{th,0} = F'(\tau\alpha)_{eff} \tag{3.16}$$

Accordingly, Duffie and Beckman (2013) describe F′ as the "ratio of the actual useful energy gain to the useful gain that would result if the collector absorbing surface had been at the local fluid temperature". In terms of heat transfer coefficients, F′ is expressed as the ratio of the heat transfer coefficient U_0, which is defined between the fluid and ambient temperature node, to the collector heat loss coefficient U_{Loss}:

$$F' = \frac{U_0}{U_{Loss}} \tag{3.17}$$

Next to this rather unintuitive definition, Duffie and Beckman provide formulae for the explicit calculation of F′ for sheet-and-tube absorbers. In addition, there are also numerical approaches for the explicit calculation of F′ for non-typical geometries (Koch et al. (2012) and Góngora-Gallardo et al. (2013)).

However, this notion of F′ is insufficient for modelling PVT collectors. The absorber temperature is a crucial parameter as both PV efficiency and heat losses depend on it, which necessitates an explicit calculation thereof. Florschuetz (1979) introduced the internal heat transfer coefficient $U_{AbsFluid}$ to couple the absorber and fluid nodes. Accordingly, the temperature difference between these two nodes is proportional to $U_{AbsFluid}$ and the useful thermal gain $\dot{q}_{useful}$:

$$\dot{q}_{useful} = U_{AbsFluid}(T_{abs} - T_m) \tag{3.18}$$

$U_{AbsFluid}$ and F′ are interrelated and can be converted into one another for a given U_{Loss}. Assuming the validity of the two-node collector model as in Figure 3.2, the following definition of F′ is derived from the definition of Duffie and Beckman in Eq. (3.17) by substituting $1/U_0$ with a serial resistance of $1/U_{Loss}$ and $1/U_{AbsFluid}$:

$$F' = \frac{\left(\frac{1}{U_{Loss}} + \frac{1}{U_{AbsFluid}}\right)^{-1}}{U_{Loss}} = \frac{1}{1 + \frac{U_{Loss}}{U_{AbsFluid}}} \tag{3.19}$$

$U_{AbsFluid}$, on the other hand, can be converted from F′ by rearranging Eq. (3.19):

$$U_{AbsFluid} = U_{Loss}\frac{F'}{1 - F'} \tag{3.20}$$

Since F′ depends on the overall heat losses U_{Loss}, a change of the thermal insulation, e.g. by the application of low-e coatings, strongly affects F′. Thus, F′ always has to be regarded in the context of the whole collector and its insulation, while $U_{AbsFluid}$ is a characteristic measure for a specific absorber. Moreover, F′ is a function of absorber temperature due to the temperature dependence of U_{Loss}. On contrary, $U_{AbsFluid}$ is less sensitive to variations of both U_{Loss} and temperature. For the mentioned reasons, $U_{AbsFluid}$ is a more suitable and practicable parameter to model the thermal coupling of absorber and fluid.

The internal heat transfer coefficient $U_{AbsFluid}$ plays a central role in PVT collectors, since it affects both electrical and thermal performances. A higher $U_{AbsFluid}$ increases the collector efficiency factor F′ and reduces cell temperatures at the same time. $U_{AbsFluid}$ is primarily influenced by design parameters such as tube spacing, tube diameter, thickness and thermal conductivity of the individual layers in the PVT ab-

sorber, bond conductance, and flow conditions of the heat transfer fluid. In the following section, both numerical and experimental approaches for the determination of $U_{AbsFluid}$ are presented and compared.

3.2.5.1 Numerical approach

The equivalent thermal network of $U_{AbsFluid}$ comprises two heat transfer coefficients connected in series: conduction from the absorber to the inner pipe wall $U_{AbsorberPipe}$ and convection from the pipe wall to the fluid $U_{PipeFluid}$ (Figure 3.5). Hereby, the heat transfer coefficient $U_{AbsorberPipe}$ contains all thermal resistances between the absorber and the pipe wall, including the fin conductance of the PVT laminate and the bond conductance between sheet and tube. While $U_{AbsorberPipe}$ is calculated with finite element methods (FEM), $U_{PipeFluid}$ is obtained from empirical correlations for heat transfer by forced convection in circular pipes.

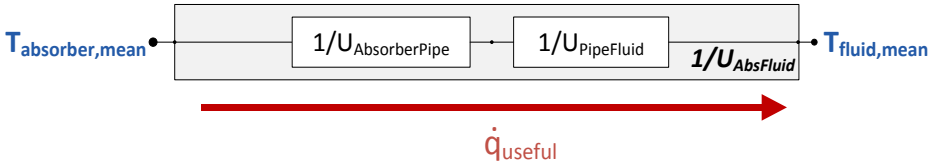

Figure 3.5: Equivalent thermal resistance network of the internal heat transfer coefficient $U_{AbsFluid}$.

Modelling $U_{AbsorberPipe}$ with the FEM approach

The PVT laminate consists of multiple layers with specific thermal conductivities and thicknesses. The fluid circulates in pipes of arbitrary geometry, which are thermally connected to the PVT laminate by gluing, clamping, welding, or other joining techniques. An analytical solution for the heat transfer problem is not trivial, which is why a FEM-based approach is used at this point. While it is possible to derive analytical solutions for a certain design, e.g. a sheet-and-tube PVT laminate with a certain order of layers, the FEM model is capable of adapting to complex geometries of both laminate and pipe design. Additionally, specific development questions can be analyzed with the FEM model, e.g. the effect of a specific absorption profile, contact resistances between two materials, or air cavities in glued compounds. Thus, the FEM approach is a universal tool for the analysis and optimization of PVT absorber designs.

The objective of the FEM approach is the determination of the conductive heat transfer coefficient $U_{AbsorberPipe}$ between the mean absorber temperature T_{abs} and the mean pipe temperature $T_{pipe,mean}$. It is convenient to exemplarily explain the approach at a typical PVT absorber. Figure 3.6 shows the cross section of a sheet-and-tube PVT absorber and the simulated absorber temperature distribution in this segment. As the absorption of solar irradiance is highest in the PV cells, the PV cells are defined as the absorber. The pipes are equally spaced in a distance of W and the fluid temperature in both parallel pipes is assumed to be equal, which corresponds to an ideal hydraulic harp configuration.

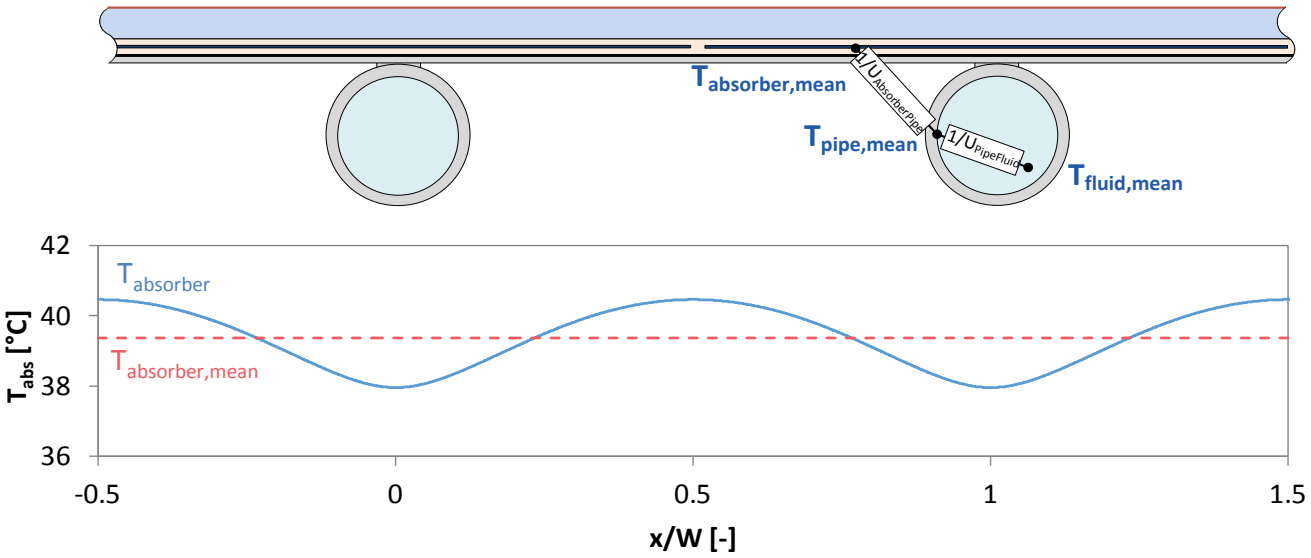

Figure 3.6: Schematic cross section of a PVT absorber with the equivalent thermal network of the internal heat transfer coefficient $U_{AbsFluid}$ (top) and the corresponding absorber temperature distribution obtained from FEM simulations (bottom).

The design and set-up of the FEM model utilizes available symmetry planes. Firstly, a two-dimensional segment is considered neglecting heat flow in the direction of fluid flow. Although the fluid temperature increases in flow direction, this temperature gradient is negligible in first order (compare Duffie and Beckman (2013)). Secondly, the lateral temperature gradient, i.e. the temperature gradient in x-direction between the pipes, equals zero at the point of minimum temperature at the centerline of the pipes at x/W = 0 and at the point of maximum temperature, which is located in the middle between two pipes at x/W = 0.5. Temperature gradients of zero imply a heat flow of zero. It is therefore convenient to model only half of an absorber segment and apply adiabatic boundary conditions at the lateral planes.

The remaining boundary conditions represent normal operating conditions for PVT collectors. Hence, heat sources are defined in the solar cell, low-e coating, PV glass, and EVA corresponding to their specific share of absorbed irradiance. Geometrical and thermodynamic properties for all employed materials are defined. Heat losses are applied to the laminate surface corresponding to U_{Loss} as modelled in chapter 3.2.4. The convective heat transfer coefficient $h_{PipeFluid}$ is applied to the inner pipe wall as described in the latter part of this section. Adiabatic boundary conditions are applied to the bottom of the PVT laminate as well as to the outer pipe surface assuming that all heat losses are dissipated from the PVT laminate surface. The resulting temperature distribution for the PVT segment is shown in Figure 3.7.

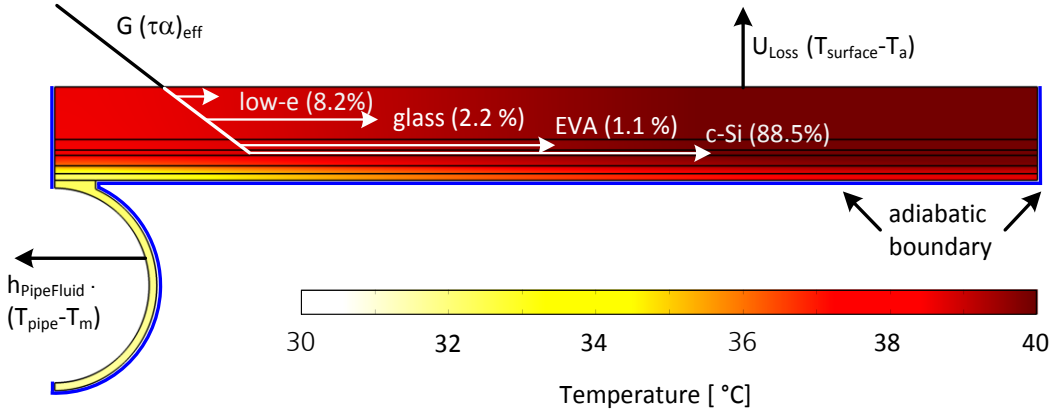

Figure 3.7: Boundary conditions and temperature distribution of a 2D FEM laminate segment for the determination of the heat transfer coefficient $U_{AbsorberPipe}$ under operating conditions $T_m = T_a = 25$ °C and G = 1000 W/m².

Based on the FEM results, $U_{AbsorberPipe}$ can be obtained by:

$$U_{AbsorberPipe} = \frac{\dot{q}_{useful}}{T_{abs,mean} - T_{pipe,mean}} \tag{3.21}$$

with the surface-averaged temperature in the PV cells $T_{abs,mean}$, the surface-averaged temperature at the inner pipe wall $T_{pipe,mean}$ and the resulting net heat flow from absorber to fluid $\dot{q}_{useful}$.

In this example, the resulting $T_{abs,mean}$ = 39.4 °C, $T_{pipe,mean}$ = 31.9 °C, and $\dot{q}_{useful}$ = 624.8 W/m² yield an overall heat transfer coefficient of $U_{Absorber,Pipe}$ = 83.7 W/m²K.

$U_{AbsorberPipe}$ is a conductive heat transfer coefficient and as such mainly influenced by the PVT absorber geometry (layer thickness, tube spacing and diameter) and material properties (thermal conductivity). Analyzing the sensitivity regarding variations of the operating conditions in realistic ranges shows an insignificant influence on $U_{AbsorberPipe}$. Varying the heat loss coefficient U_{Loss} between 3 W/m²K and 20 W/m²K leads to a variation of $U_{AbsorberPipe}$ of only 0.3 % and varying the irradiance G between 100 W/m² and 1500 W/m² leads to a variation of 0.54 %. The influence of T_m, T_a, and $h_{PipeFluid}$ is also insignificant. Due to the quasi-independence from operating conditions, it is sufficient to calculate $U_{AbsorberPipe}$ for each absorber design once for the reference conditions. Thus, a complex coupling of FEM and collector model and recalculation of $U_{AbsorberPipe}$ for every time step can be avoided. $U_{AbsorberPipe}$ is implemented into the collector model by a single heat transfer coefficient. Optionally, additional nodes can be added in order to have a higher resolution of the spatial temperature distribution (compare chapter 3.2.6).

Modelling of $U_{PipeFluid}$ with empirical correlations

The heat transfer coefficient between the pipe and fluid node in the flow regime $U_{PipeFluid}$ is calculated during every time-step in Modelica. There, thermodynamic properties as a function of fluid type, temperature and pressure are calculated and Reynolds (Re) and Prandtl (Pr) number are derived. The Nusselt number Nu is calculated based on empirical correlations of heat transfer by forced convection in a pipe according to the methodology of VDI Heat Atlas (2010). Thereby, it is differentiated between laminar, turbulent, and transitive flow conditions depending on the Reynolds number Re. Appendix B.1 describes the calculation of the Nusselt number and ΔT_{LM} in more detail.

The resulting net heat flux $\dot{q}_{useful}$ is given by:

$$\dot{q}_{useful} = \frac{Nu\ \lambda\ \pi\ l_{pipe}\ \Delta T_{LM}}{A_{ap}} \tag{3.22}$$

with the Nusselt number Nu, the thermal conductivity of the fluid λ, the total pipe length l_{pipe}, the logarithmic mean temperature difference ΔT_{LM}, and the aperture area A_{ap}.

Cross-validation of the numerical approach

A cross-validation of the presented numerical approach with analytical and FEM-based approaches for the calculation of F' was carried out. For this purpose, a conventional, non-PVT sheet-and-tube absorber segment was modeled with the geometrical design, U_{Loss}, and $h_{PipeFluid}$ as described in Koch et al. (2012). For this absorber the analytical approach of Duffie and Beckman (2013) yields a collector efficiency factor of F' = 0.942. The FEM-based approach of Koch et al. yields a slightly lower F' of 0.9408. The presented approach yields a $U_{AbsFluid}$ of 55.69 W/m²K which corresponds to a F' of 0.9408. Accordingly, both FEM-based approaches yield the identical F'. This high level of agreement is astonishing given the methodological differences of both approaches. At the same time, it proves the validity and confirms the capability of the presented numerical approach.

3.2.5.2 Experimental approach

The numerical PVT collector model necessitates an explicit input value for the internal heat transfer coefficient $U_{AbsFluid}$. The previously described numerical approach requires detailed information on the geometrical and thermal properties of the PVT absorber and assumes ideal heat transfer. This information is not always known and ideality of heat transfer cannot be assumed in all cases, e.g. due to a non-uniform fluid flow, contact resistance at the interface of two bonded materials, or in glued compounds. An experimental approach is therefore required to assess non-ideality effects and to analyze specific absorber designs without simulations.

In his Master's thesis, Panzer (2016) developed an experimental set-up to determine $U_{AbsFluid}$ based on the explicit measurement of fluid and surface temperatures of a full-size absorber while a hot fluid circulates in the pipes (Figure 3.8). The experimental approach builds up on previous work by Rummler (2008) and Karrer and Pröll (2015) with certain methodological adaptations.

While Rummler (2008) applies heat sources on the surface of the absorber, the present approach takes place without illumination with the hot fluid being the only heat source. Hence, the direction of heat flow is reversed compared to the real, illuminated operation. In contrast to Karrer and Pröll (2015), who determine local, spatially resolved values of $U_{AbsFluid}$, the present approach aims at a mean, surface-averaged result. For this purpose, an IR camera, whose signal is calibrated by a PT100 contact sensor attached to the PVT absorber, measures the surface temperature. During post-processing, the surface temperature is averaged to calculate the mean surface temperature $T_{surface,mean}$ which is required for the evaluation.

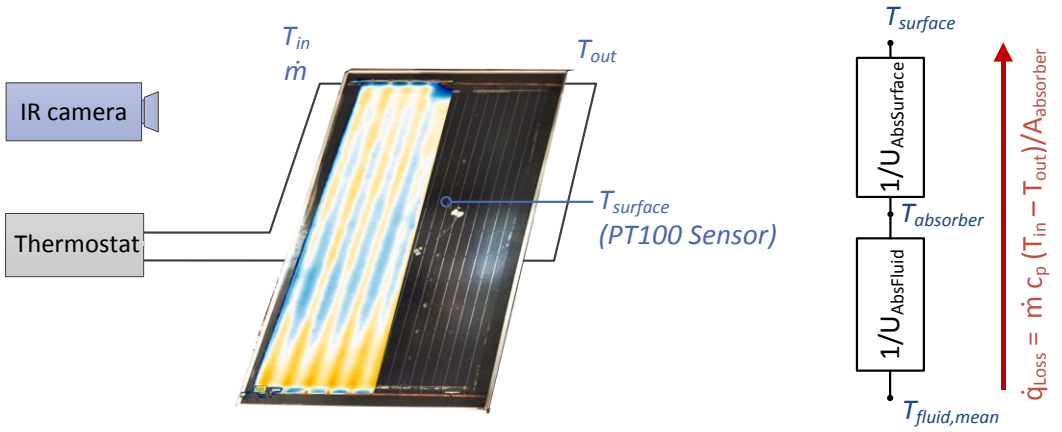

Figure 3.8: Experimental set-up for the determination of $U_{AbsFluid}$ (left) and equivalent thermal circuit (right).

The net heat flow through the absorber $\dot{q}_{Loss}$ is obtained from the energy balance of the fluid between inlet and outlet. The resulting heat transfer coefficient between surface and fluid is then given by:

$$U_{SurfaceFluid} = \frac{\dot{q}_{Loss}}{T_{fluid,mean} - T_{surface,mean}} = \frac{\dot{m}\, c_p (T_{in} - T_{out})}{A_{absorber}\left(\frac{T_{in} + T_{out}}{2} - T_{surface,mean}\right)} \tag{3.23}$$

Due to the presence of the glass pane and encapsulation material EVA, the mean cell temperatures are not directly accessible by measurement instrumentations. Therefore, $U_{SurfaceFluid}$ has to be corrected by subtracting the heat transfer coefficient $U_{AbsSurface}$ as follows:

$$U_{AbsFluid} = \left(\frac{1}{U_{SurfaceFluid}} - \frac{1}{U_{AbsSurface}}\right)^{-1} = \left(\frac{1}{U_{SurfaceFluid}} - \frac{d_{Glass}}{\lambda_{Glass}} - \frac{d_{EVA}}{\lambda_{EVA}}\right)^{-1} \tag{3.24}$$

Four sample PVT absorbers of different design and quality were examined with this approach:

- PVT absorber 1 is a glued sheet-and-tube absorber with a pipe spacing of 100 mm in double harp configuration ("PVT05-glued1"). A commercial glass-glass PV module is glued to an aluminum sheet, which is clamped to the copper tubes.
- PVT absorber 2 is an optimized version of PVT absorber 1 ("PVT06-glued2"). The difference comprises an additional aluminum sheet and higher clamping forces to increase the contact pressure between the omega-shaped sheet and tube.[3]
- PVT absorber 3 is a directly laminated sheet-and-tube PVT absorber with a pipe spacing of 75 mm in a meander configuration ("PVT01-low-e").
- PVT absorber 4 is a directly laminated rollbond PVT absorber with pipe spacing of 45 mm, in a multiply branched, fractal-like hydraulic configuration based on the FracTherm® algorithm. Instead of a protective module glass, this PVT absorber utilizes an FEP foil (Dupeyrat 2011a).

[3] PVT absorbers 1 - 2 were developed within the project PVTgen2. Further details on design and performance can be found in the corresponding project report (Lämmle et al. 2017a).

The experimental results are shown in Figure 3.9. As expected, the quality of the thermal bond and thus $U_{AbsFluid}$ differs significantly between PVT absorber 1 and 4 due to their construction and fabrication. Important factors for a high $U_{AbsFluid}$ are a small distance between absorber tubes, a high thermal conductivity of absorber layers and the absence of air cavities and contact resistance of clamped elements. These requirements stand in conflict to both economic and technical aspects. In PVT absorber 3 and 4, where the PV cells are directly laminated on the absorber sheet, the electrical isolation is a critical issue. Additionally, the different thermal expansion of the employed materials induces thermo-mechanic stress in the PVT absorber. The usage of a glass-glass-module in PVT absorber 1 and 2 eliminates these issues, yet at the cost of a lower $U_{AbsFluid}$.

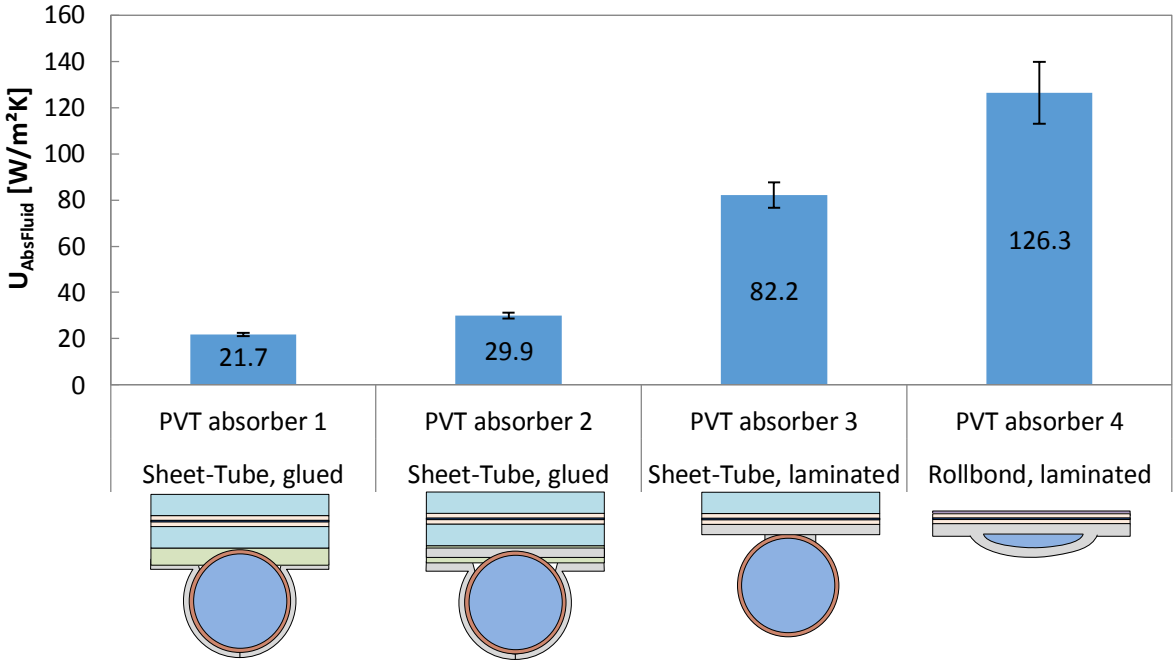

Figure 3.9: Experimental results of $U_{AbsFluid}$ of four sample PVT absorbers.

Figure 3.9 also depicts the statistical error indicator, which originates from the systematic uncertainty of the used measurement instrumentation for measuring the fluid inlet and outlet temperature, the mass flow, and the infrared thermographic surface temperature. For lower values of $U_{AbsFluid}$ the statistical error is low in absolute terms owing to the high temperature difference of surface and fluid temperature in the denominator in Eq. (3.23). Accordingly, the absolute statistical error for high values of $U_{AbsFluid}$ is higher.

A comparison of experimental and numerical results is carried out for PVT absorbers 3 and 4. Due to the unknown contact resistance of the clamped omega-tube-connection and the air cavities of the glued compound it is not possible to numerically model PVT absorbers 1 and 2 in an adequate way. The FEM model would overestimate $U_{AbsFluid}$ since it assumes perfect heat transfer at the material interfaces. Therefore the comparison is restricted to PVT absorbers 3 and 4, where an ideal heat transfer at the material interfaces can be assumed.

The numerical approach with the FEM model yields $U_{AbsFluid}$ = 82.8 W/m²K for PVT absorber 3 and $U_{AbsFluid}$ = 120.4 W/m²K for PVT absorber 4. Both values lie within range of the uncertainty of the experimental approach, where $U_{AbsFluid}$ = 82.2 W/m²K for PVT absorber 3 and $U_{AbsFluid}$ = 126.3 W/m²K for PVT absorber 4 were determined.

Despite the good agreement, it has to be mentioned that both the experimental and the numerical approach strongly depend on the fluid flow and thus heat transfer in the pipes. Numerically, the heat transfer coefficient $h_{PipeFluid}$ has a strong influence on the resulting $U_{AbsFluid}$. Experimentally, the mass flow rate and consequently the state of turbulence strongly affect the measured $U_{AbsFluid}$. The flow regime and its state of turbulence are not mainly attributable to the absorber design but to the actual operating conditions. $U_{AbsFluid}$ should therefore not be considered as a fixed value for a specific absorber design, but it also depends on the actual operating conditions.

To conclude, the described experimental approach is in general suitable to quantify the internal heat transfer coefficient $U_{AbsFluid}$ and to reproduce well the qualitative differences between different absorber designs. The rather basic test set-up with few measured variables and short duration of the experiment comes at the expense of methodological weaknesses. The experiments take place without illumination and therefore reversed direction of heat flow. Additionally, it is difficult to control the operating conditions for a high reproducibility. The correction of $U_{SurfaceFluid}$ by the thermal conductance of the glass pane and encapsulation material introduces further uncertainty to the experiments.

An alternative approach which is based on the parameter identification of $U_{AbsFluid}$ during quasi-dynamic outdoor measurements could potentially lead to better agreement. Instead of measuring temperatures, this approach correlates the electrical efficiency to the fluid temperature and useful heat flow and can thus identify $U_{AbsFluid}$ by multiple linear regression from a dynamic test sequence. This alternative approach could eliminate the methodological uncertainty of the presented experimental approach and is proposed for future research in this field.

3.2.6 Extended dynamic, multi-node PVT collector model

The previously described numerical PVT collector model is a steady-state two-node model which uses surface-averaged mean temperatures to describe the absorber and fluid nodes. According to Zondag et al. (2002a) this is a sufficient level of detail to model the thermal and electrical efficiency in stationary operation. However, specific research and development questions require a more detailed model that is capable of modeling the temporally and spatially resolved energy flows. In his Master's thesis, Böhm (2015) extended the previously described numerical model and included thermal capacities and multiple nodes. Typical applications of the extended model are, for example, the dynamic simulation of typical load scenarios, or the detailed investigation of stagnation and component temperatures.

3.2.6.1 Dynamic model extension

The required dynamic adaptions to the numerical model concern the introduction of lumped thermal capacities, the discretization of fluid volumes, and measures to ensure numerical stability.

All materials employed in the PVT collector have a thermal mass and thus contribute to the thermal inertia of the collector. Lumped thermal capacities absorb, store, and release heat and are mathematically expressed as (Modelica 2012):

$$c_p \rho V \frac{dT}{dt} = \dot{Q}_{in} \tag{3.25}$$

with the specific heat capacity c_p, the material density ρ, the material volume V, the material temperature T, and the incoming heat flow $\dot{Q}_{in}$. Thus, the heat flow $\dot{Q}_{in}$ and the thermal mass $c_p \rho V$ govern the temporal variation of the material temperature T.

The thermal masses are connected to the temperature node for every employed material with the corresponding volume and material properties. For every thermal capacity and at every time-step, Eq. (3.25) is iteratively solved until convergence, so that the material temperature T and the corresponding heat flow $\dot{Q}_{in}$ are in balance.

The usage of discretized fluid volumes compensates for the dead time resulting from the fluid flow. The change of fluid temperatures from inlet to outlet is delayed due to the physical behavior of the fluid, which is passing through the pipes while it is heated up (Norton 2014). Discretized fluid volume elements, which are coupled in series or parallel depending on the hydraulic layout, account for this effect.

In comparison to stationary simulations, dynamic simulations have stronger requirements regarding the numerical stability of the model. In a stable model, all functions, expressions, and material properties should be continuously differentiable. However, the wind speed dependence of $h_{conv,wind}$ in Eq. (3.10) and the laminar-turbulent transition of the convective heat transfer coefficient are only two examples for physical phenomena with points of discontinuity. With the operators smooth() and noEvent(), Modelica offers two practical functions which enhance the numerical stability and avoid convergence errors. Yet, it is still possible that simulations do not converge due to forbidden states or unrealistic events.

3.2.6.2 Multi-node model extension

In order increase the spatial resolution of the numerical model, the PVT absorber is subdivided into m x n segments, where m is the user-defined number of segments in the direction of flow and n is the number of pipes. The schematic division into 10 x 10 segments of a glazed, non-selective PVT absorber with a meander of 10 pipes in series is depicted in Figure 3.10. Additional nodes are introduced into each segment, and lateral and transversal heat conduction is considered between each absorber segment. Thus, each segment consists of three nodes for the minimum, maximum and mean temperature which are connected by thermal resistances derived from the FEM model in chapter 3.2.5.1.

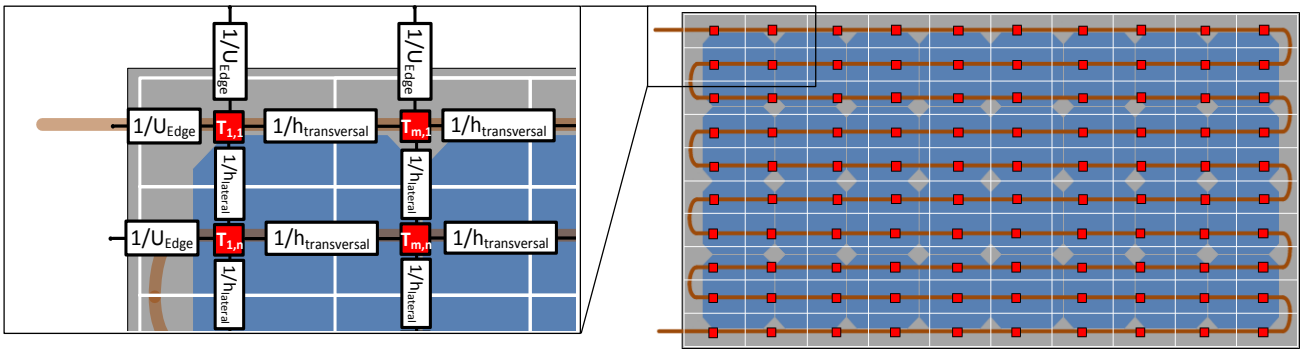

Figure 3.10: Segmentation of the PVT absorber into m x n nodes (courtesy of Böhm (2015)).

Edge losses are only incurred at the segments of the PVT absorber situated at the border of the collector frame. Radiative heat losses in the air gap between PVT absorber and cover glazing depend on the absorber temperature by the fourth power. In the 3D-model, radiative heat losses are calculated individually for each absorber segment. Thus, a more realistic model for the thermal losses is achieved, compared to

the two-node collector model, where edge and radiation losses are a function of the mean absorber temperature.

In highly conducting materials, heat spreads alongside the component resulting in a relatively homogeneous temperature distribution. It is for this reason, that a single, shared temperature node is used to model the cover glass, frame, and backside of the whole collector. The influence on the simulated thermal efficiency curve of using a multi-node model instead of a single-node model is shown in Figure B.3.

Figure 3.11 shows the temperature distribution in the PV cells during operation and stagnation. During operation, the circulating fluid heats up from an inlet temperature of $T_{fl,in}$ = 25 °C to an outlet temperature of $T_{fl,out}$ = 30.6 °C at the given operating conditions. This affects the temperature in the PV cells, which gradually increases in direction of fluid flow. The hottest temperatures are observed in the center between two pipes, due to the distance and thermal resistance to the fluid.

During stagnation, there is no fluid flow and consequently no heat transfer to the fluid. In steady-state stagnation, the absorbed irradiance is equal to the heat losses resulting in high cell temperatures. According to the model, the center of the non-selective PVT absorber reaches the highest temperatures of $T_{abs,max}$ = 124.7 °C, owing to the heat losses through the edges, which slightly cool the peripheral absorber parts. By comparison, the mean absorber temperature amounts to T_{abs} = 118.8 °C.

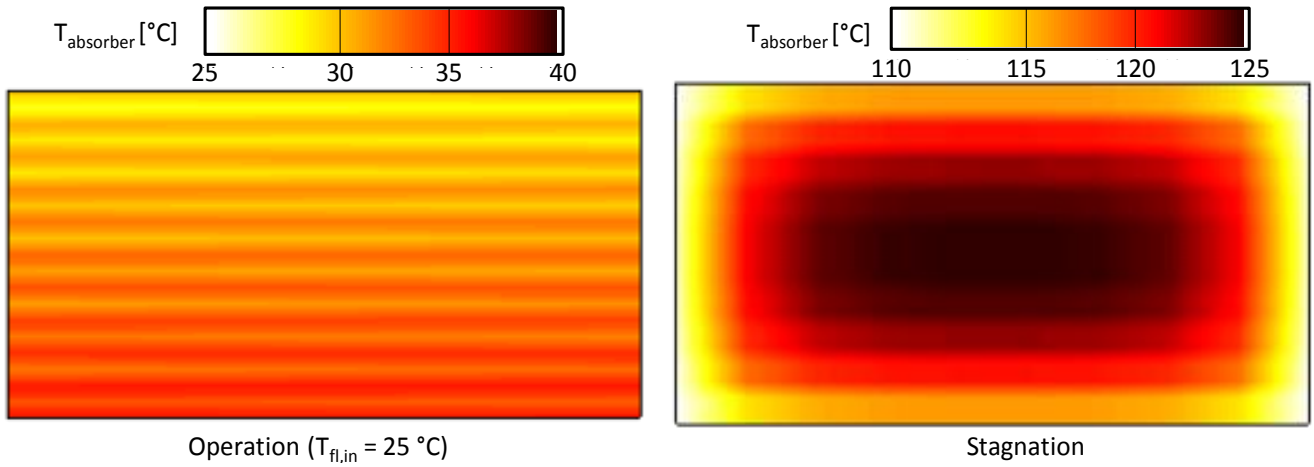

Figure 3.11: Simulated temperature distribution in PV cells during operation (left) and stagnation (right).

In real stagnation experiments on inclined collectors the highest temperatures are typically observed at an absorber height of 2/3. Due to buoyancy-driven convection in the air gap, hot air rises inside the collector resulting in typical air circulation patterns (Stieglitz 2012), which shift the maximum temperature upwards. This effect is not implemented in the model, which is why the maximum temperature is located in the center of the collector.

Next to the investigation of component and stagnation temperatures, the numerical model with multiple absorber nodes forms a basis for future investigations. The spatial resolution of the temperature distribution is a requirement for the implementation of a more elaborate PV performance model, for example PV diode models as in Haurant et al. (2015). However, the multi-node model has a significantly higher computational effort and is more complex regarding the configuration of the model. Especially the combination of dynamic and multi-node model can lead to long computation times of 24 h per simulation day. The application of the multi-node model is therefore restricted to specific research questions while typical efficiency simulations are preferably carried out in the two-dimensional model.

3.2.7 Validation of the numerical PVT collector model

The numerical PVT collector is validated by means of comparing the experimental steady-state test points with the simulated efficiency curve. This can be considered an integral validation approach, where only the final results, i.e. the efficiency curves, are assessed. The multitude of used correlations and assumptions are not validated individually, but only their combined impact on the overall efficiency. The simulated efficiency curves are obtained from the numerical model by simulating multiple steady-state test points and a subsequent multiple linear regression to the thermal and electrical models in Eq. (2.2) and Eq. (3.30), respectively.

Three PVT collector prototypes of different design and construction were both simulated with the numerical model and tested in the solar irradiance simulator at Fraunhofer ISE. The sample PVT collectors comprise an unglazed PVT collector, a glazed PVT collector ("PVT02-no low-e"), and a glazed PVT collector with low-e coating ("PVT01-low-e"). Additionally, a conventional flat plate collector is included in the validation. Figure 3.12 shows the simulated numerical results of the thermal efficiency compared with experimental test results, where the full line represents the simulated efficiency curve, the error bars belong to the steady-state test points, and the dashed line represent the corresponding experimental efficiency curve.

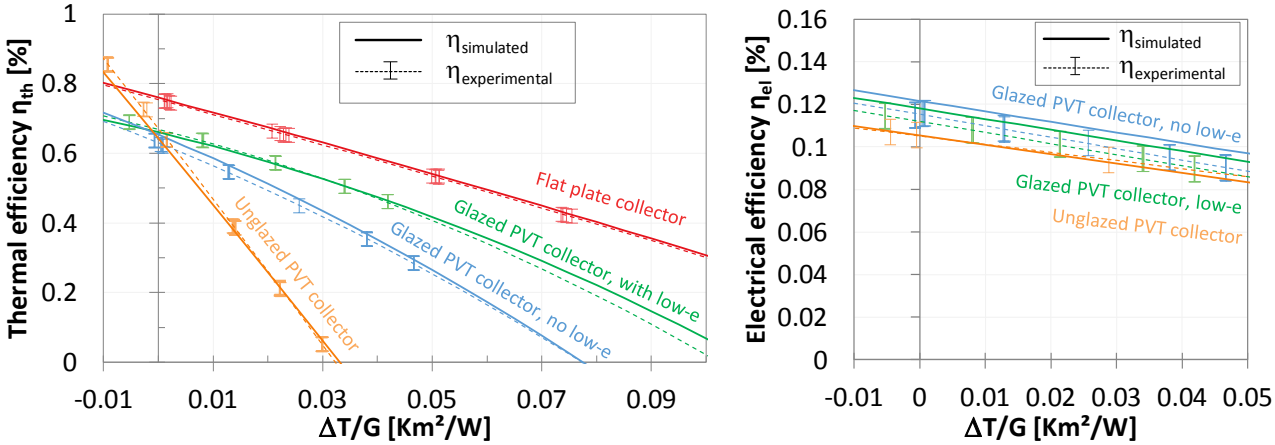

Figure 3.12: Comparison of the numerical model (lines) with experimental results (error bars and dashed lines). Efficiency based on aperture area and valid for G = 1000 W/m², u_{wind} = 3 m/s, T_a = 25 °C in MPP mode.

The uncertainty of the numerical model is assessed by two error measures. Firstly, the maximum deviation $\Delta\eta_{max}$ between experimental test points and the corresponding simulated efficiency is used as an indicator for the absolute error and is given by:

$$\Delta\eta_{max} = \mathrm{MAX}(\eta_{experiment,i} - \eta_{simulation,i}) \tag{3.26}$$

Secondly, the root mean square error RMSE is used as an indicator to summarize the overall deviation along the entire efficiency curve and is given by:

$$RMSE = \sqrt{\frac{1}{n}\sum_{i=1}^{n}(\eta_{experiment,i} - \eta_{simulation,i})^2} \tag{3.27}$$

with the number of experimental test points n.

Good agreement between the numerical model and the test data is observed in general. For all four collectors together, the overall root mean square error amounts to $RMSE_{th}$ = 1.4 $\%_{abs}$ of the thermal model and to $RMSE_{el}$ = 0.5 $\%_{abs}$ of electrical model (Table 3.2).

Table 3.2: Uncertainty assessment of the numerical model.

	Thermal efficiency		**Electrical efficiency**	
	$\Delta\eta_{th,max}$	$RMSE_{th}$	$\Delta\eta_{el,max}$	$RMSE_{el}$
Unglazed PVT	2.7%$_{abs}$	1.9%$_{abs}$	0.2%$_{abs}$	0.1%$_{abs}$
Glazed PVT	2.7%$_{abs}$	2.0%$_{abs}$	0.9%$_{abs}$	0.7%$_{abs}$
Glazed PVT low-e	1.0%$_{abs}$	0.6%$_{abs}$	0.7%$_{abs}$	0.7%$_{abs}$
Flat plate collector	1.0%$_{abs}$	0.7%$_{abs}$	-	-
Overall model error	2.7%$_{abs}$	1.4 %$_{abs}$	0.9%$_{abs}$	0.5%$_{abs}$

The thermal model shows very good agreement with experimental data for both the glazed PVT collector with low-e ($RMSE_{th}$ = 0.6 $\%_{abs}$) and the flat plate collector ($RMSE_{th}$ = 0.7 $\%_{abs}$). The unglazed PVT collector reaches a $RMSE_{th}$ of 1.9 $\%_{abs}$, which is a good result given the uncertainty involved with adjusting and measuring the wind speed during the experiment and the variations of convective heat losses $h_{conv,wind}$ found in the scientific literature. Yet, at wind speeds other than 3 m/s a higher model error is observed. For the glazed PVT collector without low-e, a relatively high uncertainty of 2 $\%_{abs}$ is observed, which might result from the production of the laminate, where the low-e coating was removed in a caustic bath after the lamination. This treatment could have led to a deterioration of the internal heat transfer coefficient $U_{AbsFluid}$ or a higher reflectance of the PVT absorber compared to the idealized assumptions in the model. For all four collectors, a systematic overestimation of the thermal efficiency at high temperatures can be observed. Most likely this is due to an underestimation of the thermal losses from idealized assumptions, e.g. neglecting thermal bridges at the edges.

The accuracy of the electrical model is good in absolute terms ($RMSE_{el}$ = 0.5 $\%_{abs}$), but comparably high in relative terms ($RMSE_{el}$ = 4.0 $\%_{rel}$). The numerical model strongly depends on accurate electrical input parameters, especially $\eta_{el,STC}$. This can be demonstrated at the examples of the glazed and unglazed PVT collectors. The electrical efficiency $\eta_{el,STC}$ of the unglazed PVT collector was measured in the flasher, resulting in a high accuracy of the electrical model ($RMSE_{el}$ = 0.1 $\%_{abs}$). For both glazed PVT collectors no flasher data was available, which is why $\eta_{el,STC}$ was calculated with the cell-to-module efficiency approach (compare chapter 3.5.1). This adds additional uncertainty to the electrical efficiency, which results in a high $RMSE_{el}$ of 0.7 $\%_{abs}$ for both glazed collectors.

Overall, the uncertainty of the numerical model lies within the range of experimental uncertainty. The confidence interval of thermal performance measurement amounts to ± 2 $\%_{abs}$ according to a round-robin test of different test laboratories (Weißmüller et al. 2012). The confidence interval of the electrical performance measurement in the solar simulator is estimated to be ± 5 $\%_{rel}$. This is mainly due to spectral differences of the artificial sun compared to the AM1.5 reference spectrum. For this reason, electrical performance measurements in the solar thermal simulators are always connected with high uncertainties and results should be viewed critically.

To conclude, the numerical model is a powerful tool for the simulation of PVT collectors of different design, which shows a good agreement between experiment and simulation. Further development should

focus on a better representation of the electrical efficiency, especially a more accurate model for the calculation of $\eta_{el,STC}$. The thermal model can be improved by heat flux measurements during tests in the solar simulator. Thus a better understanding of the composition of thermal losses could be gained, which might lead to a better model convergence at high temperatures.

3.3 Sensitivity analysis of $U_{AbsFluid}$ and U_{Loss} on gross energy yields

At an early stage in the process of developing a PVT collector, the question arises how the design of the PVT collector will ultimately affect its performance, which design parameters should be optimized and where research and development efforts should focus on. A technology-independent analysis can bring light into these questions by analyzing the influence of the four design parameters $(\tau\alpha)_{eff}$, $\eta_{el,STC}$, $U_{AbsFluid}$, and U_{Loss} on the electrical and thermal gross energy yields.

The parameters $(\tau\alpha)_{eff}$ and $\eta_{el,STC}$ scale almost linearly on the gross energy yields: an increase of 1 $\%_{rel}$ of either $\eta_{el,STC}$ or $(\tau\alpha)_{eff}$, results in an increase 1 $\%_{rel}$ of electrical or thermal yield, respectively. Assessing the influence of U_{Loss} and $U_{AbsFluid}$ is more complex because of their non-linear effect on the electrical and thermal performances. To study the influence on gross energy yields, a sensitivity analysis is therefore carried out for these parameters by coupling the numerical collector model with ScenoCalc.

A parameter sweep of the design parameters $U_{AbsorberPipe}$, ε_{373K}, d_{gap}, and $d_{insulation}$ within physically relevant limits achieves a variation of $U_{AbsFluid}$ and U_{Loss} in the numerical model. The obtained efficiency curves are then evaluated with ScenoCalc at the German location of Würzburg and the MAP weighting function according to Eq. (2.5) and Eq. (2.6) is applied. Hereby, it is assumed that the variation of U_{Loss} and $U_{AbsFluid}$ does not affect the optical performance. Accordingly, $\eta_{el,STC}$ = 12.8 % and $(\tau\alpha)_{eff}$ = 0.87 are kept at constant levels. Of course, this assumption does not hold true in reality: most measures for the reduction of thermal losses, e.g. by an external cover, low-e coating, or concentration, also reduce the optical performance.

For any combination of U_{Loss} and $U_{AbsFluid}$, the electrical and thermal performance ratios can be read from Figure 3.13. In total, 1600 individual collector and ScenoCalc simulations form the basis for the contour plot. Performance ratios instead of the specific yields are used for this assessment, as the performance ratio describes the normalized gross energy yields independently from $\eta_{el,STC}$, $(\tau\alpha)_{eff}$ and the annual rate of irradiance in the collector plane I_{tot}. Thereby, the electrical performance ratio PR_{el} is defined as the collector yield $E_{PV,MAP}$ divided by theoretical maximum yield $I_{tot}\cdot\eta_{el,STC}$:

$$PR_{el} = \frac{E_{PV,MAP}}{I_{tot} \cdot \eta_{el,STC}} \tag{3.28}$$

Correspondingly, the thermal performance ratio is defined as:

$$PR_{th} = \frac{Q_{coll,MAP}}{I_{tot} \cdot ((\tau\alpha)_{eff} - \eta_{el,STC})} \tag{3.29}$$

The specific electrical and thermal yields for a given location are obtained by multiplying the performance ratio PR with the corresponding denominator.

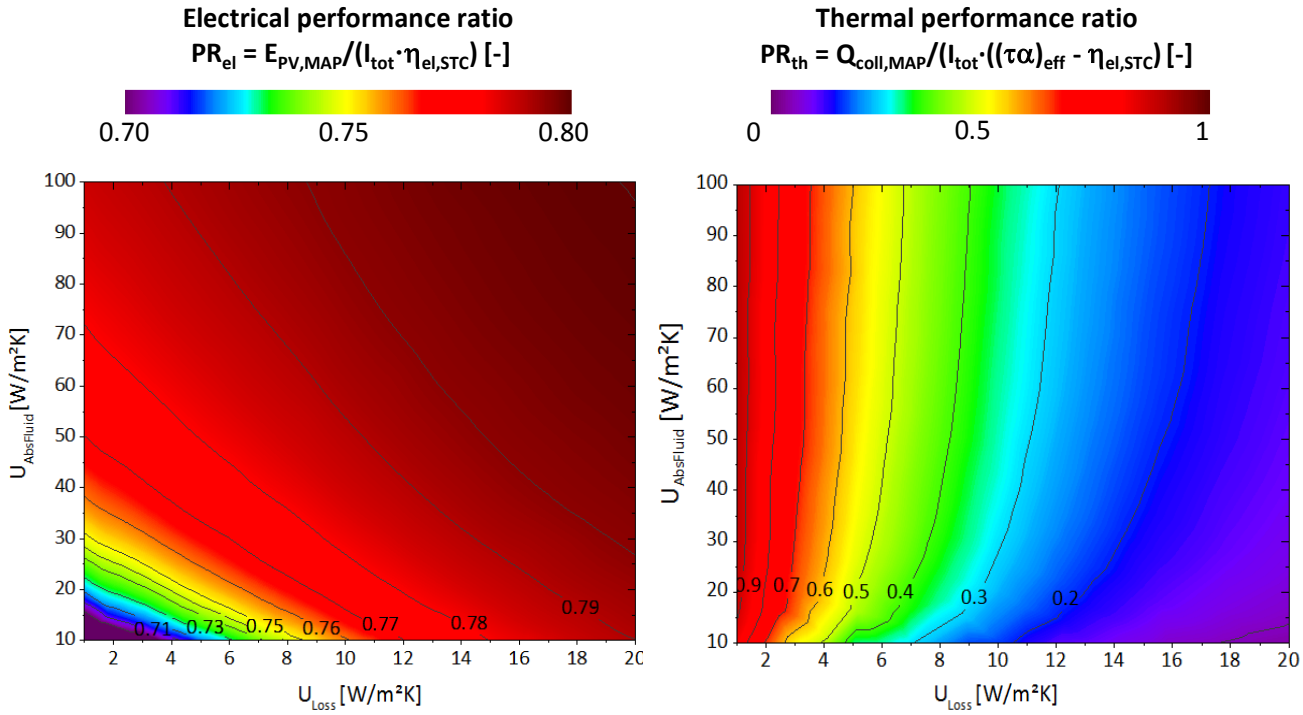

Figure 3.13: Electrical (left) and thermal (right) performance ratio of a PVT collector with varying U_{Loss} and $U_{AbsFluid}$ with applied MAP weighting function evaluated for the location of Würzburg.

For a better interpretation of the results, typical values of U_{Loss} and $U_{AbsFluid}$ are indicated in the following. U_{Loss} ranges between U_{Loss} = 10 - 20 W/m²K in unglazed collectors, U_{Loss} = 7 - 10 W/m²K in glazed collectors, and U_{Loss} = 4 - 7 W/m²K in glazed collectors with low-e. A further reduction of U_{Loss} can be achieved, for example, by noble gas fillings or vacuum insulation. $U_{AbsFluid}$ describes the quality of thermal coupling between absorber and fluid and takes values of $U_{AbsFluid}$ = 10 - 40 W/m²K for a poor coupling and values higher than $U_{AbsFluid}$ > 60 W/m²K for a good coupling.

The electrical yield benefits from high values of $U_{AbsFluid}$ and U_{Loss} through low cell temperatures. According to Eq. (3.18), a high internal heat transfer coefficient $U_{AbsFluid}$ leads to a small difference between cell and fluid temperatures. Additionally, high heat losses lead to a lower heat flux $\dot{q}_{useful}$ resulting in a small difference between fluid and cell temperatures. Consequently, high values of U_{Loss} and $U_{AbsFluid}$ achieve an efficient electrical performance.

The thermal yield benefits mainly from a low value of U_{Loss} through reduced heat losses and hence a higher thermal efficiency. Low values of U_{Loss} are especially important for challenging operating conditions with low levels of irradiance and low ambient temperatures to deliver heat at the required temperature level. The internal heat transfer coefficient $U_{AbsFluid}$ plays a secondary role regarding thermal yields, and a high value of $U_{AbsFluid}$ cannot compensate high heat losses. Nonetheless, $U_{AbsFluid}$ becomes more important for collectors with a high U_{Loss}, to reach a reasonable collector efficiency factor F'.

These results underline the importance of a good thermal coupling between PV cells and the fluid since both the electrical and the thermal yields benefit from a high $U_{AbsFluid}$. As a rule of thumb, $U_{AbsFluid}$ should exceed 50 W/m²K to achieve low cell temperatures and a high F'. As can be seen at PR_{th}, a further improvement of the thermal coupling to values above $U_{AbsFluid}$ > 50 W/m²K does not effectuate a significant increase of neither the electrical and the thermal performance ratio.

In order to reach the maximum combined electrical and thermal energy yields, low thermal heat losses are essential. Although electrical yields drop slightly through a low value of U_{Loss}, the gain of thermal yields overcompensates this effect. Hence, highest primary energy yields are achieved by a low value of U_{Loss} combined with a high value of $U_{AbsFluid}$. A maximization of the overall performance of PVT collectors therefore requires a reduction of thermal losses, without significantly reducing $\eta_{el,STC}$ and $(\tau\alpha)_{eff.}$ Low-e coatings are such an approach which will be discussed in the following sections.

For technical and economic reasons, it is unlikely that a real PVT collector will reach optimum properties for U_{Loss} and $U_{AbsFluid}$. In most cases, a trade-off between thermal insulation, the quality of thermal coupling, and optical properties is necessary. Figure 3.13 may assist in balancing between U_{Loss} and $U_{AbsFluid}$ and provide a quantitative understanding of the relationship between thermal collector properties and the gross energy yield. It has to be considered, however, that only the weighted yields for T_m = 25 °C and 50 °C are included in this analysis. Secondly, energy yields in real systems will differ from the reported gross energy yields. Thirdly, changes of the optical properties, which influence both $(\tau\alpha)_{eff}$ and $\eta_{el,STC}$, need to be taken into account.

3.4 Experimental analysis of glazed PVT collectors with low-e coating

In the research project PVTmax (Wendker et al. 2012) a low-e coating was specifically optimized for the application in PVT collectors and a prototype with this coating was built. Based on this preceding work, the isolated effect of low-e coatings on the electrical and thermal efficiency is studied hereafter by comparing the results with an identical PVT collector without low-e coating. For this purpose, the low-e coating was removed and its efficiency re-tested. This method allows an experimental comparison of the isolated effect of low-e coatings. The following section details the characteristics of the low-e coating, the design of the PVT collector, and the experimental results.

3.4.1 Optical characterization of an optimized silver-based low-e coating

At Fraunhofer ISE, a silver-based low-e coating was specifically developed and optimized for the application in PVT collectors. The optimization of the low-e coating aims at achieving a good balance between a high transmittance and a low emissivity. This objective is reached by a thin layer of Ag to realize a low emissivity in the infrared spectrum and by combining low-refractive layers of SiO_2 and high-refractive layers of TiO_2 for a high transmittance. After simulation and optimization of the multi-layer stack, the low-e coating was produced on a horizontal sputtering system at the facilities of Fraunhofer ISE. Low-iron soda lime glass with a thickness of 4 mm was used as substrate (Wendker et al. 2012).

The resulting transmittance and reflectance spectra were characterized with a spectral reflectometer equipped with an integrating sphere of 22 cm of diameter. The obtained spectra of low-e coated glass are shown in Figure 3.14 (left) together with the AM1.5 spectrum and the spectral response of a c-Si cell. In the long-wave spectrum, spectral measurements were performed accordingly and are plotted in Figure 3.14 (right). In the responsive spectrum of c-Si cells a high transmittance comparable to uncoated glass is achieved. Starting from λ = 1.0 μm, the transmittance τ decreases continuously while the reflectance ρ increases. Thus, the low-e coating achieves a low absorptance in the infrared spectrum and consequently the desired low emissivity.

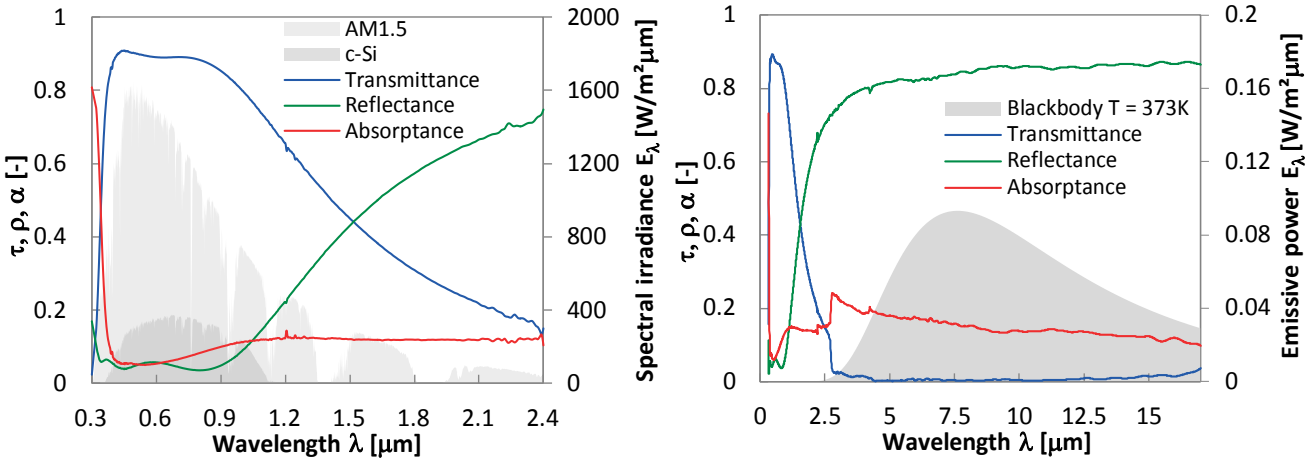

Figure 3.14: Measured transmittance, reflectance and absorptance spectra of low-e coated glass in the solar spectrum (left) and in the infrared spectrum (right).

The solar transmittance $\tau_{AM1.5}$ and reflectance $\rho_{AM1.5}$ are obtained by convolution of the measured spectra with the AM1.5 spectrum. Accordingly, $\tau_{c\text{-}Si}$ and $\rho_{c\text{-}Si}$ are obtained by convolution with the spectral response of a c-Si cell. The weighted emissivity ε_{373K} is obtained by convolution with the Planck radiation of a black body at T = 373 K according to Eq. (3.13). The optical properties of the produced low-e coating are summarized in Table 3.3.

Table 3.3: Optical properties of the produced low-e compared to uncoated low-iron glass.

Symbol	low-e glass	uncoated glass
$\tau_{AM1.5}$	0.79	0.90
$\tau_{c\text{-}Si}$	0.87	0.90
$\rho_{AM1.5}$	0.12	0.08
$\rho_{c\text{-}Si}$	0.05	0.02
ε_{373K}	0.13	0.92

3.4.2 Design of a PVT collector with low-e coating

The silver-based low-e coating was applied in a PVT collector to demonstrate the improvement of thermal efficiency and compare its performance with a PVT collector without low-e coating. A glazed, flat plate, liquid-type PVT collector with monocrystalline cells laminated to a sheet-and-tube absorber was designed for this purpose (Wendker et al. 2012). The low-e coating was applied on the upper glass surface of the PVT laminate. A schematic cross section of the PVT collector is shown in Figure 3.15.

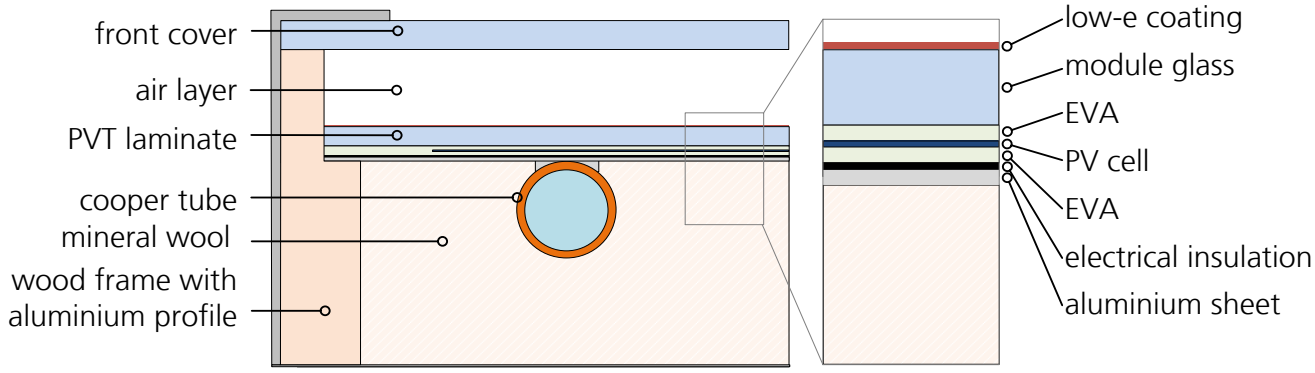

Figure 3.15: Cross section of the PVT collector with low-e coating and directly laminated sheet-and-tube absorber.

Monocrystalline silicon solar cells were selected in the present PVT collector, owing to their high conversion efficiency. 32 cells with a rated electrical efficiency of $\eta_{el,STC}$ = 18.2 % and a temperature coefficient of γ = 0.43 %/K are connected in series. A 30 mm border without PV cells avoids partial shading up to incidence angles of θ = 56°. A spacing of 2 mm between the cells as typical in PV modules was maintained. Thus, the PVT collector achieves an overall packing factor of 0.84 relative to the aperture area.

The PVT laminate consists of several layers and was manufactured as one package in a vacuum laminator at Fraunhofer ISE. For good thermal contact between cell and fluid, the cells were directly laminated on an aluminum sheet. The module glass with low-e coating forms the first layer. Two layers of EVA serve as adhesive, encapsulant and vapor barrier for the PV cells. A thin electrical insulation layer was spray-coated on the aluminum sheet before lamination. The whole stack was laminated in a vacuum laminator using standard lamination parameters for pressure, temperature and lamination time. The lamination process took place at temperatures above 140 °C at which the EVA encapsulant cross-links chemically. Owing to the different thermal expansion coefficients of aluminum and glass the laminate curves at ambient temperatures.

After lamination, the copper tubes were laser welded to the aluminum sheet of the PVT laminate. The tubes form a meander with an average tube spacing of 77 mm.

The PVT laminate is enclosed in a collector housing with a front cover and rear insulation to reduce thermal losses. A construction of dried birch screwed to an aluminum profile formed the insulated collector frame. Low-iron glass with a double-sided anti-reflective coating and a transmittance of $\tau_{AM1.5}$ = 96.2 % was used as front cover. The spacing of the air layer was set to 20 mm. However, due to the curvature of the PVT laminate, the distance varies between 15 mm and 20 mm. 40 mm of mineral wool reduce heat losses to the back. Insulation tape was applied at the edges of the PVT laminate to avoid thermal bridges.

After conducting performance tests, the low-e coating was removed in order to study the isolated effect of low-e on thermal and electrical efficiency. For this purpose, the PVT laminate was treated in a concentrated sodium hydroxide and nitric acid solution for several days. Spectral analysis of a glass sample showed a complete removal of the low-e coating by comparing the measured spectrum with that of uncoated glass. Thus, the results of the PVT collector with and without low-e are fully comparable, since the only modified design parameter is the low-e coating.

Table 3.4 summarizes the key design dimensions and of the PVT collectors with and without low-e coating, which will be referred to as "PVT01-low-e" and "PVT02-no low-e" hereafter.

Table 3.4: Key design parameters of the PVT collectors "PVT01" and "PVT02".

Design parameter	Values
aperture dimensions	1329 x 690 mm²
height air layer d_{gap}	20 mm
tube outside diameter d_{pipe}	8 mm
tube wall thickness	0.3 mm
tube spacing	77 mm
thickness EVA d_{EVA}	0.2 mm
thickness electrical insulation $d_{insulation}$	0.1 mm
thickness Al sheet $d_{aluminum}$	0.5 mm
thickness mineral wool $d_{insulation,back}$	40 mm
thickness edge insulation $d_{insulation,edge}$	18 mm

3.4.3 Performance characterization

Both collectors with and without low-e coating were tested in the indoor solar irradiance simulator at the test facilities of Fraunhofer ISE. The performance tests were carried out in steady-state conditions as described in ISO 9806 (2017). Accordingly, artificial sun, wind, and sky were applied to the collector plane. The collectors were operated in hybrid mode, i.e. with simultaneous generation of heat and electricity. For this purpose, an electrical load in the form of a maximum power point (MPP) tracker was attached to the electrical connectors. Small variations of testing conditions between the two collectors were observed and are reported in Table 3.5. The resulting curves of thermal and electrical efficiency are shown in Figure 3.16, where all efficiencies relate to the aperture area A_{ap}.

In contrast to the standardized approach, the electrical performance is expressed at this point as a function of the reduced temperature $\Delta T/G$, analogous to the thermal efficiency curve in Eq. (2.2). However, since the electrical efficiency is a function of the absolute cell temperature, the electrical performance curve is only valid for the specific test conditions with a constant rate of irradiance G. This non-standard equation is therefore a makeshift approach, which allows the comparison of the electrical performance for measurements in the solar simulator when no flasher data is available.

Performing linear regression of η_{el} to $\Delta T/G$ with the electrical steady-state test points yields the following electrical efficiency curve:

$$\eta_{el} = \eta_{el,0} - b_1 \frac{(T_m - T_a)}{G} \tag{3.30}$$

with the electrical efficiency $\eta_{el,0}$ at the temperature difference $\Delta T = T_m - T_a = 0$ K, and the linear temperature dependence factor b_1.

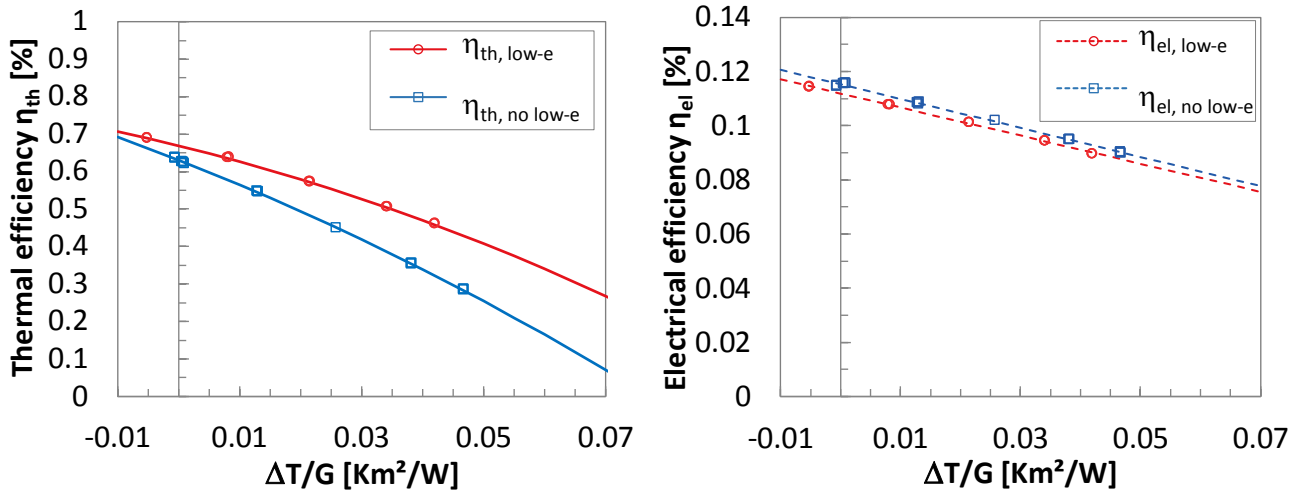

Figure 3.16: Thermal and electrical efficiency curves (lines) with test points (markers) measured in MPP mode of PVT collectors with low-e ("PVT01") and without low-e coating ("PVT02"). Efficiency based on aperture area. Electrical efficiency curve only valid for test conditions as per Table 3.5.

Table 3.5 shows the resulting thermal and electrical performance parameters obtained from least square fitting to Eq. (2.2) and Eq. (3.30). The PVT collector with low-e coating achieves a significantly improved thermal efficiency owing to the reduced radiative losses. At $\Delta T/G = 0.05$ Km²/W the thermal efficiency of the PVT collector with low-e coating is found to be 60 $\%_{rel}$ higher than that without low-e. The improvement of thermal efficiency comes at the expense of electrical efficiency, which is reduced by 3 $\%_{rel}$.

Table 3.5: Test results and test conditions from performance characterization in the solar simulator for the PVT collectors with and without low-e coating "PVT01" and "PVT02".

Parameter	Symbol	Unit	"PVT01-low-e"	"PVT02-no low-e"
Test results				
conversion factor in MPP mode	$\eta_{th,0}$	-	0.67	0.63
linear heat loss coefficient	c_1	W/(m²K)	3.98	6.37
temperature dependence of heat losses	c_2	W/(m²K²)	0.025	0.023
photovoltaic efficiency at $\Delta T = 0$ K	$\eta_{el,0}$	-	0.112	0.115
temperature coefficient of PV efficiency	b_1	W/(m²K)	0.52	0.54
Test conditions				
solar irradiance	G	W/m²	971.5	987.2
ambient temperature	T_a	°C	34.4	30.0
wind speed	u_{wind}	m/s	3	3
mass flow rate of heat transfer fluid	$\dot{m}$	kg/h	89.9	86.7

Even though great emphasis was placed on setting the same collector and test boundary conditions, the experimental comparison between the collectors with and without low-e is presented with limitations. The removal of the low-e coating by means of the caustic bath might have deteriorated optical and thermal properties of the PVT laminate. Additionally, the differing test conditions with respect to ambient temperature, mass flow rate and irradiance might cause further inconsistencies. Instead, the numeri-

cal model allows a better comparability and a more detailed analysis of energy flows. Therefore, the effect of low-e coatings on thermal and electrical efficiency is analyzed in more detail in chapter 3.5 by means of the validated numerical model, where a good agreement between simulation and experiment are observed.

3.5 Discussion of experimental results with the numerical PVT collector model

3.5.1 Effect of low-e on the electrical efficiency η_{el}

Figure 3.17 shows the waterfall charts for both collector configurations, summarizing the cell-to-module efficiency calculation according to Haedrich et al. (2014) as described in chapter 3.2.3. The efficiency of the PV cells amounts to 18.2 %. Losses due to inactive module area and cover transmittance are equal for both collectors. The inactive module area is relatively large owing to the small aperture area of A_{ap} = 0.92 m². In a PVT collector with 60 cells and identical border and cell spacing, these losses could be reduced from 3.2 $\%_{abs}$ to 1.7 $\%_{abs}$. Optical losses due to reflectance and absorptance in the PV glass amount to 1.3 $\%_{abs}$ for the low-e variant and 0.6 $\%_{abs}$ without low-e. By applying an anti-reflective coating instead, these losses could be reduced to 0.2 $\%_{abs}$. The connection losses in the collector with low-e are slightly lower because of smaller currents. In total, the low-e coating reduces the module efficiency under standard test conditions (STC) from $\eta_{el,STC}$ = 13.3 % to $\eta_{el,STC}$ = 12.7 %.

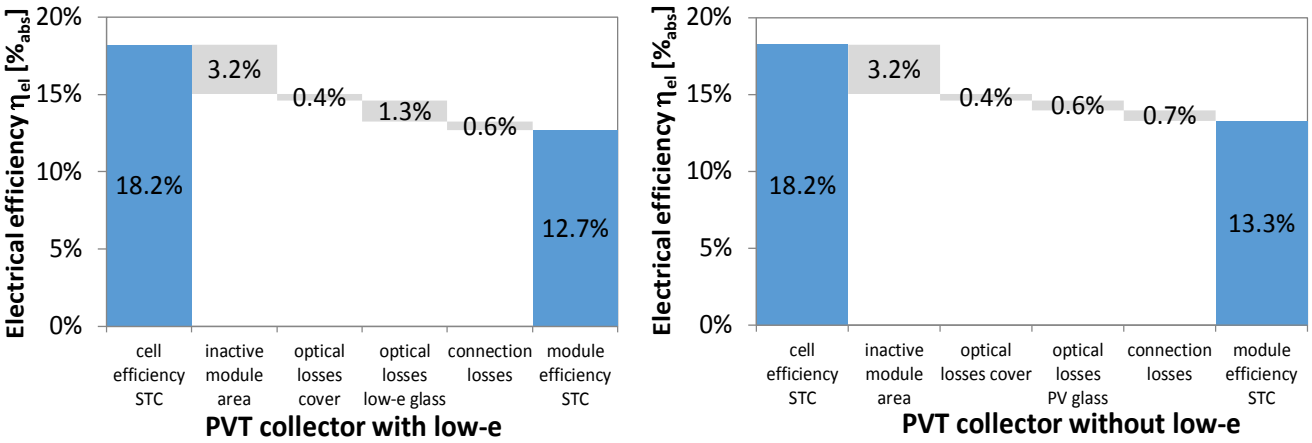

Figure 3.17: Waterfall chart for the calculation of electrical cell-to-module efficiency for a PVT collector with low-e coating (left) and without low-e coating (right).

The electrical power in standard test conditions was not tested for "PVT01" and "PVT02". Instead, the electrical efficiency curve was measured during thermal performance characterization deviating from normative procedures. There, the electrical efficiency $\eta_{el,0}$ is evaluated at the thermal operation point $\Delta T/G$ = 0 Km²/W. According to the collector model, mean cell temperatures lie 10.3 K above the ambient temperature for both collectors at this operating point. The absolute cell temperatures T_{cell} and the calculated module efficiency $\eta_{el,STC}$ employed in Eq. (2.1) yield an electrical efficiency of $\eta_{el,0}$ = 11.8 % with low-e coating and $\eta_{el,0}$ = 12.1 % without low-e coating. During performance tests $\eta_{el,0}$ = 11.2 % and $\eta_{el,0}$ = 11.5 % respectively were measured. The differences between simulation and test might result from experimental uncertainty involved with the non-standard solar spectrum of the halogen lamps as described previously.

3.5.2 Effect of low-e coatings on the overall heat loss coefficient U_{Loss}

During performance tests, cell and surface temperatures are unknown. Therefore, it is not possible to draw direct conclusions from the measured heat loss coefficients c_1 and c_2 to the radiative heat loss coefficient h_{rad} or the overall heat loss coefficient U_{Loss}. Instead, the effect of low-e on U_{Loss} is discussed by means of the numerical model.

The emissivity of the PVT absorber is a function its surface temperature $T_{surface}$. Employing the measured infrared absorptance spectra for both low-e coated and uncoated module glasses in Eq. (3.13), the emissivity as function of the module temperature is shown in Figure 3.18. Accordingly, the emissivity of the uncoated glass increases from $\varepsilon_{no\ low\text{-}e} = 0.908$ at $T_{surface} = 25$ °C to $\varepsilon_{no\ low\text{-}e} = 0.922$ at $T_{surface} = 150$ °C. In the same temperature range, the emissivity of low-e coated glass increases from $\varepsilon_{low\text{-}e} = 0.125$ to $\varepsilon_{low\text{-}e} = 0.145$.

The respective radiative heat loss coefficients h_{rad} resulting from Eq. (3.12) are also plotted in Figure 3.18 assuming a constant front cover temperature of 25 °C. For instance, the radiative heat loss coefficient at $T_{surface} = 50$ °C amounts to $h_{rad,low\text{-}e} = 0.84$ W/m²K for low-e glass compared to $h_{rad,no\ low\text{-}e} = 5.5$ W/m²K for uncoated glass. Employing these correlations in the numerical collector, where surface temperatures are computed internally, yields a reduction of the overall heat loss coefficient U_{Loss} of 71 % from 8.5 W/m²K to 4.9 W/m²K, evaluated at a surface temperature of $T_{surface} = 50$ °C.

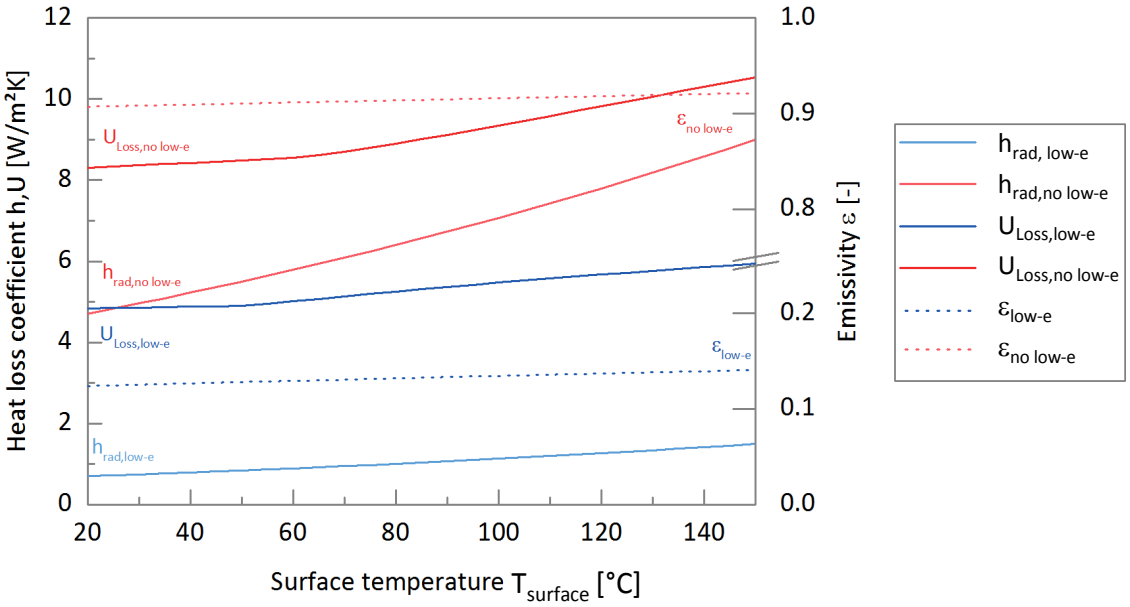

Figure 3.18: Heat loss coefficients h_{rad} and U_{Loss} and emissivity ε as function of surface temperature of the PVT absorber with and without low-e coating.

3.5.3 Effect of low-e on the conversion factor $\eta_{th,0}$

The measured conversion factor in hybrid mode amounts to $\eta_{th,0} = 0.67$ of the low-e coated and $\eta_{th,0} = 0.63$ of the uncoated PVT collector (compare Table 3.5). At first, this result looks peculiar since low-e coatings have a higher reflectance and thus lower absorptance of the PVT laminate. The higher conversion factor, however, can be attributed to the interdependence of thermal, optical, and electrical properties in F´.Resulting from the energy balance, the conversion factor $\eta_{th,0}$ under normal incidence is expressed as:

$$\eta_{th,0} = F'[(\tau\alpha)_{eff} - \eta_{el,0}] \tag{3.31}$$

with the collector efficiency factor F´, the effective transmittance-absorptance product $(\tau\alpha)_{eff}$, and the electrical efficiency at $\Delta T = 0$ K $\eta_{el,0}$.

Firstly, the higher reflectance of the low-e coating reduces $(\tau\alpha)_{eff}$. The absorptance of the PVT laminate $\alpha_{laminate}$ drops from 0.901 to 0.862 as measured in the spectrometer (Figure 3.19). Since properties of the optical stack are only changed on the first surface, the difference of absorption can be directly attributed to the additional reflection of the low-e coating.

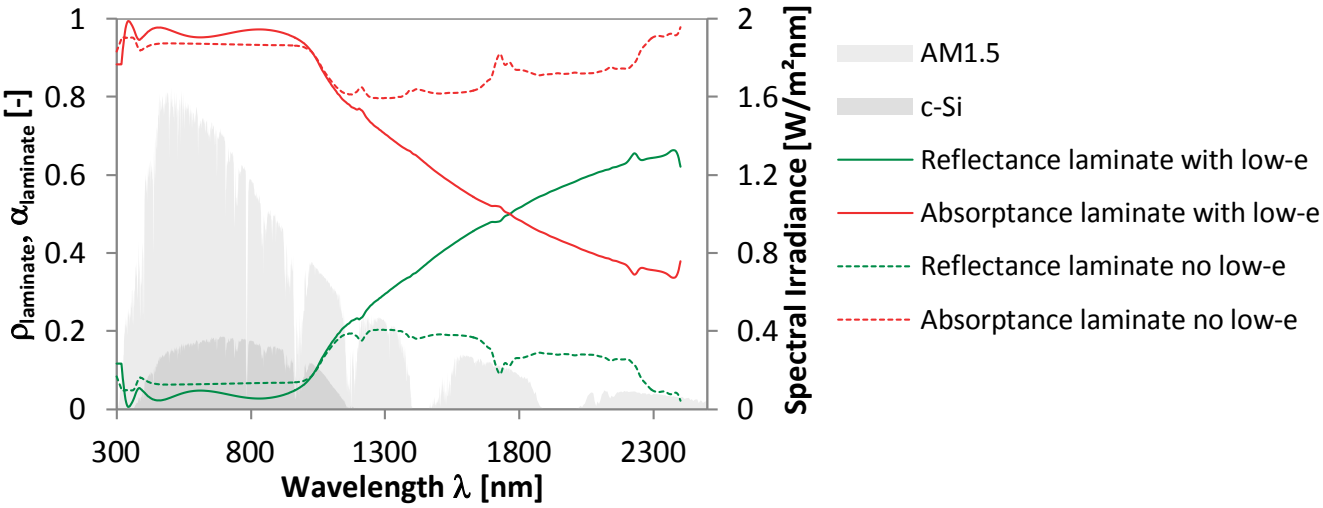

Figure 3.19: Measured reflectance and absorptance spectra of a PVT laminate with and without low-e coating.

The optical properties and resulting effective transmittance-absorptance product for the two collectors are indicated in Table 3.6. Taking into account the optical properties of the front cover and multiple reflections, the low-e coating reduces $(\tau\alpha)_{eff}$ from 0.868 to 0.832.

Table 3.6: Optical properties for the calculation of $(\tau\alpha)_{eff}$.

Parameter	Symbol	with low-e	without low-e
transmittance cover	τ_{cover}	0.962	0.962
reflectance cover	ρ_{cover}	0.029	0.029
reflectance laminate	$\rho_{laminate}$	0.138	0.099
absorptance laminate	$\alpha_{laminate}$	0.862	0.901
effective transmittance-absorptance product	$(\tau\alpha)_{eff}$	0.832	0.868

The collector efficiency factor F´ can be calculated as the ratio of the overall heat loss coefficient U_{Loss} and the internal heat transfer coefficient $U_{AbsFluid}$ (Eq. (3.19)). Low-e coatings reduce U_{Loss} resulting in a higher F´ of 0.926 compared to 0.868. At the same time $\eta_{el,0}$ drops from 12.1 % to 11.8 % (cf. chapter 3.5.1). The combined effect of F´, $(\tau\alpha)_{eff}$, and $\eta_{el,0}$ on the conversion factor $\eta_{th,0}$ is summarized in Table 3.7. Employing the obtained parameters in Eq. (3.31) yields a conversion factor of $\eta_{th,0} = 0.661$ with low-e compared to $\eta_{th,0} = 0.654$ without low-e.

To conclude, $\eta_{th,0}$ strongly depends on the properties of the low-e coating and an adequate balance between high transmittance and low emissivity is essential for an optimized conversion factor.

Table 3.7: Modelling results regarding the conversion factor $\eta_{th,0}$.

Parameter	Symbol	Unit	with low-e	without low-e
Internal heat transfer coefficient	$U_{AbsFluid}$	W/m²K	61.2	62.1
overall collector heat loss coefficient	U_{Loss}	W/m²K	4.88	8.78
collector efficiency factor	F´	-	0.926	0.876
effective transmittance-absorptance product	$(\tau\alpha)_{eff}$	-	0.832	0.868
photovoltaic efficiency at $\Delta T = 0$ K	$\eta_{el,0}$	-	0.118	0.121
thermal conversion factor	$\eta_{th,0}$	-	0.661	0.654

3.5.4 Effect of low-e coatings on the combined electrical and thermal efficiency

To summarize the effect of low-e coatings on the combined thermal and electrical efficiency of PVT collectors, the stacked efficiency curves including optical and thermal losses and useful power are shown in Figure 3.20. This rather unusual illustration of efficiency curves subdivides the incident irradiance into their effective shares of thermal and electrical gains and into the different loss mechanisms. The colored areas should not be interpreted as an integral, but for any operation point ΔT/G the breakdown of gains and losses can be read from the y-axis. The figure also nicely illustrates the effect of F': at ΔT = 0K there are already significant thermal losses due to absorber temperatures above ambient. The term "optical efficiency" is therefore inappropriate, since $\eta_{th,0}$ includes both optical and thermal losses.

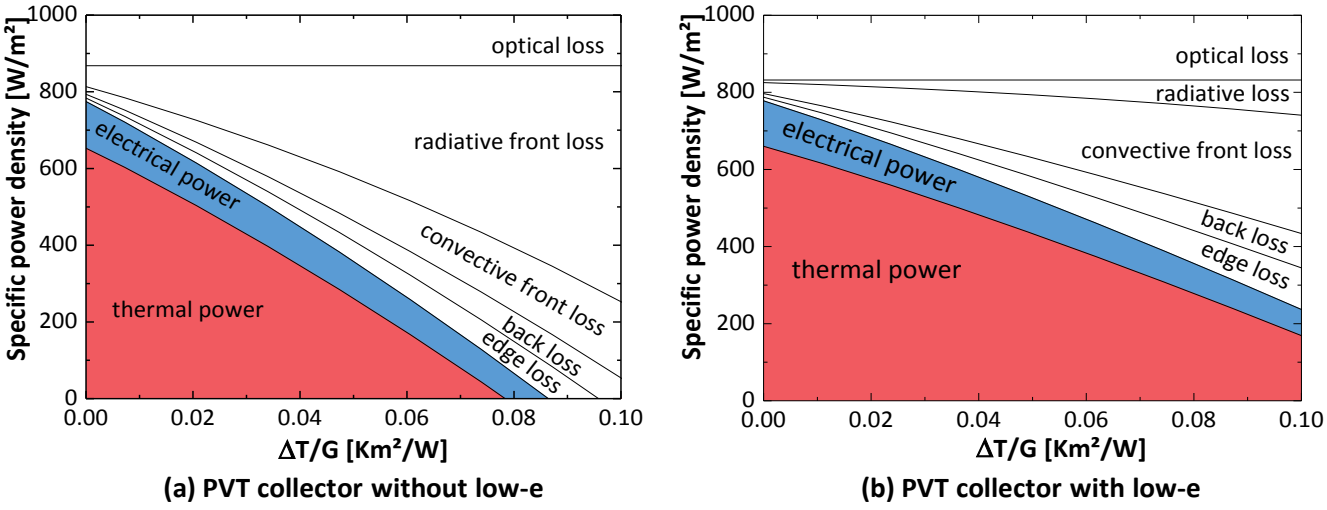

Figure 3.20: Efficiency curves with subdivided gains and losses for the PVT collector without low-e coating (left) and with low-e coating (right).

It is convenient to discuss the effect of low-e at a typical operation point of the efficiency curve, here ΔT/G = 0.05 Km²/W: The PVT collector with low-e coating has higher optical losses (+36 W/m²) owing to the higher reflectance of low-e coated glass. Radiative losses in the collector gap are significantly reduced (-247 W/m²). Although the convective heat transfer coefficient h_{conv} remains almost constant, the

convective heat losses increase by +53 W/m², which can be attributed to the higher surface temperature of the PVT absorber owing to an increased useful heat flow from the absorber to the fluid. Edge losses are relatively high in both cases (48 W/m²) due to the small collector area of A_{ap} = 0.92 m². The overall heat losses drop in total by 190 W/m² or 38 $\%_{rel}$. Consequently, the useful thermal power increases by 158 W/m² or 57 $\%_{rel}$, while the electrical power drops by 4 W/m² or 4 $\%_{rel}$ on account of the low-e coating.

3.5.5 Effect of low-e on thermal power output

It is a common misunderstanding that the reduction of thermal losses primarily aims at achieving higher temperatures. In fact, the aim of reducing thermal losses is to achieve a higher efficiency during regular operation, especially at low levels of irradiance or at low ambient temperatures. This context can be better demonstrated by means of comparing power curves. Figure 3.21 depicts the power curves of the tested PVT collector with low-e and without low-e for two standardized weather conditions: blue sky with an irradiance of G = 1000 W/m² in full line, and grey sky with G = 400 W/m² in dashed line (ISO 9806 2017).

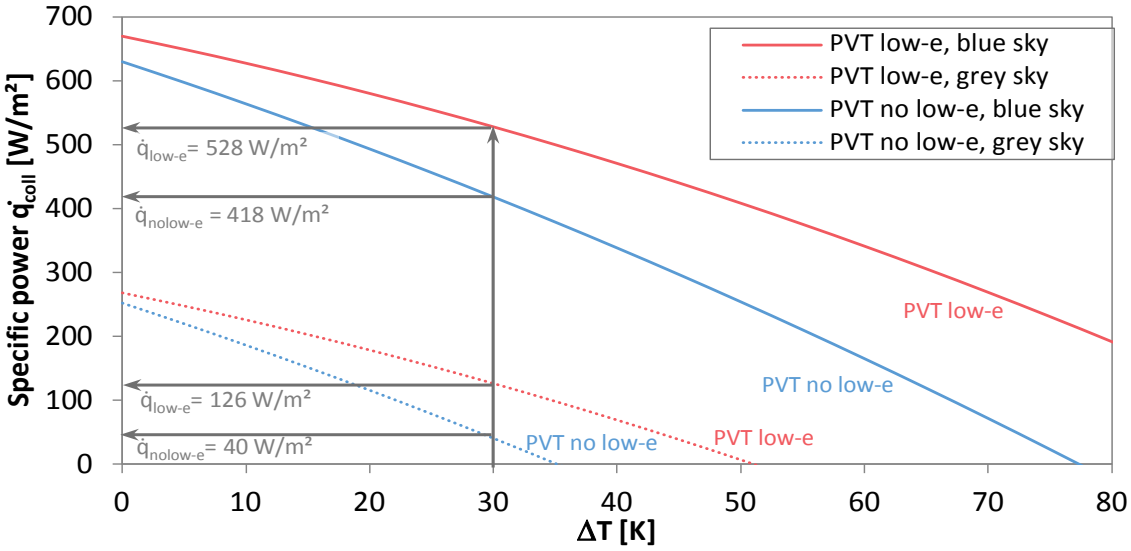

Figure 3.21: Power curves for PVT collectors with and without low-e for blue and grey sky conditions.

The specific thermal power output $\dot{q}_{coll}$ can be read from the ordinate for a given temperature difference, e.g. ΔT = 30K. At blue sky conditions, both PVT collectors deliver a reasonable thermal output of $\dot{q}_{low-e}$ = 528 W/m² and $\dot{q}_{no\ low-e}$ = 418 W/m², which equals an increase of 26 $\%_{rel}$ by the application of low-e. At grey sky conditions, however, the thermal power output drops significantly: the PVT collector without low-e falls to $\dot{q}_{no\ low-e}$ = 40 W/m² and the PVT collector with low-e still reaches $\dot{q}_{low-e}$ = 126 W/m², which equals an increase of 215 $\%_{rel}$ by low-e. At low levels of irradiance, the PVT collector without low-e often does not reach required fluid temperatures, so that the control will turn the pump off. At the same conditions, the PVT collector with low-e is still able to achieve the required fluid temperature and thus deliver solar heat to the storage.

Hence, low thermal losses are required to achieve a reasonable thermal output during demanding operating conditions, because a good thermal insulation has two effects: firstly a higher efficiency during operation and secondly longer operation periods. Both effects together result in higher annual heat

yields. The mathematical reason for this lies in the proportionality of the thermal efficiency from the temperature difference ΔT divided by the irradiance G.

As a consequence thereof, a low thermal efficiency cannot be fully compensated by larger collector areas. A collector with high thermal losses, e.g. an unglazed collector, is not able to supply any heat during challenging periods of the year with low levels of irradiance and low ambient temperatures. Increasing the collector area only increases the thermal yield during the operational periods, but not during the periods of zero efficiency. In order to increase useful annual heat gains, it is therefore not sufficient to increase the corresponding collector area, but also the collector efficiency has to be improved, for instance by reducing thermal losses. This contrasts with PV modules, where the electrical yield is primarily proportional to the area and the peak efficiency $\eta_{el,STC}$. A lower efficiency of the PV module can always be compensated by adding additional PV modules in order to reach a desired electrical yield.

3.5.6 Effect of low-e on gross energy yields

These effects are also observed in the assessment of gross energy yields with ScenoCalc. Figure 3.22 shows the electrical and thermal yields at three different mean fluid temperature levels T_{mean}. The analysis includes the previously tested glazed PVT collectors with and without low-e coatings, based on the performance data reported in Table 3.5. In addition, a PV module, an unglazed PVT collector, a low-concentrating PVT collector, and a conventional flat plate collector are also included. The low-concentrating PVT collector is a non-tracked commercial product with a concentration factor of C = 1.75 (Solarus 2017).

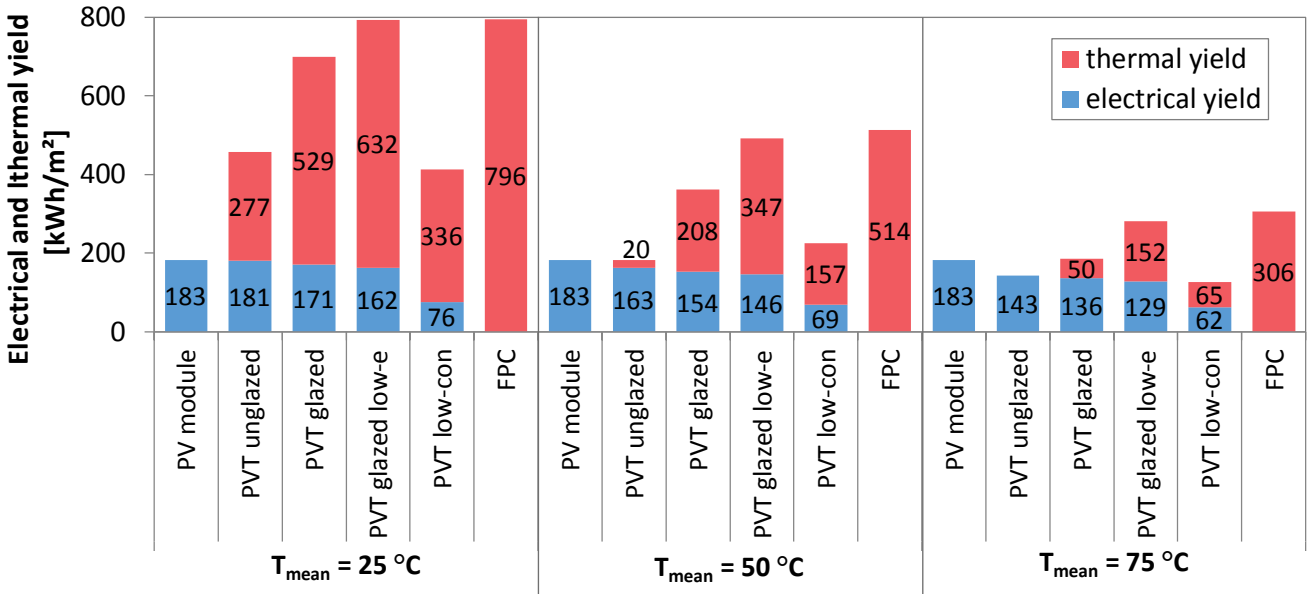

Figure 3.22: Assessment of gross energy yields for different collector technologies at the location of Würzburg.

Higher mean fluid temperatures reduce the energy yields of all collector technologies, except for the PV module, which is naturally uncoupled from the thermal operation. Next to the importance of low fluid temperatures, the assessment also illustrates the conflict between a good optical efficiency versus low thermal losses. Currently, PVT collectors reach either high electrical or high thermal yields, but not both at the same time.

Of all assessed PVT technologies, the glazed PVT collector with low-e achieves the highest thermal yields at all three temperature levels whereas the unglazed PVT collector reaches the highest electrical yields. The energy yields of the low-concentrating PVT collector lie significantly below the glazed PVT collector with low-e. Its relatively low yields can be attributed to the restricted acceptance angle of the untracked collector, resulting in incidence angle losses. Moreover, there is also the potential in concentrating PVT collectors to further reduce thermal losses by the application of low-e coatings.

Comparing both glazed PVT collectors demonstrates the effect of low-e on gross energy yields. The application of low-e increases the thermal yield by 20 $\%_{rel}$ for T_{mean} = 25 °C, by 69 $\%_{rel}$ for T_{mean} = 50 °C, and by 210 $\%_{rel}$ for T_{mean} = 75 °C. At the same time, the electrical yield drops by 3 $\%_{rel}$. Therefore, PVT collectors with low-e bring in their specific strength at a medium fluid temperature level, when the thermal efficiency of glazed PVT collectors without low-e is insufficient.

The same qualitative relationship between collector type and mean fluid temperature is also observed for other locations. Table B.2 in Appendix B.3 aggregates the yields for the locations of Athens, Davos, Würzburg, and Stockholm.

The comparison of gross energy yields represents a simplified approach, which neglects the dynamics of real systems. In decentralized building technologies, energy has to be delivered in time of demand. This can result in excessive amounts of energy, which might not be utilized when there is no current demand. Additionally, the mean fluid temperature is not constant in real systems. Domestic heat is typically stored in sensible thermal storage systems, where charging the storage increases the temperature. Instead of using ScenoCalc, the dynamic aspects of the application of PVT collectors with low-e coatings will be analyzed in depth in chapter 4 by means of system simulations.

Nonetheless, the assessment of gross energy yields shows the specific strengths and suitable fields of applications for each collector type. Only with low thermal losses, substantial thermal yields can be achieved, since an extension of collector area cannot compensate for the lower efficiency. Hence, low-e coatings enable the application of PVT collectors to systems with a higher temperature levels.

3.6 Evaluation of low-e coatings for PVT collectors

3.6.1 Screening of available low-e coatings

A high transmittance in the solar spectrum is a prerequisite for the application of low-e in PVT collectors. Only few low-e coatings with a high transmittance can be found on the market or are described in the scientific literature. This is due to the still insignificant market for these types of high-transmittance coatings. For manufacturers of architectural glass, the optimization towards a low emissivity has a higher priority than achieving a high transmittance.

The screening of potentially suitable low-e coatings was carried out within the research projects PVTmax (Wendker et al. 2012) and PVTgen2 (Lämmle et al. 2017a) and the findings are summarized briefly in Table 3.8. The low-e samples were characterized with the Fourier spectrometer with Ulbricht sphere at Fraunhofer ISE and optical parameters are subsequently weighted with the respective spectra.

Table 3.8: Screening of highly transparent low-e coated glasses.

Manufacturer	Product name	Material	Optical parameters			
			ε_{373K}	$\tau_{c\text{-}Si}$	$\tau_{AM1.5}$	$\alpha_{AM1.5}$
Guardian	SunGuard	Ag	0.04	0.64	0.59	0.11
f-glas/Interpane	ILS ipawhite	Ag	0.08	0.82	0.75	0.07
Fraunhofer ISE	ISE low-e	Ag	0.13	0.87	0.79	0.09
Pilkington	K Glass N OW	SnO_2:F	0.14	0.82	0.78	0.11
Pilkington	K Glass N OW + AR coating	SnO_2:F + AR (TiO_2)	0.15	0.86	0.80	0.12
Euroglas	silverstar free vision white	ZnO:Al_2O_3	0.30	0.90	0.86	0.06
Centrosolar	HiT	white glass	0.92	0.91	0.92	0.02
Centrosolar	HiT C	white glass + AR (TiO_2)	0.92	0.94	0.94	0.02

Guardian SunGuard is a typical architectural low-e glass with a silver-based low-e coating for window glasses and has a low emissivity, but also a relatively low transmittance. Interpane ILS ipawhite is also a silver-based low-e coating for windows, yet with improved solar transmittance. The Fraunhofer ISE low-e coating is the aforementioned coating, which was applied in the PVT prototype and specifically optimized for this purpose. Pilkington K-Glas N OW is a pyrolitic, fluorine doped tin oxide (SnO_2:F) coating and achieves both low emissivity and high transmittance. With an additional anti-reflective coating, which can be spray-coated on the glass, the transmittance can be further improved especially in the PV responsive spectrum. However, the combination K-Glass + AR is not available commercially but was produced on lab scale at Fraunhofer ISE. Euroglas silvestar free vision white is a highly transparent low-e coating based on aluminum doped zinc oxide (ZnO:Al_2O_3). It was developed in the joint research project HFK Glas by Euroglas and ISFH and is optimized for the application in solar collectors with a high transmittance and medium emissivity (Föste et al. 2013).

Two samples of soda free low-iron glass (white glass) without low-e are also included in Table 3.8 for comparison purposes, where Centrsolar HiT C features a single anti reflective coating based on TiO_2.

As can be seen from this summary, the lower emissivity typically comes at the expense of a lower transmittance, which reduces note only the electrical but also the thermal performance. Therefore, a good balance between a low emissivity ε and a high transmittance τ is desired.

3.6.2 Evaluation of optical parameters

The optical parameters of the low-e coating determine the resulting performance of the PVT collector. A rating function for the optical parameters is suitable to evaluate existing low-e coatings, assess their suitability for PVT collectors, and develop new, optimized low-e coatings. In fact, such a target function was used for the optimization of the silver-based low-e coating developed at Fraunhofer ISE (Lämmle et al. 2016a). This target function was based on empirical assumptions and served as a starting point for the more precise rating function, which is described in the following section.

Figure 3.23 illustrates the methodology with which this rating function is determined. The notion of this approach is to correlate the optical properties of the low-e coating with the primary energy savings of a PVT collector employing this coating. Thus, the rating function directly links the optical parameters of any low-e coating with the primary energy yield of the PVT collector.

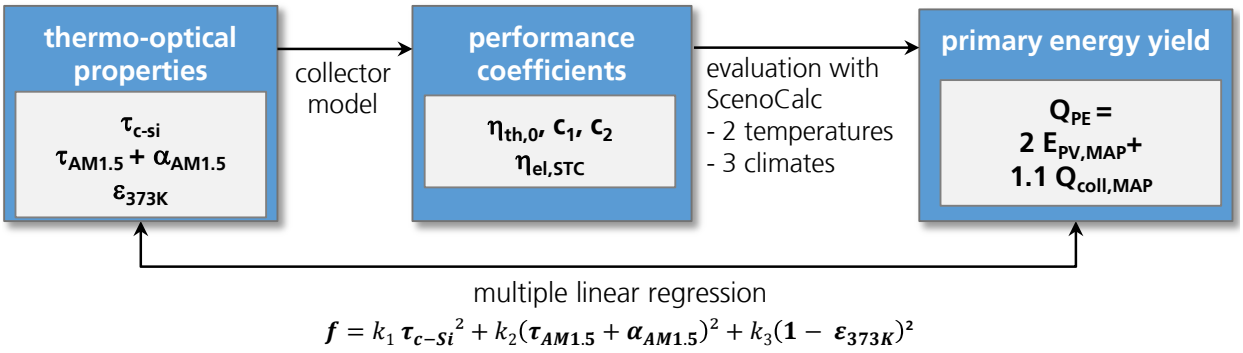

Figure 3.23: Methodology for the deduction of the rating function.

In the first step, the relevant thermo-optical coating properties are identified based on the discussions in chapter 3.5.3. The low-e coating only affects the optical properties at the first optical interface. Accordingly, the electrical efficiency depends on the transmittance of the coating in the PV spectrum $\tau_{c\text{-}Si}$. Secondary reflections from the external cover can be neglected because of the low reflectance of AR glazing of $\rho_{c\text{-}Si} = 0.04$. The overall absorbed energy of the PVT collector as expressed by $(\tau\alpha)_{eff}$ is influenced by the low-e coating through the transmittance in the solar spectrum $\tau_{AM1.5}$ plus the absorptance in the low-e coating $\alpha_{AM1.5}$. Thermal losses in the given PVT collector design depend on the coating's emissivity ε_{373K}.

In the second step, performance coefficients of the PVT collector are calculated with the PVT collector model. The collector construction and design parameters of the PVT prototype "PVT01-low-e" are applied. The rating function is therefore valid for this type of glazed, flat-plate PVT collectors with low-e applied on the PVT absorber surface.

In the third step, the primary energy savings for these collectors are calculated with ScenoCalc. The thermal and electrical gross energy yields E_{PV} and Q_{coll} are evaluated at three locations Athens, Würzburg, and Stockholm at the relevant mean fluid temperatures of 25 °C and 50 °C, applying the MAP weighting function. The primary energy savings Q_{PE} are assessed and averaged for these locations using the previously defined primary energy factors for electricity and gas.

In the fourth step, the correlation between the primary energy yields and thermo-optical properties is analyzed. In total, 125 PVT collectors are sampled varying the three parameters $\tau_{c\text{-}Si}$, $\tau_{AM1.5}+\alpha_{AM1.5}$, and ε_{373K}, which are treated as if they were independent from each other. A rating function f is introduced, which normalizes the primary energy yields in the sense that the ideal coating ($\tau_{c\text{-}Si} = 1$, $\tau_{AM1.5} + \alpha_{AM1.5} = 1$, $\varepsilon_{373K} = 0$) takes the value of f = 1 and the worst coating ($\tau_{c\text{-}Si} = 0$, $\tau_{AM1.5} + \alpha_{AM1.5} = 0$, $\varepsilon_{373K} = 1$) takes a value of f = 0. The analysis of the correlation between the new rating function and the thermo-optical properties shows a quadratic relationship for all three variables. This leads to the following form of the rating function f with the weighting factors k_1, k_2, k_3:

$$f = k_1 \tau_{c-Si}^2 + k_2 (\tau_{AM1.5} + \alpha_{AM1.5})^2 + k_3 (1 - \varepsilon_{373K})^2 \tag{3.32}$$

The weighting factors k_1, k_2, k_3 are then identified via multiple linear regression, which achieves a good correlation with a Pearson coefficient of $R^2 = 0.99$ and is shown in Figure 3.24. The resulting rating function f with the identified weighting factors k_1, k_2, and k_3 is given by:

$$f = 0.24\, \tau_{c-Si}^2 + 0.59\, (\tau_{AM1.5} + \alpha_{AM1.5})^2 + 0.17\, (1 - \varepsilon_{373K})^2 \tag{3.33}$$

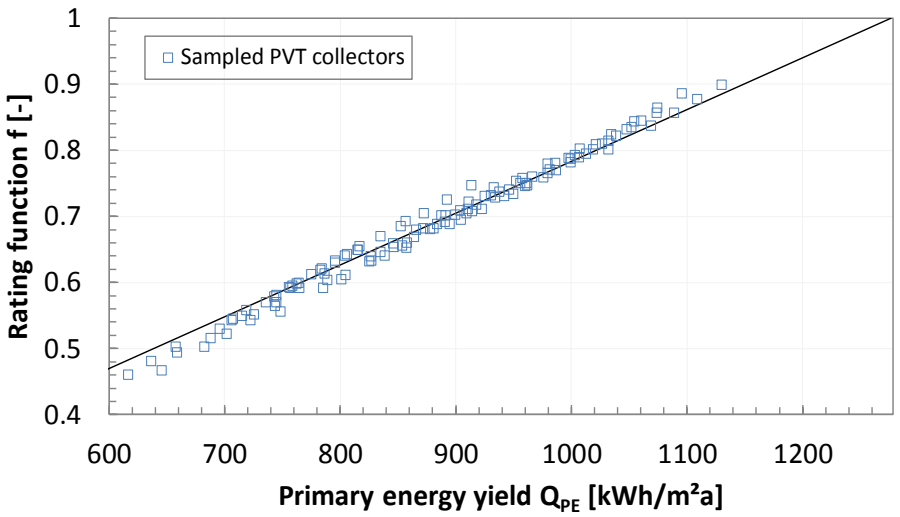

Figure 3.24: Correlation analysis and multiple linear regression for the rating function f.

The rating function can be illustrated as follows: the higher the rating function f, the more suitable is the coating. A high transmittance over a wide spectrum is of utmost importance since it is beneficial for both $\tau_{c\text{-}Si}$ and $\tau_{AM1.5}$ and thus electrical and thermal yields. Although the weighting factor for emissivity k_3 is the lowest, it should be noted that the emissivity typically ranges between 0.04 and 0.92, while transmittance normally exceeds 0.6. The emissivity is therefore an effective lever for achieving a high rating function, and thus high primary energy yields.

Due to the normalization, an increase of the rating function by 1 $\%_{rel}$ equals an increase of 1 $\%_{rel}$ in primary energy yield $Q_{PE.}$ The rating function differs slightly from the empirical function described by Lämmle et al. (2016a): the new rating function assumes a quadratic relationship in contrast to a linear one. Due to the fact that the multiple linear parameter identification is based on gross energy yields, the thermal yields are overestimated compared to electrical yields. As a result, the focus is slightly shifted from electrical to thermal priority resulting in a comparably lower weighting factor for $\tau_{c\text{-}Si}$.

The simplicity of the rating function comes at the expense of restricted validity and accuracy. Of course, the balance between the thermo-optical parameters also depends on assumptions regarding primary energy factors, collector design, and collector location. Assuming a primary energy factor for electricity of $f_{p,el} = 3$ instead of 2 results in a shift from heat to electricity priority with weighting factors of $k_1 = 0.32$, $k_2 = 0.53$, and $k_3 = 0.15$. Regarding collector location and orientation the rating function appears to be robust: the weighting factors k_1, k_2, and k_3 differ by only ±2 $\%_{abs}$ between Athens, Würzburg, Davos, and Stockholm.

An exemplary application of the rating function is given in Table 3.9. The seven screened low-e coatings from Table 3.8 are evaluated with the rating function by employing their optical properties in Eq. (3.33). Thermal and electrical gross energy yields for these coatings are calculated by running collector simulations with the optical parameters of the low-e coatings and a subsequent assessment of gross energy yields with ScenoCalc. The detailed efficiency curves of the PVT collectors with varying low-e coatings as simulated with the numerical collector model are also presented in Appendix B.3.

The primary energy yield Q_{PE} correlates well with the rating figure: it reproduces not only the ranking of low-e coatings but also the relative difference of gross energy yields. This shows that the rating function

is a suitable tool to quickly assess the optical properties of low-e coatings for the application in PVT collectors without performing elaborate collector and yield simulations.

Table 3.9: Applied rating function for seven low-e coatings compared to thermal, electrical, and primary energy yields.

Parameter	Unit	Guardian SunGuard	f-glas ILS ipawhite	Fraunhofer ISE low-e	Pilkington K Glass NOW + AR	Euroglas free vision white	Centrosolar HiT	Centrosolar HiT+C
$\eta_{el,STC}$	-	8.6%	11.0%	11.5%	11.7%	12.6%	13.4%	13.7%
$\eta_{th,0}$	-	0.54	0.62	0.66	0.70	0.68	0.67	0.68
c_1	W/m²K	3.72	3.78	4.04	4.24	4.72	6.48	6.34
c_2	W/m²K²	0.01	0.01	0.02	0.01	0.02	0.02	0.02
$E_{PV,MAP}$	kWh/m²a	106	137	146	149	160	173	179
$Q_{coll,MAP}$	kWh/m²a	415	523	563	608	554	465	484
$Q_{PE,MAP}$	kWh/m²a	667	850	912	966	930	857	890
Rating function f	-	0.54	0.70	0.77	0.80	0.78	0.72	0.76

3.6.3 Evaluation of humidity and condensation resistance with "Task X" tests

Next to the optical properties, humidity and condensation resistance is an important criterion regarding durability and lifetime assessment. To characterize the stability of low-e coatings under high humidity and condensation conditions, five selected coatings underwent accelerated ageing tests within the project PVTgen2 (Lämmle et al. 2017a). These so-called "Task X tests" were originally developed for absorber coatings (ISO/FDIS 22975-2 2014), but can be adapted for low-e coatings due to similar micro climatic conditions inside the collector.

The test procedure is divided into four phases:

- Phase 0: Initial characterization
- Phase I: Condensation induced ageing in a climate chamber at T = 40 °C, relative humidity ϕ = 90 $\%_{rel}$ and sample temperature T = 30 °C for 600 h
- Phase II: Condensation induced ageing in a climate chamber at T = 65 °C, relative humidity ϕ = 95 $\%_{rel}$ and sample temperature T = 60 °C for 85 h
- Phase III: Outdoor weathering/exposition: exposition for six days in Freiburg

After each phase, the samples' emissivity and transmittance were measured in order to monitor their ageing process.

Figure 3.25 shows the measured emissivity ε_{373K} of five samples after the corresponding ageing phases. While ILS ipawhite and Fraunhofer ISE low-e coating suffered from major degradation effects, both K Glass samples and the Euroglas coating registered no measured degradation. The application of the latter coatings is therefore recommended with respect to humidity and condensation resistance.

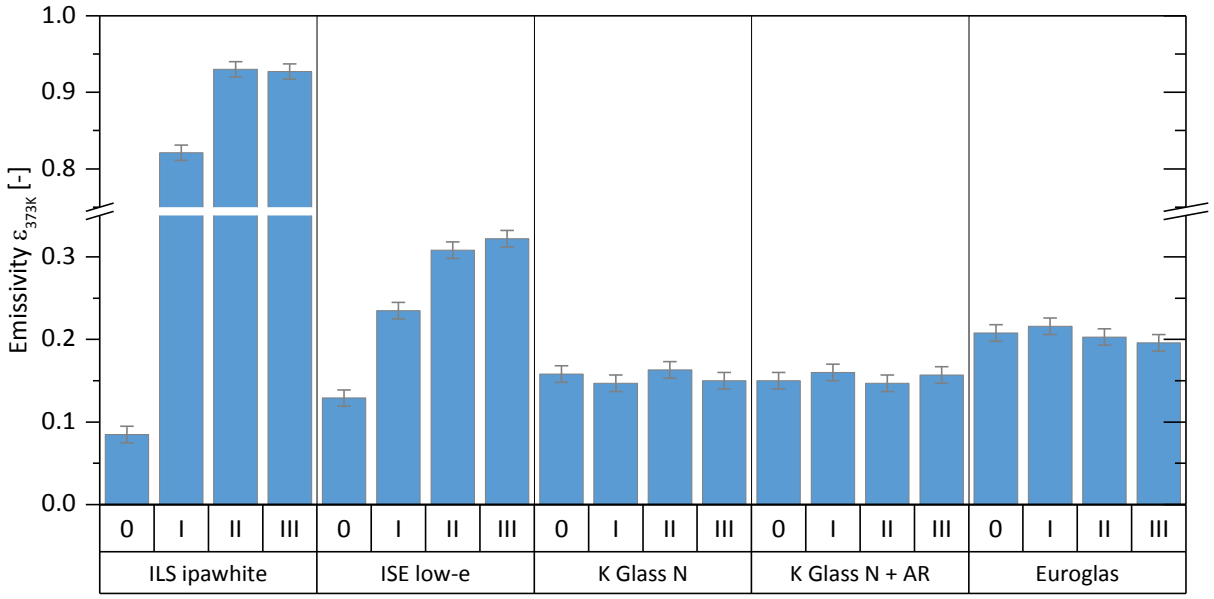

Figure 3.25: Emissivity of five low-e samples after phases 0 - III of the condensation ageing tests adapted from Task X test.

The emissivity of the ILS ipawhite sample increased from an initial $\varepsilon_{373K} = 0.08$ to $\varepsilon_{373K} = 0.93$ after phase III. At the same time the transmittance increased from $\tau_{AM1.5} = 0.71$ to $\tau_{AM1.5} = 0.84$. The high emissivity similar to uncoated glass and the increased transmittance suggest that the coating was destroyed almost completely.

After three ageing phases, the ISE low-e coating reaches an emissivity of $\varepsilon_{373K} = 0.32$ from initially $\varepsilon_{373K} = 0.13$. There is no indication whether the emissivity decreases further beyond that point or stabilizes around $\varepsilon_{373K} = 0.32$. The transmittance was not affected by the ageing process and remains at a constant level of $\tau_{AM1.5} = 0.79$.

No change of optical properties of both K Glass samples, with and without AR coating, were observed, not even after six days of outdoor exposure with strong rainfall. The same applies for the Euroglas coating. Note that the Euroglas sample differs from the low-e coating in Table 3.8 having an initial emissivity of $\varepsilon_{373K} = 0.21$ and transmittance of $\tau_{AM1.5} = 0.82$. However, the good humidity resistance should be identical for both Euroglas samples given the almost identical coating layout.

Both silver-based low-e coatings seem to corrode faster than the tin and zinc oxide coatings. This finding is in line with the results of Stazi et al. (2016), who found that "films with elevate silver percentages registered the worst physical and chemical resistances" after ageing. However, according to the authors, there exist approaches to increase the moisture resistance by means of doping with additional metals or additional thin films of moisture barrier.

3.7 Application aspects in glazed, unglazed and concentrating PVT collectors

In the previous sections, glazed PVT collectors were discussed, where the low-e coating was directly applied on PVT absorber surface. However, low-e coatings can theoretically be applied to all emitting surfaces to suppress radiative heat losses. Accordingly, the application on the front glazing may also be an

interesting option. Next to glazed PVT collectors, low-e coatings are also a suitable measure to reduce radiative heat losses in unglazed and concentrating PVT collectors. In the following section, efficiency aspects and practical considerations of the application of low-e coatings in glazed, unglazed, and concentrating PVT collectors are discussed.

Following the notation typically used in window glazing, Figure 3.26 illustrates the positions of low-e coatings in PVT collectors. Position 1 directly faces the environment and is thus exposed to humidity and external factors. Position 2 is located on the internal side of the front glazing. The position on the PVT laminate in glazed or concentrating collectors is defined as position 3.

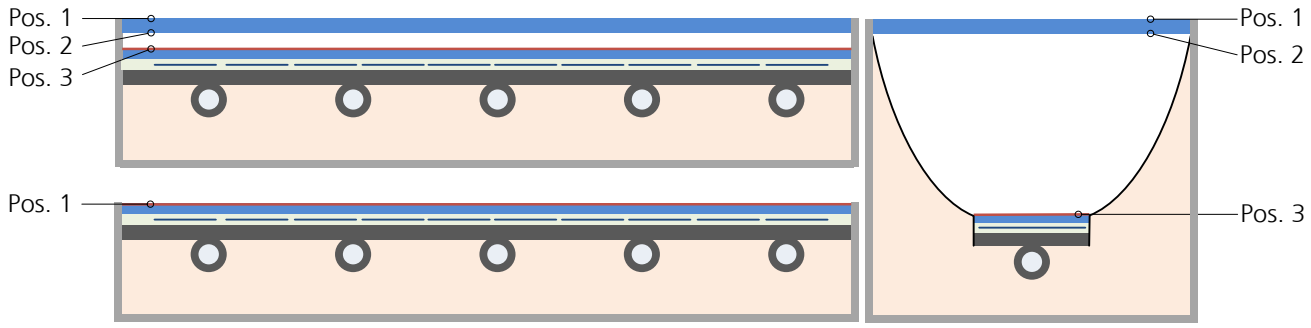

Figure 3.26: Applications of low-e coatings on different positions in a glazed collector (top), unglazed collector (bottom), and concentrating collector (right).

The favorable application of low-e directly on the module glass on position 3 is not always technically feasible. Firstly, some PVT collectors use materials other than glass for the protection of the PV cells. Instead of glass, polymer films such as FEP or ETFE (Dupeyrat et al. 2011c), protective silicone lacquers, or gas-filled encapsulation-free PV modules (Mittag et al. 2015) can be used. In these cases, the feasibility of applying low-e coatings on each specific substrate needs to be verified individually. Secondly, the introduction of low-e coated, thermally toughened module glass in the production process might cause problems. If commercial PV modules "from the shelf" are used, the low-e coating needs to be deposited on each PV module after lamination individually at potentially high costs. Preferably, low-e coated, thermally toughened glass is inserted directly in the production process, provided the availability at desired thickness and type of the glass substrate. In case the application of low-e on position 3 proves to be unfeasible, low-e coatings can be alternatively applied on position 1 or position 2, however with a lower thermal efficiency.

Different configurations of glazed, unglazed, and concentrating PVT collectors are implemented in the numerical collector model to study the influence of low-e at different positions on $(\tau\alpha)_{eff}$, U_{Loss}, and the thermal and electrical efficiency. As boundary condition, the position of the low-e coating is varied, while all other glass surfaces have an AR coating. The optical properties of the ISE low-e coating are used for the simulation study because of its medium rate of absorptance. Simulation results are summarized in Table 3.10 and the corresponding thermal efficiency curves are depicted in Figure 3.27.

Table 3.10: Variation of the low-e position in glazed, unglazed, and concentrating PVT collectors.

Collector design	Description	Pos. 1	Pos. 2	Pos. 3	$\eta_{el,STC}$ [-]	$(\tau\alpha)_{eff}$ [-]	$U_{Loss,\Delta T=50\ K}$ [W/m²K]	$\eta_{th,0}$ [-]	c_1 [W/m²K]	c_2 [W/m²K²]
glazed PVT	no low-e	AR	AR	AR	13.8%	89.5%	8.8	0.67	6.4	0.03
	ISE low-e Pos. 1	low-e	AR	AR	12.7%	76.2%	7.9	0.58	5.9	0.03
	ISE low-e Pos. 2	AR	low-e	AR	12.7%	76.2%	5.4	0.59	4.0	0.02
	ISE low-e Pos. 3	AR	AR	low-e	12.7%	83.2%	5.4	0.66	4.0	0.02
unglazed PVT	no low-e	-	-	AR	14.2%	92.7%	20.5	0.50	13.4	0.02
	ISE low-e Pos. 1	-	-	low-e	13.0%	86.0%	13.8	0.54	9.9	0.03
concentrating PVT	no low-e	AR	AR	AR	10.7%	81.9%	6.1	0.68	3.99	0.01
	ISE low-e Pos. 1	low-e	AR	AR	9.9%	69.6%	5.8	0.58	3.85	0.01
	ISE low-e Pos. 2	AR	low-e	AR	9.9%	69.6%	3.9	0.58	2.31	0.01
	ISE low-e Pos. 3	AR	AR	low-e	9.9%	76.1%	3.9	0.65	2.42	0.01

Applying low-e on position 1 on the front surface of the cover minimizes radiative losses from cover to ambient. In glazed collectors, the heat loss coefficient is thus reduced from U_{Loss} = 8.8 W/m²K to 7.9 W/m²K at ΔT = 50 K according to the numerical model. Convective heat losses by wind convection dominate U_{Loss}, reducing the effect of low-e at this position. This results in a lower efficiency in glazed PVT collectors compared to configuration without low-e, owing to the significant reduction of $(\tau\alpha)_{eff}$ by 13.2 $\%_{abs}$.

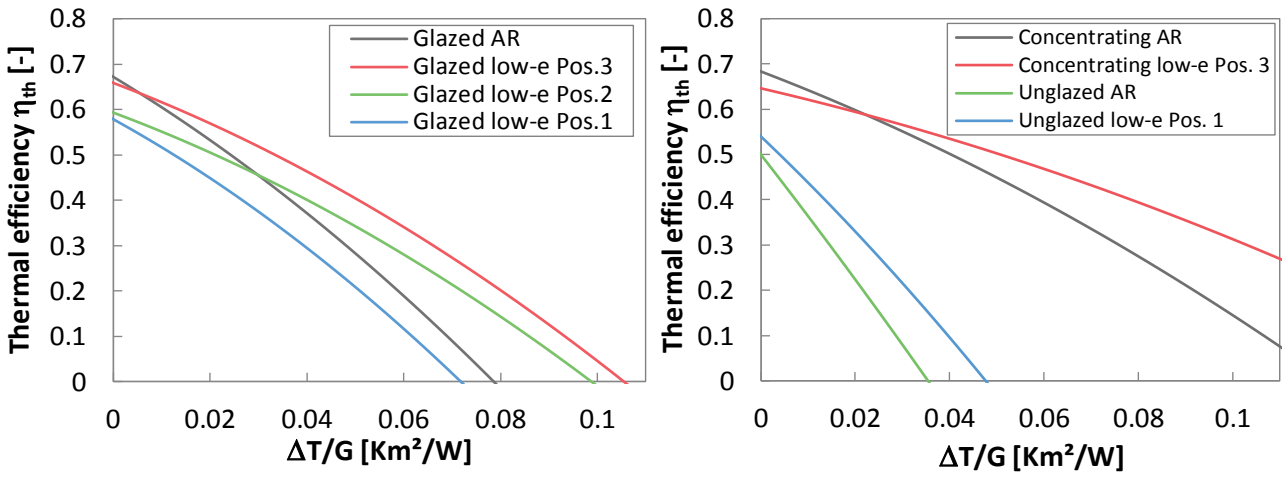

Figure 3.27: Application of low-e coatings in a glazed PVT collector on three different positions (left). Application of low-e in unglazed PVT collectors and concentrating PVT collectors (right).

Nonetheless, low-e coatings at the front cover are an interesting option for unglazed PVT collectors, where the surface temperature and thus radiative losses are higher (Giovannetti et al. 2014). In the simulated configuration, the low-e coating reduces the overall heat losses from U_{Loss} = 20.5 W/m²K to 13.8 W/m²K resulting in an increase of the standard stagnation temperature from T_{stg} = 80 °C to 93 °C. Resistance to weathering, humidity, and soiling poses a challenge for low-e coatings on position 1.

Owing to the symmetry of Eq. (3.12), the radiative heat loss coefficient h_{rad} and consequently U_{Loss} remain unaffected whether the coating is applied at position 2 or position 3. However, due to the increased absorptance in the metal layers, the absorbed heat in the low-e coating is not utilized if low-e is applied at the front cover. The vast majority of energy absorbed in the front cover is lost to the ambient because of the poor thermal contact between front cover and fluid, resulting in a drop of the effective transmittance-absorptance product $(\tau\alpha)_{eff}$. Low-e coatings with a low absorptance $\alpha_{AM1.5,}$ e.g. Euroglas low-e coating, are recommended for the application on position 2.

The application of low-e in concentrating PVT collectors is also promising, although the concentration of irradiation itself has the effect of reducing hot absorber areas and thus radiative heat losses. That being the case, low-e has the biggest benefit in low concentrating collectors, where radiative heat losses account for a substantial share of heat losses. The same qualitative considerations as for glazed, flat plate PVT collectors also hold true for low-e in concentrating PVT collectors on position 1, 2, and 3. However, since already the concentration itself decreases the optical efficiency, low-e on position 3 is recommended to avoid a further reduction of $(\tau\alpha)_{eff}$. Another advantage of low-e on position 3 is a smaller coating area, which could potentially reduce coating costs. Collector simulations were performed for a low-concentration PVT collector design with concentration ratio of C = 2.4 based on the collector design parameters given in Pröll et al. (2016). For the simulations, the numerical model was adapted in order to include concentration, while the convective heat loss model was not modified. According to the numerical results, the overall heat loss coefficient can be reduced from U_{Loss} = 6.1 W/m²K to 3.9 W/m²K at ΔT = 50 K by applying low-e to position 2 or 3.

To conclude, low-e coatings are a suitable measure of reducing radiative heat losses in all types of PVT collectors. Next to the favorable application directly on the module glass, low-e can also be applied to the front cover. However, this reduces $(\tau\alpha)_{eff}$ significantly, depending on the absorptance of the low-e coating. The effect of the position of low-e on the electrical efficiency is negligible.

4 ASSESSMENT OF PVT SYSTEMS

The following chapter concerns the assessment of electrical and thermal yields in PVT systems with the following research questions:

- Which factors influence electrical and thermal yields?
- Which PVT technology is suitable for which application, especially concerning PVT collectors with low-e?
- What are the energetic benefits and the economic expenses of PVT systems?

Firstly, chapter 4.1 presents an empirical performance model of PVT collectors based on standard efficiency parameters, which is suitable for annual system simulations. In chapter 4.2, the simulation framework is defined concerning the reference electrical and thermal PVT systems and investigated PVT technologies. Chapter 5.3 contains the detailed assessment of the electrical and thermal collector yields in these systems. Chapter 4.4 describes the novel characteristic temperature approach, the correlation of T_{char} with collector yields, and possible fields of application. After the detailed analysis of collector yields, chapter 4.5 evaluates the system performance concerning useful system yields and the added value of PVT collectors. Based on their thermal operation within the system context, chapter 4.6 draws conclusions on an optimized engineering of PVT collectors. Finally, chapter 4.7 analyses the economic feasibility of the PVT system by a techno-economic assessment of collector prices, system costs, and the levelized costs of electricity and heat. [4]

4.1 PVT collector performance model

4.1.1 Introduction, motivation and literature review

The assessment of annual yields of PVT collectors under "real" operating conditions can only be carried out on the system level. There, the collector, weather, load profile, storage, control and their interaction are taken into consideration. For simulating PVT systems, a PVT collector performance model based on standardized performance parameters is necessary. The use of a detailed, physical collector model as described in chapter 3.1 is impractical due to high computation times and, what is even more important,

[4] The major findings of the following chapter are also published in the paper "PVT collector technologies in solar thermal systems - a systematic assessment of electrical and thermal yields with the novel characteristic temperature approach" (Lämmle et al. 2017b). Chapters 4.1, 4.2, 4.3, 4.4, and 4.5.3 contain literal fragments of the paper. These fragments are not marked as citations to facilitate the legibility for the reader. While acknowledging the co-authors valued contributions, the author claims authorship and responsibility for these sections. An explicit citation of literal fragments is therefore omitted.

the unavailability of collector data, which is required for the consistent comparison of different types of collectors. Manufacturers, test certificates, and scientific publications mainly include standard performance parameters. Therefore, the simulation of annual yields of PVT systems requires a PVT collector performance model, which is based on standard performance parameters, but nonetheless considers the interdependence of simultaneous electrical and thermal operation (Figure 4.1).

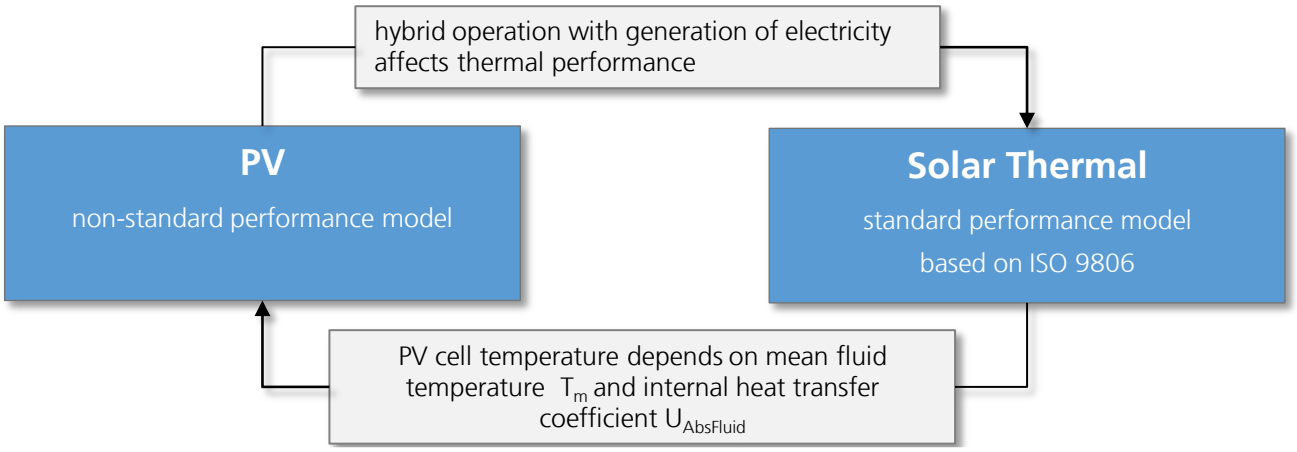

Figure 4.1: Interaction of electrical and thermal performance in PVT collectors.

Current standards do not address the interaction of thermal and electrical operation in PVT collectors with regards to a standardized approach for characterizing and modelling their performance (Kramer and Helmers 2013).

The characterization of the electrical performance according to the corresponding standard IEC 61853 (2011) includes, amongst others, standard test conditions, nominal operating conditions, and the measurement of temperature coefficients. Yet, the operation in a PVT collector differs from these standard measurements due to the influence of the flow of heat transfer fluid and the resulting temperature distribution in the PV cells.

The standard for solar thermal collectors ISO 9806:2013 allows tests in both open circuit (OC) and maximum power point (MPP) conditions, despite the known influence of the electrical operation on the thermal performance. Nonetheless, the Solar Keymark Network guidelines (SKN 2015) specify the requirements for PVT collector certification, according to which the PVT collector should be operated in MPP mode.

Regarding modelling the PVT performance, the most basic approximation sets the cell temperature equal to the mean fluid temperature, which is for instance used in the simulation software Polysun (Vela Solaris 2013). A more accurate approach was brought forward by Florschuetz (1979), who extended the Hottel-Whillier-Bliss equation and coupled the cell temperature to the fluid temperature by a heat transfer coefficient. This approach is the most widely used approach in the literature to model the electrical performance of PVT collectors (e.g. Zondag et al. (2002b), Chow (2003), Perers et al. (2012), Bilbao and Sproul (2015)).

Stegmann et al. (2012) developed a PVT performance model for TRNSYS which uses standard performance parameters but is restricted to unglazed PVT collectors. Fritzsche et al. (2014) and Zenhäusern et al. (2015) developed an empirical correlation to couple cell and fluid temperature by measuring an equivalent cell temperature during stationary, indoor performance tests and correlating the equivalent cell temperature with irradiance, fluid temperature, and the wind velocity. In a different approach, Helmers and Kramer (2013) extended the quasi-dynamic method to simultaneously characterize the elec-

trical and thermal performance in outdoor conditions, where the relevant performance parameters are identified by multiple linear regression.
All models have their specific strengths and weaknesses, which are discussed in Schmidt et al. (2017). There is, however, currently no standardized modelling and testing approach, while research activities in this field are ongoing to harmonize the characterization of collectors and their underlying performance models.
To bridge this gap, a custom, empirical performance model was developed. This PVT model builds up on the two-node model by extending the standardized thermal model with an explicit node for the mean cell temperature T_{cell}, which is coupled to the mean fluid temperature T_m by the internal heat transfer coefficient $U_{AbsFluid}$. Hence, the performance model can mostly use the standardized electrical and thermal performance models and their corresponding set of performance data.

4.1.2 Electrical performance model for PV modules

A consistent comparison between the electrical yield of PV modules and PVT collectors requires a performance model with consistent assumptions for both technologies. The major difference between PV modules and PVT collectors concerns the governing cell temperature, which is primarily determined by the fluid temperature in PVT collectors, and by the steady-state module temperature in PV modules.

The electrical performance model takes into account loss effects of incidence angle, irradiance, temperature, cable and inverter during every time step by modelling their specific contribution to the performance ratio. The performance ratio is a useful indicator to compare the quality of a PV system on an annual basis at different locations and is defined as (Goetzberger and Hoffmann 2005):

$$PR_{tot} = \frac{E_{PV}}{\eta_{STC} \cdot I_{tot}} \tag{4.1}$$

The instantaneous performance ratio due to incidence angle losses can be expressed as (Duffie and Beckman 2013):

$$PR_{IAM} = 1 - \mathrm{b}_0 \left(\frac{1}{\cos \theta} - 1 \right) \tag{4.2}$$

with a typical value of $b_0 = 0.07$ for PV modules (King et al. 2004).

The temperature dependence of the electrical efficiency is expressed as (Skoplaki 2008):

$$PR_T = 1 - \gamma \left(T_{cell,PV} - 25\,°C \right) \tag{4.3}$$

with a typical power temperature coefficient of $\gamma = 0.43$ %/K.

The temperature of the PV module is calculated by (Faiman 2008):

$$T_{cell,PV} = T_a + \frac{G}{U_0 + U_1\, u} \tag{4.4}$$

with the constants of a crystalline PV module $U_0 = 30.02$ W/m²K and $U_1 = 6.28$ Ws/m³K (Koehl et al. 2011).

The low irradiance behavior is described by (Heydenreich et al. 2008):

$$PR_G = a\,G + b\,ln(G+1) + c[\frac{(\ln(G+e))^2}{G+1} - 1] \tag{4.5}$$

with the irradiance G in the unit W/m² and the dimensionless Euler's number e [sic!]. Typical values for crystalline PV modules are a = -0.0000109 m²/W, b = -0.047, and c = -1.40.

On the system side, cable and inverter losses are considered. The performance ratio reduction due to the effect of ohmic cable losses is modelled by:

$$PR_C = 1 - 0.02\,(\frac{P_{PV}}{P_{STC}})^2 \tag{4.6}$$

assuming a maximum of 2 $\%_{rel}$ losses during peak operation (Santbergen et al. 2010).

The performance ratio of the inverter is given by (Schmidt and Sauer 1996):

$$PR_I = -\frac{1+v_{switch}}{2r_{ohm}p_{DC}} + \sqrt{\frac{(1+v_{switch})^2}{(2r_{ohm}p_{DC})^2} + \frac{p_{DC}-p_{own}}{r_{ohm}p_{DC}^2}} \tag{4.7}$$

with the direct current PV output p_{DC}, and the inverter specific constants p_{own} = 0.016, v_{switch} = -0.0046, r_{ohm} = 0.047, which represents an inverter with a peak efficiency of 95 %.

Altogether, the overall instantaneous performance ratio PR_{tot} consists of:

$$PR_{tot} = \mathrm{PR}_{IAM} \cdot \mathrm{PR}_T \cdot \mathrm{PR}_G \cdot \mathrm{PR}_C \cdot \mathrm{PR}_I \tag{4.8}$$

The instantaneous specific electrical power output p_{PV} is then given by:

$$p_{PV} = \eta_{\mathrm{el,STC}} \cdot \mathrm{PR}_{tot} \cdot G \tag{4.9}$$

The correlations for the PV performance in Eqs. (4.1) - (4.9) are implemented into TRNSYS by a generic performance model. The electrical performance model disregards effects due to air mass and corresponding spectral variations (compare King et al. 2004) because their impact on the annual performance was found to have an negligible effect on annual yields. Furthermore, it is assumed that the PV module remains unshaded throughout the year, and no power degradation of the module efficiency takes place.

Figure 4.2 summarizes the annual performance ratio of a c-Si PV module and depicts the contribution of the individual loss mechanisms to the annual performance ratio. IAM, temperature, and irradiance loss are assigned to the module losses, while cable losses and inverter losses are assigned to system losses.

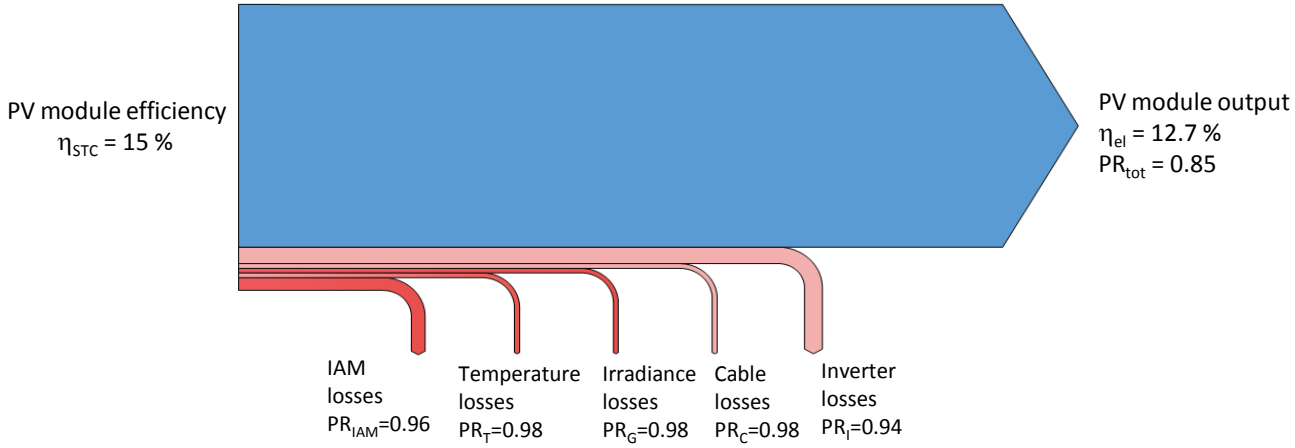

Figure 4.2: Sankey diagram for the annual electrical performance of a c-Si PV module in Würzburg.

4.1.3 Solar thermal collector model (ISO 9806)

The versatile quasi-dynamic model forms the basis for the thermal PVT collector performance model, which takes into account the dependence on direct and diffuse radiation, fluid temperature, wind speed, incidence angle effects, and capacity (ISO 9806 2013):

$$\dot{q}_{useful} = \eta_0(K_{\theta b}(\theta)G_b + K_{\theta d}(\theta)G_d) - c_6 uG - c_1(T_m - T_a) - c_2(T_m - T_a)^2 - c_3 u(T_m - T_a) + c_4(E_L - \sigma T_a^4) - c_5 dT_m/dt \quad (4.10)$$

The performance coefficients $\eta_{th,0}$ and $c_1 - c_6$ can be evaluated by multiple linear regression after outdoor characterization of the collector. Depending on the collector technology, some of the coefficients $c_1 - c_6$ may show an insignificant sensitivity and can therefore be set to zero.

For example, the coefficient for wind speed dependence of thermal losses c_3 is typically not evaluated for glazed collectors but set to zero. Nonetheless, the heat losses increase with higher wind speeds despite the front cover. As a result, the efficiency and also stagnation temperatures depend on the wind speed and the performance coefficient c_3. To investigate this effect, two sample PVT collectors ("PVT03-vented" and "PVT06-glued2") were tested outdoors and, deviating from the standardized procedure, the parameter c_3 was identified. A wind speed dependence of c_3 = 0.27 J/m³K (PVT03) and c_3 = 0.22 J/m³K (PVT06) was found for these collectors, which is slightly lower than typical values for flat plate collectors (c_3 = 0.36 J/m³K, Fischer 2011), due to the predominant influence of radiative heat losses in PVT collectors.

4.1.4 PVT collector performance model

The two-node collector model, which is also used for the physical collector model in chapter 3.1, forms the basis for the empirical PVT collector performance. Accordingly, the mean cell temperature $T_{cell,PVT}$ is equal to the absorber temperature T_{abs}, which according to the two-node model is given by:

$$T_{cell,PVT} = T_{abs} = T_m + \frac{\dot{q}_{useful}}{U_{AbsFluid}} \quad (4.11)$$

$T_{cell,PVT}$ is used as an explicit value to calculate the temperature-related electrical performance ratio PR_T with Eq. (4.3) during every time step. Except for the different procedure for calculating cell temperatures,

the identical performance model is used as for PV modules for modelling IAM, irradiance, cable, and inverter losses. Regarding the incident angle modifier, the electrical IAM is set equal to the thermal IAM if no separate test data for the characterization of the electrical IAM is available (Perers et al. 2012).

The electrical mode of operation has a significant impact on the thermal efficiency (Hofmann et al. 2010). It is for this reason that the collector has to be operated in its realistic electrical mode during testing, i.e. in hybrid operation with the electrical power tracked in maximum power point (MPP).

Theoretically, it is also possible to convert the thermal efficiency from open circuit (OC) mode to the MPP mode. However, the interaction of electrical and thermal operation is physically complex and the mathematical conversion relies on several assumptions on the internal heat transfer and the nature of heat loss paths (Helmers and Kramer 2013). Accordingly, a mere subtraction of the electrical power from the thermal power in OC mode is physically incorrect.

A new procedure for the conversion of OC to MPP performance coefficients was specifically developed for the purpose of performing system simulations for PVT collectors tested in OC mode. Appendix C.2 presents the mathematical background and a comparison of the thermal performance of PVT collectors, which were tested in both MPP and OC modes including the theoretical conversion.

Nonetheless, the direct characterization of the thermal performance coefficients in MPP mode is more accurate, due to the involved modelling assumptions of the new conversion procedure. Therefore, the PVT performance model neglects the feedback of electrical output on the thermal gains and the performance coefficients in Eq. (4.10) refer to the operation in MPP mode in any case.

There has been previous research on the two-node performance collector model for solar thermal collectors with different motivations. Rockendorf et al. (1993) compared the heat loss measurement without irradiance with efficiency measurement under irradiance by means of a two-node collector model. Wittwer and Rommel (1996) used the two-node model to model variable flow rates and a variable collector efficiency factor F'. Fischer and Müller-Steinhagen (2009) developed the two-node model further and they expect a significant reduction of test duration and therefore suggest to include the extended model to the European standard EN 12975.

All of the previous work utilize the two-node model because of the explicit notation of the mean absorber temperature T_{abs}. Thus, the two-node model extends the simple ISO 9806 model with the single temperature node T_m by an additional node for the absorber temperature T_{abs} without altering its validity. Figure 4.3 shows the one-node model juxtaposed to the two-node model for PVT collectors. In the following section, the differences between both models are explained, and a consistent procedure to obtain the additional input parameters, which are not characterized by the ISO 9806 tests, is presented.

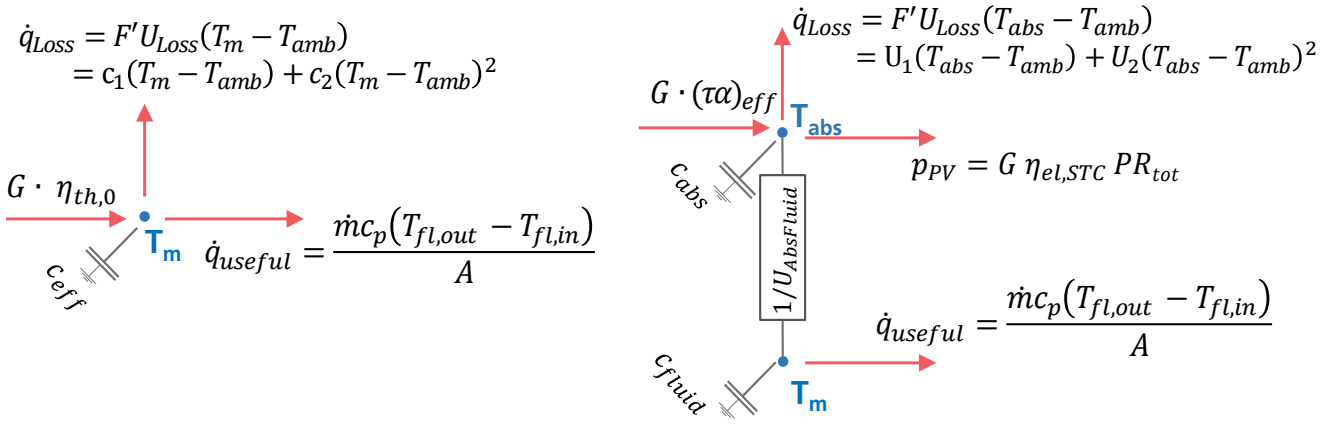

Figure 4.3: Comparison of one-node model for solar thermal collectors (ISO 9806) and the two-node model for PVT collectors (based on Fischer and Müller-Steinhagen 2009).

Analogous to the physical model, the two-node model couples the two nodes T_m and T_{abs} by the internal heat transfer coefficient $U_{AbsFluid}$. As discussed in chapter 3.2.5, numerical and experimental approaches can be used to determine $U_{AbsFluid}$ for a specific absorber design. However, the required absorber-specific parameters are mostly unknown for commercial PVT collectors, where typically test reports or data sheets are the only available source of information. In this case, a makeshift procedure can be applied, which uses measured test data to derive $U_{AbsFluid}$ on basis of the collector efficiency factor F'. For a description of the procedure, refer to Annex 0.

In contrast to the one-node model, where thermal losses are expressed as a function of T_m, the thermal losses in the two-node model are calculated as a function of T_{abs}. The latter represents a more exact representation of the physical phenomena, since T_{abs} governs the heat losses. However, this also needs to be taken into account when specifying the input parameters for the performance model. Instead of the standardized parameter set of $\eta_{th,0}$, c_1, and c_2, the parameters need to be corrected with the collector efficiency factor F' according to Table 4.1.

Table 4.1: Input parameters for the one-node and two-node collector model.

Input parameter	One-node model (ISO 9806)	Two-node model (PVT collector)
conversion factor	$\eta_{th,0}$	$(\tau\alpha)_{eff} = \eta_{th,0}/F'$
linear heat loss coefficient	c_1	$U_1 = c_1/F'$
quadratic heat loss coefficient	c_2	$U_2 = c_2/F'$

In contrast to the single, effective capacity c_{eff} in the one-node model, the two-node model uses the discrete thermal capacities c_{abs} and c_{fluid} for each node. For this purpose, c_{eff} has to be distributed on c_{abs} and c_{fluid}:

$$c_{eff} = c_{abs} + c_{fluid} \tag{4.12}$$

A good agreement between experiment and simulation is observed, if c_{eff} is halved and distributed equally on c_{abs} and c_{fluid}:

$$c_{abs} = c_{fluid} = \frac{c_{eff}}{2} \tag{4.13}$$

Weißmüller et al. (2012) observed high deviations of the effective capacity c_{eff} in a round-robin test, if c_{eff} is characterized with the quasi-dynamic method. This may be due to a small variance of T_m in the test sequences. A significantly improved agreement with experimental results is achieved if c_{eff} is calculated from the material properties of the collector, applying the weighting factors according to ISO 9806. For instance, the quasi-dynamic method for "PVT06-glued2" yielded c_{eff} = 80.0 kJ/m²K, while the calculated capacity amounts to c_{eff} = 15.9 kJ/m²K. Owing to the entailed issues with using the capacity term identified by the quasi-dynamic method, the usage of the calculated capacity is highly recommended for conducting annual system simulations.

Stagnation is an important operating condition which existing performance models do not cover. PVT collectors continue to generate electricity during stagnation, whereas stagnation is irrelevant for the annual yields of solar thermal collectors. For PVT systems, a correct model is however important and can have a strong influence on the simulation of yields. Therefore, the state of stagnation is specifically analyzed for the new PVT performance model.

During stagnation, the thermal power $\dot{q}_{th}$ is zero and as a consequence of the two-node model, the cell temperature equals the mean fluid temperature $T_{cell,PVT} = T_m$. Comparing the simulated model output with the experimental electricity output, an acceptable agreement is observed (Figure 4.5, day 3). Therefore, Eq. (4.10) describes the cell temperatures with sufficient accuracy for the case of stagnation. Due to the good agreement, no additional correlations for stagnation are required. This is an important finding for achieving a high accuracy of the electrical performance model during stagnation conditions.

An even higher accuracy is achieved if the wind speed dependence of thermal losses c_3 is also taken into account. For instance, c_3 of "PVT06-glued" was experimentally determined as c_3 = 0.27 J/m³K. Taking into account this factor, the absorber would reach a stagnation temperature of T_{abs} = 128 °C at wind speeds of u_{wind} = 3 m/s according to simulations for a sunny summer day. In still air conditions at the otherwise identical day, the absorber temperatures reaches T_{abs} = 139 °C, which would result in a difference of the electrical efficiency of 4.7 $\%_{rel}$.

The two-node model according to Fischer and Müller-Steinhagen (2009) is already implemented in TRNSYS type 832 (Haller et al. 2012), which is also regarded as the most accurate and flexible solar thermal collector type currently available. Type 832 is therefore used for the system simulations, where the electrical performance model is coupled to type 832 via the mean absorber temperature T_{abs}.

4.1.5 Validation of the PVT collector performance model

The PVT performance model is validated by comparing simulation data with experimental measurements. For this purpose, two glazed PVT collectors, one with low-e coating ("PVT03-vented") and one without low-e coating ("PVT06-glued2") were monitored for 15 days at the outdoor test fields of the accredited test lab at Fraunhofer ISE. Both PVT collectors were fixed on a rack, connected to a thermostat, and attached to a MPP tracker. The thermostat emulated dynamic inlet temperature profiles in order to achieve realistic operating conditions. Highly accurate laboratory measurement equipment measured the weather

data and electrical and thermal collector power output. Prior to the monitoring period, the thermal input parameters were characterized based on the quasi-dynamic method. The electrical input parameters were characterized in a flasher at Fraunhofer ISE CalLab.

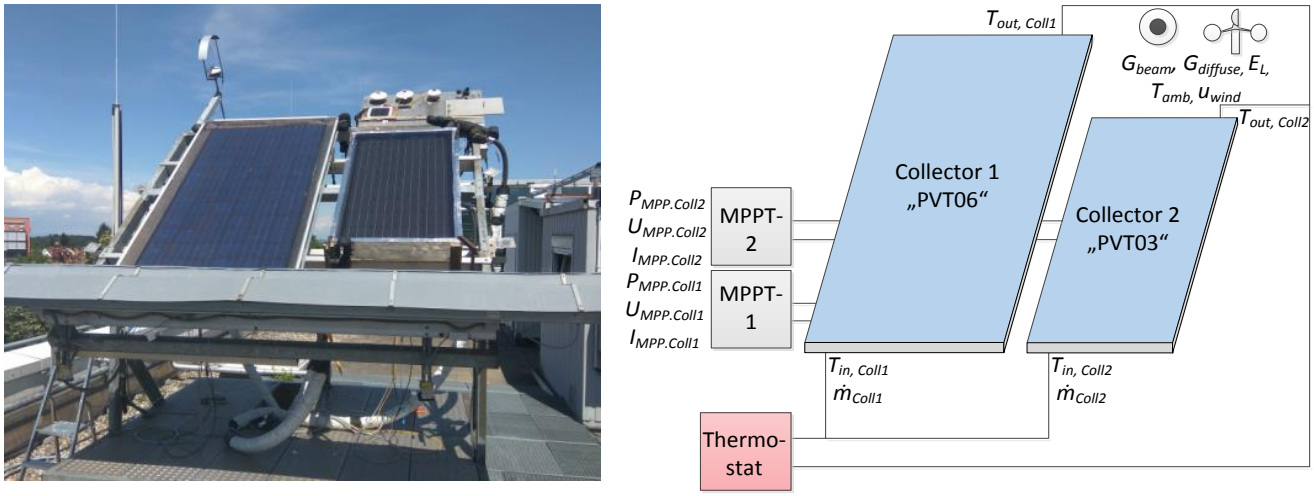

Figure 4.4: Set-up of the outdoor test-stand with two full-size, glazed PVT collectors: photo (left), and measurement schema (right).

In order to validate the PVT performance model, the same 15 days were simulated in TRNSYS in 0.1 h time steps using the measured weather data, collector inlet temperature, and mass flow rate as input data. Figure 4.5 depicts the experimental and simulated electrical and thermal power output on three representative test days of collector 2. The fluctuations in the thermal power of day one and two result from variations of the irradiance and the inlet temperature. On day three, the pump was switched off during noon in order to achieve stagnation conditions.

Good agreement between simulated and experimental results is observed. The thermal model reproduces accurately the steady-state situations, for instance during the morning and afternoon of day 3. However, the capacity term c_{eff} in Eq. (4.10) is not able to fully describe the dynamic behavior with varying levels of irradiance and inlet temperatures. The electrical model shows good agreement during most of the measurement period. Only at a high angle of incidence in early morning and late afternoon, the collector frame partially shades the PV cells, which results in a drop of the measured electrical power. The electrical performance model does not consider this effect, which explains the deviations between experiment and simulation.

The objective of system simulations is the accurate prediction of annual yields. Therefore, the major requirement of the performance model is a good reproduction of the cumulative thermal and electrical energy balance. The exact representation of the instantaneous power output plays a secondary role and small deviations may be accepted, if the effect on the cumulative energy balance is small. With this background, the model accuracy is assessed by means of the mean relative error of the electrical and thermal yield cumulated over the measurement period. In contrast to the validation of the numerical collector model, the root mean square error is not expedient here, because this error indicator overrates large deviations at singular time steps, e.g. when the pump is turned back on after stagnation.

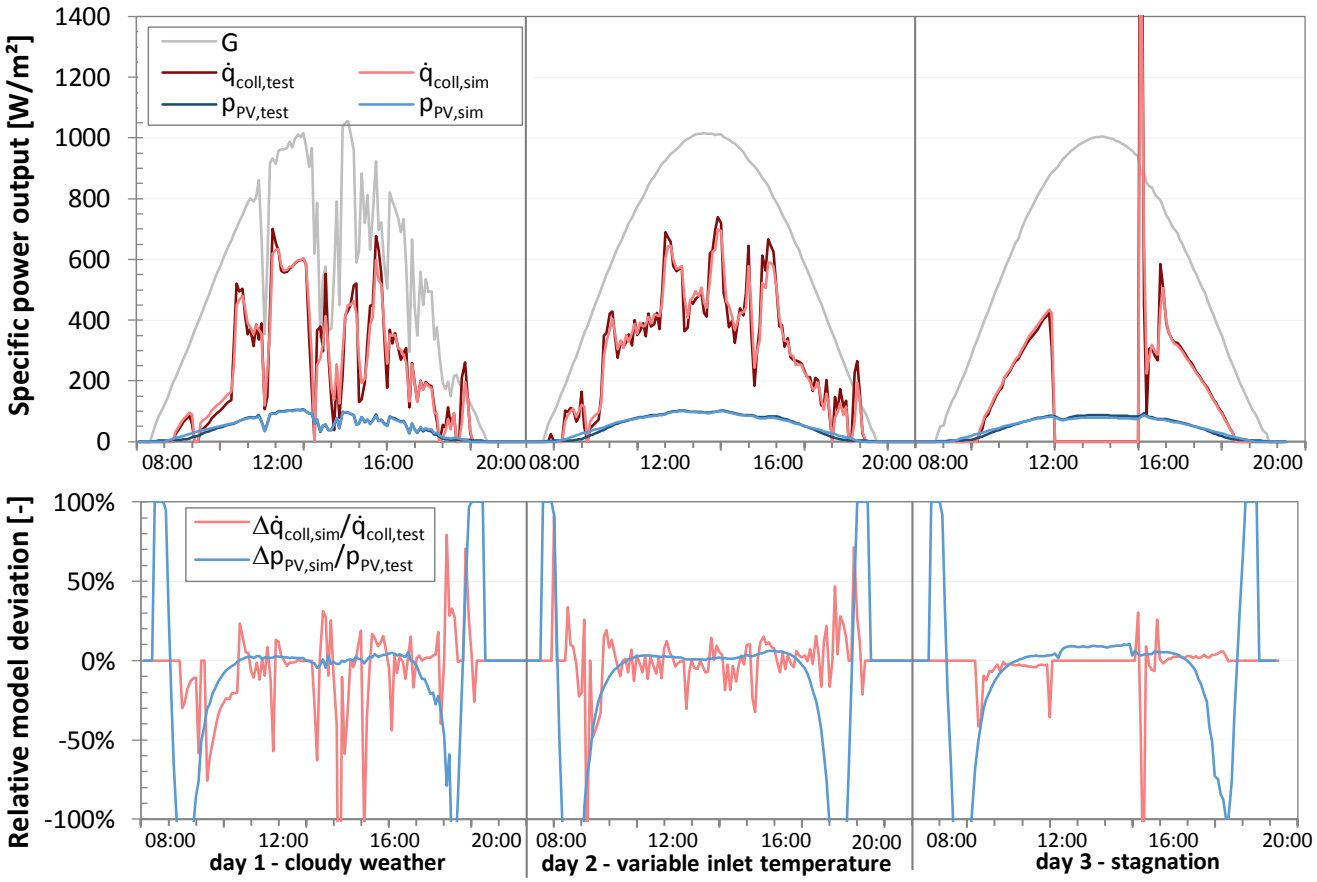

Figure 4.5: Validation of the PVT collector performance model: comparison of experiment and simulation at three reference days for "PVT03-vented".

The cumulative electrical yield E_{PV} is given by the integral over the power output:

$$E_{PV} = \int p_{PV}\, dt \tag{4.14}$$

The mean relative error ΔE_{PV} is then given by:

$$\Delta E_{PV} = \frac{E_{PV,test} - E_{PV,sim}}{E_{PV,test}} = \frac{\int (p_{PV,test} - p_{PV,sim})\, dt}{\int p_{PV,test}\, dt} \tag{4.15}$$

The cumulative thermal yield Q_{coll} and the thermal mean relative error ΔQ_{coll} are defined correspondingly. Table 4.2 documents the resulting mean relative error for both tested PVT collectors and for the combined overall PVT performance model.

The simulation model slightly underestimates the electrical yield with a mean relative error of ΔE_{PV} = -0.8 $\%_{rel}$ of PVT03 and ΔE_{PV} = 1.5 $\%_{rel}$ of PVT06. The thermal yield is overestimated with a mean relative error of ΔQ_{coll} = 0.6 $\%_{rel}$ of PVT03 and ΔQ_{coll} = 3.9 $\%_{rel}$ of PVT06. It is worth mentioning, that the fully standardized thermal performance model has a relatively large mean relative error of ΔQ_{coll} = 1.6 $\%_{rel}$ for the overall model, while the non-standard electrical performance model shows a better agreement with a mean relative error of ΔE_{PV} = 0.5 $\%_{rel}$. This might be caused by the measurement uncertainty, which is larger for the thermal power than for the electrical power. The measurement error of the electrical yield is estimated to be ±1 – 3 $\%_{rel}$ mainly due to the uncertainty of the MPP tracker, while the uncertainty of the thermal yield lies in the range of ±2 – 5 $\%_{rel}$.

Altogether, the accuracy of the PVT performance model lies within an acceptable range, which allows the conduction of annual simulations on the system level.

Table 4.2: Uncertainty assessment of the PVT performance model.

	PVT03-vented		**PVT06-glued2**		**Overall model**	
	Electrical	Thermal	Electrical	Thermal	Electrical	Thermal
Measured yield E_{test}, Q_{test} [kWh/m²]	6.09	30.75	7.89	29.27	13.98	60.02
Simulated yield E_{sim}, Q_{sim} [kWh/m²]	6.14	30.56	7.77	30.44	13.92	61.01
Mean relative error ΔE_{PV} / ΔQ_{coll} [-]	-0.8 $\%_{rel}$	0.6 $\%_{rel}$	1.5 $\%_{rel}$	-4.0 $\%_{rel}$	0.5 $\%_{rel}$	1.6 $\%_{rel}$

4.1.6 Discussion and outlook

Despite the good agreement with experimental results, the performance model is subject to several assumptions and is therefore limited in its validity.

Firstly the performance model is based on the two-node collector model with its underlying notion that the thermal losses are solely governed by the absorber temperature, a constant internal heat transfer coefficient $U_{AbsFluid}$ couples the absorber and fluid temperatures, and the mean cell temperature equals the mean absorber temperature. While the two-node collector model shows a relatively good agreement with glazed PVT collectors, its validity for unglazed PVT collectors is doubtful when comparing model results with experimental observations.

Secondly, the additional model parameters $U_{AbsFluid}$ and c_{fluid} have to be determined from standardized test results with an alternative, makeshift approach. This approach underlies model assumptions and involves high levels of uncertainty. For instance, small variations of the performance parameters $\eta_{th,0}$, $(\tau\alpha)_{eff}$ and F' result in high variations of $U_{AbsFluid}$ during its calculation from F'.

Thirdly, the feedback of electrical operation on the thermal performance is neglected in the performance model. Therefore, it is essential that the thermal performance coefficients are determined during MPP operation. Then the electrical efficiency of simulation and test only differs due to variations of irradiance and absolute temperature. With a conservative estimate, this influence on the instantaneous thermal efficiency can be narrowed down to a maximum deviation of less than 2 $\%_{abs}$.

Future research should aim at a standardized performance model for PVT collectors, where all required model parameters are obtained from standardized collector characterization procedures. With such a harmonized model, more accurate simulation results can be expected due to a more realistic determination of performance coefficients. Additionally, a standardized performance model facilitates the comparison of PVT collectors which were tested in different facilities and in different test conditions. Some interesting approaches have been brought forward, e.g. by Helmers and Kramer (2013), Fritzsche et al. (2014), and Zenhäusern et al. (2015), but a consensus on a standardized model has not yet been reached.

4.2 Definition of PVT system simulations framework

The objective of the simulation study is the analysis and comparison of the yields and system performances of different PVT collector technologies in a wide band of different solar thermal applications. The following chapter introduces and defines the boundary conditions for this simulation study.

4.2.1 Definition of reference PVT collector technologies

One objective of the assessment of PVT systems is the comparison of collector technologies to identify suitable fields of applications. Flat plate, liquid-type PVT technologies are in the focus of the system assessment in addition to reference technologies, namely a PV module and a flat plate collector. All input data for the collectors originate from measurements on real PVT prototypes at Fraunhofer ISE. The following three PVT collector technologies are assessed:

- The **unglazed PVT collector** is a commercial product without back insulation featuring a high internal heat transfer coefficient $U_{AbsFluid}$ and mono-Si PV cells.
- The **glazed PVT collector** features mono-Si PV cells, directly laminated on a sheet-and-tube absorber made of aluminum and copper ("PVT02-no low-e").
- The **glazed PVT collector with low-e** features the same PV cells and identical collector design, but it is additionally equipped with the silver-based low-e coating by Fraunhofer ISE with $\varepsilon_{373K} = 0.14$ on the surface of the PV module ("PVT01-low-e").

In addition to the PVT collectors, a conventional PV module and flat plate collector are included as reference and technology benchmark:

- The reference **PV module** is a commercial glass-glass module with mono-crystalline PV cells and a rated module efficiency of $\eta_{el,STC} = 15$ %, corresponding to the efficiency and cell technology of the assessed PVT technologies.
- The reference **flat plate collector** represents the European market average and is a standard sheet-and-tube collector with spectrally selective absorber coating.

Figure 4.6 depicts the corresponding efficiency curves and Table 4.3 summarizes the electrical and thermal input parameters.

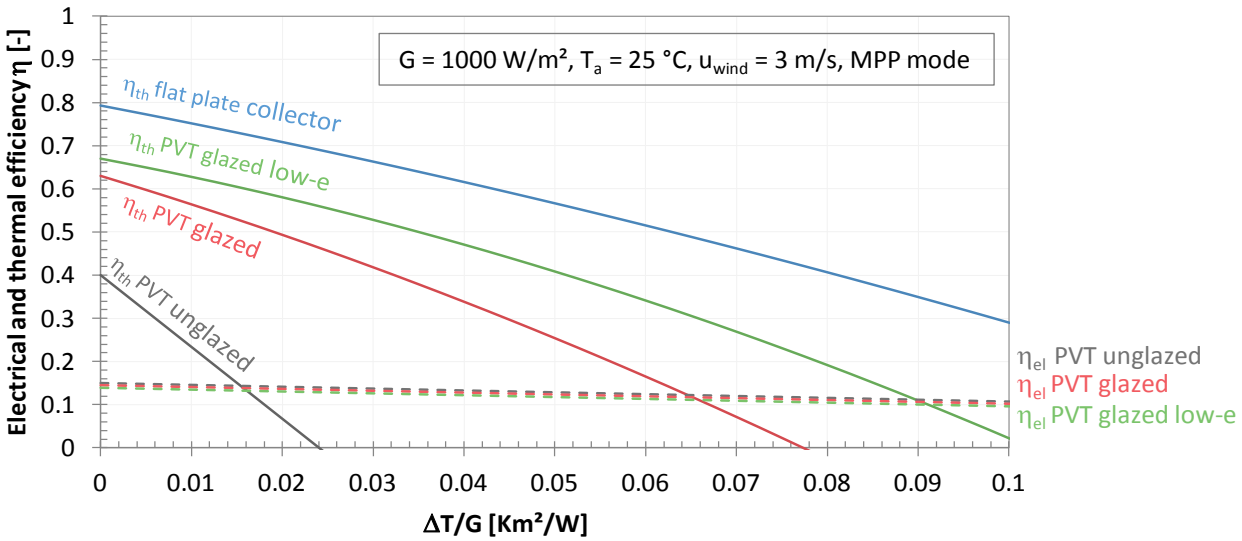

Figure 4.6: Electrical and thermal efficiency curves of the investigated collectors.

The precise definition of collector area has a substantial influence on the evaluation of PVT technologies, as shows the following example. Figure 4.7 illustrates the relevant areas of the glazed PVT prototype "PVT01-low-e". The PV module areas covers only 88 % of the aperture area to avoid partial shading from the collector frame. Furthermore, the inactive collector frame occupies 13 % of the gross collector area, owing to the small collector dimensions. Relating the energy yield to the gross area A_g, aperture area A_{ap} or PV module area A_{PV} makes a difference of up to 22%.

Table 4.3: Electrical and thermal performance coefficients of the investigated collector technologies.

	Parameter	Unit	PV mod-ule	PVT unglazed	PVT glazed	PVT glazed low-e	Flat plate collector
Electrical	$\eta_{el,STC}$	-	15.0%	15.0%	14.5%	13.9%	
	γ	%/K	0.43	0.43	0.43	0.43	
Thermal	$\eta_{th,0}$	-		0.58	0.63	0.67	0.793
	c_1	W/m²K		12.5	6.37	3.98	4.03
	c_2	W/m²K²			0.023	0.025	0.01
	c_3	-		1.38			
	c_6	s/m		0.06			
	c_{eff}	kJ/m²		16.3	10.143	10.143	5.2
	b_0	-		0.09	0.15	0.17	0.09
Thermo-electrical coupling	$U_{AbsFluid}$	W/m²K		65.5	62.1	61.2	

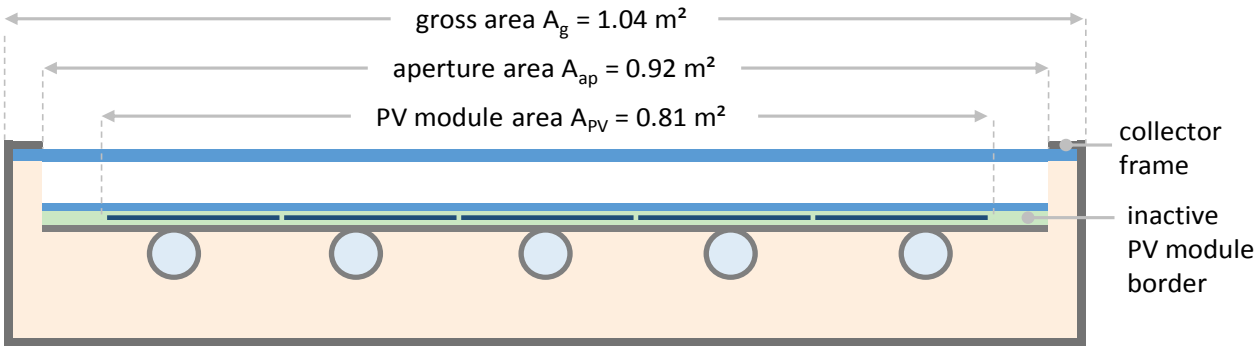

Figure 4.7: Definition of gross, aperture, and PV module area at the example of "PVT01-low-e".

Based on these considerations, the following conventions apply. The efficiency and specific yields are reported relative to the technologically relevant areas. For the electrical efficiency this means the PV module area A_{PV}, and for the thermal efficiency the aperture area A_{ap}. Thus, the inactive areas of the collector frame and module border are disregarded for the yield assessment. For the comparison of PVT systems with regards to utilization of roof area, effective gross areas are used. While for PV modules and unglazed PVT collectors gross, aperture and PV module areas are equal ($A_g = A_{ap} = A_{PV}$), the following aspect ratios are used for glazed PVT collectors corresponding to a PVT collector of 2 m² size: A_g/A_{ap} = 1.09, and A_{ap}/A_{PV} = 1.09.

4.2.2 Definition of reference solar thermal systems

The solar thermal system in which the PVT collector is operated in substantially affects the electrical and thermal yields. Amongst others, the system is characterized by its hydraulic layout, the sizing of storage and collector field, design temperatures of the heat supply system, and the system control. Considering the specific interplay between the collector, system components, weather, control, and user behavior, it is essential to always regard the collector yield within its system context.

While numerous studies and existing publications focus on one specific system, the present approach implies the simulation of varying PVT collector technologies in different systems. To date, only Zondag et al. (2001) compared the performance of unglazed and glazed PVT collectors in different PVT systems (DHW, combi, and heat pump in S/R configuration). Since that time, however, there was significant progress in the development of PVT collectors, especially concerning low-e coatings.

Four reference systems are investigated, which cover a broad range of potential applications with varying levels of operating temperatures.

- **System (a) - Heat pump (HP) system in a single-family house (SFH)** supplies space heat and domestic hot water by a ground coupled brine-water heat pump. A synergetic integration of PVT collectors can be reached when the PVT collector is coupled to the heat pump as heat source or for the regeneration of a ground heat exchanger, which potentially offers lowest collector temperatures.
- **System (b) - Domestic hot water (DHW) system in a multi-family house (MFH)** is typically dimensioned in such a way that a relatively low solar fraction is reached. Hence, the water is mostly preheated and operating temperatures in the collector circuit are lower.

- **System (c) - Domestic hot water (DHW) system in a single-family house (SFH)** is the classical system for solar thermal collectors and is therefore considered a promising application with a potentially big market for PVT collectors (Zondag et al. 2006).
- **System (d) - Combined DHW and space heating (Combi) system in a single-family house (SFH)** is a challenging application with high requirements for the thermal efficiency of the PVT collector, since the heat demand occurs mostly in winter, with low levels of irradiance and low ambient temperatures.

The basic hydraulic layout of the four systems with corresponding reference collector and storage dimensions are depicted in Figure 4.8. The reference dimensions of collector and storage are chosen according to typical values found in the reviewed publications, which are presented with more detail in the following paragraph.

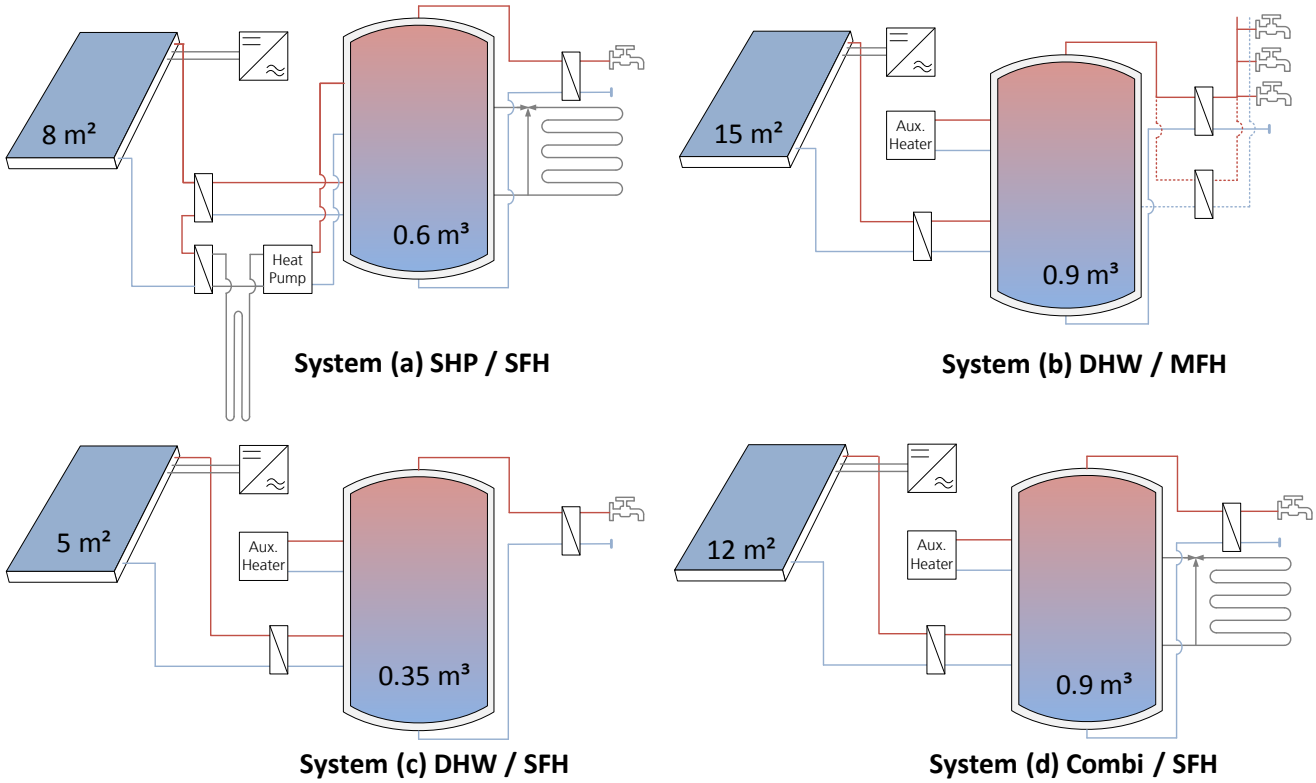

Figure 4.8: Hydraulic layout of the solar thermal systems (a) – (d) with reference dimensions of collector aperture area A_{ap} and storage volume V_{stor}.

4.2.2.1 System (a) – SHP + SFH

System (a) is a solar heat pump (SHP) system to provide domestic hot water and space heat to a single-family house (SFH). The heat pump delivers heat to a central storage tank, and a PVT collector array constitutes an additional heat source. The combination of PVT collectors and heat pump systems bears the advantage of low collector temperatures.

Solar thermal heat pump systems offer several hydraulic integration concepts (Ruschenburg et al. 2013). In the parallel configuration (P), PVT collectors operate independently from the heat pump and the solar heat feeds directly to the storage. The serial configuration (S) describes the coupling of the PVT collector to the evaporator as an exclusive or additional source for the heat pump. Furthermore, PVT collectors can

be used for the regeneration (R) of a ground source. Typical systems comprise a combination of the parallel, serial, and regeneration configurations. The performance of unglazed PVT collectors was assessed in a P/S/R system by Bakker et al. (2005), in a S/R system by Bertram et al. (2012), and in P, P/S, and P/S/R systems by Ille et al. (2014).

The reference PVT heat pump system in this assessment is a P/R system, meaning that the solar heat can be used to directly deliver heat to the storage (P), or to regenerate the borehole (R). Under energetic considerations, the parallel operation is advantageous since the heat can be directly used without an additional conversion step of the heat pump.

The vertical borehole serves as a heat source for the brine-water heat pump. During regeneration (R), the PVT collector delivers heat to the borehole heat exchanger and thus avoids an undesired cooling of the ground in proximity to the borehole. Thus, the dimensions of the borehole heat exchanger can be reduced compared to a system without borehole regeneration (Bertram et al. (2012)). Moreover, the PVT collector raises the source temperature to reach a higher coefficient of performance (COP) of the heat pump. Concerning the operation of the PVT collector, regeneration reduces collector temperatures due to low ground temperatures and avoids stagnation of the collector array.

The option for a serial operation (S) is not considered, due to high variations of PVT collector outlet temperatures. Therefore, the solar heat always passes through the ground heat exchanger before entering the heat pump, so that temperature peaks are avoided.

In PVT heat pump systems, the electrical output of the PVT collector can be directly used to drive the compressor of the heat pump. However, the electrical performance of the heat pump is beyond the scope of this assessment. Therefore, it is also acceptable that the hydraulic implementation of the heat pump is not optimized towards a maximum COP of the heat pump, which for instance could be achieved by a sophisticated control strategy ensuring low heat pump outlet temperatures.

4.2.2.2 System (b) – DHW + MFH

System (b) is a multi-family home (MFH) system with solar thermal domestic hot water preheating. The hot water for ten households is supplied by a storage tank with an auxiliary gas heater and the solar heat is used to preheat the cold water in the bottom of the storage tank.

Rommel et al. (2014) assessed the performance of unglazed PVT collectors, and Matuska et al. (2015) compared the performance of unglazed, glazed, and glazed PVT collectors with low-e coatings in DHW systems in multi-family houses.

The set temperature for hot water draw-off amounts to T_{tap} = 60 °C at the households' tap with an overall daily hot water consumption of V = 1000 l/d, assuming a stochastically distributed tapping profile. In addition to the hot water demand, heat losses originating from circulation are considered. To avoid the formation of legionella, a permanent circulation of hot water at T = 60 °C has to be maintained in this four-pipe-configuration (Streicher 2012). The circulation line is reheated by an external heat exchanger and the recovered heat feeds back into the storage.

Due to a relatively constant heat load and relatively small dimensions of the collector array, DHW systems in multi-family houses have a low solar fraction and hence moderate collector temperatures. PVT collectors might be a suitable solution for multi-family homes as they potentially make optimum use of the limited available roof space in relation to the high energy demand of the building.

The hydraulic layout and load profile of system (b) is very similar to solar thermal systems for hotels, hospitals, and office buildings. A PVT collector system is installed for field tests in the new town hall buildings of the city of Freiburg, which is designed as the biggest plus energy building in Europe. There, glazed PVT collectors substitute the originally planned flat plate collectors to provide hot water to the kitchen and office taps.

4.2.2.3 System (c) – DHW + SFH

System (c) is a single-family house system with solar-assisted domestic hot water (DHW) preparation. This configuration is considered the classical solar thermal application with a potentially big market for PVT collectors (Zondag et al. 2006).

As such, system (c) is the most widely reviewed PVT system. Amongst others, Zondag et al. (2002b), Kalogirou and Tripanagnostopoulos (2006), and da Silva and Fernandes (2010) assessed the yields of glazed PVT collectors in DHW systems. Moreover, Santbergen et al. (2010) analyzed the effect of anti-reflection and low-emissivity coatings in glazed PVT collectors and Dupeyrat et al. (2014) compared the performance of unglazed and glazed PVT collectors.

The set temperature for the hot water draw-off of system (b) amounts to T_{tap} = 45 °C with a stochastically distributed tapping profile and daily draw-off rates of V = 175 l/d. This corresponds to a typical four-person household, which is also used as simulation boundary condition for the single-family house systems (a) and (d).

4.2.2.4 System (d) – Combi + SFH

System (d) is a single-family house system with combined solar hot water preparation and space heating. In Europe, combi systems are an important application and represent a share of 20 % of the solar thermal market (Mauthner et al. 2016).

The application of PVT collectors in combi systems was assessed by Fraisse et al. (2007) for unglazed and glazed PVT collectors with and without low-e, by Fortuin et al. (2014) for glazed PVT collectors with low-e, and by Good et al. (2015) for unglazed and glazed PVT collectors.

The space heating in system (d) is implemented by a floor heating system with low supply temperatures of 40 °C and the hot water preparation is identical to system (c). In general, the hydraulic system layout, control, and parametrization follow the reference heating system developed within the IEA SHC Task 32 (Heimrath and Haller 2007).

As the demand for space heating mainly occurs in winter and the transitional period with low levels of irradiance, sufficiently large collector areas and storage volumes are required. Amongst the investigated systems, the combi system imposes the most challenges for PVT collectors, because high temperatures are reached in summer due to a low heat demand. During the harsh climatic conditions of winter, a high thermal efficiency is required, where PVT collectors underperform compared to flat plate solar thermal collectors. Although the required floor heating supply temperatures are low, storage temperatures typically exceed this temperature, because the heat has to be stored for a longer period, which is achieved by a sensible increase of storage temperature.

Concerning the operation of the PVT collector, the combi system with auxiliary heater bears no significant differences to a solar thermal heat pump system in parallel configuration (P).

4.2.2.5 General boundary conditions of the solar thermal systems

The operation of the solar loop is controlled by a differential controller with a fixed mass flow rate of $\dot{m}$ = 45 kg/h per square meter of collector area. When the difference between collector outlet and storage is above ΔT = 6 K, the pumps in the primary and secondary collector loop are turned on. When the difference falls below ΔT = 4 K, the pumps are turned off again. Regarding the regeneration of the ground source, a more complex control algorithm is implemented, where priority is granted to charging the storage directly: when the temperature level of the collector is insufficient for storage charging, the heat is used to regenerate the borehole.

Load profiles for hot water tapping and space heating are provided in TRNSYS as an input file. The stochastic distribution of draw-offs is obtained with DHWcalc (Jordan and Vajen 2005) for both single and multi-family homes. The location-specific annual variation of cold water temperature is calculated according to DIN EN 12977-2 (2012). The heat demand of the building is obtained following the methodology of Task 32 for the reference building with a heated floor area of 140 m² and a specific heat demand of 60 kWh/m²a for the climatic conditions of Zurich (Heimrath and Haller 2007). The components and TRNSYS types are listed in Table 4.4 and resulting hot water and space heating loads are reported in Table 4.5 for the four reference locations.

Table 4.4: List of components and used TRNSYS types.

Component	Type	Comment
Solar thermal collector	Type 832	Dynamic collector model (Haller et al. 2012)
PV module		Custom PV model (chapter 4.1.2)
PVT extension		Custom PVT model (chapter 4.1.4)
Storage	Type 805	Multiport Store model (Drück 2006)
Heat exchanger	Type 91	TESS Library
Differential controller	Type 2	TRNSYS 17 library
Auxiliary heater	Type 6	TRNSYS 17 library
Heat pump	Type 42b	Quasi steady-state performance map model
Vertical borehole heat exchanger	Type 451	EWS model (Wetter 1997)
Flow diverter	Type 11b	TRNSYS 17 library
Tee-piece	Type 11h	TRNSYS 17 library
Pipes	Type 31	TRNSYS 17 library
Variable speed pump	Type 110	TESS Library

4.2.3 Definition of the electrical PVT system including battery storage

The electrical PVT system in the basic grid-connected configuration consists of the PV generator and an inverter. The PV generator is formed by an array of PV modules, PVT collectors or a combination of both. Their respective electrical yields are modelled with the performance model described in chapter 4.1.

As is generally known, the value of generated PV electricity is subject to temporal fluctuations. With high proportions of renewable electricity from sun and wind in the grid, the value of electricity is lower and

hence market prices drop. On the contrary, PV electricity has a higher value in situations with lower proportions of renewable energy from sun and wind. Therefore, a mere analysis of the net energy generation is not sufficient, but also the temporal distribution of PV generation is relevant, i.e. when and how much electricity is produced.

In contrast to PV systems, which can also be grid-connected, most solar thermal systems are per se decentral. For a consistent comparison of the amount of produced electricity and heat, the system boundaries for PV and solar thermal need to be defined consistently. Either the net, cumulated energy is assessed at the collector level, or the decentral, local energy consumption is assessed on a system level.

Following these considerations, a simple, decentral home battery system based on the battery model by Staudacher and Eller (2012, 2015) is implemented in TRNSYS. This model allows the analysis of self-consumption rates and electrical solar fractions within the decentral boundaries of a home battery system. Thus, the value of generated PV electricity is taken into consideration within the context of the decentral battery system to cover the local electricity load.

Figure 4.9 shows the electricity flow chart of a decentral battery system. The battery charge controller priorizes the self-consumption to cover the local load. If the instantaneous PV generation surpluses the local load, the excess PV yield is stored in a battery under consideration of the current state of charge, maximum depth of discharge, maximum charging and discharging rates, and conversion efficiency of the battery. Only if the battery is fully charged, the surplus electricity feeds into the grid. The dynamic load profile with a required high temporal resolution based on stochastical user behavior is generated with Synpro (Fischer et al. 2015) for single-family and multi-family houses.

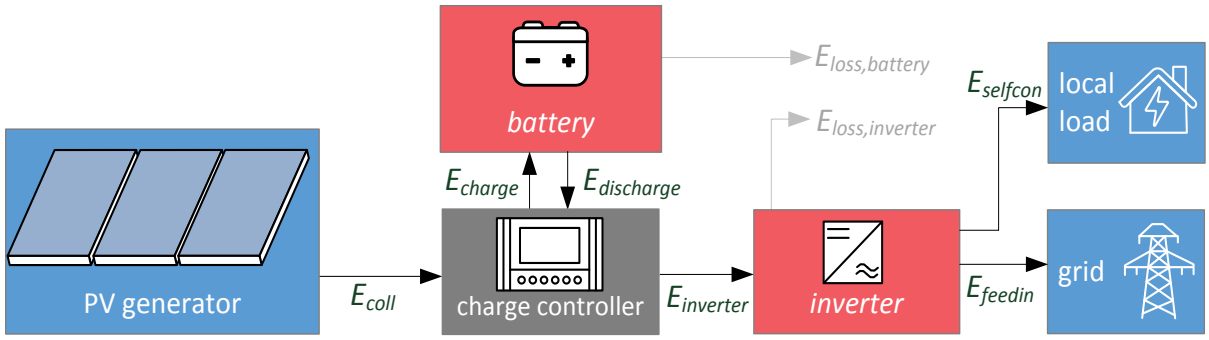

Figure 4.9: Energy flow chart of a decentral PV battery system (own illustration based on Staudacher and Eller 2012).

4.2.4 Definition of reference locations

The assessment of PVT system includes the four European locations of Athens, Davos, Würzburg, and Stockholm. These reference locations as defined by EN 12977-2:2012 represent the different European climatic conditions. Their weather data is obtained from Meteonorm (Meteonorm 2016). Climatic details and the resulting annual hot water and space heating demand are reported in Table 4.5 for the four reference locations.

Table 4.5: Location-specific weather and load characteristics.

Parameter	Unit	Athens	Davos	Würzburg	Stockholm	Comment
Average ambient temperature T_a	°C	16.2	4.4	10.2	7.7	Meteonorm weather data
Irradiance on tilted plane I_{tot}	kWh/m²a	1823	1732	1293	1177	Meteonorm weather data
Tilt angle	°	25°	30°	35°	45°	latitude minus 15° and rounded to the nearest 5° step
Hot water demand SFH	kWh/a	2060	2948	2617	2746	V = 175 l/d, T_{tap} = 45 °C
Hot water demand MFH	kWh/a	23498	28523	26651	27415	V = 1000 l/d, T_{tap} = 60 °C + circulation heat losses
Space heating demand SFH	kWh/a	1998	9803	8516	10341	Task 32 reference building (60 kWh/m²)

4.3 Assessment of electrical and thermal yields in PVT systems

In the following section, the electrical and thermal yields are assessed with regards to collector technology, system type, and location. Hereby, the specific electrical and thermal yields are summed without taking into account primary energy factors or exergetic efficiencies. E_{PV} and Q_{Coll} specify the annual cumulative electrical and thermal collector yields per square meter, where the electrical yield relates to the PV module area and the thermal yield to the aperture area as defined in the collector specifications.

E_{PV} disregards cable and inverter losses and balances the photovoltaic output behind the PVT collector and PV module:

$$E_{PV} = \frac{\int P_{PV}\ dt}{A_{PV}} \tag{4.16}$$

with the instantaneous electrical gain of the PV collector P_{PV} and the PV module area A_{PV}

Q_{Coll} specifies the annual thermal output disregarding piping and storage losses:

$$Q_{Coll} = \frac{\int \dot{Q}_{Coll}\, dt}{A_{ap}} \tag{4.17}$$

with the instantaneous thermal collector gain $\dot{Q}_{Coll}$ and the collector aperture area A_{ap}. In the solar heat pump system (a), Q_{Coll} is subdivided into heat delivered to the storage $Q_{Storage}$ in parallel operation and heat delivered to the borehole Q_{Regen} for regeneration.

Before comparing collector technologies, systems, and locations in more detail, Figure 4.10 shows the specific collector yields at the location of Würzburg. A more detailed summary of the yields at all four reference locations can be found in Table C.3.

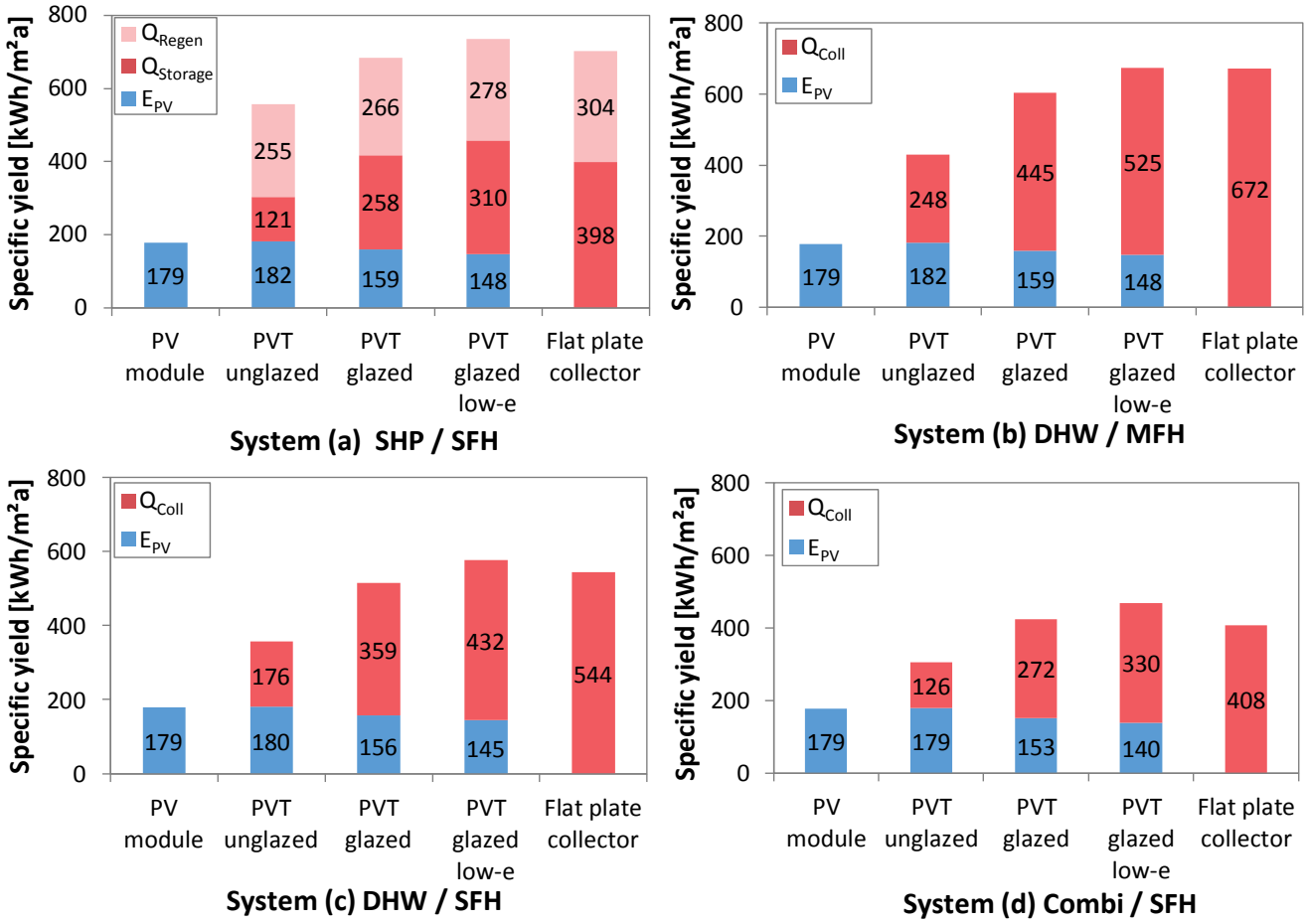

Figure 4.10: Comparison of annual electrical and thermal yields of different collector technologies for systems (a) – (d) in Würzburg.

4.3.1 Comparison of PVT collector technologies

The differences between the PVT collector technologies are discussed exemplarily for the multi-family home water preheating system (b) in Würzburg (Figure 4.10, top right). The qualitative differences between collector technologies are observed similarly for the other system configurations and locations.

The electrical yields of the investigated PVT collectors vary between 148 kWh/m² and 182 kWh/m² depending on the employed collector technology. By comparison, the PV module achieves a specific yield of 179 kWh/m² or 1.5 $\%_{rel}$ below the unglazed PVT collector. This is due to the cooling of the unglazed PVT collector, whose average, irradiance-weighted cell temperature amounts to $T_{cell,mean}$ = 27.9 °C compared to $T_{cell,mean}$ = 28.9 °C of the PV module.

The lower electrical yields of the glazed PVT collectors are caused by the reduced rated module efficiency $\eta_{el,STC}$ and higher cell temperatures. The front glazing with its additional optical interfaces and reflections reduces $\eta_{el,STC}$ by 3.3 $\%_{rel}$. The low-e coating further reduces the module efficiency by 4.1 $\%_{rel}$. Moreover, the better thermal performance increases storage temperatures and thus fluid and cell temperatures. This results in an average, irradiance-weighted cell temperature of $T_{cell,mean}$ = 38.2 °C of the glazed PVT collector and $T_{cell,mean}$ = 41.8 °C of the glazed PVT collector with low-e. Compared to the PV module, the electrical yield in system (b) drops by 11.1 $\%_{rel}$ for the glazed PVT collector and by 17.0 $\%_{rel}$ for the glazed PVT collector with low-e.

In addition to the electrical output stands the thermal yield, which ranges between 248 kWh/m² of the unglazed PVT collector and 672 kWh/m² of the flat plate collector. Both glazed PVT collectors rank in-between with a thermal yield of 445 kWh/m² of the glazed PVT collector and 525 kWh/m² of the glazed PVT collector with low-e. Hence, the thermal yield follows the oppositely directed trend than the electrical yield. Each PVT collector technology achieves either high electrical or high thermal yields, but not both at the same time.

High thermal yields result from a good thermal insulation, which increases both the instantaneous efficiency and the collector availability. The latter point can be demonstrated by means of the annual operation time, which amounts to 1415 h for the unglazed PVT collector compared to 2240 h for the glazed PVT collector with low-e. During most of the year, the efficiency of the unglazed PVT collector is insufficient to deliver heat at the required temperature level. A higher thermal efficiency is achieved technologically by a better thermal insulation, e.g. an external glazing or a low-e coating. However, the gain in thermal yield comes at the expense of a drop of electrical yield.

To conclude, a conflict of objectives between a high electrical and a high thermal yield is observed analogous to the previous findings in chapter 3.5.6. This originates from the conflict between a high optical efficiency versus a high level of thermal insulation. If high electrical yields are desired, a collector technology with a good optical efficiency is advantageous whereas for high thermal yields a collector technology with a good thermal insulation is required. For the investigated PVT collectors, a better thermal insulation results in a reduced optical efficiency. This is why a compromise between electricity and heat generation has to be made.

4.3.2 Comparison of system configurations

The yield of PVT collectors in various system configurations is discussed exemplarily for the glazed PVT collector without low-e at the location of Würzburg (Figure 4.11). The qualitative differences are observed similarly for the other collector technologies and locations. The focus of the assessment is placed on the PVT collector yields within its system context disregarding system performance indicators such as the solar thermal fraction, the seasonal performance factor of the heat pump, or the avoided CO_2 emissions.

The electrical and thermal yields vary significantly between the four system types. Both electrical and thermal yield decrease from system (a) to system (d), with the electrical yield dropping by 4 $\%_{rel}$ and the thermal yield by 48 $\%_{rel}$. Thus, the thermal yield is affected more profoundly by challenging system requirements.

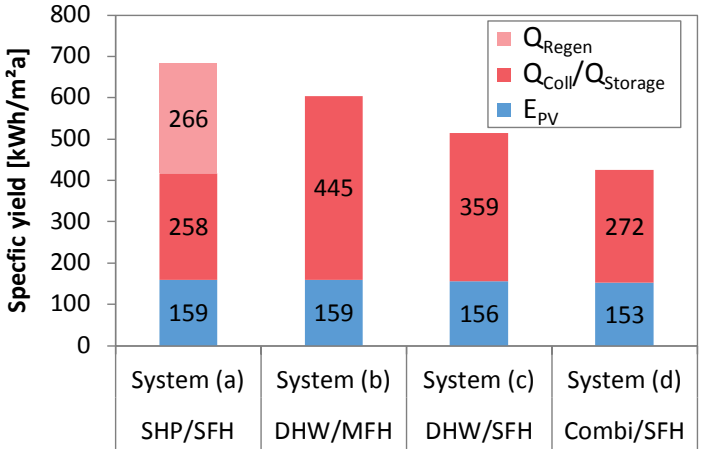

Figure 4.11: Comparison of specific annual yields of a glazed PVT collector in different system configurations in Würzburg.

The differences of the yields are caused by various factors. Dimensions of collector area and storage volume, temperature of the heat supply system, varying load profiles, coincidence of supply and demand, control of collector and auxiliary heating, storage stratification and mixing are just a few factors on the system level which have a significant influence on the collector yields. However, the influence on the collector performance can be reduced to the temporal distribution of the mean fluid temperature T_m in the collector field. This temperature governs the operation of the collector and significantly affects the thermal losses through Eq. (4.10) and the cell temperatures through Eq. (4.11).

Due to the central importance of T_m, the characteristic temperature T_{char} is introduced as a new indicator, which describes the irradiance-weighted mean fluid temperature of the collector within the system context and is defined as:

$$T_{char} = \frac{\int G \cdot T_m dt}{\int G \; dt} \tag{4.18}$$

The reason for weighting the mean fluid temperature T_m with the irradiance in the collector plane G can be demonstrated by the notion that T_m does not affect the collector performance during night and has a lesser influence during low levels of irradiance. Weighting T_m with G filters the night events with zero irradiance and considers the proportionality of both electrical and thermal yields to the irradiance G.

Evaluating T_{char} for the glazed PVT collector in the four investigated systems reveals the different governing operating temperatures. A characteristic temperature of T_{char} = 32.0 °C is reached in system (a), T_{char} = 33.7 °C in system (b), T_{char} = 36.8 °C in system (c), and T_{char} = 41.7 °C in system (d). The increase of the characteristic temperature correlates with the decrease of corresponding yields. Although also solar thermal collectors in general prefer low operating temperatures, this is even more important for PVT collectors since not only the thermal yields but also electrical yields benefit from a low T_{char}.

To conclude, significant differences between the thermal yields in the four systems are found which result from different operating temperatures of the collector. The characteristic temperature T_{char} is a new indicator, which characterizes the mean operating temperature of a solar thermal system and with which the differences in electrical and thermal yields can be explained. A more detailed analysis of the correlation between yields and T_{char} will be presented in chapter 4.4.

4.3.3 Comparison of locations

The electrical and thermal yields at the four reference locations differ in particular due to the annual rates of irradiance in the collector plane I_{tot}. Therefore, the usage of utilization ratios is useful, which relate the annual yields to the rate of irradiance. The electrical and thermal utilization ratios UR_{el} and UR_{th} are defined as (VDI 6002):

$$UR_{el} = \frac{E_{PV}}{I_{tot}} = \frac{\int p_{PV}\, dt}{\int G\, dt} \tag{4.19}$$

$$UR_{th} = \frac{Q_{Coll}}{I_{tot}} = \frac{\int \dot{q}_{coll}\, dt}{\int G\, dt} \tag{4.20}$$

The utilization ratio thus normalizes the yield with regards to climate and collector orientation, which makes it particularly useful for the comparison of yields at different climatic conditions.

Nearly constant utilization ratios for each PVT system can be observed, when comparing utilization ratios instead of specific yields for the four assessed locations of Athens, Davos, Würzburg, and Stockholm (compare Table C.3).

The electrical utilization ratio UR_{el} for PV modules varies by $\Delta UR_{el,max}$ = 0.4 $\%_{abs}$, primarily due to variations of ambient temperature and wind speed. For PVT collectors, a deviation of $\Delta UR_{el,max}$ = 1.2 $\%_{abs}$ is observed, which results from the dependence of the electrical efficiency on T_m and $\dot{q}_{Coll}$. Very good agreement of UR_{el} in Würzburg and Stockholm is found because of similar weather conditions.

Regarding thermal performance, slightly higher variations of the utilization ratio are observed. System (a) shows the largest regional differences due to the sensitive charging control with the two heat sinks of storage and borehole. This results in significant deviations of Q_{Regen} and $Q_{Storage}$ between the four locations. The differences between Stockholm and Würzburg of the thermal utilization ratio UR_{th} are relatively low due to similar climatic conditions with a maximum deviation of $\Delta UR_{th,max}$ = 0.6 $\%_{abs}$ for system (b) to system (d). The thermal utilization ratios in Athens and Davos are lower compared to the more northern locations in Würzburg and Stockholm. In Athens, this is mainly due to overdimensioned systems resulting in higher operation temperatures ($\Delta UR_{th,max}$ = -6.2 $\%_{abs}$). In Davos, the lower utilization ratio is attributable to colder ambient temperatures ($\Delta UR_{th,max}$ = -4.2 $\%_{abs}$). Regarding variations of UR_{th} between collector technologies, the highest variations are observed for unglazed PVT collectors due to their strong dependence on wind speed.

In summary, the regional variations with regards to the utilization ratios UR_{el} and UR_{th} are relatively small between the investigated locations. For this reason, the qualitative observations for Würzburg in the previous sections also hold true for other European locations.

4.4 Characteristic temperature approach

In the previous section, the electrical and thermal yields in specific system and collector configurations were assessed. For a better interpretation of the differences between the system types, the characteristic temperature T_{char} was introduced in Eq. (4.18). Both thermal and electrical yield depend on the fluid and cell temperatures, which is why the correlation between T_{char} and yields is now analyzed in more detail.

This novel approach is proposed to systematically assess the suitability of systems for the application of PVT, select the most suitable PVT collector for a specific system, pre-assess the electrical and thermal yields or to evaluate optimization measures. The approach should not be regarded as a substitute to dynamic system simulations, but as an additional evaluation indicator to compare collector yields of different systems in a systematic way.

4.4.1 Dependence of collector yield on T_{char}

In order to draw generalized conclusions, the simulation results are analyzed by means of correlating the yields with the characteristic temperature T_{char}. For this purpose, a parameter variation was conducted for the main dimensions of collector area and storage volume of the four reference systems. Additionally, the heat load, temperature level of hot water, stratification characteristics of the storage, and circulation losses were varied. The parameter variation is limited to the location of Würzburg, and system (a) is only considered in the parallel configuration without borehole regeneration. In total, over 1000 annual system simulations in the four reference systems were carried out. Their corresponding yields are plotted altogether in Figure 4.12, where each point represents a specific simulation case for one system configuration with one collector technology.

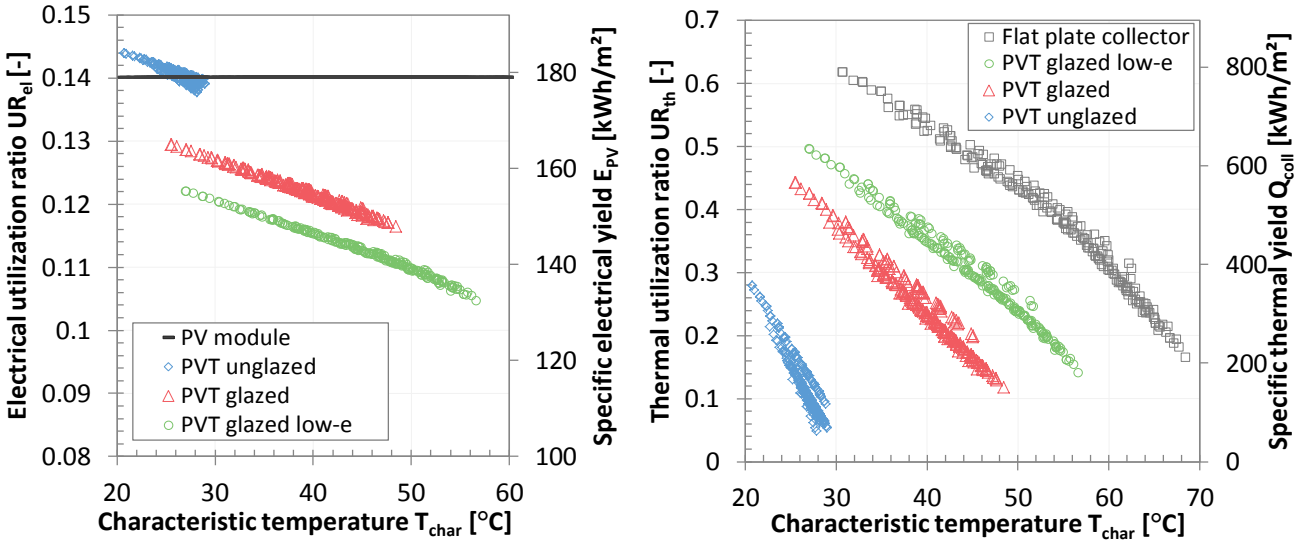

Figure 4.12: Correlation between characteristic temperature T_{char} and electrical (left) and thermal (right) utilization ratio, or yields indicated for Würzburg, with varying PVT collector technologies.

A strong correlation between T_{char} and the electrical and thermal yields can be observed, as both yields decrease with a higher characteristic temperature.

While the electrical yield of the three PVT technologies is almost proportional to T_{char}, the PV module operates independently from T_{char}. Naturally, the cell temperatures in PV modules are uncoupled from fluid temperatures unlike in PVT collectors. A better thermal coupling between PV cells and the fluid in PVT collectors through an improved internal heat transfer coefficient $U_{AbsFluid}$ leads to higher electrical yields at a constant T_{char} due to a reduction of the cell temperatures. The electrical utilization ratio UR_{el} of the PVT collector technologies drops by 0.45 - 0.48 $\%_{rel}$/K, which is in the range of the power dependence γ of the PV cells.

The thermal yields also follow an almost linear trend, yet the yields are scattered more diffusely compared to the electrical correlation. This is due to a more complex interaction of collector and system, where collector control, weather, and storage temperatures introduce a higher uncertainty. Nonetheless, a characteristic curve can be observed for each collector technology, which resembles the thermal efficiency curve and clearly denotes their different thermal performance characteristics. The thermal utilization ratio UR_{th} drops by 1.1 - 1.4 $\%_{abs}$/K for the glazed PVT collectors and by 2.5 $\%_{abs}$/K for the unglazed PVT collector, which is evidently more sensitive to a higher T_{char}.

In general, the thermal yields depend much stronger on the characteristic temperature than the electrical yields. An increase of T_{char} by 10 K reduces the electrical yield of a glazed PVT collector by 4.6$\%_{rel}$, while the thermal yield drops by 36 $\%_{rel}$. It is worth mentioning that both electrical and thermal yields benefit from low characteristic temperatures. The lower T_{char}, the more symbiotic is the application of PVT collectors, resulting in higher specific yields. However, the temperature level as required by the system has to be met, since high characteristic temperatures may be necessitated by the application.

By its definition, the characteristic temperature T_{char} describes the governing fluid temperature of the collector field and thus summarizes the influence of the system on the collector. On an annual basis, the system configuration, storage volumes, and aperture area are the most relevant factors influencing T_{char}. Yet at the same time, T_{char} itself also depends on the thermal performance of the collector and its interaction with the system. With higher thermal yields, the storage heats up, and consequently the collector inlet temperatures and T_{char} increase. Therefore, T_{char} can be interpreted as an indicator for the mean operating temperature of a given collector-system-combination.

The characteristic temperature approach puts the operating temperatures in the collector array into the focus. Hence, T_{char} is the central criterion to assess the applicability of a PVT collector technology for a given system configuration. The approach bears some similarities but also significant differences with the FSC method developed by Letz et al. (2009). The FSC method aims at comparing system performances with varying hydraulic schemes and components, correlating the fractional energy savings f_{sav} to the fractional solar consumption FSC. In contrast, the characteristic temperature approach aims at comparing collector performances by linking the collector with the system by T_{char}.

4.4.2 Relationship of T_{char} and system type

Electrical and thermal yields of PVT collectors correlate strongly with T_{char} as shown in the previous section. Hence, these yields can be estimated roughly when T_{char} is known. However, it may be difficult to estimate T_{char} due to its dependence from the exact system configuration and collector performance. Therefore, the following section details the relationship between T_{char} and the type of system.

An interesting observation was made while analyzing simulation results. Different collector technologies yield a similar T_{char} if the collectors deliver the same thermal yield and thus the same solar fraction f_{sol} of the solar thermal system. This hypothesis was investigated for the previously defined systems (a) - (d). Apparently, T_{char} is relatively constant for identical system configurations with a constant f_{sol}, with the characteristic temperatures varying only in a small range.

Based on this observation, typical ranges for T_{char} can be identified for systems (a) – (d) with a given f_{sol}. Figure 4.13 shows a box plot indicating the quantiles of T_{char} for each system with varying levels of solar

fractions, and varying operation modes for the solar heat pump system (a). The above-mentioned parameter variation for the characteristic curves in Figure 4.12 provides the basis for the indicated ranges.

Figure 4.13 gives an orientation of typical values of T_{char} for the discussed systems, independent from the employed PVT collector technology. With the knowledge of T_{char}, the preliminary yields of the PVT system can be pre-estimated and a suitable collector technology can be selected.

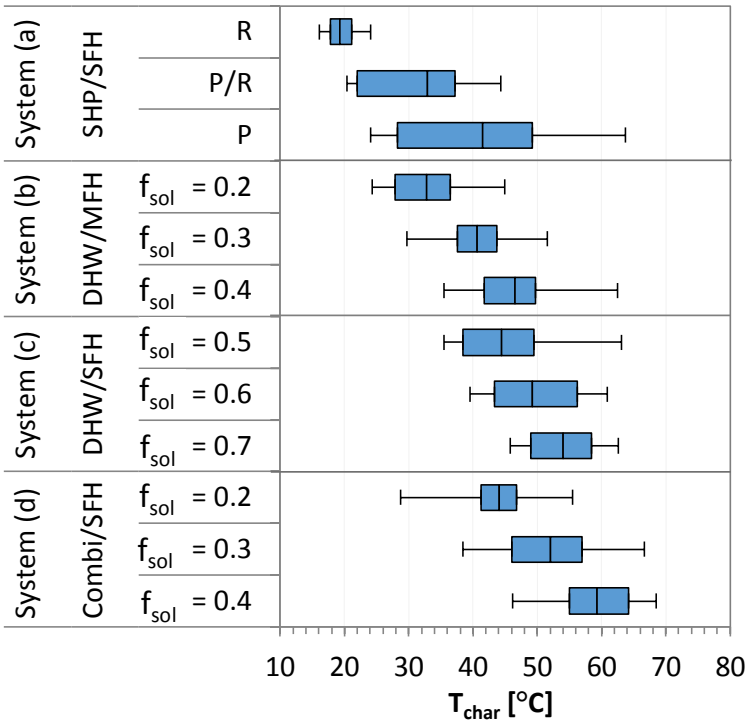

Figure 4.13: Box plot of the ranges of the characteristic temperature T_{char} for the four reference systems indicating the four quantiles.

The median of T_{char} indicates typical temperature levels for each system configuration. As expected, the solar fraction has a strong influence on T_{char}. With a higher solar fraction, the characteristic temperature T_{char} increases, reducing specific electrical and thermal yields at the same time. Also the mode of operation of the solar heat pump system has a strong impact on temperatures and thus T_{char}. While regeneration (R) of the borehole achieves the lowest T_{char}, the combined parallel/regeneration (P/R) increases T_{char} due to higher collector inlet temperatures from the storage. With respect to T_{char}, the parallel mode without regeneration (P) bears no differences to the combi system (d) resulting in a wide band of possible characteristic temperatures.

4.4.3 Identification of suitable fields of application for PVT collectors

The process of selecting the worthwhile PVT collector for a specific PVT system is not trivial. Due to the aforementioned technological conflict between a high optical efficiency and a good thermal insulation, either highest electrical yields or highest thermal yields can be reached, but not both at the same time. This is why there is not the perfect PVT collector for all applications, but it is even more important to specifically select the most suitable PVT collector for the given PVT system with its individual requirements. As the PVT collector has to match the operating temperatures, the characteristic temperature is a suitable indictor for the process of selecting a suitable PVT collector.

The lower the operating temperature, the more symbiotic is the application of PVT collectors in general, as both electrical and thermal efficiency prefer low temperatures. With increasing operating temperatures, a higher degree of thermal insulation is required to reach a sufficiently high thermal efficiency in the operating range. For instance, the thermal efficiency of an unglazed PVT collector is insufficient for the characteristic temperature of a domestic hot water system, which is why a glazed PVT collector with a transparent front glazing should be preferred, although this reduces the electrical performance.

As a rule of thumb, the thermal insulation should be as little as possible in order to reach high electrical yields. At the same time, the thermal insulation has to be as high as required, i.e. matching the given T_{char}, in order to reach a high heat output. In low temperature systems, e.g. heat pump systems with ground regeneration, unglazed PVT collectors may reach sufficient thermal yields, so that high electrical yields can be achieved due to their poor thermal insulation. In medium temperature systems, e.g. multi-family homes with low solar fractions, glazed PVT collectors offer a good balance between electrical and thermal yields. In medium to high temperature systems, such as domestic hot water and combi systems, glazed PVT collectors with low-e coating offer relatively high thermal yields, while maintaining acceptable electrical yields. For systems with high characteristic temperatures, concentrating PVT technologies or non-hybrid side-by-side installations may be the suitable solution.

The analysis of primary energy yields provides a more scientific explanation of this rule of thumb. The maximization of locally produced solar energy is a major motivation for the application of PVT collectors. To quantify the combined production of electricity and heat, Figure 4.14 plots the characteristic curves for the specific primary energy yield instead of showing the electrical and thermal yield separately next to each other. Primary energy factors as defined in chapter 2.2.5 are used for the conversion from electricity and heat into primary energy.

The glazed PVT collector with low-e coating achieves the highest primary energy yields in a wide temperature range. Its higher thermal yields overcompensate its lower electrical efficiency. Even at lower characteristic temperatures, the glazed PVT collector with low-e achieves higher primary energy yields than without low-e. Although unglazed PVT collectors reach the highest electrical yields, their primary energy yields are significantly lower than that of glazed PVT collectors. In systems with characteristic temperatures above 50 °C, conventional flat plate collectors reach higher overall yields than the investigated PVT technologies. This overall picture might however change, when different primary energy factors are taken as a basis for the assessment.

Furthermore, the maximum characteristic temperature T_{char} of each collector technology limits their fields of application. For instance the unglazed PVT collector reaches a maximum characteristic temperature of T_{char} = 30 °C. Therefore, this collector is not applicable in systems exceeding this characteristic temperature, as larger collector areas cannot compensate for the low specific yields at these temperatures.

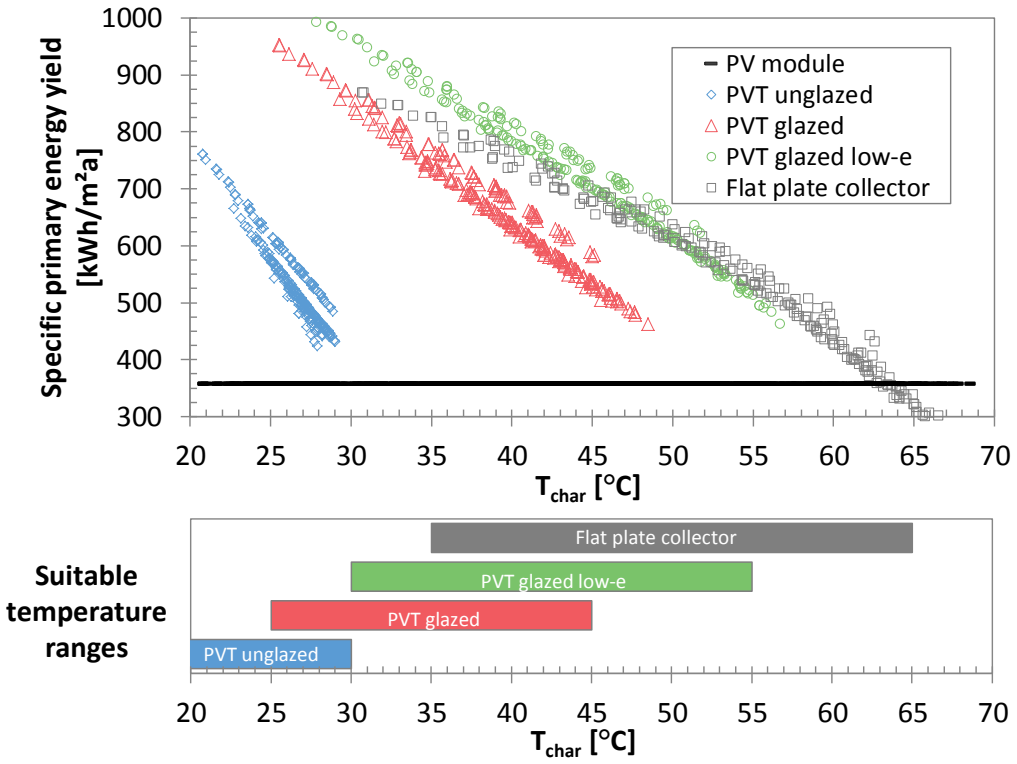

Figure 4.14: Primary energy yields and recommended temperature ranges per collector technology.

From these considerations, typical fields of applications and suitable temperature ranges can be recommended for each PVT collector technology, which are also added to Figure 4.14:

- The application of unglazed PVT collectors is limited to low operating temperatures near or below ambient temperatures of $T_{char} < 30$ °C.
- Glazed PVT collectors are suitable for low to medium operating temperatures in the range of T_{char} between 25 °C and 45 °C.
- Glazed PVT collectors with low-e coatings can be applied for a wide temperature range of T_{char} between 30 °C and 55 °C.
- For higher temperatures, concentrating PVT collectors or a side-by-side installation of flat plate collectors and PV modules might result in highest overall primary energy yields.

4.4.4 Exemplary application of the characteristic temperature approach for the preliminary assessment of a PVT system at the new town hall building in Freiburg

The new town hall building in the Freiburg district of Stühlinger is an administrative building for approximately 830 employees. With a net floor area of 21,500 m² it is designed to be the largest European building with a net zero energy standard. A sophisticated energy concept is required to reach this ambitious target and cover the high electricity and heat demand with locally generated energy. Next to a full coverage of the roof area with highly efficient PV modules, the façade is activated by building-integrated

PV panels. A ground water coupled heat pump delivers energy-efficient heating and cooling for the building.

Within the research project "NVZ-Freiburg", the originally planned solar thermal system was substituted with a PVT system to increase the primary energy yields. The solar thermal pre-heating system provides hot water for the kitchen and for the office facilities and is designed to achieve a relatively low solar fraction of $f_{sol} = 0.15$, while the supplementary heat is provided by a biogas boiler. Concerning its thermal characteristics, the planned PVT system is similar to the domestic hot water system (b) in a multi-family home. However, the specific load profile, thermal demand, location, climate, and storage volumes differ to the previously assessed system.

This example demonstrates the application of the characteristic temperature approach for the selection of PVT collectors and for preliminary dimensioning the collector array. In six steps, the most important performance parameters of PVT collectors are derived:

1) **Identify T_{char}:** the first step concerns the identification of the characteristic temperature. T_{char} can be calculated by a single system simulation, it can be obtained from the diagram in Figure 4.13, or it has to be estimated based on experience and expert knowledge. In this example, T_{char} amounts to 28.0 °C and was obtained from the simulation of the reference solar thermal system with flat plate collectors.

2) **Read utilization ratio from yield estimation tableau:** for the given characteristic temperature T_{char}, the corresponding electrical and thermal utilization ratios per collector technology can be read from the yield estimation graph in Figure 4.15.

3) **Assess specific yields:** by multiplying the utilization ratios with the total annual rate of irradiance on a tilted collector plane I_{tot}, the specific electrical and thermal yields are given by:

$$E_{PV} = UR_{el} \cdot I_{tot} \tag{4.21}$$

$$Q_{Coll} = UR_{th} \cdot I_{tot} \tag{4.22}$$

4) **Set total thermal output**: since the PVT system substitutes a conventional solar thermal system, the total thermal output is given by the replaced reference system. In this specific case, the system aims at a solar fraction of $f_{sol} = 0.15$ which corresponds to a total thermal output of $Q_{tot} = 22$ MWh.

5) **Calculate required collector area**: the collector aperture area A_{ap}, which is required to meet the thermal output, is given by:

$$A_{ap} = Q_{tot}/Q_{Coll} \tag{4.23}$$

6) **Determine electrical PVT output**: the total annual electricity output of the PVT array is given by the following equation under consideration of the ratio between aperture and PV module area A_{ap}/A_{PV}:

$$E_{tot} = E_{PV}\, A_{ap} \cdot \frac{A_{PV}}{A_{ap}} \tag{4.24}$$

By means of the characteristic temperature approach, different PVT technologies can thus be compared and specific yields, required areas, and surplus electrical yields can be preliminary assessed without con-

ducting a single simulation run (Figure 4.15). In comparison to detailed system simulations, which were conducted for the precise dimensioning of the system, the results are very similar. The exact simulations yield a required collector area of A_{ap} = 29.4 m² for the flat plate collector, A_{ap} = 38 m² for the glazed PVT collector with low-e, and A_{ap} = 44 m² for the glazed PVT collector. The required areas as obtained with the characteristic temperature approach amount to A_{ap} = 36 m² and A_{ap} = 43 m² and the detailed results from all six steps are also given in Table 4.6

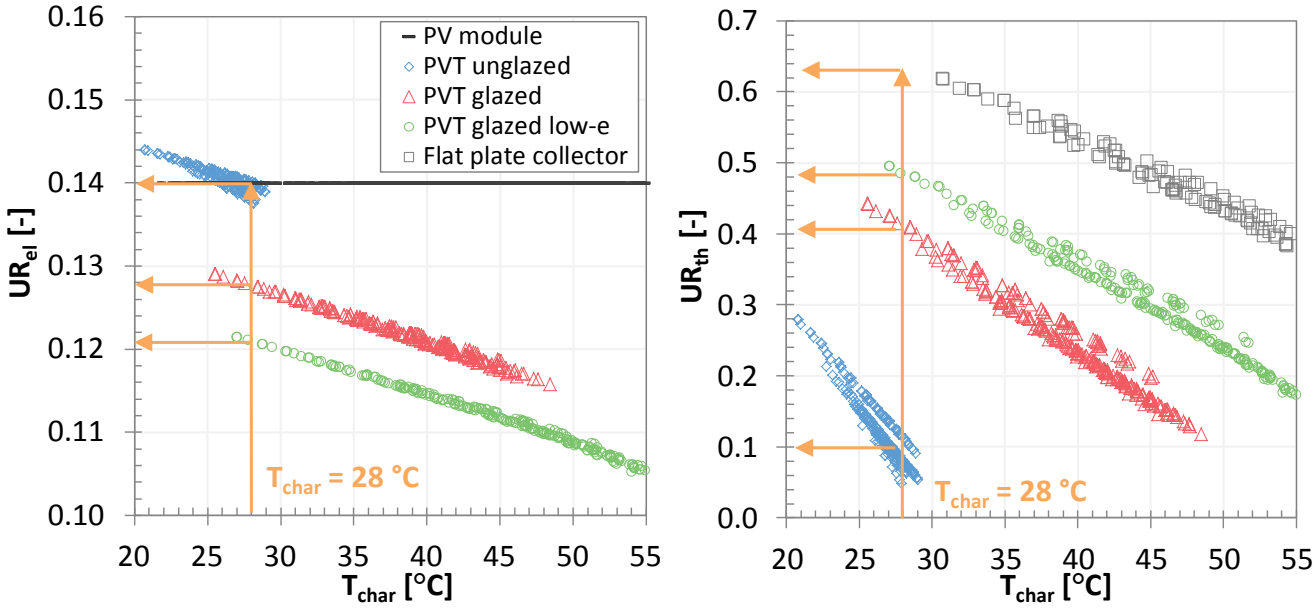

Figure 4.15: Yield estimation tableau for the characteristic temperature approach with the example of the new town hall in Freiburg.

After the completion of the new town hall building, 22 glazed PVT collectors with a total aperture area of 44 m² were installed. The performance of this PVT system will be monitored for one year to assess the actual electrical and thermal performance, and optimize the systems operation. Unfortunately, no monitoring results were available at the time of finishing this PhD thesis.

Table 4.6: Preliminary assessment of performance indicators for different collector technologies in the new town hall in Freiburg, following the six steps of the characteristic temperature approach.

Step	Parameter	Unit	Unglazed PVT	Glazed PVT	Glazed PVT low-e	FPC
(1) Identify T_{char}	T_{char}	[°C]		28.0		
(2) Read utilization ratios	UR_{el}	[-]	0.14	0.128	0.121	0
	UR_{th}	[-]	0.11	0.41	0.49	0.64
(3) Assess specific yields	E_{PV}	[kWh/m²]	175	160	151	0
	Q_{Coll}	[kWh/m²]	138	513	613	801
(4) Define total thermal output	Q_{tot}	[MWh]		22.0		
(5) Calculate required collector area	A_{ap}	[m²]	160	43	36	27
(6) Determine electrical PVT output	E_{tot}	[MWh]	28	6.3	5.0	0

4.4.5 Discussion of the characteristic temperature approach

The operating temperatures of PVT systems are centrally important with regards to the performance of PVT collectors. The novel characteristic temperature approach puts these temperatures into the focus by introducing the characteristic temperature T_{char} as a new indicator to describe the irradiance-weighted mean fluid temperatures. This indicator can be considered as the central link between collector and system due to its strong correlation with electrical and thermal yields. Therefore, the characteristic temperature is proposed as a new indicator for the thermal characterization of solar thermal systems.

Different application possibilities for the characteristic temperature were presented. The approach can be used to pre-assess electrical and thermal yields, preliminarily size a PVT system, compare the performance and select suitable PVT collector technologies. Furthermore, the characteristic temperature is also a suitable indicator to identify, quantify and evaluate optimization measures, which reduce the operating temperature in PVT systems. Chapter C.4 in the Appendix discusses four cases studies for optimizing collector yields and their implication on T_{char}.

From all these considerations, it becomes clear that the operating temperatures have a major influence on electrical and thermal yields. Hence, an optimization of the PVT system always implies a reduction of T_{char}. An adequate sizing of the PVT collector array and storage volume, and the selection of a suitable PVT collector technology are therefore the key to a well-balanced PVT systems with high overall yields.

Being at an early stage, the characteristic temperature approach needs to be developed further. The validity of the correlation between T_{char} and thermal and electrical yields needs to be verified by field monitoring and by simulations for other types of PVT technologies and solar thermal systems. A simple method has to be developed to obtain the characteristic curve for a collector at a specific location depending on performance and weather data. Additionally, the factors determining T_{char} of a given system need to be identified, so that in the future T_{char} can be easily estimated from system characteristics.

Nonetheless, the characteristic temperature is a versatile indicator, which has to prove its practical applicability in the future. Above all, T_{char} is especially helpful to bring a structure into the discussion of PVT systems by focusing on operating temperatures.

4.5 Assessment of system performance

Up to now, the focus of the assessment was placed on collector yields. However, the collector performance and its heat and electricity output have to be seen in the context of the system. It is in the nature of decentral systems that yields need to meet the corresponding energy demand. A closer look at the system performance allows an analysis of the performance of decentral PVT systems and a comparison with a side-by-side installation of conventional flat plate collectors and PV modules.

To begin with, chapter 4.5.1 describes the selected assessment approach of sizing the PVT collector array to achieve the same thermal output as the reference system with flat plate collectors. In chapter 4.5.2., the system performance is assessed using the example of the domestic hot water system (c) with glazed PVT collectors with low-e. In doing so, indicators for the characterization of the performance on system

level are introduced and explained. However, the performance indicators for the separate electrical and thermal system do not take into account the central benefit of PVT collectors concerning the efficient co-generation of electricity and heat on limited areas. Therefore, a new approach to describe the energetic added value of PVT systems is presented in chapter 4.5.3. Finally, chapter 4.5.4 discusses the newly defined system performance indicators for worthwhile PVT systems, where suitable PVT technologies are selected for synergetic collector-system combinations.

4.5.1 Approach for the assessment of PVT system performance

The previous assessment of collector yields in chapter 4.3 analyzed PVT systems with a fixed collector area and compared their specific yields. However, fixing the collector area is not a fair approach for the assessment of system performance. If PVT collectors are regarded as a substitute to conventional flat plate collectors (FPC), it is a common assessment approach to compare a PVT system with a FPC system delivering both an equal heat output. For example, this approach was also conducted in the new town hall in Freiburg. Accordingly, the approach of comparing systems, which achieve the same solar fraction and operate at similar characteristic temperatures, enables a fairer benchmark methodology.

Therefore, the total thermal yield of PVT and FPC systems is set to be equal throughout chapter 4.5. Instead of comparing PVT and FPC systems with fixed areas, we now compare PVT and FPC systems with a fixed thermal output. To reach this goal, the collector area of the PVT collectors has to be increased. Increasing the PVT collector array, however, reduces the specific collector yield, because T_{char} increases due to higher storage temperatures. Consequently, PVT collectors require more area to provide the same thermal yield as FPCs.

This approach of fixing the total thermal yields instead of fixing collector areas imposes more challenging conditions for the PVT operation. Relatively high solar fractions and large collector arrays result in a higher characteristic temperature and thus lower yields than the yields obtained during the assessment of PVT collector yields in chapter 4.3.

4.5.2 Exemplary assessment of the system performance of system (c) with glazed PVT collectors with low-e

This section exemplarily presents the system performance for the domestic hot water system (c) in a single-family house with a glazed PVT collector with low-e coating and introduces indicators for characterizing the system performance. These system indicators show how PVT collectors provide electricity and heat to the single-family house and how the extensively discussed collector yields affect the system performance.

Neither a comparison with alternative system configuration nor a full coverage of known indicators for PV and solar thermal systems will be given at this point. The focus is much rather placed on a selection of interesting aspects regarding the system integration of PVT collectors.

4.5.2.1 System characteristics

The domestic hot water system can be considered the "classic" solar thermal system worldwide and is also a suitable example for explaining PVT aspects due to its hydraulic simplicity. The glazed PVT collectors with low-e coatings are selected as they match the characteristic temperature of the system.

To achieve the same total thermal yield as a system with flat plate collectors, the area of the PVT collector array has to be increased. In system (c), a PVT array with an area of A_{PVT} = 8.5 m² delivers the same total thermal yield of Q_{tot} = 2.7 MWh as a FPC array with A_{FPC} = 5 m² as defined in the reference system in Figure 4.8.

The electrical and hydraulic layout of the system is shown in Figure 4.16. The thermal system is equal to the previously discussed domestic hat water system with a storage volume of V_{stor} = 0.35 m³, an auxiliary heater, and a daily hot water demand of V = 175 l/d at T_{tap} = 45 °C. Additionally, a simple grid-coupled PV home battery system with an effective battery capacity of 5 kWh is considered. The battery system aims at increasing the rate of locally covered and consumed solar electricity.

The characteristic temperature of the system amounts to T_{char} = 49.1 °C. This indicates challenging operating temperatures for the PVT collector and relatively low electrical and thermal yields can be expected.

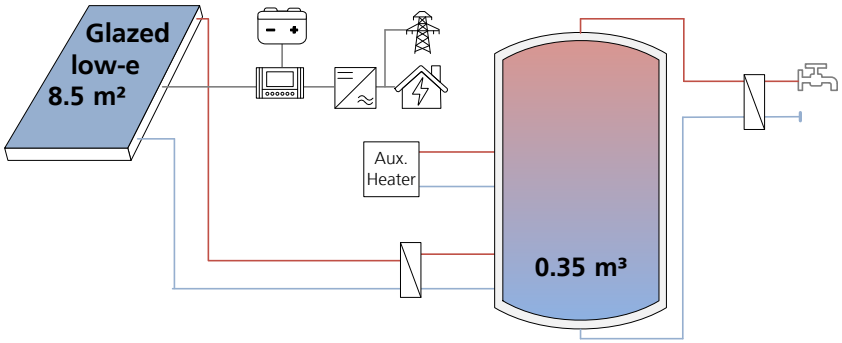

Figure 4.16: Electrical and hydraulic layout of PVT system (c) including PVT technology, collector area A_{coll} and storage volume V_{stor}.

4.5.2.2 Visualization of energy flows

To begin with, the annual energy flows in the system are visualized in Figure 4.17. This diagram gives an excellent overview of the energy flows in a PVT system by comparing the supply side (PVT collector) with the demand side (local power and heat demand) and by juxtaposing gains and losses of collector and system. The green arrows show the optical energy flows and their respective losses, the blue arrows the electrical energy flows, and red arrows the thermal energy flows.

Here, the irradiance in the collector aperture area $I_{tot,ApertureArea}$ = 11.0 MWh is defined as 100 %. By multiplying the values given in percentage with this value, all energy flows can be transformed to their absolute value.

The first two arrows in green stand for the annual rate of irradiance in the gross and aperture area. The inactive area of the collector frame already reduces the usable irradiance by 9 %. Moreover, the PV cells only cover 91 % of the aperture area to avoid partial shading of the cells from the collector frame. While the share of irradiance on the inactive absorber area can be utilized for thermal operation, it is lost for electricity generation. This shows the importance in glazed PVT collectors to reduce inactive areas of collector frame and absorber to achieve a maximized utilization of the solar irradiance. Unglazed PVT collectors do not have this issue, as the PV module area is basically equal to the aperture area.

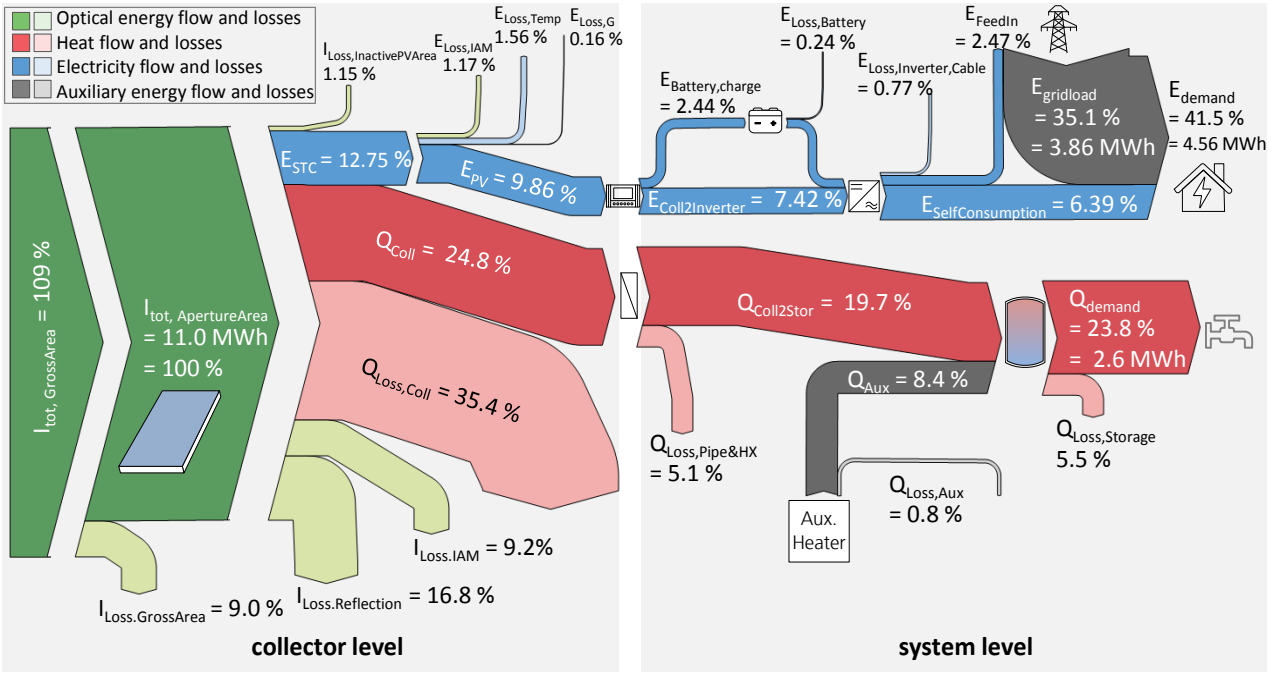

Figure 4.17: Visualization of optical (green), electrical (blue), and thermal (red) energy flows of PVT system (c) in a Sankey diagram.

On collector level, the losses are dominated by the heat losses of the collector $Q_{Loss,Coll}$ (35.5 %). Next to heat losses during operation, these losses also include the solar energy which is not used while the collector pump is switched off during periods of insufficient thermal efficiency. Optical losses from non-absorption and reflection ($I_{Loss,Reflection}$ = 16.8 %) and from high angles of incidence ($I_{Loss,IAM}$ = 9.2 %) together amount for more than a quarter of the incident solar irradiance. Compared to this, the electrical PV losses due to elevated cell temperatures ($E_{LossTemp}$ = 1.56 %), high incidence angles ($E_{LossIAM}$ = 1.17 %), and low levels of irradiance ($E_{Loss,G}$ = 0.16 %) are relatively low.

On system level, electricity losses from the battery, inverter and cable reduce the electrical collector yield E_{PV}. In this system, the major share of the PV gain is consumed locally to cover the local electricity demand. Only a smaller share of the PV gain feeds into the power grid.

Heat losses in the solar thermal system reduce the collector gain Q_{Coll}. Firstly, heat losses of pipes and accessories need to be considered. Secondly, there are heat losses at the heat exchanger between collector and storage circuit. Due to the limited UA-value of the heat exchanger, heat may not be transported from the collector to the storage circuit. Thirdly, heat losses of the storage need to be considered ($Q_{Loss,Storage}$ = 5.5 %).

4.5.2.3 Collector performance

Figure 4.18 gives a closer look at the monthly collector yields juxtaposed to the available solar resource I_{tot}, the electricity demand E_{demand}, and the heat demand Q_{demand}. This approach is also known as the fractional savings method FSC, which was developed to characterize the performance of combi systems (Letz et al. 2009).

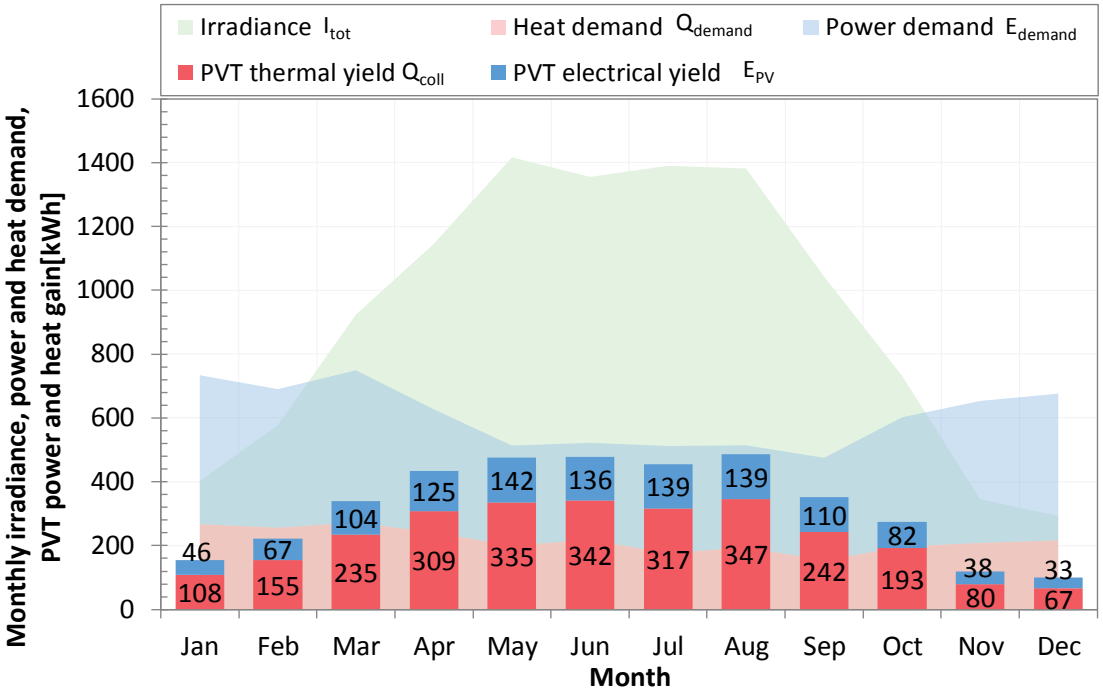

Figure 4.18: Monthly irradiance, electricity and heat demand, electrical and thermal yield of PVT system (c).

The monthly electrical utilization ratio UR_{el}, as ratio of electrical yield and I_{tot}, is relatively low in this system and ranges between UR_{el} = 10.0 % in summer at high cell temperatures and 11.5 % in winter. The monthly thermal utilization ratio ranges between UR_{th} = 22.9 % in winter with low levels or irradiance and cold ambient temperatures and UR_{th} = 26.9 % in summer. While the electrical efficiency matches better the demand side, the thermal efficiency reaches its peaks during the periods with low heat demand.

The major share of electrical and thermal yields is generated between May and August with high levels of irradiance. While the monthly electrical gain is always below the electricity load, the thermal yield exceeds the monthly demand during summer. In this period, the excessive thermal yields heat up the storage, with the consequence of higher storage losses, higher collector inlet temperatures and a more frequent occurrence of stagnation.

This assessment demonstrates that merely examining the quantitative value of annual collector yields (E_{PV}, Q_{Coll}) is insufficient for an analysis of system performance. Losses on the system level have to be considered, which are strongly influenced by the coincidence of energy production and energy demand. Storage capacities for electricity and heat are not sufficient to store energy for longer periods of time but only for a couple of days. In the optimal case, the supply side (collector gain) coincides with the demand side (energy load).

4.5.2.4 Electrical system performance

The application of PVT collectors aims at achieving a certain level of energetic self-sufficiency by increasing the local production of renewable energy. As PVT collectors reach lower electrical yields than PV modules, it is interesting to investigate the system performance with regards to coverage of the electrical load and compare PVT systems with PV systems.

The following indicators are used to characterize the electrical system performance:

The electrical coverage rate f_{cov} indicates the contribution of locally generated and consumed electricity $E_{selfcon}$ to the local electrical load E_{demand} and is defined as (Staudacher and Eller 2012):

$$f_{cov} = \frac{E_{selfcon}}{E_{demand}} \tag{4.25}$$

Accordingly, f_{cov} describes how much of the local electricity demand is covered by the PV battery system and is an indicator for the electrical autarchy level.

By contrast, the self-consumption rate $f_{selfcon}$ is defined as the ratio of self-consumed electricity $E_{selfcon}$ to the total PV generation E_{PV} (Staudacher and Eller 2012):

$$f_{selfcon} = \frac{E_{selfcon}}{E_{PV}} \tag{4.26}$$

Thus, the self-consumption rate describes how much of the total PV output is consumed locally and is an important parameter for the sizing of a PV or PVT collector array.

These two indicators are evaluated for the glazed PVT collector with low-e in system (c) and compared with a PV module. Each case is simulated for a PV system with and without battery, and for different module areas between 2.5 m² and 15 m². Figure 4.19 shows the resulting electrical coverage rate f_{cov} and self-consumption rate $f_{selfcon}$.

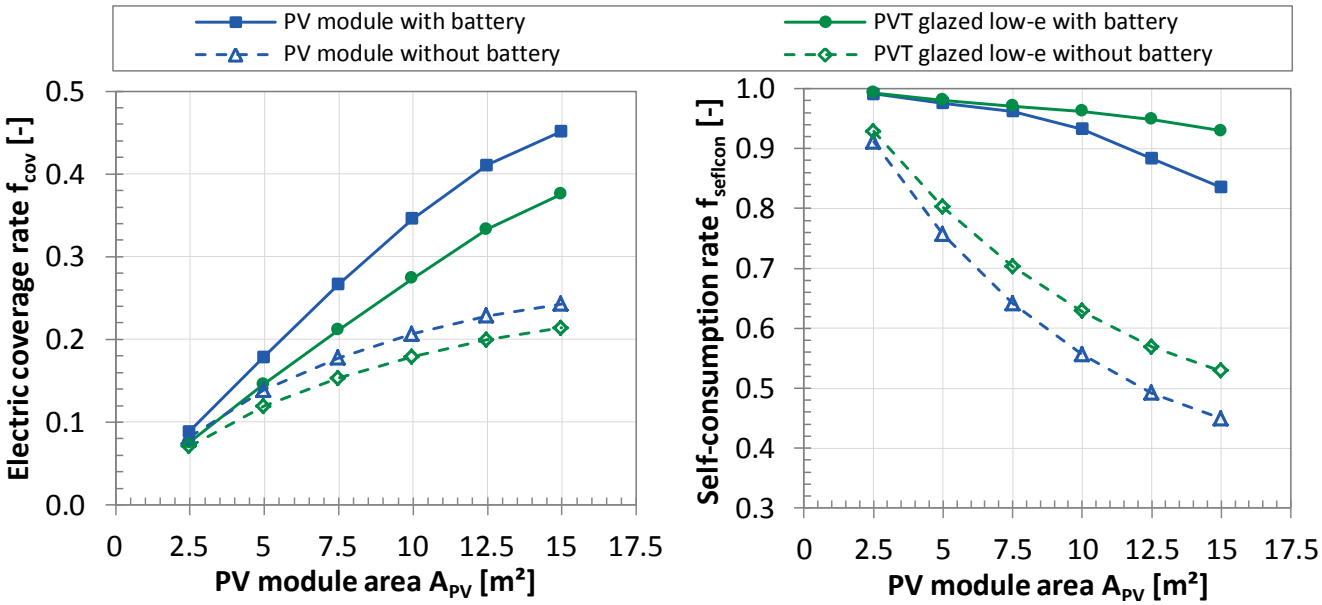

Figure 4.19: Electrical coverage rate f_{cov} and self-consumption rate $f_{selfcon}$ for PV modules and glazed PVT collectors with low- e in system (c).

While the PV system reaches higher electrical coverage rates, the PVT systems achieve a higher self-consumption rate. Employing a battery increases both the coverage rate and the self-consumption rate.

On account of their higher efficiency $\eta_{el,STC}$ and lower cell temperatures T_{cell}, the PV modules achieve significantly higher electrical coverage rates than the PVT collectors. Consequently, larger PVT collector arrays are required to reach the same coverage rate. For the present example, the PVT array with a module area of A_{PV} = 8.5 m² achieves a coverage rate of f_{cov} = 16 % without battery and f_{cov} = 24 % with bat-

tery. The PV module achieves the same coverage rates with a module area of A_{PV} = 6.5 m². The differences between the required areas are in line with the differences of the electrical yield.

It is interesting to mention, that the differences of f_{cov} and $f_{selfcon}$ are smaller in the other investigated PV and PVT systems (compare Figure C.8, Figure C.15, and Figure C.23 in the Appendix). Apparently, the gap between the curves of f_{cov} and $f_{selfcon}$ for PV modules and PVT collectors tends to become lower with larger module areas.

4.5.2.5 Thermal system performance

The main objective of solar thermal systems is the reduction of the consumption of conventional energy in the heating system. Typically, the following indicators are used to describe the thermal system performance:

The solar fraction f_{sol} specifies the contribution of the solar thermal collector to the heating system and is defined as the useful collector output divided by the heat demand (DIN EN 12977-2:2012):

$$f_{sol} = 1 - \frac{Q_{Aux}}{Q_{demand}} \tag{4.27}$$

with the delivered auxiliary heat Q_{Aux}, and the heat demand Q_{demand}. f_{sol} is regarded as the central parameter to describe a solar thermal heating system and is the thermal pendant to the electrical coverage rate $f_{cov.}$

The fractional energy savings f_{sav} are an extension of f_{sol} and quantify the reduction of required auxiliary energy achieved by the application of solar thermal (EN ISO 9488:1999). While f_{sol} disregards losses of a conventional heating system, f_{sav} consider these, which is why f_{sav} is a more benefit-oriented indicator describing the real advantage of using solar thermal for the end-user. DIN EN 12977-2:2012 defines the fractional energy savings f_{sav} as:

$$f_{sav} = 1 - \frac{Q_{Aux}}{Q_{conv}} \tag{4.28}$$

with the heat demand in a conventional heating system Q_{conv} as sum of the heat demand Q_{demand} plus heat losses of a conventional heat system $Q_{Loss,conv}$, which amount to 487 kWh for system (c).

Figure 4.20 compares the resulting solar fraction f_{sol} and the fractional solar savings f_{sav} for different collector technologies as function of the collector area.

The qualitative shape of the curves of f_{sol} and f_{sav} resembles the curve for total thermal yields Q_{Coll}, where a saturation of the collector yield can be observed with increasing collector areas. However, f_{sol} additionally includes losses on the system level and is therefore a better indicator for the thermal system performance than the total overall collector yield Q_{tot}. The fractional solar savings f_{sav} are slightly higher than f_{sol} since the former indicator also considers heat losses of a conventional heating system. Yet, their shape of curves is very similar.

In order to achieve the solar fraction of f_{sol} = 0.65, A_{coll} = 5 m² of flat plate collectors, A_{coll} = 8.5 m² of glazed PVT collectors with low-e, and A_{coll} = 17.5 m² of glazed PVT collectors without low-e coatings are

required. The thermal efficiency of the unglazed PVT collector is insufficient to reach the required solar fraction.

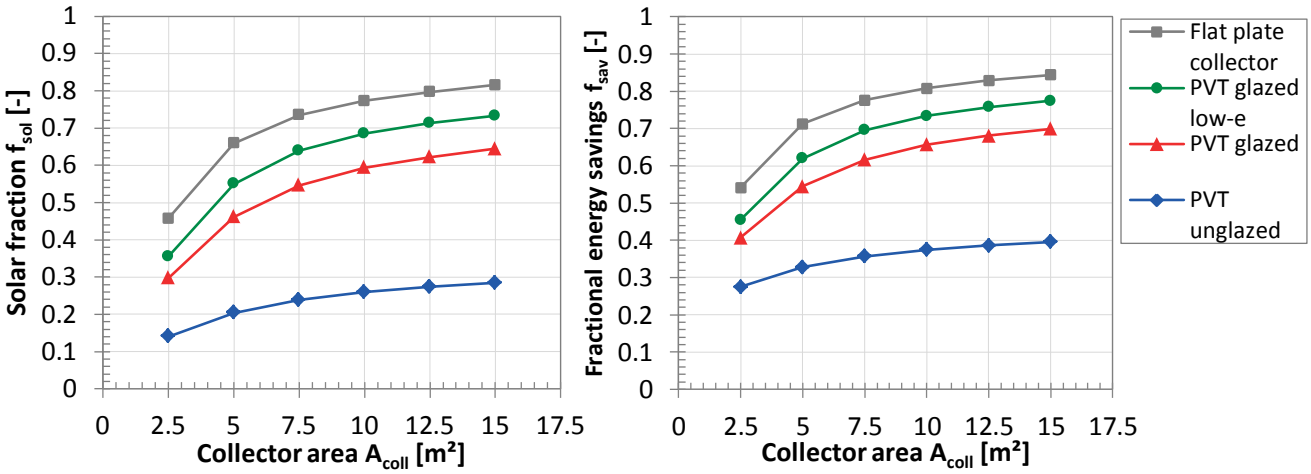

Figure 4.20: Solar fraction f_{sol} and fractional energy savings f_{sav} as function of the collector area A_{coll} in system (c).

This again demonstrates the difficulty of PVT collectors to reach high solar fractions, respectively high fractional solar savings. High solar fractions require a good thermal efficiency, so that the collector produces heat also during periods of challenging operating conditions with low ambient temperatures and low levels of irradiance. This is why PVT systems should aim towards systems with low characteristic temperatures and thus low solar fractions.

4.5.3 Assessing the energetic added value of PVT collectors on limited areas

Neither the collector yield and utilization ratio (chapter 4.3) nor the described system indicators for PV systems and solar thermal systems (chapter 4.5.2) illustrate the beneficial dual use of co-generating electricity and heat in a single component on limited areas. If PVT collectors are compared with either PV modules or solar thermal collectors, they will always underperform, since the electrical efficiency of PVT is lower than that of PV modules and the thermal efficiency is lower than that of solar thermal collectors. But the advantage of PVT collectors, to generate both electricity and heat on each square meter of collector area, is not considered by these considerations.

The assessment of the energetic added value of PVT on limited areas is an alternative, novel approach, which compares the energy yield of a PVT installation with a side-by-side installation of FPC and PV modules on limited areas. In the planning process of PVT collector systems, this approach of viewing limited areas showed a high practical relevance when high solar yields were required. Since glazed PVT collectors typically aim at substituting conventional solar thermal collectors, their added value can be seen in the electrical surplus yield of a PVT installation, which covers the same thermal load but additionally provides solar electricity.

The described approach builds up on the work by Dupeyrat (2011a) and Delisle and Kummert (2014). However, instead of looking at a fixed roof area with either PVT+PV or FPC+PV, the new approach only compares the energy yield of the area occupied by PVT collectors in comparison with a FPC+PV installa-

tion. Thus, the assessment is independent from the random choice of the reference roof area and the absolute values of the resulting indicators are more meaningful.

For this assessment approach, the PVT collector array is sized in such a way, that both types of installations, FPC+PV and PVT, generate the same thermal yield. The corresponding area of PVT collectors has to be increased to compensate for the lower thermal performance of PVT collectors compared to FPC. The PV module array is sized in such a way that the flat plate collectors and PV modules cover the same roof area as the PVT collectors. Since both side-by-side and PVT installations generate the same thermal output, the surplus electrical output of the PVT array is the sole indicator to characterize the added value of using PVT collectors.

Figure 4.21 illustrates the comparison of a side-by-side installation with a PVT collector installation exemplarily for system (c). The areas of the FPC, PV and PVT array result from the following considerations:

1. The area of the flat plate collector amounts to A_{FPC} = 5 m², as previously defined in the reference systems.
2. By definition, the thermal yields of the PVT array have to equal the yields of the flat plate collector array. An area of A_{PVT} = 8.5 m² of glazed PVT collectors with low-e are required to meet the target of Q_{coll} = 2.7 MWh.
3. The differential area between PVT and flat plate collectors is filled by PV modules, so that both installations occupy the same roof area. Here, the difference between gross, aperture, and PV module area of glazed PVT collectors has to be considered, which leads to a PV module area of A_{PV} = 3.5 m².

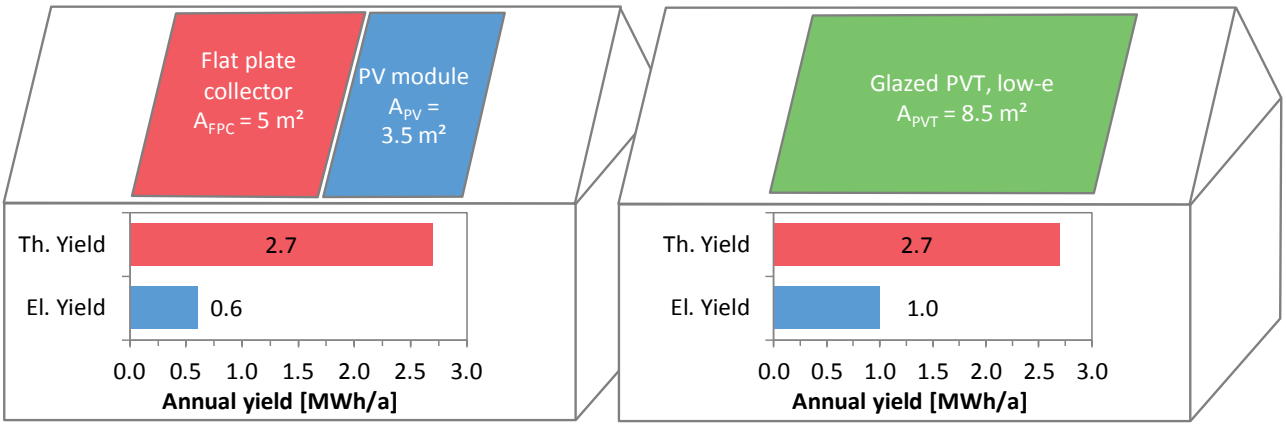

Figure 4.21: Limited area assessment of system (c), Würzburg. Comparison of a side-by-side installation of flat plate collectors (FPC) and PV modules with a PVT installation of same thermal overall output on the same roof area.

By definition, both installations generate the same thermal yields. However, the PVT array generates 1.0 MWh of electricity compared to 0.6 MWh of the PV array. This increase of +60 $\%_{rel}$ is due to the fact that the whole area is covered by PVT collectors generating electricity. On the contrary, PV modules only cover a small fraction of the area in the side-by-side installation.

Two new indicators are introduced here to describe the area requirement and the additional electrical yield of a PVT system relative to a side-by-side installation.

The area requirement factor f_{area} specifies the additional area, which is required to reach a design solar fraction f_{sol} by taking into account the reduced thermal efficiency of PVT collectors compared to refer-

ence FPCs. In order to compensate for the lower specific thermal yields of PVT collectors, the PVT collector area has to be enlarged. f_{area} is defined as the ratio of PVT collector aperture area A_{PVT} divided by the reference collector area A_{FPC} which both produce the same annual thermal yield:

$$f_{area} = \frac{A_{PVT}}{A_{FPC}} \tag{4.29}$$

The surplus electricity rate $f_{surplus}$ quantifies the rate of additional electricity generated by a PVT array compared to a side-by-side installation of reference collectors and PV modules on the same area. Thus, $f_{surplus}$ quantifies how much more electricity is generated by a PVT array compared to a side-by-side installation with identical heat generation and is defined as the ratio of the total electrical output of the PVT collectors E_{PVT} compared to the total electrical output E_{PV} of the PV modules in the side-by-side installation $E_{PV:}$

$$f_{surplus} = \frac{E_{PVT}}{E_{PV}} \tag{4.30}$$

The electrical surplus rate $f_{surplus}$ varies between different systems and also depends on the PVT and reference technologies. Accordingly, $f_{surplus}$ characterizes the energetic added value of co-generating electricity and heat in a single component on limited areas.

Evaluating these two new indicators for the above-mentioned example yields an area requirement factor f_{area} of 1.70 and a surplus electricity rate $f_{surplus}$ of 1.60. This means that 70 % more collector area is required to reach the same thermal output, but 60 % more electricity is generated on the same roof area.

The same procedure for assessing the energetic added value of PVT on limited areas was applied for the three investigated PVT collector technologies in the four systems (a) - (d). Table 4.7 compares the resulting, newly introduced indicators f_{area} and $f_{surplus}$. Owing to the different total areas of each case, the overall electrical yields of each case should not be compared, but only the highlighted area requirement factor f_{area} and the surplus electricity rate $f_{surplus}$.

The differences between systems (a) – (d) can be attributed to the characteristic temperature. The higher the characteristic temperature, the higher is the area requirement factor and the lower is the surplus electricity rate. This underlines the importance of low characteristic temperatures for the synergetic applicability of PVT collectors.

The unglazed PVT collectors do not reach the required thermal target of systems (b) – (d). Increasing the collector area further would not yield higher overall thermal yields, because the characteristic temperatures of systems (b) – (d) are too high for unglazed PVT collectors. Glazed PVT collectors with low-e coatings require significantly smaller collector areas to achieve the targeted thermal yield, resulting in a lower area requirement factor $f_{area.}$ A high thermal efficiency is therefore essential to reduce the necessary collector area.

The glazed PVT collectors in system (c) and system (d) do reach the required thermal output and the electrical surplus rate is smaller than 1. This means, that the PVT installations achieve a lower electrical yield than side-by-side installations owing to the drop of electrical efficiency of the PVT collectors compared to PV modules. Therefore, the application of glazed PVT collectors in systems (c) and (d) is not beneficial, under mere energetic considerations.

Table 4.7: Area requirement and surplus electrical yields comparing a side-by-side and PVT installation with equal thermal yields covering the same combined roof area.

	System (a)			System (b)			System (c)			System (d)		
	Un-glazed	**Glazed**	**Glazed low-e**	**Un-glazed**	**Glazed**	**Glazed low-e**	**Un-glazed**	**Glazed**	**Glazed low-e**	**Un-glazed**	**Glazed**	**Glazed low-e**
Area FPC +PV [m²]	8 +10.5	8 +3.6	8 +2	target not met	15 +22.6	15 +7.9	target not met	5 +12.4	5 +3.5	target not met	12 +30	12 +8.4
Area PVT [m²]	18.5	11.6	10		37.6	22.9		17.4	8.5		42	20.4
f_{area}	**2.3**	**1.4**	**1.2**		**2.5**	**1.5**		**3.5**	**1.7**		**3.5**	**1.7**
Q_{tot} FPC/PVT [MWh/a]	5.6	5.6	5.6		10.1	10.1		2.7	2.7		5.0	5.0
E_{tot} FPC+PV [MWh/a]	1.7	0.6	0.3		4.0	1.4		2.2	0.6		5.3	1.5
E_{tot} PVT [MWh/a]	3.1	1.5	1.2		4.8	2.8		2.2	1.0		5.2	2.3
$f_{surplus}$	**1.79**	**2.42**	**3.53**		**1.20**	**1.98**		**0.98**	**1.60**		**0.97**	**1.56**

Particularly PVT collectors with low-e coatings show a high energetic benefit with an increase of electrical output of up to 253 %. Even under challenging conditions in a combi system, PVT collectors with low-e achieve an electrical output 56 % higher than a side-by-side installation. 20 - 70% more area of PVT collectors compared to flat plate collectors are necessary to reach the required thermal output.

In conclusion, PVT collectors can achieve a significantly higher electrical output on limited areas while maintaining the same thermal output as a side-by-side installation of flat plate collectors and PV modules. To assess this aspect quantitatively, two new indicators were introduced and discussed. The added value of the hybrid PVT concept can be assessed by means of the electrical surplus rate $f_{surplus}$. The additional collector area, which is required to meet the same thermal output, is specified by the area requirement factor $f_{area.}$

4.5.4 Comparison of the system performance of PVT systems (a) - (d)

To conclude the assessment of the performance of PVT systems, worthwhile PVT systems are compared in the following and their performance is evaluated with the newly introduced indicators.

First of all, suitable PVT technologies have to be selected for the PVT systems (a) - (d). The previous considerations on the characteristic temperature clearly demonstrate that the PVT collector has to match the operating temperatures of the system and a suitable PVT collector should be selected according to the level of T_{char}. Following this approach, suitable PVT technologies are now selected for the previously defined systems (a) - (d) and their collector array is sized to meet the required thermal demand.

System (a) has low operating temperatures (T_{char} = 21.3 °C), system (b) medium operating temperatures (T_{char} = 44.4 °C), and systems (c) and (d) reach slightly higher operating temperatures (T_{char} = 49.1 °C and T_{char} = 54.2 °C). Following the recommendation of suitable PVT collector technologies per temperature range in Figure 4.14, unglazed PVT collectors are selected for system (a) and glazed PVT collectors with

low-e for systems (c) and (d). An exception from the recommendation is made in system (b). The glazed PVT collector is selected, although T_{char} is higher than the recommended temperatures. This is to show a possible use case also for the glazed PVT collector technology.

Analogous to the procedure described in chapter 4.5.1, the area of the PVT collector array is enlarged to deliver the same total heat output as the reference FPC array. Figure 4.22 indicates the required area for the PVT collector arrays and the employed PVT collector technology. Note that system (c) is identical to the PVT system discussed in chapter 4.5.2.

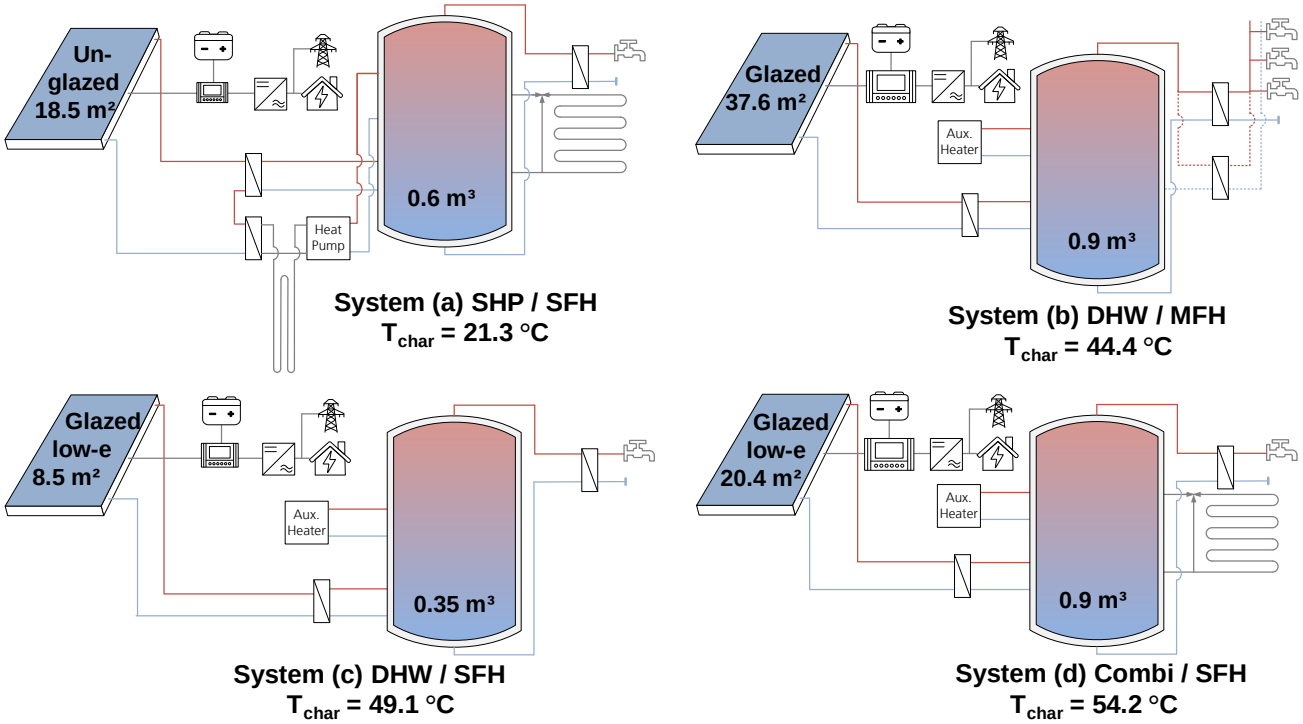

Figure 4.22: Electrical and hydraulic layout of PVT systems (a) - (d) including PVT technology and required collector area.

System simulations were conducted for these systems, and their performance is summarized in Table 4.8 with regards to the previously introduced system performance indicators. This synopsis illustrates how the selected system indicators characterize the performance of PVT systems comprehensively. Most performance indicators are dimensionless quantities, allowing a comparison and transformation between different types of collectors, systems, and locations.

- The collector performance indicators characterize the collector yields either by the specific electrical and thermal yields E_{PV} and Q_{coll} or by the utilization ratios UR_{el} and UR_{th}. The utilization ratio is a dimensionless quantity, which normalizes the collector yields through division with the annual irradiance I_{tot}. The collector performance indicators are particularly important for the selection of a PVT technology and for assessing the economic feasibility.
- The electrical system performance can be characterized by the electrical coverage rate f_{cov} and the self-consumption rate $f_{selfcon}$. The former indicator f_{cov} characterizes the share of the electricity demand which is covered by the locally generated solar electricity. The share of locally consumed electricity is characterized by the self-consumption rate $f_{selfcon}$. The indicators f_{cov} and $f_{selfcon}$ are particularly useful for analyzing the match of PV generation and electricity load, and for sizing a PV bat-

tery system and the module array, which might also consist of PVT collectors and PV modules side-by-side.

- The thermal system performance can be characterized by the solar fraction f_{sol} and the fractional energy savings $f_{sav.}$ These indicators illustrate the rate of heat load which is covered by solar heat allowing an assessment of the level of autarchy, the reduction of conventional energy consumption, primary energy savings, or avoided CO_2 emissions. Furthermore, the solar fraction f_{sol} was found to be suitable for sizing a PVT collector array through its relationship with the characteristic temperature T_{char} (compare Figure 4.13).
- In addition to the extensively discussed characteristic temperature T_{char}, two new indicators were specifically defined for comparing PVT systems with conventional systems. The surplus electricity rate $f_{surplus}$ describes the potential of PVT to generate more solar energy on limited areas compared to a side-by-side installation. On the other hand, the area requirement factor f_{area} illustrates the additional area, which is required to achieve the same thermal output as a conventional solar thermal system. Thus, the PVT specific indicators quantify the benefits (more energy) and the downsides (more collector area) of PVT systems compared to non-PVT systems.

For a more detailed assessment of the PVT systems (a) – (d), the interested reader is referred to Appendix C.6. There, a detailed analysis of the system performance is also given for the other PVT systems (a), (b), and (d), analogous the presented procedure for system (c). Detailed scorecards for each PVT system with a comparison of system performance indicators are presented, showcasing possible use cases for the investigated PVT technologies. Moreover, Table C.7 comprehensively summarizes the performance of collector and system of the PVT systems. Their performance can be compared with the electrical and thermal performance of conventional PV or FPC systems Table C.5 and Table C.6.

Table 4.8: Synopsis of system performance indicators of PVT systems (a) – (d).

Performance indicator	Symbol	Unit	Definition	Sys (a) SHP/SFH	Sys (b) DHW/MFH	Sys (c) DHW/SFH	Sys (d) Combi/SFH
System characteristics							
Collector technology				unglazed PVT	glazed PVT	glazed PVT with low-e	glazed PVT low-e
Collector aperture area	A_{ap}	m²		18.5	37.6	8.5	20.4
Collector performance							
Specific electrical yield	E_{PV}	kWh/m²a	Eq. (4.16)	182	152	139	135
Specific thermal yield	Q_{coll}	kWh/m²a	Eq. (4.17)	307	273	321	237
Electrical utilization ratio	UR_{el}	-	Eq. (4.19)	0.14	0.12	0.11	0.10
Thermal utilization ratio	UR_{th}	-	Eq. (4.20)	0.24	0.21	0.25	0.18
Electrical system performance							
Electrical coverage rate	f_{cov}	-	Eq. (4.25)	0.50	0.13	0.21	0.44
Self-consumption rate	$f_{selfcon}$	-	Eq. (4.26)	0.75	1.00	0.97	0.87
Thermal system performance							
Solar fraction	f_{sol}	-	Eq. (4.27)	0.05[5]	0.31	0.65	0.28
Fractional energy savings	f_{sav}	-	Eq. (4.28)	0.09[5]	0.35	0.70	0.31
PVT specific indicators							
Characteristic temperature	T_{char}	°C	Eq. (4.18)	21.3	44.4	49.1	54.2
Area requirement factor	f_{area}	-	Eq. (4.29)	2.3	2.5	1.7	1.7
Surplus electricity rate	$f_{surplus}$	-	Eq. (4.30)	1.8	1.2	1.6	1.6

4.5.5 Discussion of results

Chapter 4.5 assessed the performance of PVT systems where PVT collectors substitute conventional flat plate collectors and their collector array is sized to achieve the same overall thermal yield as flat plate collectors. This leads to demanding thermal requirements with relatively high characteristic temperatures

[5] The indicators f_{sol} and f_{sav} alone are not suitable to characterize the thermal system performance of the solar heat pump system, as the PVT collectors provide solar heat to the storage and the borehole. The indicators f_{sol} and f_{sav} only consider the heat which is directly delivered to the storage in parallel operation but disregard the heat for regenerating the borehole. According to the system simulations, the regeneration of the borehole increases the mean evaporator temperatures of the heat pump from 9.5 °C to 11.8 °C. This effect, combined with the reduced heat demand through the parallel operation, reduces the electricity demand of the heat pump by 9 %.

T_{char}. Consequently, only low utilization ratios are achieved compared to the yield assessment in chapter 4.3. In particular, this can be seen in system (b), where the PVT collectors underperform owing to an oversized collector array and too high operating temperatures for the glazed PVT technology.

The previous findings lead to the following three requirements for a viable and synergetic application of PVT collectors:

1) The system should have a considerable heat and electricity demand, which ought to be covered by solar energy. This is the principle motivation for generating solar electricity and heat locally.

2) The available areas for the application of solar energy should be limited. For buildings with extensive roof areas, a side-by-side installation of flat plate collectors and PV modules might be a better solution.

3) The characteristic temperature of the PVT system should be as low as possible. Small solar fractions and small dimensions of the PVT collector array can achieve this requirement. Furthermore, PVT systems with a relatively constant heat demand a more suitable due to the rarer occurrence of stagnation.

An additional point has to be stressed. PVT collectors should not be seen as a one-to-one replacement of solar thermal collectors with the added functionality of PV generation. On the contrary, PVT systems should be specifically designed for the requirements of PVT collectors. As a consequence, the concept of co-generating electricity and heat should not only be restricted to the collector but expanded to a sector-coupled energy concept for the building as a whole. Ideally, this also leads to holistic, synergetic PVT systems. Solar heat pump systems with PVT collectors are one worthwhile example where solar electricity and heat are used to cover the local power and heat demand while the heat pump transforms electricity into heat.

4.6 Thermal analysis of PVT collectors within PVT systems

The objective of the following section is to gain insights into the operation of PVT collectors within typical PVT systems. The system-oriented component development approach aims at optimizing the collector according to the specifications and requirements which are derived from the system the collector is operated in.

In this thesis so far, we optimized the PVT collector by applying low-e coatings and subsequently studied its system performance. Now, we would like to analyze how the system affects the collector operation and use the insights to further improve the collector design and its construction in the future.

Up to now, the operating conditions of the PVT collector were characterized by the characteristic temperature. T_{char} is defined as the irradiance-weighted mean fluid temperature T_m and, as such, can be considered the governing operating temperature of the collector. Yet, operating conditions deviate from the mean value of T_{char} over the year. Moreover, the temporal probability distribution of operating temperatures is of interest. For this purpose, the collector operation of the four previously defined systems is thermally analyzed by means of two novel diagrams, the temperature duration curve and the collector operating map.

4.6.1 Temperature duration curve

The load duration curve is a tool frequently used in the power generation sector to analyze a power plant utilization or dimension a co-generation plant (Zahoransky et al. 2010). The analysis of the load duration curve illustrates the operating hours and temporal variation of operating temperatures and thus shows how often certain fluid temperatures occur throughout the year. This tool is now applied to PVT collectors to analyze the frequency distribution of the mean fluid temperature.

To generate the temperature duration curve, the hourly time series of the simulation results are analyzed. Only those temperatures are considered where the collector is operational. This is achieved by filtering the events when the pump is turned off. Then, the valid temperatures are sorted from high to low values, so that a sorted annual temperature duration curve is obtained. The resulting temperature duration curves for systems (a) – (d) are shown in Figure 4.23. For comparison purposes, T_{char} is also added to the graph.

The temperature duration curves of systems (b) – (d) are very similar and almost linear over a wide range T_m. Hence, there are no operating temperatures with particularly frequent occurrences. Temperatures up to T_m = 93 °C are reached in systems (b) - (d), but only for a short duration annually. The solar heat pump system (a) has a very different temperature duration curve, as the unglazed PVT collector is operated at lower temperatures for regenerating the borehole.

The total utilization time is influenced by the system temperatures and the thermal performance of the PVT collector. The unglazed PVT collector in system (a) is operational for 995 hours per year owing to its low thermal efficiency. The collectors in system (b) and (c) are operational for 1587 h/a, respectively 1543 h/a. Despite its higher thermal efficiency, the glazed PVT collector with low-e in system (d) achieves an annual utilization time of 1256 h/a, as high storage temperatures in summer reduce the total utilization time.

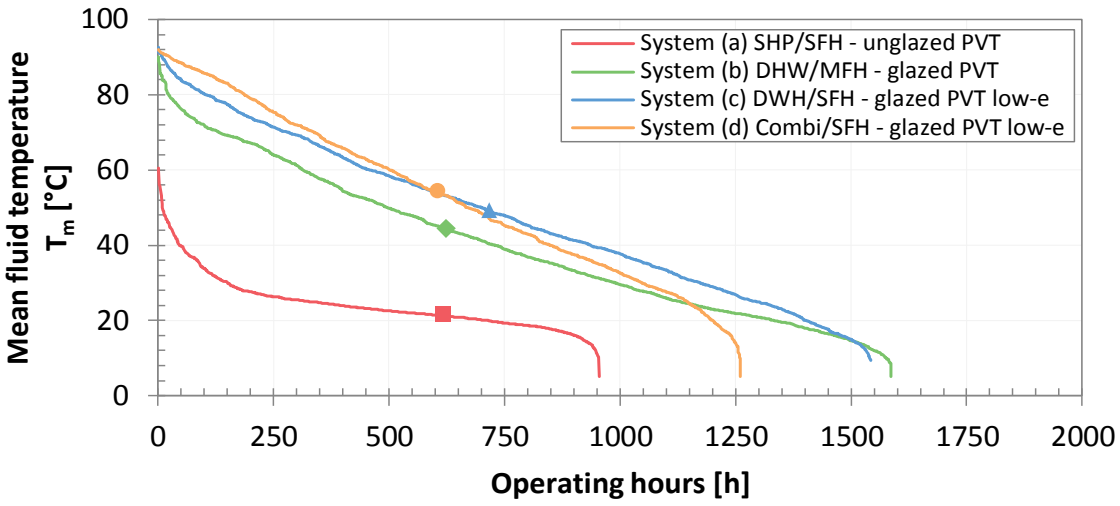

Figure 4.23: Temperature duration curves for PVT systems (a) - (d). The marker represents the characteristic temperature T_{char}.

4.6.2 Collector operating map

The discussion about the efficiency of solar thermal collectors and PVT collectors usually revolves around the efficiency curve. There, the efficiency is plotted as a function of the reduced temperature ΔT/G, i.e.

the temperature difference of mean fluid to ambient temperature $\Delta T = T_m - T_a$ divided by the incident irradiation G. It is however not clear which part of the efficiency curve is utilized during operation in real systems. The analysis of the novel collector operating map gives a good understanding at which temperatures and which levels of irradiance thermal yields are generated in typical systems and which part of the efficiency curve needs to be optimized.

The collector operation map plots the thermal yields in a two-dimensional, Cartesian carpet plot with the temperature difference $T_m - T_a$ as x-coordinate and the irradiance G as y-coordinate. To generate the collector operation map, the collector yields are grouped in bins of the respective $T_m - T_a$ and G intervals in which they are harvested. Afterwards, the yields are normalized so that their sum equals unity. Thus, the collector operation map is basically a histogram in two dimensions. As additional information, the mean, yield-weighted temperature difference $T_m - T_a$, is added to the graph as a white crosshair.

Figure 4.24 depicts the resulting collector operation maps for the four PVT collectors in systems (a) - (d). An interesting shape of the yield probability distribution with a characteristic form of the color map can be observed. During low levels of irradiation, only low temperature differences are achieved. During high levels of irradiation, also higher temperature differences are reached. This effect can partly be attributed to the fact that the temperature lift from T_{in} to T_{out} is affected by the instantaneous thermal heat gain, resulting in higher mean fluid temperature during higher levels of irradiance.

A high share of thermal yield is harvested at medium levels of irradiance. The yield-weighted mean irradiance amounts to G = 630 – 670 W/m². Instead of the typical G = 1000 W/m² peak power, which is used in efficiency curves, G = 650 W/m² is therefore a more representative value for the typical irradiance in western European climates.

The unglazed PVT collector operates mostly in the range of ambient temperatures and even at negative temperature differences, i.e. fluid temperature below ambient. In the other PVT systems, the mean operating temperature difference ranges between $\Delta T = 27.4$ K of the glazed PVT collector in system (b) to $\Delta T = 46.7$ K of the glazed PVT collector with low-e in system (d).

The highest temperature differences are $\Delta T = 40$ K of the unglazed PVT collector in system (a), $\Delta T = 60$ K of the glazed PVT collector in system (b), and $\Delta T = 67.5$ K of the glazed PVT collector with low-e in systems (c) and (d). The maximum temperature difference ΔT is thus significantly lower than the depiction of the efficiency curve, which is typically plotted up to the stagnation temperatures at the intersection of the efficiency curve with the x-axis. A value of $\Delta T = 70$ K is therefore a more representative value for the maximum temperature difference to be shown in an efficiency curve.

Low heat losses and as consequence the low inclination of the efficiency curve are required to harvest solar heat at medium temperature and low levels of irradiance. The minimization of heat losses is thus required to reach an adequate efficiency in the operating range, and not to reach high temperatures as temperature difference remains below $T_m - T_a = 70$ K in all PVT systems. Hence, the right part of the efficiency curve is not utilized in real operation.

This is an important observation with regards to the issue of overheating. High temperatures, respectively high temperature differences, are not desired by the system, but are only an undesired side effect of the basic requirement of low heat losses. Consequently, the principle solution of an overheating protection can be applied for PVT collectors. The overheating protection is only activated in periods without heat demand and frequent occurrences of stagnation. During periods with higher heat demand, the

overheating protection remains deactivated and the PVT collector achieves low heat losses and a high thermal efficiency. The principle of overheating protection will be studied theoretically and experimentally in the following chapter 5.

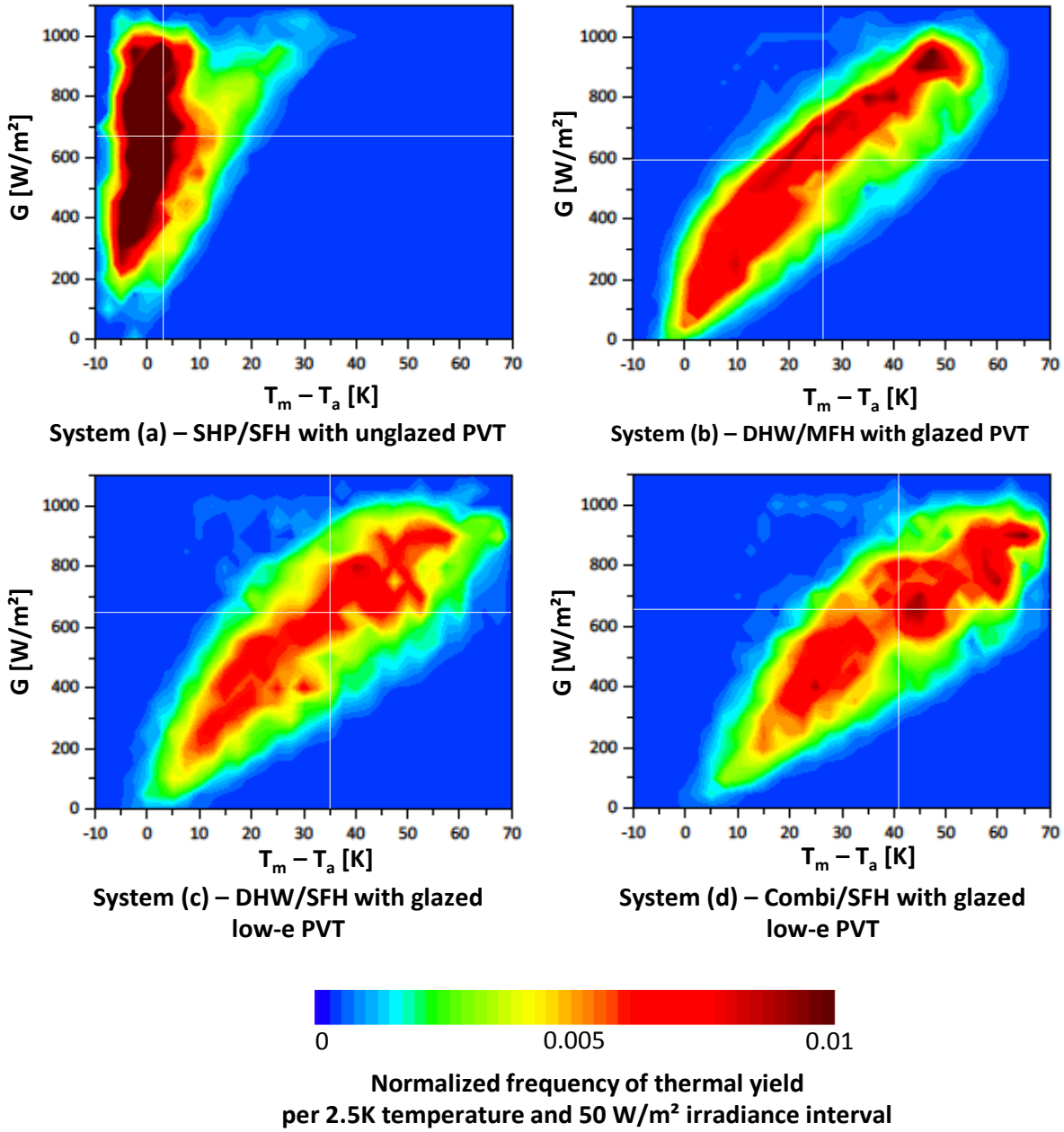

Figure 4.24: Frequency distribution of thermal yields per temperature difference and irradiance interval. The white crossfade refers to the mean, yield-weighted level of irradiance G and temperature difference T_m - T_a.

4.7 Techno-economic assessment of PVT systems

Next to the technical performance of PVT systems with regards to annual yields, the economic feasibility is also a crucial factor to determine the future success of PVT collectors in the market. To investigate this point, the costs of heat and electricity of PVT systems are analyzed and benchmarked with PV and solar thermal (ST) systems.

First, the net list prices of PVT collectors are analyzed by means of a market review of existing PVT products. Then, the costs of an exemplary PVT system are presented, including required component and installation costs. Finally, the levelized costs of heat and electricity are assessed by combining the previous yield simulations with the economic cost data.

Cost data that was assessed in the Master's thesis of Pfänder (2015) form the basis for the following chapter. Her thesis was updated with more recent data. Furthermore, the assessment of levelized costs of energy was extended to also include decentral PV battery systems.

4.7.1 Cost analysis of PVT collectors

The net list prices of existing PVT products on the market allow a benchmark with competitive technologies. After a thorough market screening of available products, net list prices for various products of PV modules (thin-film, poly crystalline, mono crystalline PV) and collectors (swimming pool absorbers, flat plate collectors, evacuated tube collectors) were obtained for the German market.

No publicly available data on the prices for PVT collectors are available. Therefore, we sent enquiries on list prices to the manufacturers. In total, seven unglazed PVT collectors and three glazed PVT collectors are thus included in the cost assessment. PVT collectors with low-e coatings are not available on the market and consequently no cost data is available.

Figure 4.25 summarizes the net list prices of PV, ST and PVT technologies indicated in Euro per square meter collector area. The net list prices, which explicitly exclude taxes, are plotted against the primary energy collector yield. The electrical yields for the location of Würzburg assume a constant performance ratio of 93 % for all PV technologies. The thermal yields refer to the gross collector yields as obtained with ScenoCalc applying the MAP rating function. This diagram illustrates the energetic potential of the different technologies juxtaposed to their corresponding price level.

The average net list price of the unglazed PVT collector was found to be 417 €/m². The glazed PVT collectors at 455 €/m² are slightly more expensive. By comparison, the PV module price lies around 102 €/m² of a polycrystalline PV module and 143 €/m² of a monocrystalline PV module, while the flat plate collector ranges around 271 €/m² and the evacuated tube collector at 463 €/m². A surprisingly accurate approximation of the list price of unglazed PVT collectors is given by the sum of an average mono-Si PV module plus a flat plate collector.

The net list price, however, should not be mistaken with production costs. The most recent overview of the cost structure of flat plate collectors by Frick (2014), who updated a previous study by Mangold (1996), shows that the production costs amount to only 24 % of the net list price of flat plate collectors. More than half of the price for collectors ends up in margins at retail and wholesale. The global PV market, on the other hand, is highly competitive and margins for PV modules are rather small with the ongoing overcapacity in the PV module production (ITRPV 2017).

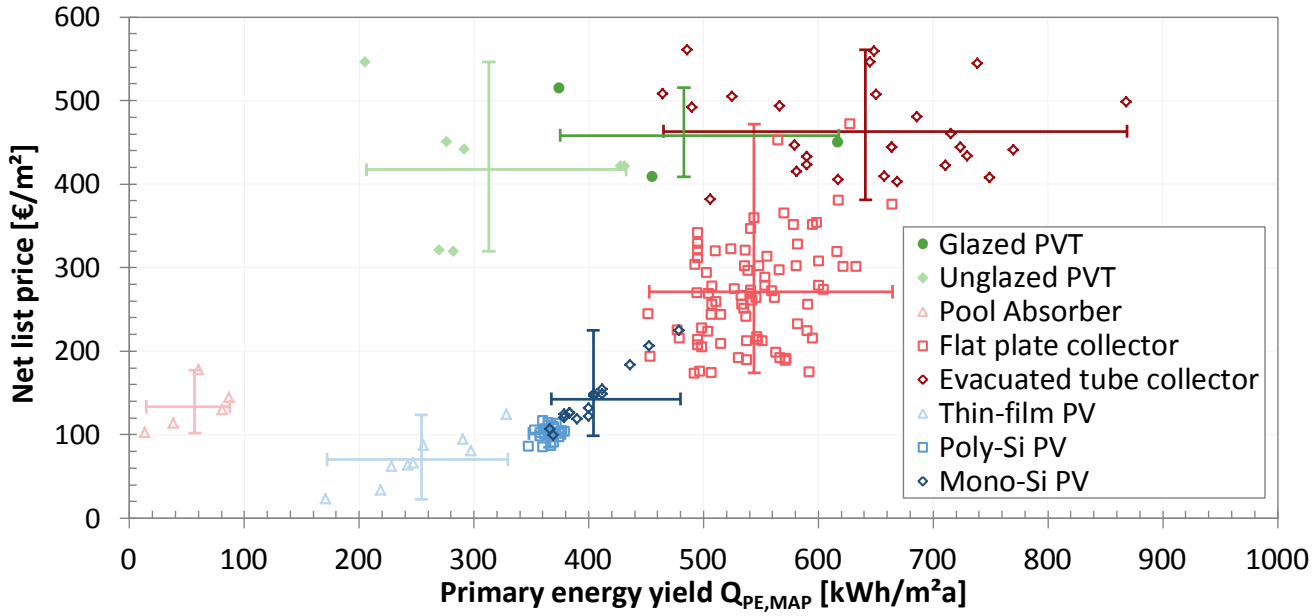

Figure 4.25: Net list prices of PVT collectors compared to conventional PV modules and ST collectors based on cost data by Pfänder (2015), updated with recent data.

Undoubtedly, there is a significant potential to reduce the costs of PVT collectors, as the PVT market is at an early stage with only few manufacturers and small collector areas being produced. The potential for reducing production costs is found in combining components that are used in both PV modules and the collector, e.g. the collector frame. In future production lines, costs could also be reduced by approaching the production of the PVT collector as an integrated process, rather than a simple combination of a PV module and a collector. One possible approach for the integrated production process is the lamination of the PVT absorber in a single production step (Dupeyrat et al. 2011b) instead of gluing a PV module to an absorber sheet. Also beyond production costs, there is certainly a cost reduction potential in terms of indirect costs. A reliable estimation of cost reduction potential is, however, not possible on the basis of the available data.

In contrast to the available list prices for market-available PV modules or ST collectors, the net list price of the glazed PVT collector with low-e coating has to be estimated on the basis of available cost data. On average, the net list price of glazed PVT collectors without low-e lies at 455 €/m². The market screening on highly-transparent low-e coatings, as discussed in chapter 3.6, found list prices of 8 - 15 €/m² of low-e coated glass. As discussed above, the production costs are only responsible for approximately one quarter of the final net list price, when a similar price structure as for flat plate collectors is assumed. Accordingly, the additional costs for the low-e coating cannot be simply added, but the internal cost calculation of the manufacturer has to be considered.

As indicative estimate, the additional costs for the application of the low-e coating are assumed to be in the range of 30 €/m². This includes costs for the coating of approximately 8 €/m² and 22 €/m² for external costs. The resulting, estimated net list price of glazed PVT collectors with low-e coatings amounts to approx. 485 €/m². Additional costs for adapted materials or an overheating protection are not included in this cost estimate.

4.7.2 Cost analysis of PVT systems

In addition to the PVT collectors, a PVT system consists of various other components that ensure the electrical and thermal operation. Moreover, installation labor and material costs make for a substantial share of the overall system costs for the end customer. In this section, a cost analysis will be presented exemplarily for the domestic hot water system (c) with glazed PVT collectors with low-e as discussed in chapter 4.5.2. This analysis includes all costs for the end customer, including components, installation and planning costs, and taxes of 19 % on top of the net list price.

In first approximation, a PVT system can be regarded as a PV system plus a solar thermal system. The costs for these separate systems are covered extensively in the scientific literature (e.g. Morris et al. (2013) for PV systems and Eicker (2012) for ST systems). However, a major difference to conventional systems concerns the installation costs. As a single collector technology has to be installed instead of two separate technologies, installation costs may be significantly lower. To study the installation costs in more detail, enquiries were sent to installers, who were asked to quote their prices for installing PV and ST systems. The costs data was analyzed in order to estimate installation costs for PVT systems with the following findings:

- Only one mounting system is required. Costs for the mounting system amount to 10 – 18 €/m² for PV modules and 10 - 25 €/m² for flat plate collectors. In the light of the heavier construction of PVT collectors, their mounting system costs are expected in the range of flat plate collectors, and are incurred at an average price of 16 €/m².
- The labor costs for the on-roof installation of flat plate collectors were explicitly quoted by only one installer at 41 €/m². It is assumed that labor costs for mounting the PVT collectors are identical to that of flat plate collectors.
- Specific installation tasks are required for the electrical and hydraulic systems where no cost reductions can be expected. The electrical installation costs include electricity works and cabling materials for the PV system. The installation of a ST system is more labor intensive. Typical tasks include the installation of storage and components, piping, and hydraulic balancing. These PV and ST specific tasks may require two trained professionals, one electrician and one plumber, for the installation of PVT collectors.

Figure 4.26 presents the full picture of the PVT system costs. The underlying cost assumptions for the individual costs are indicated therein, next to the percentage of the total system costs of 13,239 €. In accordance with the data presented in chapter 5.5.1, system (c) consists of 8.5 m² of glazed PVT collectors with low-e, a storage tank with a volume of 350 l, an inverter with a rated power of 1.25 kWp, and a battery storage with a capacity of 5 kWh.

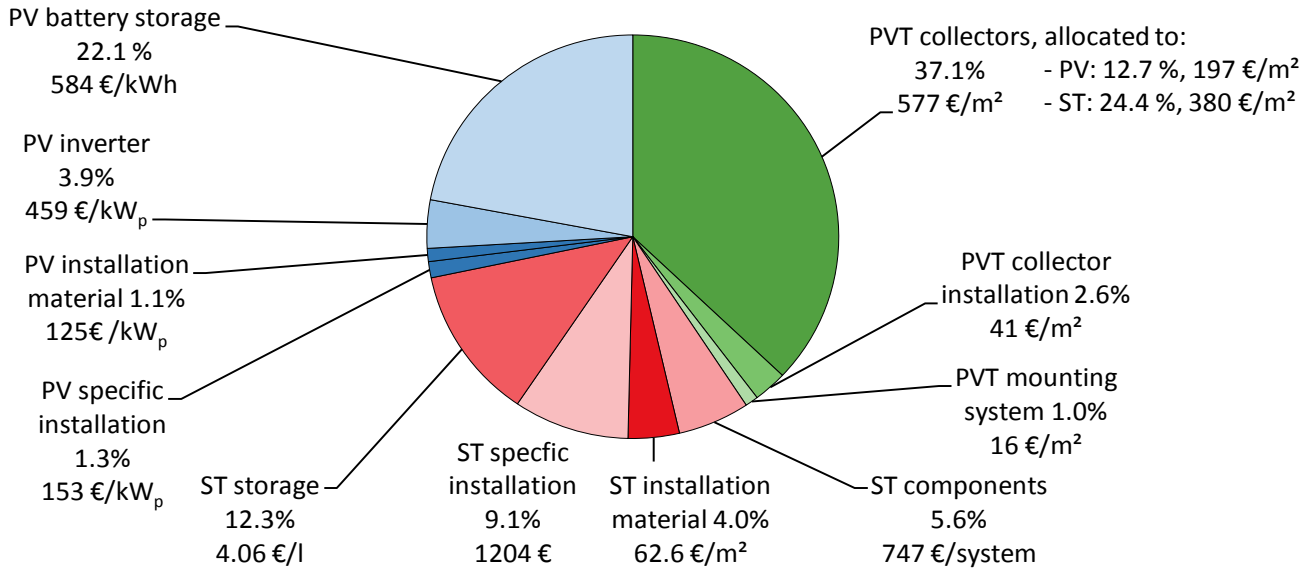

Figure 4.26: Breakdown of system investment costs for PVT system (c) with 8.5 m² of glazed PVT collectors with low-e at total system costs of 13,239 €.

With 4,906 €, or 37.1 % of the total system costs, the PVT collectors account for the major share of the system costs. For a side-by-side system of PV modules and flat plate collector, which achieve the equal thermal and electrical yield, a 6.1 m² array of PV modules and 5 m² array of flat plate collectors would be required. The corresponding costs amount to 1,024 € for the 6.1 m² of PV modules and to 1,612 € for the 5 m² of flat plate collectors. Thus, the costs for the PVT collector components are 86 % higher than the corresponding component costs in the side-by-side installation. The main reason for the increased system costs are the high costs for the PVT collectors of 577 €/m². At the same time, larger collector areas are required to generate the same energy output. This underlines the importance of high-efficiency components for the reduction of system costs.

The second largest cost item is the PV battery storage, which accounts for 22.1 % of the total system costs. However, the battery capacity can be considered oversized for the small installed electrical power of 1.1 kW_p. As the batteries are a comparably expensive investment, an additional PV array would be combined with the PVT array for the given electrical storage capacity in a real installation. Thus, the relative costs of the battery are reduced, making the PV battery system more profitable.

The installation costs for the PVT collectors amount to 485 € in the PVT installation in comparison to 570 € in the side-by-side installation. Thus, installation costs of 10 €/m² can be saved by installing PVT collectors instead of separate collectors and modules. These savings for collector installation are relatively small, compared to the high overall collector and system costs.

The total costs for the PVT system of 13,239 € are significantly higher than the combined costs for a side-by-side installation of PV modules and flat plate collectors with the same annual electrical and thermal yield. The total costs of these systems are estimated to lie around 4,813 € for the PV system and 6,094 € for the ST system. The total system costs of the hybrid PVT system are thus 21 % higher than the combined costs for the separate, non-hybrid systems.

4.7.3 Levelized costs of electricity and heat

The levelized costs of electricity LCOE and the levelized costs of heat LCOH are commonly used indicators to describe the cost for generating energy with different energy technologies. They are used to assess and compare the techno-economic viability by combining the technical characteristics, i.e. energy yields, with the economic characteristic, i.e. investment and operational costs.

The levelized costs of electricity are defined as (Konstantin 2009):

$$LCOE = \frac{I_0 + \sum_{t=1}^{t=n} \frac{OC_t}{(1+i)^t}}{\sum_{t=1}^{t=n} \frac{E_{tot}}{(1+i)^t}} \tag{4.31}$$

with the initial investment costs I_0 as in Figure 4.26, the annual operational costs OC = 1.5 %·I_0 (VDI 2014), the summation index t, the assumed lifetime n = 20 years, and the interest rate i = 2.5 %. No degradation is considered within this approach. Hence, the annual total collector yield E_{tot} is assumed constant over the entire lifetime.

A simpler notation of the LCOE without the sums can be obtained by multiplying the initial investment costs with the annuity factor $f_{annuity}$:

$$LCOE = \frac{I_0 \cdot f_{annuity} + OC}{E_{tot}} \tag{4.32}$$

with:

$$f_{annuity} = \frac{1 - (1+i)^{-n}}{i} \tag{4.33}$$

The levelized costs of heat LCOH are defined analogously (Louvet et al. 2017), but naturally incur the total thermal collector yield Q_{tot} instead of E_{tot}.

Due to the nature of the hybrid concept, it is necessary to divide the combined investment costs of the PVT system into their respective share of costs for electricity and for heat production. While this is clear for most of the system costs (the ones in blue and red in Figure 4.26), the combined costs in green are divided according the following rules: the non-allocatable PVT installation costs and the PVT mounting system are evenly split. The PVT collector costs are allocated with 34 % to electricity and with 66 % to heat, which equals the ratio between PV module and flat plate collector list prices.

It is important to compare the LCOH and LCOE on a common basis. Solar thermal systems are per se a decentral technology as they come with a heat storage and all produced heat is consumed on-site. PV systems can be carried out either grid-connected to feed excess electricity to the grid, or decentral with a battery storage. The LCOE is assessed for both scenarios: $LCOE_{grid}$ for a central, grid-connected system, and $LCOE_{storage}$ for a decentral battery system. The former $LCOE_{storage}$ can be used for comparison with the solar thermal system, and the latter $LCOE_{grid}$ for comparison with technologies or studies, where only the grid-connected LCOE is calculated.

The basis for calculation differs between $LCOE_{grid}$ and $LCOE_{storage}$: Firstly, different investment costs I_0 need to be considered. $LCOE_{grid}$ disregards the costs for a PV battery system, while these costs are included in the calculation of $LCOE_{storage}$. Secondly, different energy yields E_{tot} need to be considered. $LCOE_{grid}$

considers both the self-consumption and feed-in electricity, whereas $LCOE_{storage}$ only considers the self-consumed electricity. Thirdly, different sizes of the PV array are considered. $LCOE_{grid}$ regards a PVT system with 8.5 m² PVT collectors and PV module array with 6.1 m². $LCOE_{storage}$ requires a larger PV array to offset the high investment costs of the battery. Therefore, the assessment assumes an array size of 20 m² as a basis for the PV case. Correspondingly, the PVT case assumes a PVT array of 8.5 m² combined with a PV array of 13.9 m², which together achieve the equal electrical yield as the PV case. The costs for the battery storage are divided correspondingly, and $LCOE_{storage}$ is reported for the PVT collector array alone.

Now that the LCOE and LCOH are clearly defined, we can compare the levelized costs of the PVT system with the non-hybrid flat plate collector and PV systems in Figure 4.27.

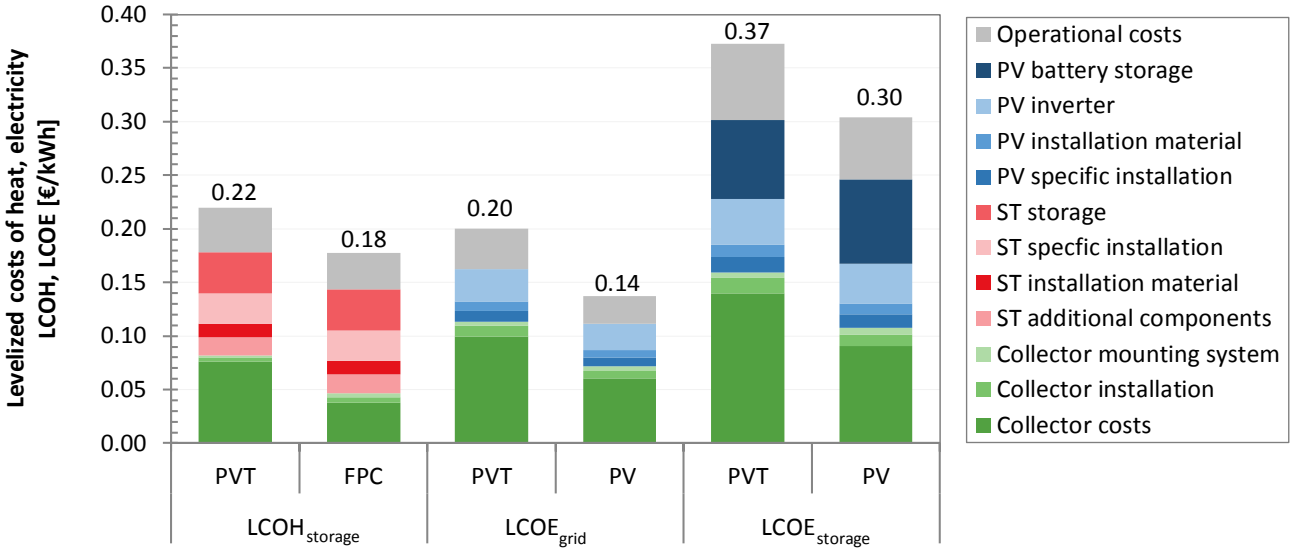

Figure 4.27: Breakdown of levelized costs of heat LCOH and electricity LCOE for system (c) with PVT collectors, flat plate collectors (FPC) and PV modules. The LCOE are reported for a grid-connected system ($LCOE_{grid}$) and for a decentral system with battery storage ($LCOE_{storage}$).

The resulting levelized costs of heat amount to $LCOH_{PVT}$ = 0.22 €/kWh and $LCOH_{FPC}$ = 0.18 €/kWh for the per-se decentral PVT and FPC system. The grid-connected levelized costs of electricity amount to $LCOE_{grid,PVT}$ = 0.20 €/kWh for the PVT system and $LCOE_{grid,PV}$ = 0.14 €/kWh for the PV system. Due to the additional battery system costs and a smaller rate of self-consumed electricity, the LCOE of the decentral PVT battery systems are significantly higher ($LCOE_{storage,PVT}$ = 0.37 €/kWh and $LCOE_{storage,PV}$ = 0.30 €/kWh).

The breakdown of LCOH and LCOE illustrates the contribution of the different costs to the levelized costs of heat and electricity. The collectors (PVT, FPC, PV) account for the largest share in almost all cases, followed by the costs for storage of electricity and heat. In solar thermal systems, the installation costs are an important factor, due to the high labor intensity of the installation. The expensive electrical battery accounts for a large share of the $LCOE_{storage}$ in both PVT and PV cases.

Comparing the PVT systems with the non-hybrid PV and FPC systems, an increase of levelized costs between 21 % and 46 % is observed. In general, there may be two possible reasons for higher levelized costs: higher investment costs I_0 and lower specific yields. In the present study, the differences can be narrowed down to the investment costs, as the PV and the FPC systems are sized to generate the same electrical and thermal yields as the PVT system.

Accordingly, the 24 % higher LCOH of the PVT system are caused by the increased investment costs of 24 %. The higher $LCOE_{grid}$ of the PVT system is also attributable to the corresponding 46 % higher investment costs. As discussed in the previous section, the high costs for the PVT collector are primarily responsible for the increased investment costs.

The decentral levelized costs of electricity $LCOE_{storage}$ are significantly higher than $LCOE_{grid}$, but also the value of the self-consumed electricity has to be ranked higher than the value of feed-in electricity. It is therefore important to not only look at the costs of electricity, but also at the benefit from a system perspective. Concerning the calculation of $LCOE_{storage}$, both PV and PVT system achieve an electrical coverage rate of $f_{cov} = 0.52$. The absolute difference of $LCOE_{storage}$ between PVT and PV amounts to 0.07 €/kWh, which corresponds to a relative increase of 22 %.

Compared with the costs for electricity purchased from the grid of 0.29 €/kWh (BDEW 2017b), the $LCOE_{storage}$ of the PV system are in a similar range, while the $LCOE_{storage}$ of the PVT system are 27 % higher. According to BDEW (2017a), the LCOH of a heating systems with a condensing gas or oil boiler amount to 0.10 – 0.20 €/kWh, the LCOH of an air-to-water heat pump amounts to 0.12 – 0.25 € /kWh, and of a wood pellet system to 0.15 – 0.21 €/kWh. Depending on the benchmark technology, the LCOH of the assessed PVT system may be cost-competitive already now.

As PVT collectors are a novel technology, it is interesting to analyze the sensitivity of the net list price of PVT collectors on the total levelized costs of heat and electricity LCOH and LCOE. For this purpose, the net list price of PVT collectors with low-e coatings is varied, while all other parameters remain at constant levels. Figure 4.28 shows the resulting sensitivity of the net list price on the LCOH and LCOE for PVT systems compared to the conventional PV and FPC systems Due to the large share of the PVT collector costs, a reduction of the collector list price of 50 % leads to a significant reduction of $LCOH_{storage}$ of 21 $\%_{rel}$ and $LCOE_{grid}$ of 32 $\%_{rel}$.

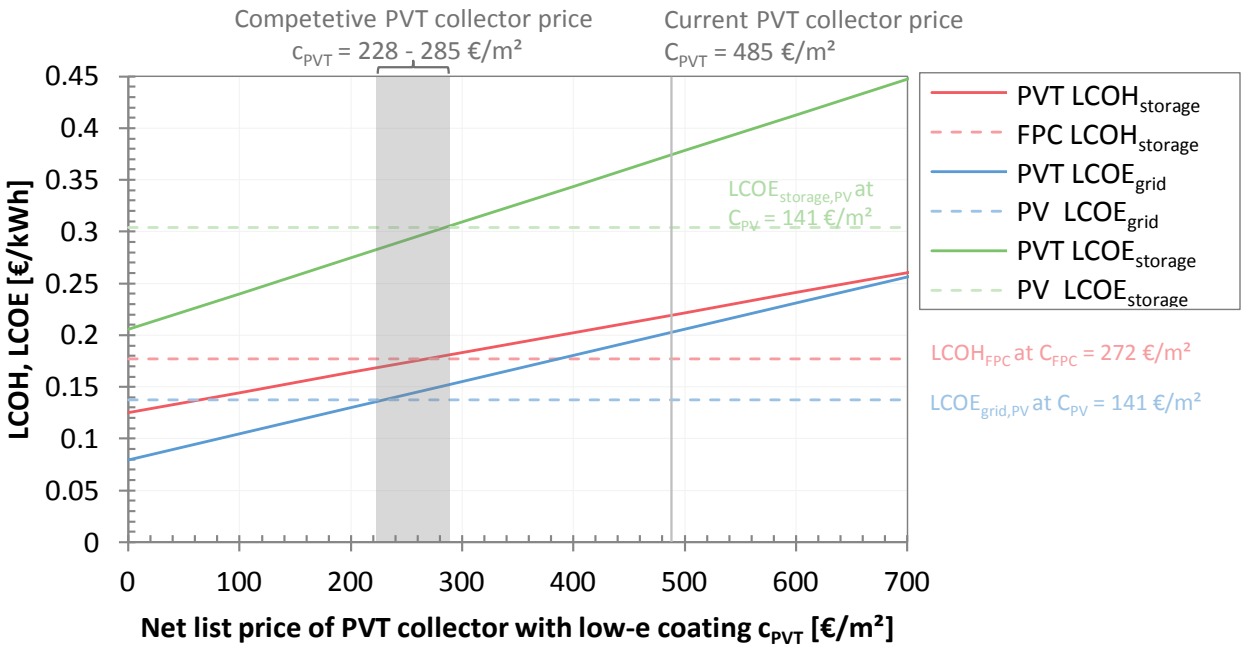

Figure 4.28: Sensitivity analysis of the net list price of the PVT collector with low-e coating on LCOE and LCOH. The reference technologies are assumed at constant module and collector price levels and are indicated in dotted lines.

It is particularly interesting to assess the PVT collector price, for which cost parity between the PVT system and the conventional system is reached. In Figure 4.28, this price of break-even can be read from the intersection of the cost curves of the PVT system with the constant energy costs of the conventional PV and FPC systems. Accordingly, PVT collectors are competitive as soon as the PVT collector price falls below c_{PVT} = 228 - 285 €/m². This corresponds to a cost reduction by almost a half compared to the current price level of c_{PVT} = 485 €/m². Keeping in mind, that the current price level of PV modules and flat plate collectors leads to a theoretical combined list price of c_{PV+FPC} = 413 €/m², this target seems ambitious too reach. Measures to reduce costs should therefore be accompanied with a further improvement of the electrical and thermal efficiency and a reduction of the balance of system costs.

4.7.4 Discussion of results

The higher energy output per square meter of PVT systems comes at the expense of higher energy costs than for the conventional side-by-side installations. At its current early commercial stage, PVT collectors are economically not competitive yet. This is due to higher costs for the components and lower specific electrical and thermal yields.

The average net list price of glazed PVT collectors amounts to 455 €/m² and can be thus more or less approximated by the sum of a separate PV module plus a solar thermal collector. It is expected that there is still a potential to reduce the collector costs by an optimized production process and by reduced external costs.

Regarding system costs, little synergies were found for the installation. Only minor cost reductions in the range of approximately 10 €/m² for installation system and labor costs may be achieved by the two-in-one PVT collector. Comparing the high costs for the PVT collectors to the non-hybrid technologies, the small cost reductions for installing PVT collectors are of subordinate importance.

Due to higher investment costs and lower specific yields, the levelized costs of electricity LCOE and heat LCOH are higher than that of separate PV and solar thermal systems. For the exemplary domestic hot water system (c), it was found that the LCOE lies 0.06 €/kWh and the LCOH lies 0.04 €/kWh above the costs for a side-by-side installation of equal electrical and thermal output. Cost competitiveness can be reached if the price of glazed PVT collectors with low-e drops below 228 - 285 €/m², which has to be considered an ambitious cost target. From this, the conclusion is reached that the value proposition of PVT collectors does not necessarily lie in low energy costs, but rather in a more effective usage of available area.

Other PVT systems with high specific yields, e.g. through low characteristic temperatures or through high annual rates of irradiance, potentially achieve lower levelized costs of energy. For instance, in system (b) lower LCOH and LCOE can be expected due to the higher specific yields. The previous considerations on low characteristic temperatures by an appropriate sizing of PVT array and storage volumes remain crucial for the economic feasibility of PVT systems at the current cost level of PVT collectors.

5 PVT COLLECTORS WITH OVERHEATING PROTECTION

The assessment of system performance in the previous chapter made clear that an improved thermal efficiency is the key to a higher overall efficiency and optimized primary energy yields. Low-e coatings are therefore an essential requirement to achieve a sufficiently high thermal efficiency in the operating range whereas yields at high temperatures are irrelevant for the system performance. Excessive temperatures during stagnation are, however, a negative side-effect of the improved thermal insulation and may lead to faults, ageing, and reliability issues. Furthermore, the PV cells underperform at elevated cell temperatures, resulting in a drop of the electrical efficiency. To solve this problem, either an inherently temperature-resistant PVT absorber construction has to be developed, or the collector has to be protected against overheating (Fortuin et al. 2014) .

The following chapter pursues the latter approach and concerns the demonstration of overheating protection (OHP) concepts in PVT collectors with the following research questions:

- What are the thermal requirements of the materials employed in PVT collectors?
- Which overheating protection concepts are suitable for the application in PVT collectors?
- How does the overheating protection influence temperatures and yields?

Chapter 5.1 gives an overview on the research of overheating protection in solar collectors and motivates the application of OHP in PVT collectors. Chapter 5.2 describes the thermal requirements of PVT collectors concerning temperature load, fault mechanisms and suitable material temperatures. Chapter 5.3 presents a classification and evaluation of existing OHP concepts following their physical effect on the absorber temperatures. In chapter 5.4, innovative PVT collectors with OHP are developed and the effect of the OHP on efficiency and stagnation temperature is characterized. Chapter 5.5 assesses the annual energy yields and temperatures of PVT collectors with OHP by system simulations.

5.1 Motivation for the application of overheating protection in PVT collectors

High stagnation temperatures have been a challenge ever since spectrally selective coatings were introduced to conventional solar collectors. Research on overheating protection (OHP) concepts for solar collectors is ongoing with different motivations and objectives.

Avoiding excessive collector and system temperatures is the central motivation for applying OHP. The potential benefits lie mainly in an increased durability and safety of collector and system. This is achieved by minimizing degradation effects on materials and the heat transfer fluid, resulting in an improved performance of collector and system over the lifetime. Furthermore, the temperature limitation avoids damage to hydraulic components in the solar thermal system, which thus increases the safety of collector and system (Harrison and Cruickshank 2012). Preventing overheating is also an important aspect in large

collector arrays, e.g. in process heat installations, where the safety issue is seen even more critically due to the bigger thermal power of the collector arrays (Frank et al. 2014).

OHP in polymeric collectors is an approach to apply cheap polymer materials in collectors with a high thermal efficiency, but avoid excessive temperatures through activating the OHP during stagnation (Lang et al. 2013; Reiter 2014). Substituting metallic materials with polymers primarily aims at reducing material and production costs. Moreover, polymeric materials are potentially more environmentally friendly with a smaller environmental footprint, as life cycle analyses show (Köhl 2015). Major drawbacks of polymer materials are, however, the reduced temperature and pressure stability.

The reduction of the thermal loads is also an objective in the development of heat pipe collectors. When the temperature in the heat pipe exceeds the dry-out limit, the operation of the heat pipe is cut off and the heat flux from the absorber to the heat transfer fluid in the manifold ceases. The complexity is thus transferred from the system to the collector, which might lead to a more reliable, simpler, and potentially cheaper system (Jack and Rockendorf 2013; Jack et al. 2014). However, heat pipes with inherent temperature limitations only reduce the temperature load in the secondary fluid circuit and not in the heat pipe and absorber sheet.

The idea of applying an active OHP in glazed PVT collectors to solve the stagnation issues was brought forward by Zondag (2008). The first research on OHP in glazed PVT collectors was carried out by Dupeyrat (2011a), which culminated in the application of a patent on an OHP mechanism for PVT collectors (Dupeyrat 2011b). Subsequently, different approaches for overheating in PVT collectors were analyzed by Wendker et al. (2012). In the same project, a PVT collector prototype with a switchable vacuum insulation was developed (Fortuin et al. 2014). Moreover, the British company NakedEnergy developed a glazed PVT collector where the PV cells are laminated on a heat pipe located in a vacuum tube. Overheating is avoided by an external heat exchanger, which is activated by a thermally controlled valve in the double condenser heat pipe (Boyle et al. 2012).

Applying OHP in PVT collectors combines the benefits of conventional solar collectors, polymer collectors and heat pipe collectors. In addition, the electrical efficiency also benefits from lower collector temperatures, making OHP particularly interesting for PVT collectors. Thus, the advantages can be summarized as follows:

- Increase the durability of the PVT collector by reducing temperature-induced aging and degradation
- Employ standard PV components and thus participate from the low cost level of PV modules
- Reduce costs of the collector by substituting expensive metal by low-cost materials, e.g. polymers
- Reduce temperature load in system and thus reduce the temperature requirements of external components
- Increase the electrical efficiency of PVT collectors by lower cell temperatures

5.2 Thermal boundary conditions for overheating protection

In this section, the technical requirements for an overheating protection with regards to reducing absorber temperatures are assessed. Firstly, typical temperatures occurring in PVT collectors are analyzed. Then, potential failure modes that are caused by elevated temperatures are summarized. Finally, the ma-

terial requirements and their maximum temperatures are discussed through experiments and literature review.

5.2.1 Stagnation temperatures

The highest collector temperatures are reached during stagnation, which VDI 6002-2014 defines as a "system state in which the heat transfer fluid in the collector loop does not circulate and the radiation energy absorbed and converted into heat is not supplied to a storage tank or consumer."

ISO 9806 (2013) allows two methods for characterizing stagnation temperature: either by direct measurement or by extrapolation from the efficiency curve. Both methods yield different stagnation temperatures, which is why a clear notion of the stagnation temperature is required. The following definitions apply in the following.

The maximum absorber temperature $T_{abs,max}$ refers to the measured stagnation temperature at the absorber. For its characterization, the collector is exposed to an incident irradiation of G = 1000 W/m² at ambient temperatures of T_a = 30 °C and a surrounding air velocity of u_{wind} < 1 m/s. The temperatures are measured at 2/3 height of the absorber in dry conditions, i.e. without fluid in the tubes, when steady-state conditions are reached.

The alternative extrapolation method calculates the stagnation temperature from the efficiency curve at its intersection with the x-axis. This temperature is referred to as standard stagnation temperature T_{stg} and is given by (ISO 9806):

$$T_{stg} = T_a + \frac{-c_1 + \sqrt{c_1^2 + 4\,G\,\eta_{th,0}\,c_2}}{2c_2} + 20\,°C \tag{5.1}$$

with standard stagnation conditions of T_a = 30 °C and G = 1000 W/m², and the coefficients $\eta_{th,0}$, c_1, and c_2 from performance measurements.

Normatively, a margin of 20 °C is added to compensate the higher wind speeds during performance measurement than during the experimental approach. Although not explicitly stated in the standard, another reason for the margin of 20 °C lies in the temperature inhomogeneity of the absorber during stagnation. While the heat losses are in first order proportional to the mean absorber temperature, the maximum absorber temperature $T_{abs,max}$ refers to the local maximum at the absorber. Numerical simulations with the multi-node collector model showed that if edge losses are considered for the glazed PVT collector, the local maximum temperature is 5.8 K higher than the average absorber temperature (compare chapter 3.2.6).

Helminger (2012) compared the measured absorber temperature $T_{abs,max}$ with the extrapolated stagnation temperature T_{stg} of 59 types of flat plate collectors. He did not incorporate the above-mentioned margin of 20 °C and found on average an mean deviation of $T_{abs,max}$ - T_{stg} = 14.9 K. Hence, the margin of 20 °C is justifiable if looking at the mean deviation only. Yet, there were also statistical spikes from $T_{abs,max}$ - T_{stg} = -20 K up to +60 K. The deviations for evacuated tube collectors were even spread more widely.

Therefore, the extrapolated stagnation temperatures T_{stg} have to be viewed critically, and if possible, measured stagnation temperatures $T_{abs,max}$ should be used. The measured method is considered to be more accurate than the extrapolation method, as the temperature is determined directly and no mathe-

matical conversion is required. However, the measured method is not always applicable, for instance if the absorber is not accessible for measurement instrumentation, or if the collector would be destroyed.

To wrap-up the considerations on stagnation temperatures, Table 5.1 summarizes typical standard stagnation temperatures of PVT collectors compared with flat plate collectors and evacuated tube collectors. Furthermore, Table 5.1 indicates the water saturation pressure p_{sat} at stagnation temperatures based on VDI (2010). If p_{sat} exceeds the system pressure, vapor formation will occur resulting in large volumes of steam formation, which can have critical implications. In conventional solar thermal collectors, the formation of steam is considered a critical problem for the hydraulic components (Rommel et al. 2007; Scheuren 2008).

Steam formation is a minor problem in PVT collectors. Since stagnation temperatures are lower than in solar thermal collectors, the water saturation pressure is also lower (compare Table 5.1). Thus, steam formation occurs more rarely, and if it happens, less volumes of steam are produced. Instead, the exposure of PV modules and their polymer components are considered the critical point of stagnation.

Table 5.1: Standard stagnation temperatures and corresponding saturation pressure of water for different collector technologies.

Collector technology	Standard stagnation temperature T_{stg} [°C]	Water saturation pressure at T_{stg} p_{sat} [bar]
Unglazed PVT collector	75 – 95	0.4 – 0.8
Glazed PVT collector	120 – 145	2.0 – 4.2
Glazed PVT collector with low-e	140 – 165	3.6 – 7.0
Flat plate collector	160 – 200	6.2 – 15.5
Evacuated tube collector	250 – 300	39.8 – 85.9

5.2.2 Annual frequency distribution of absorber temperatures

The stagnation temperature specifies the maximum absorber temperature, which occurs under worst-case, steady-state conditions. By contrast, the annual absorber temperatures that actually occur throughout a year depend on multiple factors such as climate, system operation, collector orientation, and dynamic effects, just to name a few.

System simulations were conducted to assess the typical temperature load of PVT collectors. The PVT performance model, which was presented in chapter 4.1, is also valid for stagnation conditions. The temperature load is analyzed for glazed PVT collectors with and without low-e. Both collector technologies were simulated in combi system (d) and in permanent stagnation conditions. The simulation boundary conditions from the previous section, i.e. location of Würzburg, southern orientation, tilt angle of 35°, PVT array of 20.4 m², and storage volume of 900 l, were applied.

The annual distribution frequency is obtained by analyzing the temperatures of the absorber node at every time step. The absorber temperatures are then grouped in temperature intervals in bins of 10 K. Typically, this type of histogram is plotted as a bar diagram. Instead, to show the four different cases together in a single graph, each data point represents the corresponding bar in Figure 5.1.

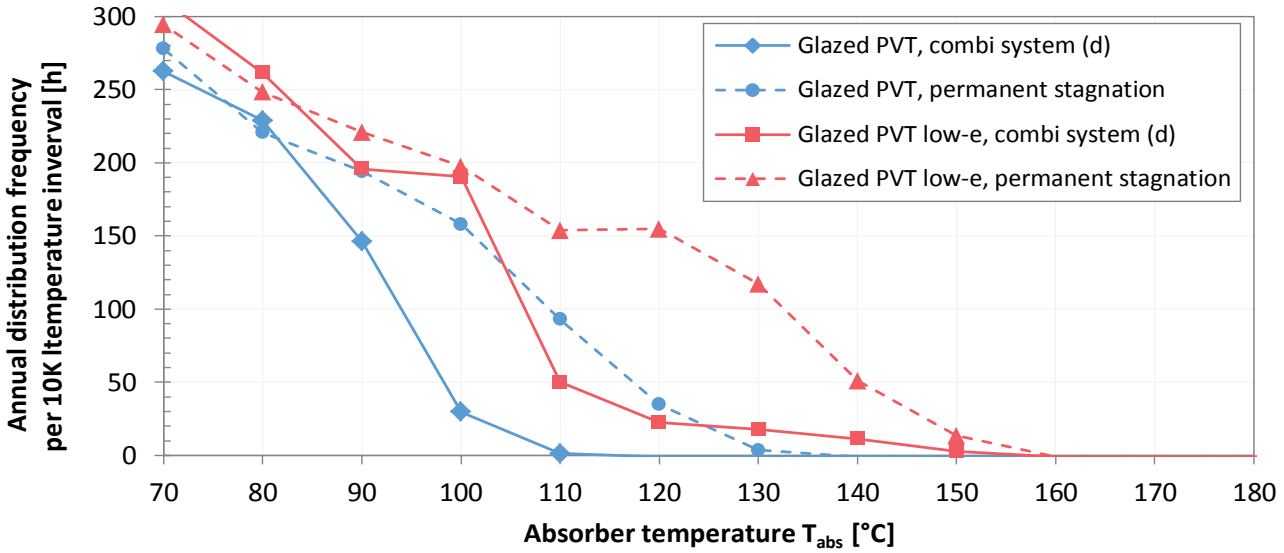

Figure 5.1: Annual distribution frequency of absorber temperatures for glazed PVT collectors with and without low-e at the location of Würzburg. Operation of PVT collectors in MPP mode throughout the year.

As can be expected, the PVT collectors face the most challenging temperature load under permanent stagnation without heat extraction. The maximum annual absorber temperatures amount to $T_{abs,max}$ = 130.8 °C for the glazed PVT collector and to $T_{abs,max}$ = 153.9 °C for the glazed PVT collector with low-e. The glazed PVT collector exceeds critical temperatures above 130 °C for only 4 h during permanent stagnation. The application of low-e increases the occurrence of critical temperatures significantly. The glazed PVT collector with low-e has to withstand absorber temperatures above 130 °C for 32 h in the combi system and for 182 h during permanent stagnation.

During permanent stagnation, the occurrence of high absorber temperatures is naturally more frequent than in the combi system in normal operation. Stagnation also occurs in the combi system when the storage is fully charged and the pump is off. However, this event is relatively rare resulting in a less frequent occurrence of absorber temperatures T_{abs} > 80 °C than during permanent stagnation. Correspondingly, absorber temperatures below T_{abs} < 80 °C are more frequent in the combi system in normal operation, as this is the typical operating range of PVT collectors in this system and the fluid cools the PVT absorber compared to the PVT collector in stagnation.

When analyzing the time series of the combi system simulations, it is interesting to notice that high absorber temperatures occur even while the pump is operational and the fluid circulates. A gradual heating-up of the collector circuit causes this effect if the heat is not efficiently transferred to the secondary circuit due to a too low heat transfer capability of the heat exchanger. Apparently, the effectiveness of the heat exchanger between primary and secondary circuit is an important parameter and should therefore not be underestimated during sizing the heat exchanger in a PVT system.

Nevertheless, the simulation results should be regarded as indicative temperature ranges, whereas monitoring results need to confirm these findings. A system failure or power outage in system (d) may shift the temperature loads into the direction of permanent stagnation. Furthermore, operating the PVT collector in OC mode instead of MPP mode also results in higher temperature loads than the simulated ones.

5.2.3 Failure mode and effects analysis

To assess the effect of elevated temperatures on the different components of glazed PVT collectors, a failure mode and effects analysis (FMEA) is presented. The approach is based in its idea on the design FMEA according to IEC 60812 (2006), which will be carried out with a reduced scope in the following.

Table 5.2 summarizes potential failures as observed in past research on PV module reliability (Yedidi et al. 2014; Köntges et al. 2014) and PVT collector development (Affolter 2000; Zondag 2008; Dupeyrat 2011a; Wendker et al. 2012; Gomes et al. 2015; Lämmle et al. 2017a). The list covers the most relevant failure modes from a reliability point of view with no claims to be exhaustive.

Two major potential causes for failure are observed: thermo-mechanical stress and exceedance of the material's maximum temperature.

Thermo-mechanical stress is induced by the thermal expansion of two different materials in bonded connections. The relative elongation δ_{rel} between two components of different materials is given by (Grote and Feldhusen 2011):

$$\delta_{rel} = (\alpha_1 - \alpha_2)\, l\, (T_{max} - T_0) \tag{5.2}$$

with the thermal expansion coefficients α_1 and α_2, the components' length l, and the maximum temperature difference $T_{max} - T_0$.

Hence, the relative elongation δ_{rel} can be reduced by matching the thermal expansion coefficients α_1 and α_2 of the bonded materials, reducing the length of the bonded a components l, and by reducing the maximum temperature T_{max}, which the materials are exposed to. Furthermore, using elastic materials, e.g. elastic glue to bond absorber sheet and PV module, also reduces the thermo-mechanical stress in the components.

Exceeding the maximum temperatures of the materials is the second cause of failure. These temperature limitations mostly apply for polymeric materials where their specific glass transition and softening temperature should not be exceeded. This is especially relevant for polymer encapsulation materials such as the PV standard ethylene vinyl acetate (EVA) where a degradation of the encapsulant can cause critical failures such as browning and delamination.

While thermo-mechanical stress can be reduced by an adapted design with the aforementioned measures, the maximum material temperatures are a strict limitation, which can only be overcome by a substitution of materials. Therefore, the maximum material temperatures for PV modules are analyzed in more detail in the following section.

Table 5.2: Failure mode and effects analysis for high temperatures in PVT collectors.

Component	Potential failure mode	Potential causes for failure	Potential effect of failure
PV cells	micro-cracks, cell breakage	thermo-mechanical stress	reduced cell and module efficiency, total module failure
	corrosion, oxidation	humidity intake from degraded EVA	
cell connectors	cracked, broken cell connectors	thermo-mechanical stress, material fatigue	increase of series resistance, string failure
EVA	yellowing, browning	oxidation of EVA at elevated temperatures	degraded optical efficiency
	delamination	production of acetic acid at elevated temperatures	corrosion of PV cells
bypass diodes	defective bypass diode	thermo-mechanical stress, exceeding max. temperature	formation of hot spots, burn marks, fire
junction box	loss of adhesion deformation, destruction	thermo-mechanical stress, exceeding max. temperature	short-circuit, module failure
glue	failure of adhesion, e.g. between PV module and absorber	mechanical degradation, loss of elasticity or tensile strength	reduction of $U_{AbsFluid}$ and F'
PVT absorber	cracks, breakage	thermo-mechanical stress, internal temperature shock	destruction of PVT absorber
	excessive bending	bi-metal effect of bonded compounds	increased heat losses from smaller d_{gap}
weld-seam between absorber and tube	debonding of tubes	thermo-mechanical stress, fatigue failure	reduction of $U_{AbsFluid}$ and F'
absorber tubes	internal pressure resistance	material failure from excess temperatures, thermo-mechanical stress	water leakage, destruction of PVT absorber
insulation	degradation of insulation	exposition to excessive material temperatures, degradation	increased heat losses, burn marks, fire

5.2.4 High temperature exposure of materials employed in PVT collectors

Within the project PVTgen2 (Lämmle et al. 2017a), high temperature tests have been conducted on adhesives, encapsulants, single-cell PV modules, and full-size PV modules to analyze their temperature stability and identify maximum material temperatures. Different research groups at Fraunhofer ISE carried out these tests. The results are briefly summarized at this point due to their central importance on the specifications and requirements of overheating protection.

Mechanical characterization of adhesives

Different types of adhesives were tested on their applicability in PVT collectors for gluing the absorber sheet to the PV module. Their mechanical properties of tensile strength and maximum elongation were characterized in a standard tensile strength setup. The samples were retested after exposition to high temperatures of 120 °C, damp heat and thermal cycling.

Both tested polyurethane-based adhesives failed after the high temperature exposure when they turned brittle. Two out of five silicone-based adhesives failed the thermal cycling and the damp heat tests. Two other silicone-based adhesives have insufficient elasticity in the initial, unaged state. Only one silicone and one acrylic-based adhesive had satisfactory initial mechanical properties and were able to withstand the temperature exposure to 120 °C, thermal cycling, and damp heat test. While there are suitable candidates, these adhesives have to be selected carefully for the application in PVT collectors.

Dynamic mechanical analysis of PV encapsulants

Typical PV encapsulants underwent the dynamic mechanical analysis before and after temperature exposure to test the thermal properties of the encapsulants. The samples included two products of EVA and two products of polyolefins. Already prior to the temperature exposure, a loss of the storage modulus was registered at increasing sample temperatures as the glass transition temperature of EVA lies below 0 °C. The dynamic-mechanical properties, however, did not change significantly after temperature exposure of 500 h at 150 °C and no difference was observed between the four samples.

Silicone encapsulants were not included in the dynamic mechanical analysis, but they are known to be more suitable for higher temperatures. Mickiewicz et al. (2011) compared the dynamic mechanical properties of silicone encapsulants to EVA and concluded that the storage modulus of silicone is more constant over a wide temperature range. Eltermann et al. (2012) exposed three silicone encapsulants to temperatures of 150 °C to test their application for concentrating PV receivers. Only a minor reduction of optical properties was observed for one sample, while two samples showed no indication of optical degradation. Given their good thermal, mechanical, and optical properties, silicone encapsulants are therefore considered more suitable for higher temperatures than EVA and polyolefines. This is why silicone is used as an encapsulant in different high-temperature PVT collectors, which were developed recently (Matuska et al. 2015; Gomes et al. 2015; Proell et al. 2017).

Optical analysis of single-cell PV modules with EVA

The degradation of small-sized PV modules with EVA encapsulant was assessed through optical Fourier spectroscopy and visual inspection after ageing at various temperature levels. Single-cell module samples were specifically manufactured for the tests. The samples feature an mono-Si PV cell embedded between two layers of EVA and glass sheets on front- and backside.

For the accelerated ageing tests, these samples were exposed at 105 °C, 120 °C, 130 °C, and 140 °C for a duration between 106 h and 652 h. The Fourier measurements did not show a systematic degradation of the module's transmittance. However, the samples that were exposed at 130 °C and 140 °C registered degradation effects in the form of browning of EVA in the peripheral areas of the PV modules. These effects might originate from an oxygen-induced reaction of the encapsulant at high temperatures caused by breaking the polymer chains and the subsequent formation of chromophores. Therefore, temperatures above 130 °C have to be seen critical for PV modules with EVA encapsulant.

Analysis of full-size PV modules

Four types of full-sized glass-glass PV modules were exposed at 120 °C, 135 °C, and 150 °C. After each ageing phase, the electrical power was measured in a flasher at standard test conditions. The samples included three modules with EVA encapsulant and one module with silicone encapsulant.

After the three accelerated ageing phases, a reduction of the electrical power of 1.2 $\%_{rel}$ was observed for one of the three EVA modules and a reduction of 1.0 $\%_{rel}$ for the silicone module. On the two other modules, the temperature exposition did not have any negative effects and no micro-cracks were found in any of the PV modules. However, the junction box of two PV modules was deformed severely, which might be a potential source for an electrical short-circuit.

Conclusion

Despite numerous tests, it is not possible to define a certain maximum temperature for the materials employed in PV modules and PVT collectors. No systematic failure modes above specific temperature levels could be registered by mechanical, optical, dynamic mechanical, and electrical characterization. Hence, degradation is not caused by exceeding a specific maximum temperature level. Instead, degradation has to be considered as a stochastic effect where the probability of degradation increases with elevated temperatures. Nonetheless, it is clear that temperatures above 130 °C are especially critical for EVA. But also other materials (adhesives, interconnectors) and components (junction box, bypass diodes) are subject to ageing at elevated temperatures.

Another way of looking at the ageing processes in PVT collectors delivers the Arrhenius equation. According to this model, the aging rate r is exponentially proportional to the activation energy E_a divided by the temperature T and the Boltzmann's constant k (Kurtz et al. 2011):

$$r \propto \exp(-\frac{E_a}{kT}) \tag{5.3}$$

Hence, every increase in temperature also effectuates an increase of the reaction rate. For PV modules, an activation energy of E_a = 1.1 eV can be assumed (Kurtz et al. 2011). Increasing the temperature from 85 °C, up to which PV modules are certified, to 130 °C, which is the maximum temperature of the glazed PVT collector, effectuates an increase of the reaction rate by 53 times. At temperatures of 150 °C, the stagnation temperature of glazed PVT collectors with low-e, the reaction rate is even 238 times faster than at 85 °C.

This clearly demonstrates the importance of maintaining low temperatures in the PVT collector to avoid ageing, degradation and critical failures.

5.3 Evaluation of overheating protection concepts for PVT collectors

5.3.1 Classification and literature review of overheating protection concepts

Multitudes of concepts for OHP are discussed in scientific literature and are registered in various patents. Reiter (2014) and Frank et al. (2014) provide a good overview of existing OHP concepts and a mere repetition of these concepts is avoided. Instead, all existing OHP concepts are classified in a new topology, which provides a systematic analysis where energy flows can be switched.

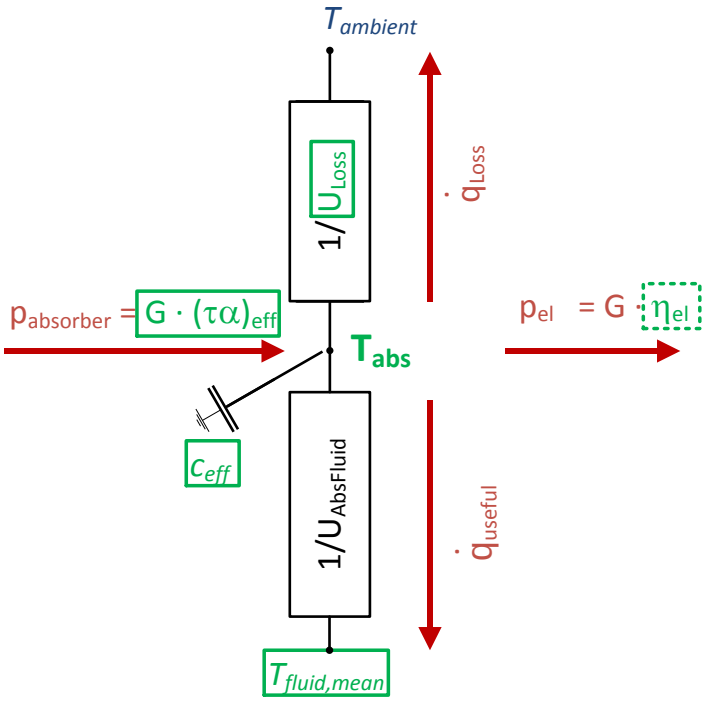

Figure 5.2: Equivalent thermal circuit of a two-node PVT collector model. The suitable parameters to lower the absorber temperature T_{abs} are highlighted in green.

The two-node energy balance for PVT collectors in Figure 5.2 forms the basis for the new topology. The central aim of all OHP concepts is the reduction of absorber temperatures T_{abs}. Any possible measure to lower T_{abs} can be derived from the two-node model by analyzing energy flows and parameters that affect T_{abs}.

Accordingly, all concepts to reduce T_{abs} can be classified in the following four OHP categories:

1) **Reduce $G(\tau\alpha)_{eff}$:** this OHP category aims at switching-off, or at least reducing, the heat source $p_{absorber}$ which is responsible for overheating in the first place. There are three possibilities for reducing $G(\tau\alpha)_{eff}$. Firstly, the transmittance of the transparent cover can be reduced, e.g. by shadowing the absorber. Secondly, the absorption in the PV cells can be adjusted, e.g. by a switchable layer that increases reflection. Thirdly, the incident irradiance can be reduced, e.g. by defocusing a concentrating collector. Applying this OHP category in PVT collectors, however, also reduces the electrical power output p_{el}, which is considered a major drawback.

2) **Increase U_{Loss}:** OHP concepts of the second category lower the absorber temperature by increasing the heat loss rate $\dot{q}_{Loss}$ through an increased heat loss coefficient U_{Loss}. As the high level of insu-

lation in glazed PVT collectors with low-e aggravates the issue of overheating and is the main cause for excessive stagnation temperatures, it is an obvious approach to deal with the issue by switching from low to high value of U_{Loss} in the case of stagnation. This is either achieved by changing the characteristics of existing heat loss paths, e.g. by a switchable emissivity of the absorber coating. Alternatively, U_{Loss} can be increased by activating new loss paths, e.g. by opening flaps in the collector housing to ventilate the collector.

3) **Reduce $T_{fluid,mean}$:** the mean fluid temperature $T_{fluid,mean}$ determines the absorber temperature during regular operation. By maintaining fluid circulation and keeping the collector inlet temperatures at a low level, $T_{fluid,mean}$ can be used to avoid stagnation and cool the absorber temperature. For this purpose, the fluid has to dissipate its heat to the ambient. The heat dissipator can be either integrated on the collector level or on the array or system level, e.g. by an external finned-tube heat exchanger (Frank et al. 2014). A central challenge of this OHP category is the maintenance of circulation of the heat transfer fluid and a passive and fail-safe operation. Control based concepts, e.g. night cooling of the storage, also fall amongst this category.

4) **Increase c_{eff}:** the last OHP category aims at buffering high absorber temperatures by increasing the heat capacity c_{eff} of the collector. Thus, excessive heat is stored in thermal masses preventing a rise of absorber temperature. Phase change materials (PCM) are an ideal solution to the problem, as they store sensible heat at a constant temperature after exceeding a defined temperature limit. For this purpose, PCM has to be thermally coupled to the absorber and regenerated at night to release the stored heat. The high costs and temperature stability of PCMs are however a limiting factor of this OHP approach.

Apparently, the electrical efficiency η_{el} also has an influence on the energy balance and $T_{abs.}$ Yet, η_{el} is limited by its rated efficiency $\eta_{el,STC}$. Therefore, it is not possible to actively increase η_{el} and use p_{el} as an active measure for an OHP concept. Nevertheless, η_{el} influences the maximum absorber temperatures, which can be seen at the differing stagnation temperatures of PVT collectors operated in MPP and OC mode. Likewise, the ambient temperature is considered a constant boundary condition that cannot be altered but influences the absorber temperature.

The four OHP categories with their corresponding subcategories are illustrated in Figure 5.3. Combinations of the four categories are also possible, but will not be subject to further investigations.

The physical effects that are responsible for a temperature reduction are identical inside each category, because the physical two-node model of the collector forms the basis for the topology. The same mathematical and physical approaches for dimensioning OHP concepts can be applied as a consequence. For instance, all OHP concepts of category 2 are based on reducing U_{Loss}. To achieve a certain temperature reduction, U_{Loss} has to be switched in a given switching range ΔU_{Loss}. The required switching range ΔU_{Loss} is independent from the technological construction, whether by switching the absorber emissivity or by venting.

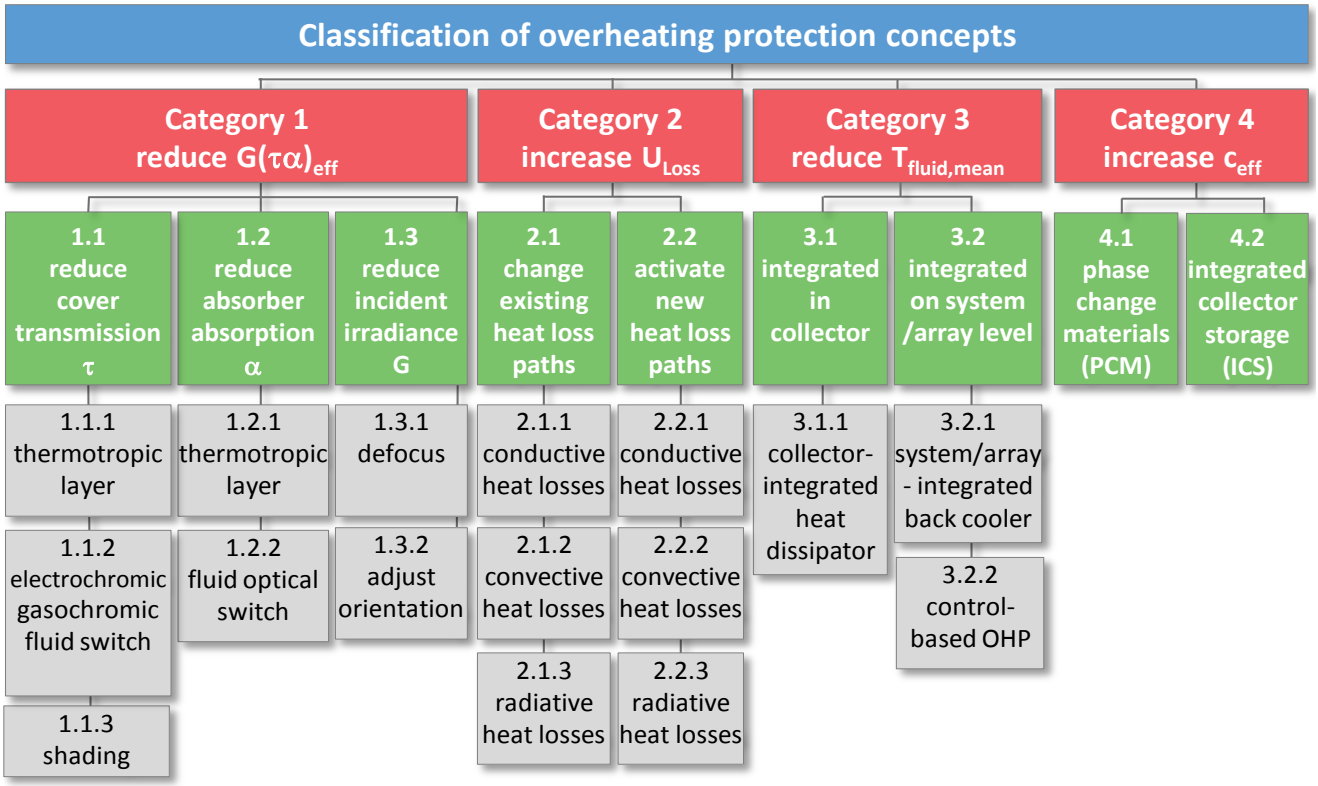

Figure 5.3: Classification of overheating protection concepts into four main categories according to their physical effects on the energy balance of the collector.

Useful nomograms to preliminary dimension OHP concepts for each category are presented in Appendix D.1. These nomograms summarize the crucial factors that influence the stagnation temperature. Furthermore, the dimensioning tools allow a quick assessment of the suitability of the OHP in terms of temperature reduction potential.

Besides the mentioned classical OHP approaches that utilize a switch of the thermal efficiency, there is also the possibility to engineer the collector in such a way that critical temperatures are inherently avoided. This is achieved by reducing the thermal insulation to a subcritical level. Fortuin et al. (2014) call this approach "LT-resist" as the materials are resistant to the inherently low temperatures. Unglazed PVT collectors can be grouped into this category, and this approach is also applied for polymer collectors (e.g. Dursun et al. (2014) and Reiter et al. (2014)). However, permanently high heat losses are not expedient, as a good thermal efficiency is required for regular operation conditions. Therefore, all OHP concepts must be able to switch from a high and to a low thermal efficiency, either actively of passively.

Besides that, air-type PVT collectors have a reduced risk for overheating compared to water-type PVT collectors. As air collectors are typically operated in open systems, a worthwhile OHP approach comprises venting heated air to the atmosphere to avoid excessive temperatures and thus maintain low cell temperatures (Cartmell et al. 2004). Air as heat transfer has the additional advantage that there is no risk of steam formation.

Table 5.3 categorizes OHP concepts into the four categories, based on a thorough literature review of existing OHP concepts for solar thermal collectors, PV modules, and PVT collectors. For each OHP concept a short description and corresponding references are also stated.

Table 5.3: Novel classification existing overheating protection concepts.

Category	Description of overheating protection (OHP)	Reference
1) Reduce G $(\tau\alpha)_{eff}$		
1.1) Reduce τ	1.1.1 Thermotropic layer changes its transmittance depending on temperature of said layer	Nitz (1999), Resch and Wallner (2009)
	1.1.2 Fluid-optical switch to either transmit or reflect incident irradiation depending on presence of fluid	Stephens (1981), Slaman and Griessen (2009)
	1.1.2 Electrochromic or gasochromic glazing which switches its transmittance by an applied voltage or the presence of gases	Lampert (1998), Georg et al. (1998)
	1.1.3 Shading the absorber by blocking incident irradiation	
	- Rollable curtain covers the aperture on either the inside or outside of the collector	Products available e.g. by Orionsolar, Heijasolar, Radiant Floor Company
	- Shading of solar thermal absorber with PV cells	Gillmann (2010), Fischer et al. (2016)
1.2) Reduce α	1.2.1 Thermotropic layers and 1.2.2 Fluid-optical switch can also be applied directly on the absorber to increase reflectance and thus reduce absorptance	Resch and Wallner (2009), Slaman and Griessen (2009)
1.3) Reduce G	1.3.1 Defocus concentrating collectors	Witt and Mesquite (1984)
	1.3.2 Adjust orientation, e.g. by adjusting azimuth or tilt angle	
2) Increase U_{Loss}		
2.1) Change existing heat loss paths	2.1.1. Switchable insulation integrated in the back of the collector, e.g. by releasing hydrogen in a metal container	Benson et al. (1994)
	2.1.2 Adjust distance between absorber and glazing and thus switch convective heat losses	
	- Transparent front cover, which is flexible and potentially inflatable, can be moved towards and brought in contact with absorber to increase convective and radiative losses	Patents by Moore (1983), Sharpe (1984), Raetz (1998), Mueller and Wemhoener (2013)
	- Absorber can be moved towards glazing	Dupeyrat (2011b)
	2.1.2 Switchable vacuum insulation between absorber and glazing	
	- active: vacuum pump stand maintains pressure; flooding the gap with air increases pressure and thus U_{Loss}	Wendker et al. (2012), available as product by UniKoll (UniKoll 2015)
	- passive: temperature-induced desorption of water inside a vacuum container	Henning et al. (2011)
2.2) Activate new heat loss path	2.2.2 Venting the collector by opening flaps in the collector housing, e.g. passively by a memory shape metal actor, buoyancy-driven natural convection of ambient air cools the collector	
	- Ventilation of back side between absorber and insulation	Cadafalch (2002), Harrison et al. (2004), Hussain and Harri-

		son (2015)
	- Ventilation of front side and back side	Kearney et al. (2005), Ramschak et al. (2016)
	2.2.2 Switchable heat pipes transfer heat to an external heat exchanger	
	-Valve with shape memory metal opens after exceeding a set temperature	Mahdjuri (1999), Mahjouri (2004), Boyle et al. (2012). Applied in products by Naked Energy and Kingspan
	- Sorption heat pipe is activated after exceeding a set temperature	Klier (2013), mechanism also explained in Vasiliev (2004) and Frank et al. (2014). Product by TIGI Solar.
3) Reduce $T_{fluid,mean}$		
3.1) Collector integrated	3.1.1 Thermosiphonic-driven fluid circulation sets in when valve opens after exceeding a set fluid temperature	
	- heat dissipator attached to collector frame	Cummings (1977), Konetsu and Torrens (2004), product by Konetsu S.L.
	- heat dissipator integrated into the collector's rear side	Thür and Hintringer (2013)
3.2) System integrated	3.2.1 Thermosiphonic-driven fluid circulation setting in after valve opens when exceeding set fluid temperature. Heat dissipator integrated on array or system level.	Baer (1984), Butler (2002), Konetsu and Torrens (2004), product by Konetsu S.L.
	3.2.2 Thermo-electric peltier devices generate electricity to run a fan which cools the heat transfer fluid	Martínez et al. (2014)
	3.2.3 Control-based strategies to reduce storage temperature	
	- Night cooling of storage by utilizing the collector as heat sink by recirculation hot water from storage	Becker et al. (2006), Scheuren (2008), Kusyy and Vajen (2011)
	- Actively increase collector temperature by low mass flows to reduce thermal collector efficiency	Lustig (2002), Scheuren (2008), Kusyy and Vajen (2011)
	- Tank fluid purging: release hot tank water to drain	Magalhães et al. (2016)
	- Actively pumped and controlled external back cooler for stagnation cooling	Hausner et al. (2003), Becker et al. (2006),
4) Increase c_{eff}		
4.1) PCM	4.1.1 Phase change material (PCM) is coupled to the PV module or absorber to buffer temperatures	
	- in PV modules	Du et al. (2013), Makki et al. (2015)
	- in solar thermal collectors in façade applications	Hengstberger et al. (2016)
	- in PVT collectors	Bouzoukas (2008), Di Su et al. (2017)
	4.1.2 PCM slurries	Serale et al. (2014)
4.2) ICS	4.2 Integrated collector storage (ICS) to increase collector capacity	Smyth et al. (2006)

5.3.2 Evaluation of overheating protection concepts for PVT collectors

The suitability of existing and novel OHP approaches for the application in PVT collectors varies from concept to concept. Objective and systematic evaluation criteria are required to assess and compare the individual approaches.

Reiter (2014) developed a multi-dimensional evaluation approach for OHP concepts in polymer collectors. On a scale from 1 to 5, he evaluates multiple OHP concepts in the six dimensions of intrinsic safety, temperature reduction, universal applicability, operational costs, efficiency reduction, and manufacturing costs. This comprehensive study is highly recommended for any reader who is interested in the evaluation of the individual OHP concepts.

The requirements for OHP concepts in PVT collectors, however, differ from the requirements of polymer collectors. In polymer collectors, the sole objective of OHP is the limitation of the absorber temperature. In PVT collectors, also the electrical efficiency benefits from the reduced temperature load. Therefore, the evaluation criteria of Reiter (2014) are adapted slightly to also take into account the specific requirements of PVT collectors. The adapted evaluation criteria for OHP in PVT collectors are discussed in the following paragraph, highlighting the specific requirements of PVT collectors.

1. Temperature reduction

The first and most important evaluation criterion concerns the potential to reduce absorber temperatures during stagnation, which can be quantified by the temperature switching range $\Delta T_{OHP} = T_{stg,normal} - T_{stg,OHP}$. While high stagnation temperatures would occur in the normal operation mode, the OHP limits the absorber temperature during stagnation. Thus, the OHP reduces cell temperatures for a higher electrical efficiency and reduces the temperature load to avoid ageing and degradation.

Depending on the corresponding category, the temperature switching range ΔT_{OHP} can be assessed preliminarily from the switching range of $(\tau\alpha)_{eff}$ in category 1, the switching range of U_{Loss} in category 2, the heat dissipator capacity in category 3, and the effective capacity c_{eff} in category 4. The dimensioning nomograms for the four OHP concepts in Appendix D.1 are also suitable to assess the temperature reduction ΔT_{OHP}.

2. Intrinsic safety

The intrinsic safety criterion specifies whether the OHP operates fail-safe and is activated even during irregular operating conditions. Reiter (2014) classifies the intrinsic safety of OHP concepts into permanent protection (A), protection during power failure (B1), protection during system failure (B2), and protection only during operation (C). A permanent protection is, of course, always desired, but not all OHP approaches can be realized in such a way.

With regards to the intrinsic safety, it can also be differentiated between active and passive OHP concepts. In this context, active refers to an OHP that consumes electricity or relies on active control algorithms. A passive concept, on the other hand, activates its OHP automatically if temperatures exceed a certain threshold, or if fluid flow falls below a minimum level.

Both active and passive OHP concepts can be carried out in a fail-safe manner. For instance, an active system is permanently protected if the OHP is activated automatically during power and system fail-

ures. A specialty of OHP in PVT collectors is the internal generation of electricity during critical states. High stagnation temperatures only occur during high levels of irradiance, so that the PVT array would generate sufficient electricity to operate its own active OHP. Furthermore, longer intervals of power failures could also be bridged when a backup battery system is utilized. An active OHP in combination with a PVT battery system would be classified as B1 – protection during power failures, as system failures are not covered in this example.

Guaranteeing intrinsic safety is a challenge for all OHP approaches. Especially in active and control-based OHP concepts of category 3 it is difficult to achieve a permanent protection.

3. Efficiency reduction

It is clear that the OHP reduces the thermal efficiency $\eta_{th,OHP}$ when it is activated. However, some OHP approaches also reduce the thermal efficiency during normal operation $\eta_{th,normal}$. For instance, thermotropic layers suffer from a reduced transmittance in its transparent state, compared to conventional glazing. A reduction of thermal efficiency $\Delta\eta_{th,normal}$ results in an undesired drop of optical performance and lower annual thermal yields compared to a collector without OHP.

Electricity is generated during normal operation but also during stagnation. Hence, a reduction of electrical efficiency is also critical when the OHP is active. In this respect, the reduction of the electrical efficiency during stagnation $\Delta\eta_{el,stg}$ has a lesser influence on annual electricity yields than a reduction of the normal efficiency $\Delta\eta_{el,normal}$, given the much rarer occurrence of stagnation. Yet, all approaches in OHP category 1 reduce the optical efficiency during stagnation, which might reduce annual electrical yields significantly. OHP category 1 is therefore less suitable for PVT collectors where a high electrical efficiency is also required during stagnation.

4. Additional costs

Most OHP concepts imply additional manufacturing and operational costs. The manufacturing costs concern the additional components for the OHP mechanism. Operational costs concern the additional energy consumptions of the overheating-protected collector. Depending on the OHP technology, electricity is either consumed during normal operation, e.g. to maintain a vacuum pressure for high thermal performance, or it is consumed during stagnation to activate and operate the OHP.

Passive OHP concepts in categories 1, 2 and 4 typically have less operational costs, but the manufacturing costs are higher. Control-based OHP approaches in category 3 have no manufacturing costs, but higher operational costs. For instance, night cooling by recirculating hot water in the collector loop requires no additional equipment, but it consumes electricity to operate the pumps.

5. Potential synergies

Evaluation criterion 5 considers all potential synergies of applying OHP in PVT collectors. Potential synergetic effects can be found in an increased electrical or thermal efficiency by a higher optical or thermal performance during normal operation. Cost reductions in the collector and system through lower temperature requirements or substituting components by the OHP are also a potential benefit of OHPs. Moreover, new possible applications may arise through an OHP. For example, the hot air of a vented PVT collector could be utilized, or the collector performance in a heat pump system could be increased by opening the ventilation channels when operated below ambient temperatures.

Also, the flexible, demand-oriented operation of the PVT collector is a potential synergy. By actively and purposely lowering the absorber temperatures, it is possible to switch between operation with heat-priority and electricity-priority. Thus, annual yields can be potentially increased. This aspect is analyzed in more detail in chapter 5.5.

Any overheating concept can be evaluated with these five evaluation criteria on a custom scale or on a scale as proposed by Reiter (2014) by taking into account the individual construction, design, and realization of each concept. Although the previously defined OHP categories base on the same physical effect, it is not possible to rate these categories on a consistent basis. Instead, the evaluation has to be carried out for each OHP concept individually.

5.4 Demonstration of overheating protection concepts in PVT collectors

The objective of the following section is the building and testing of highly efficient PVT prototypes with low-e coatings, which are protected against overheating. Thus, the effect of OHP on temperatures and the instantaneous efficiency under real stagnation conditions can be analyzed experimentally and the applicability of overheating protection for PVT collectors can be assessed.

By means of three case studies, different OHP concepts for PVT collectors are evaluated and compared:

- **PVT collector with ventilation:** this state-of-the-art OHP concept is applied first-in-time to a glazed PVT collector with low-e coating.
- **PVT collector with switchable film insulation:** in this innovative OHP concept, an inflatable polymer film substitutes the rigid glass front cover. This opens the possibility to vary the gap distance between the PVT absorber and polymer film and thus switch convective and radiative heat losses.
- **PVT collector with sorption-based switchable insulation:** this passive OHP concept approach is based on the temperature-dependent desorption characteristics of adsorbents in a vacuum chamber. A feasibility study with small-scale experiments and numerical simulations of the PVT collector is presented.

5.4.1 PVT collector with ventilation

5.4.1.1 Description of the OHP concept

Venting of the collector is one of the most discussed OHP approaches for flat plate collectors in the scientific literature (Cadafalch 2002; Harrison et al. 2004; Kearney et al. 2005; Hussain and Harrison 2015; Ramschak et al. 2016). The idea of venting the collector is simple: ventilation channels are integrated into the collector. During normal operation, the channels are closed. During stagnation, cool ambient air enters the collector through the opened channels. The air takes up heat so that its temperature increases, its density decreases and the air rises upwards. Thus, the passive, buoyancy-driven airflow evacuates excessive heat from the collector and thus lowers the absorber temperatures. For the first time, this established OHP concept is now applied to PVT collectors.

The design of the PVT collector with ventilation "PVT03-vented" is analogous to the PVT collector "PVT01-low-e". It uses the same PVT absorber dimensions, same PV cells, and the same construction of

the direct-laminated sheet-and-tube PVT absorber. However, a low-e coating from Euroglas, which features an emittance of $\varepsilon_{373K} = 0.30$ and a transmittance of $\tau_{AM1.5} = 0.89$, is applied on the PV module glass. This PVT collector comes without anti-reflection coating on the front glazing, resulting in a relatively low transmittance-absorptance product of $(\tau\alpha)_{eff} = 0.83$. Due to these constructive differences, the performance in normal operation is expected to be slightly lower than that of "PVT01-low-e".

Within his Master's thesis, Panzer (2016) constructed the collector casing and integrated inlets and outlets into the frame, allowing the ventilation of channels above and beneath the absorber. During stagnation, the channels can be opened to allow air circulation and avoid overheating. To enhance the heat transfer from the absorber to the air, V-shaped aluminum fins with a thickness of 0.2 mm are glued to the rear side of the absorber.

Figure 5.4 depicts a schematic cross section of the PVT collector with ventilation and its equivalent thermal circuit. Opening the ventilation channels activates the parallel resistance $1/U_{Vent}$, resulting in the additional heat flux $\dot{q}_{Vent}$.

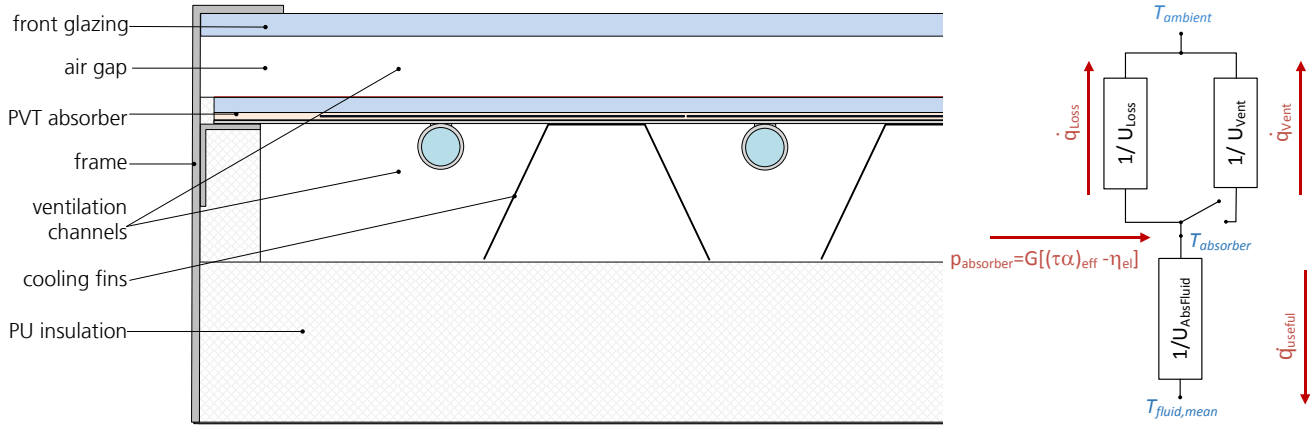

Figure 5.4: Schematic cross section of the PVT collector with the option to vent above or beneath the absorber (left); equivalent thermal circuit of the PVT collector indicating the switchable ventilation losses (right).

In the present prototype, the channels have to be opened manually. There are, however, available technical solutions for opening the channels passively. Thermally controlled shape memory alloy springs can be used to open the channels, once its temperatures exceed the threshold (Harrison et al. 2004; Kessentini 2014). The integration of such an automated mechanism was, however, beyond the scope of this collector development.

Figure 5.5 shows photos of the collector at the outdoor test field of the TestLab Solar Thermal Systems at Fraunhofer ISE. In the left photo, the collector is in normal operation with closed channels. In the right photo, the OHP is activated through the opened ventilation channel below the absorber.

Figure 5.5: Photos of the PVT collector "PVT03-vented" during outdoor testing with closed vents (left) and opened vents (right).

5.4.1.2 Experimental characterization of U_{Loss}

The heat loss coefficient U_{Loss} was experimentally determined for several design variants in the fluid dynamic test rig at Fraunhofer ISE using the "dark" method of characterizing heat losses without incident irradiance. This formerly normative method (DIN 4757) is still a popular approach to reduce test time (Fischer 2011; Beikircher et al. 2014). In the dark method, hot fluid is circulated through the collector. Given the absence of irradiance, the heat dissipates from the fluid to the ambience, resulting in an inverted heat flow from absorber to ambience and consequently a lower fluid outlet than inlet temperature.

The heat loss rate $\dot{q}_{Loss}$ is obtained from measuring the mass flow rate $\dot{m}$ and balancing the fluid inlet and outlet temperatures $T_{fluid,in}$ and $T_{fluid,out.}$ Then the heat transfer coefficient U_0, which is defined between the nodes of mean fluid temperature T_m and ambient temperature T_a, is obtained with:

$$U_0 = \frac{\dot{q}_{Loss}}{\Delta T} = \frac{\dot{m}\, c_p (T_{fluid,in} - T_{fluid,out})}{A_{aper}(T_m - T_a)} \tag{5.4}$$

In the dark case without irradiance, the thermal resistance $1/U_0$ can be regarded as a serial connection of $1/U_{AbsFluid}$ and $1/U_{Loss}$. With the previously determined $U_{AbsFluid}$ (compare experiments in chapter 3.2.5), U_{Loss} is expressed as:

$$U_{Loss} = \frac{1}{1/U_0 - 1/U_{AbsFluid}} \tag{5.5}$$

The stagnation temperature T_{stg} can be estimated from U_{Loss}, which allows a better interpretation of the experimental results. Assuming a security margin of 20 °C, the stagnation temperature is given by:

$$T_{stg} = T_a + G\frac{(\tau\alpha)_{eff} - \eta_{el}}{U_{Loss}} + 20\,°C \tag{5.6}$$

The resulting stagnation temperatures T_{stg} in Figure 5.6 are indicated for $(\tau\alpha)_{eff}$ = 0.832, G = 1000 W/m² and T_a = 30 °C in OC mode with η_{el} = 0.

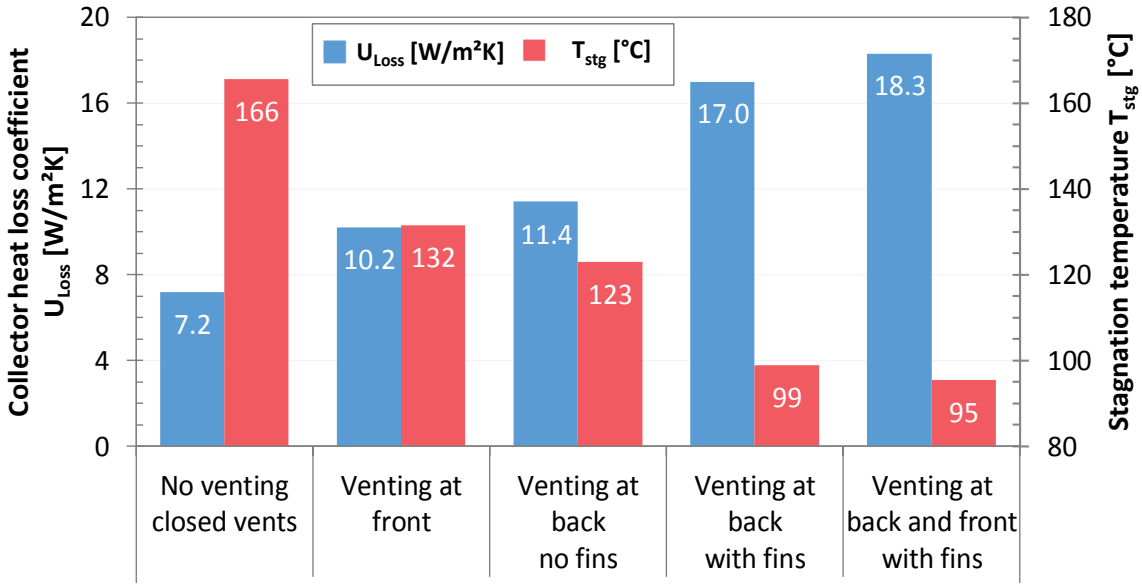

Figure 5.6: Measured heat loss coefficient U_{Loss} at ΔT = 39 K and derived stagnation temperature T_{stg} of the vented PVT collector in several design variants.

During normal operation with closed ventilation channels, a low heat loss coefficient of U_{Loss} = 7.2 W/m²K was measured, which corresponds to high stagnation temperatures of T_{stg} = 166 °C. Activating the overheating protection by venting the front channel lowers the stagnation temperature to T_{stg} = 132 °C. Venting the rear channel without fins results in stagnation temperatures of T_{stg} = 123 °C while venting the rear channel with fins yields T_{stg} = 99 °C. The lowest stagnation temperatures of T_{stg} = 95 °C are achieved by venting both the front and rear channel.

Accordingly, the switch of U_{Loss} by venting the front channel is insufficient to avoid critical temperatures above 130 °C. On the contrary, ventilation of the rear channel with added fins achieves the temperature reduction target.

However, the measured values for U_{Loss} and the derived stagnation temperatures have a limited validity and should be primarily used for comparing the different variants. The operating conditions of the fluid dynamic test rig, i.e. ambient temperatures, radiation background, and wind speed distribution in the collector plane, are difficult to control. Although measurements were carried out at four discrete temperature levels of T_m = 58 °C, 63 °C, 67 °C, and 71 °C and U_{Loss} was averaged for these temperatures, stagnation levels were not reached to avoid destroying the collector. Moreover, the method entails uncertainty for the prior determination of $U_{AbsFluid}$. Therefore, the values of U_{Loss} and T_{stg} serve as an approximate estimate to compare the variants and to pre-assess the potential of the OHP concept. The exact stagnation temperatures are therefore determined by thermal performance measurement according to ISO 9806 (2016).

5.4.1.3 Characterization of collector performance

The thermal and electrical performance of the collector were measured in outdoor conditions with the quasi-dynamic test method according to ISO 9806 in the hybrid MPP mode, i.e. with simultaneous thermal and electrical operation. The efficiency curves in Figure 5.7 were characterized in two modes:

1) Normal operation mode with closed ventilation channels
2) Vented OHP with activated overheating protection and open ventilation channels behind the absorber with fins

A dynamic switch during operation between these two efficiency curves is possible by opening the ventilation channels, which is indicated by the green line in Figure 5.7.

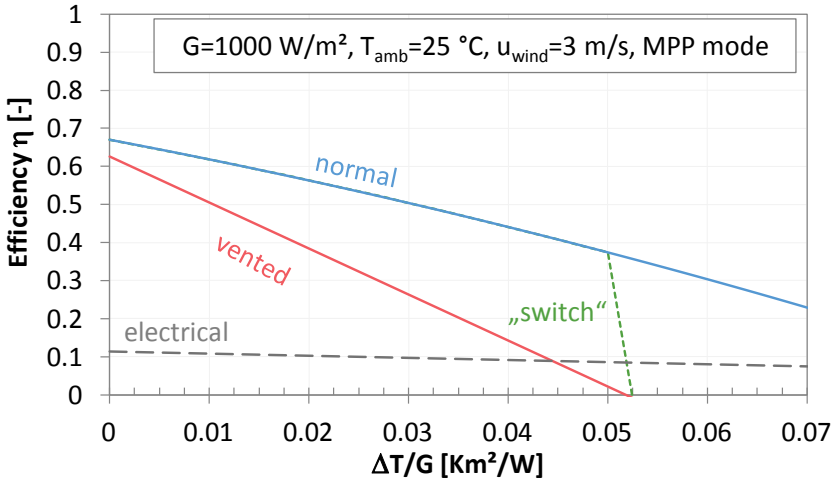

	normal operation	vented OHP
$\eta_{th,0}$	0.67	0.63
c_1 [W/m²K]	4.973	12.09
c_2 [W/m²K²]	0.019	0
T_{stg} [°C]	148.9	101.8
$U_{Loss,stg}$ [W/m²K]	7.8	14.3
$\eta_{el,stg}$	6.5 %	8.9 %

Figure 5.7: Efficiency curves for the PVT collector with ventilation "PVT03-vented" in normal mode with closed channels and OHP mode with opened channels.

During normal operation, the PVT collector achieves a high thermal efficiency with relatively low heat losses. A slightly lower thermal and electrical efficiency is observed compared to "PVT01-low-e" in chapter 3.4. This is due to the aforementioned higher emissivity of ε = 0.30 of the Euroglas coating compared to ε = 0.14 of the ISE coating. Additionally, the front glazing is not equipped with AR coating resulting in a reduced optical efficiency.

During stagnation or periods of low heat demand, the OHP can be activated by opening the ventilation channels. The ventilation increases the heat losses significantly and lowers stagnation temperatures. The resulting standard stagnation temperature amounts to T_{stg} = 148.9 °C during normal operation and to T_{stg} = 101.8 °C in overheating protection mode.

The heat loss coefficient during stagnation U_{Loss} can also be estimated from the efficiency curve parameters. During no flow conditions, the incident power on the absorber equals the heat losses. Solving the energy balance of the two-node model to U_{Loss} leads to:

$$U_{Loss,stg} = \frac{G \cdot [(\tau\alpha)_{eff} - \eta_{el}]}{T_{stg} - T_a} = \frac{G\left[(\tau\alpha)_{eff} - \eta_{el}\right] 2c_2}{\sqrt{c_1^2 + 4\eta_{th,0}c_2 G} - c_1} \tag{5.7}$$

The derived heat loss coefficients $U_{Loss,stg}$ = 7.8 W/m²K with closed channels and $U_{Loss,stg}$ = 14.3 W/m²K with opened channels, are in the range of the previously assessed values with the dark method.

As positive side effect of the overheating protection, the electrical efficiency also benefits from lower stagnation temperatures. According to the measurement, the drop of cell temperatures increases the electrical efficiency during stagnation from η_{el} = 6.5 % with closed channels to η_{el} = 8.9 % with opened ventilation channels. During regular operation, the instantaneous electrical efficiency remains unaffected by the overheating protection.

5.4.1.4 Dynamic operation of the OHP

The PVT collector was monitored at the outdoor test rack on the roof of Fraunhofer ISE to test the overheating protection under real operating conditions. A typical stagnation sequence was emulated for this purpose, while temperature, thermal and electrical power, and operating conditions were monitored. Figure 5.8 shows the measured curve of temperature and power during an exemplary test day with a longer stagnation period.

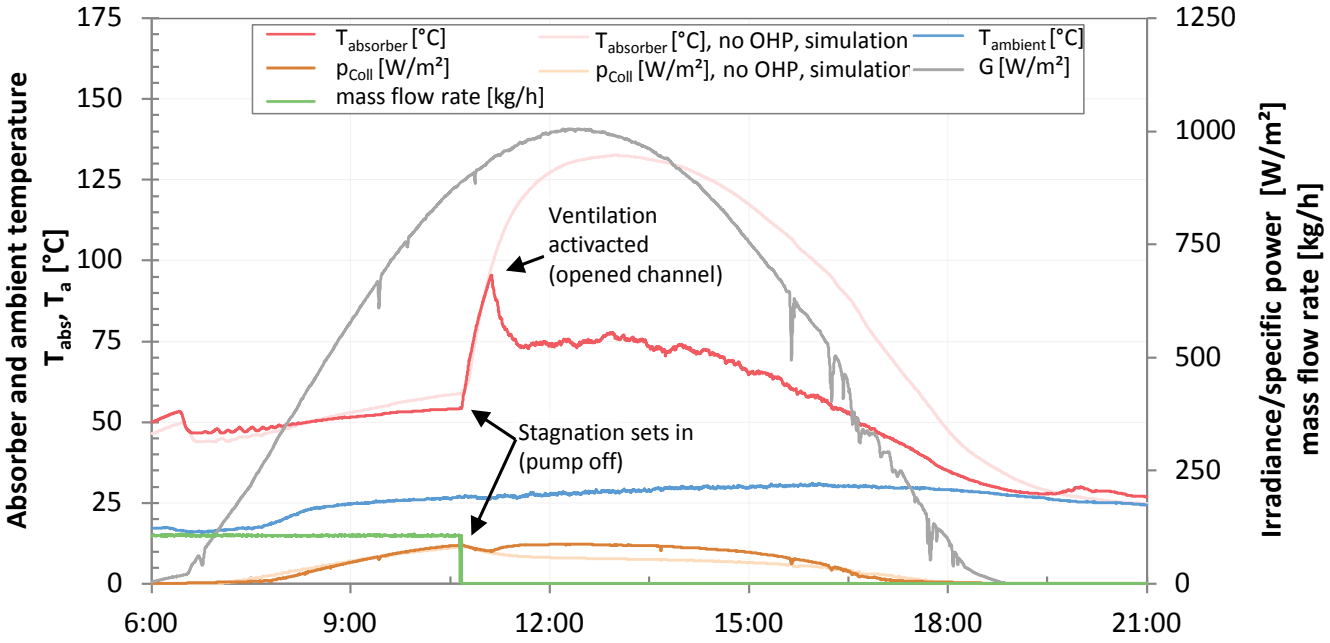

Figure 5.8: Measured temperature as well as electrical and thermal power of "PVT03-vented" during stagnation.

On a hot and sunny day with nearly no clouds, the PVT collector was first operated in normal operation mode with simultaneous thermal and electrical operation. At 10:40 am, the collector pump was turned off and the collector began to stagnate. Owing to the almost complete cease of heat transfer to the fluid, the collector began to heat up rapidly. After 30 minutes, the absorber temperatures, which were measured at 2/3 height of the collector, reached T_{abs} = 99.5 °C. At this point in time, the OHP was activated manually by opening the ventilation channel behind the PVT absorber. Immediately, an air stream began to flow through the collector and thus cooled the PVT absorber. Within 30 minutes, the absorber temperature stabilized around T_{abs} = 75 °C, with some minor temperature fluctuations.

Simulations of the same test day were conducted to analyze temperature and electrical power during stagnation, assuming no activation of the overheating protection. These simulated absorber

temperatures are shown in Figure 5.8 in light red. According to the simulations, the absorber would have reached a daily maximum temperature of T_{abs} = 132.6 °C without OHP. Compared to the maximum measured absorber temperature of T_{abs} = 77.8 °C, this equals a temperature reduction of ΔT_{abs} = 54.8 K.

The effect of the overheating protection on the specific electrical collector power p_{coll} is indicated by the orange curves. Directly after stagnation sets in, the electrical efficiency drops from η_{el} = 10.0 % to η_{el} = 7.9 %. After opening the ventilation channels, the electrical yield increases again and stabiles around η_{el} = 9.3 % due to lower cell temperatures. Comparative simulations showed that without OHP, the electrical efficiency drops to as low as η_{el} = 5.6 % during the temperature peak at noon. The measured, daily electrical yield with OHP amounts to E_{Coll} = 1.17 kWh/m² compared to simulation results of E_{Coll} = 1.04 kWh/m² without OHP, which equals a difference of 11 $\%_{rel}$.

5.4.2 PVT collector with switchable film insulation

5.4.2.1 Description of collector concept

An innovative overheating protection concept based on an inflatable glass-film cushion was specifically developed for PVT collectors. The PVT absorber itself is inherently rigid and protected against damage from hail by the presence of the PV module glass. Therefore, a flexible film can substitute the glass cover on the front. During regular operation, the film cover reduces heat losses by establishing an insulating air layer above the PVT absorber. During stagnation, the film is brought in contact with the PVT absorber. This increases both convective and radiative heat losses and lowers stagnation temperatures. Thus, the switchable film insulation falls under OHP category 2.1 - switchable U_{Loss} by changing the properties of existing heat loss paths. Selected results of the following section were also published in Lämmle (2016b).

The switchable collector insulation is realized by an inflatable fluoropolymer film which is sealed at its edges with the PVT absorber. A small air pressure stabilizes the cushion during regular operation. Removing the air from the cushion, e.g. by a small negative pressure, deflates the cushion so that the polymer film directly contacts the low-e-coated PVT absorber.

Fluoropolymer films such as ETFE, FEP, or PTFE are mainly used in architectural applications for building envelopes (Robinson-Gayle et al. 2001) and in greenhouses. Max et al. (2012) investigated various inflatable glass-film-combinations for a switchable greenhouse insulation. In solar thermal collectors, fluoropolymer films are used as additional convection barrier between absorber and glazing. Moore (1983) used a switchable film insulation in a solar thermal collector for overheating protection, while Mueller and Wemhoener (2013) aim at variable heat dissipation rates by adjusting convective heat losses with a switchable film insulation.

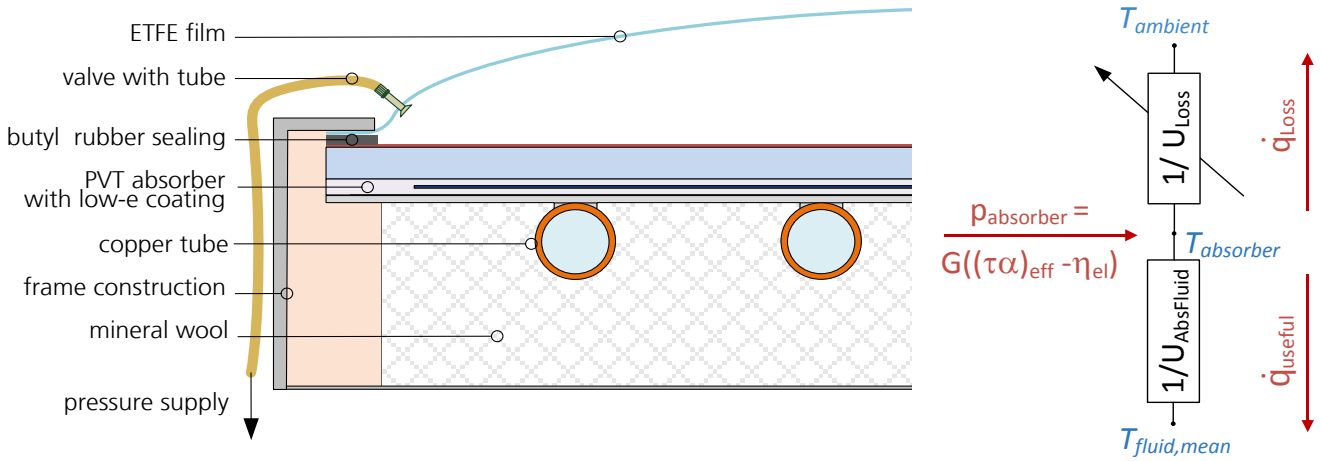

Figure 5.9: Schematic cross section of the PVT collector with switchable film insulation (left); equivalent thermal circuit of the PVT collector indicating the switchable convective and radiative heat losses (right).

The PVT absorber has the same design as the glazed PVT collector with low-e ("PVT01-low-e"). 32 mono-Si cells are laminated within a sandwich of EVA, low-e-coated module glass, and a sheet-and-tube absorber with an aluminum sheet and copper tubes. This PVT collector also utilizes the silver-based low-e coating with an emissivity of ε_{373K} = 0.14 produced at the laboratory of Fraunhofer ISE.

The only differences between this PVT collector and PVT01 are the front glazing and the collector frame. An ETFE film with a thickness of 100 µm is used. At its edges, the film is hermetically sealed with butyl rubber. To ensure air-tightness over longer periods, the film, butyl rubber, and PVT laminate are pressed together during production. Moreover, the film is sealed under tension, so that it forms a naturally curved form of a cushion with a maximum distance between absorber and film of d_{gap} = 35 mm. However, the distance between absorber and film is not constant, so that convection losses are slightly higher than in a collector with parallel glass panes.

A small internal pressure in the range of 20 mbar guarantees the mechanical stability of the cushion. For this purpose, a small and cheap electrical air pump was used. This air pump, which can both suck and blow, is typically used for inflating and deflating air mattresses. An automotive valve is inserted into the ETFE film and is also sealed with butyl rubber.

The heat loss rate can be adjusted according to current heat demand by regulating the air pressure in the cushion. In periods of low thermal demand and high storage temperatures, the cushion is actively deflated and thus prevents overheating. In the case of a power failure, the air slowly evades from the cushion. A valve that automatically opens during power failure can accelerate the process of deflating the collector. Thus, a fail-safe overheating protection can be achieved.

Figure 5.10: Photos of PVT collector with switchable film insulation "PVT04-film" during indoor testing in normal, inflated mode (left and center) and in protected, deflated mode (right).

5.4.2.2 Characterization of radiative heat losses $\dot{q}_{rad}$

The radiative heat losses $\dot{q}_{rad}$ during normal operation and in OHP mode are of great interest, as they determine the applicability of polymer films as transparent cover in PVT collectors with switchable film insulation. As thin polymer films are partly transparent for radiation in the near infrared spectrum, radiative heat losses are expected to be slightly higher during regular operation, compared to a PVT collector with transparent glass cover. Moreover, it is essential that the collector can switch between low $\dot{q}_{rad}$ in regular operation to high $\dot{q}_{rad}$ in OHP mode, when the film is brought in contact with the PVT absorber with low-e coating.

For these reasons, the radiative heat losses of the glass-film combination were analyzed with an infrared thermographic experimental set-up as shown in Figure 5.11 (left). The graphic output signal of the infrared camera was calibrated with several samples of known emissivity. Measurements were conducted at different surface temperatures under consideration of background radiation. Thus, the temperature output signal of the IR camera was calibrated and can be converted into the radiative heat flux $\dot{q}_{rad}$.

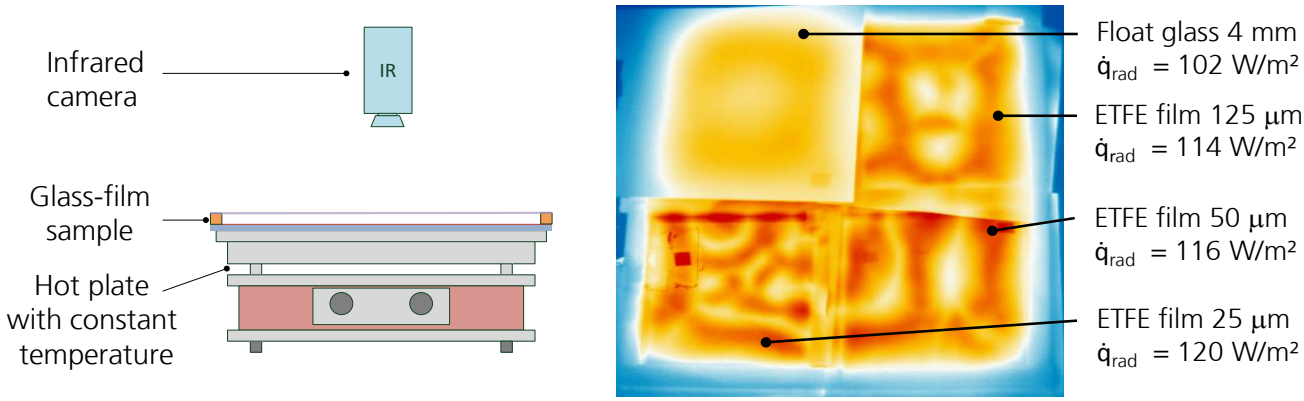

Figure 5.11: Thermographic analysis of radiative heat losses of polymer films in combination with a low-e coated glass: experimental set-up (left) and thermographic image of four film-glass samples with low-e glass at T = 74 °C (right).

Analysis of radiative heat losses of polymer films as front cover

Heß (2014) reports that the transmittance of polymer films in the infrared spectrum is relevant concerning radiative heat losses. While glass can be considered opaque, the effect of infrared transmittance on the overall heat losses is not negligible for polymer films.

In Fourier spectroscopy measurements, we characterized an ETFE film with a thickness of 100 µm in the infrared spectrum up to λ = 17 µm. An infrared transmittance of τ_{373K} = 0.23 was obtained by weighting the measured spectrum with the Planck spectrum of a black body at 373 K. This suggests that radiative heat losses might increases significantly when using polymer films instead of glass as front cover. Comparison with previous measurements of Heß (2014) show that the variance between different types of polymer films (FEP, PFA, PTFE) is small. Yet, thinner films also have a higher transmittance for infrared radiation up to τ_{373K} = 0.49 at a film thickness of 25 µm.

To study the influence of the infrared transmittance on the overall radiative heat losses in the PVT collector, ETFE films of various thicknesses were investigated with the hot plate thermography measurement set-up. The glass-film-sample comprises three films and one glass substrate that are mounted on a wood frame. This frame spaces the samples in distance of 20 mm to a low-e-coated glass pane which is heated by a hot plate of constant temperature. The set-up corresponds to the typical construction of a PVT collector with low-e on position 3. The resulting infrared thermographic image of the heat flux of three film samples compared to glass is shown in Figure 5.11 (right).

12 % - 18 % higher radiative heat losses were observed for the ETFE films ($\dot{q}_{rad}$ = 114 - 120 W/m²) compared to conventional float glass ($\dot{q}_{rad}$ = 102 W/m²). This is due to the mentioned infrared transmittance τ_{373K} of the polymer films. With a higher emissivity of the glass pane, e.g. in a PVT collector without low-e coating, this effect becomes more important, as the radiative heat losses are responsible for a significant share of the collector heat losses. If low-e coatings are applied, the share of radiative heat losses emitted from the PVT absorber are relatively small compared to the convective heat losses.

Numerical collector simulations for the two PVT prototypes "PVT01-low-e" and "PVT02-no-low-e" illustrate this relationship. Substituting the glass cover with an ETFE film would increase the overall collector heat loss coefficient U_{Loss} at ΔT = 50 K by 6.9 % for the PVT collector without low-e, but only by 1.5 % for the PVT collector with low-e. The slightly higher radiative heat losses during normal operation are therefore not seen critically for PVT collectors with low-e coatings.

Analysis of the radiative heat losses of switchable glass-film insulation

A small-scale, inflatable glass-film cushion with the dimensions of 400 mm x 400 mm was built to characterize the switching range of the radiative heat losses. The construction bases on a full-size, inflatable PVT collector and comprises a low-e-coated glass with an emissivity of ε_{373K} = 0.05, a 100 µm thick ETFE film, a butyl rubber edge compound, and a Schrader valve to inflate and deflate the cushion. The heat loss rate $\dot{q}_{rad}$ was studied at this small-scale sample for different filling states with the hot plate thermography measurement set-up. Figure 5.12 shows the thermographic image of the cushion during a deflation sequence at a hot plate temperature of $T_{surface}$ = 74.5 °C.

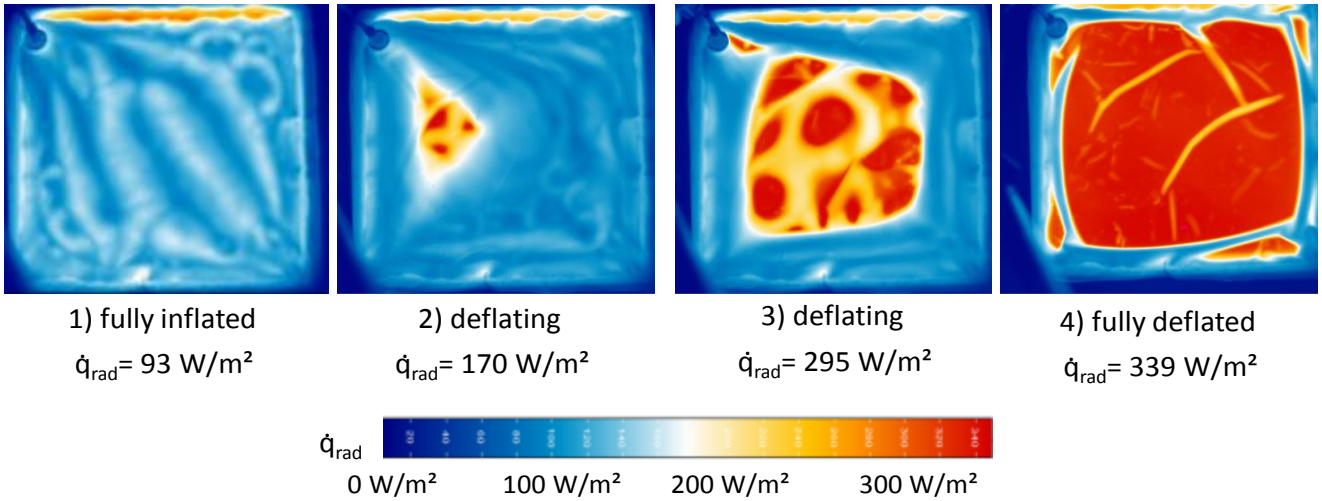

Figure 5.12: Thermographic images of a glass-film cushion in fully inflated and deflated state and during deflation at a hot plate temperature of $T_{surface}$ = 74.5 °C.

In the fully inflated state in image (1), the average radiative heat loss rate amounts to $\dot{q}_{rad}$ = 93 W/m². Only the top edge of the butyl sealing acts as a thermal bridge with consequently high heat losses. It is interesting to observe the movement of the air inside the cushion through the thin film. Due to the small thermal capacity of the film, dynamic changes of the air temperature are visible in the thermographic image through changes of the surface temperature. Slow, billowing movements in the shape of organic structures are observed during the experiment that are attributable to the movement of hot air and its natural convection cells.

Shortly after the deflation process starts, the film begins to contact the glass directly (image (2)). With less air volume in the cushion, more and more area of the low-e glass is in direct contact with the film. The lighter yellow spots in image (3) are air bubbles, where only a thin air film separates the low-e glass and the film. Image (4) shows the fully deflated state with a radiative heat loss rate of $\dot{q}_{rad}$ = 339 W/m². A glass sheet with an emittance of ε_{373K} = 0.91 achieves similar heat dissipation rates. The air is now almost entirely removed from the cushion, so that the contact between film and glass is smooth and only few remaining wrinkles and air intake at the edges are visible.

From all this follows that a glass-film cushion can effectively switch between low radiative heat losses in the inflated state to high radiative heat losses in the deflated state. In the inflated mode, the heat loss rate lies in the range of a conventional PVT collector setup. In the deflated mode, the heat loss rate is similar to an uncoated glass without additional front cover. This shows that the low-e coating is basically deactivated when brought in contact with the film, because conductive heat transfer dominates the heat loss mechanisms in this configuration.

5.4.2.3 Experimental characterization of U_{Loss}

Next to the radiative heat losses, convective heat losses are also triggered by deflating the glass-film cushion. The overall collector heat losses were characterized at the full-size PVT prototype with switchable glass-film insulation using the "dark method" as described in section 5.3.1.2.

Figure 5.13 compares the resulting overall heat loss coefficient U_{Loss} in three different modes:

- In the air-inflated mode, the heat loss coefficient during normal operation amounts to U_{Loss} = 7.8 W/m²K, corresponding to a stagnation temperature of T_{stg} = 157 °C.
- Alternatively, the ETFE cushion can be filled with argon instead of air to suppress convective heat losses. For the argon inflated mode, a heat loss coefficient of U_{Loss} = 6.7 W/m²K was measured. Using argon instead of air thus reduces U_{Loss} by 16 $\%_{rel}$. Noble gas fillings are therefore an interesting option to increase the thermal performance during normal operation, with the advantage to not affect the optical performance.
- In the deflated mode, the application of a negative pressure inside the cushion attracts the film and deactivates the low-e coating. Furthermore, convective heat losses increase due to the attached film cover. An artificial wind with a wind speed of u_{wind} = 1.2 m/s in the collector plane was applied during the dark method measurements. The measured heat loss coefficient amounts to U_{Loss} = 18.9 W/m²K, corresponding to a stagnation temperature of T_{stg} = 94 °C.

To conclude, the inflatable film insulation achieves a large switching range of ΔU_{Loss} = 11.1 W/m²K for air filling and ΔU_{Loss} = 12.2 W/m²K for argon filling. This is an unprecedented switching range, which enables a good performance during normal, inflated operation and an effective overheating protection with a deflated cushion.

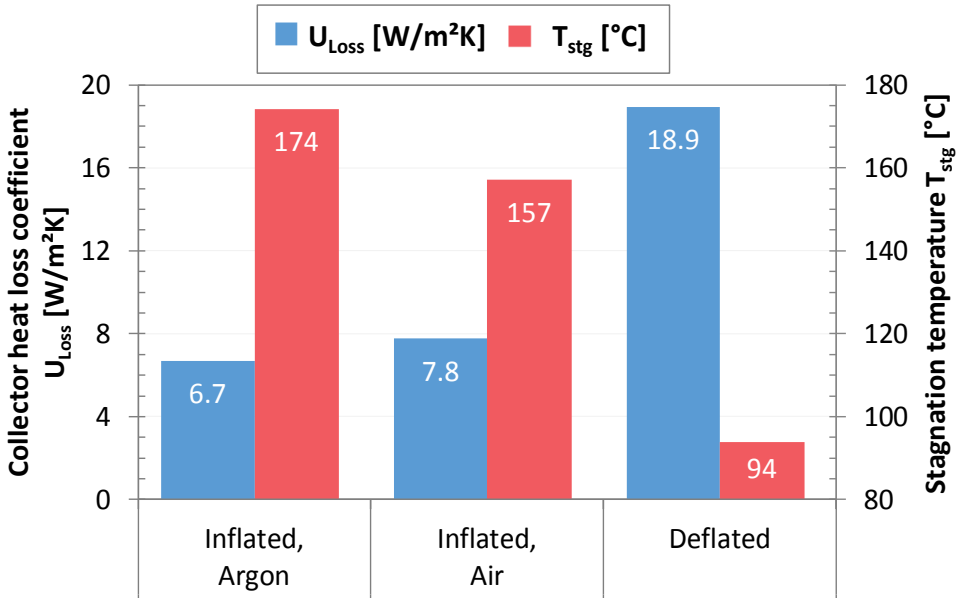

Figure 5.13: Measured heat loss coefficient U_{Loss} at ΔT = 50 K and calculated stagnation temperature T_{stg} of the film PVT collector in inflated and deflated mode.

5.4.2.4 Characterization of collector performance

The thermal performance of the PVT collector with switchable film insulation was characterized based on ISO 9806 in the indoor solar simulator of Fraunhofer ISE. Throughout the performance measurements, the PVT collector was operated in the simultaneous MPP mode and an artificial wind with u_{wind} = 3 m/s was applied in the collector plane. The thermal efficiency was characterized in both the air-inflated and deflated operation mode.

Figure 5.14 shows the resulting efficiency curves and corresponding standard performance coefficients. The results of the performance characterization of the full-size PVT collector confirm the previous, non-standard measurements of $\dot{q}_{rad}$ and U_{Loss}.

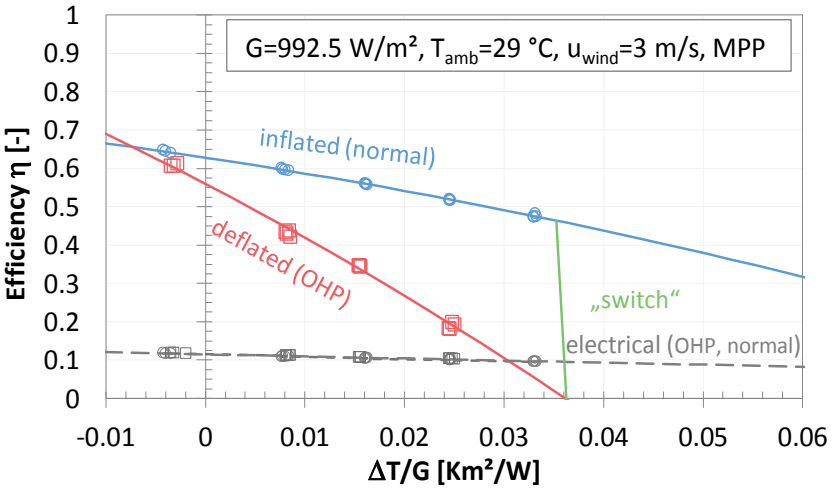

	inflated (normal)	deflated (OHP)
$\eta_{th,0}$	0.63	0.56
c_1 [W/m²K]	3.92	13.5
c_2 [W/m²K²]	0.021	0.056
T_{stg} [°C]	154.0	94.5
$U_{Loss,stg}$ [W/m²K]	6.8	22.8
$\eta_{el,0}$ at $\Delta T = 0$ K	11.5 %	11.5 %
$\eta_{el,stg}$ during stagnation	5.9 %	9.6 %

Figure 5.14: Thermal and electrical efficiency curves with steady-state test points of "PVT04-film" measured in the solar simulator.

The PVT collector reaches a high thermal performance with low heat losses in the inflated mode. The thermal efficiency is comparable to "PVT01-low-e", given the similar characteristics of the low-e coating. However, the conversion factor of the film collector is 4 $\%_{abs}$ lower ($\eta_{th,0} = 0.63$ compared to $\eta_{th,0} = 0.67$) because of a reduced transmittance of the ETFE film ($\tau_{AM1.5} = 0.92$) compared to double sided AR glass ($\tau_{AM1.5} = 0.97$).

In the deflated mode, the PVT collector achieves low stagnation temperatures with high heat losses. The characteristics of the PVT collector with activated overheating protection are similar to those of an unglazed PVT collector with insulated backside.

To compare stagnation temperatures and heat loss rates, the standard stagnation temperature T_{stg} is evaluated with Eq. (5.1) and the overall collector heat loss coefficient during stagnation $U_{Loss,stg}$ is evaluated with Eq. (5.7). Accordingly, the overheating protection reduces the standard stagnation temperature from 154 °C to 94.5 °C. This corresponds to an increase of $U_{Loss,stg}$ from 6.8 W/m²K to 22.8 W/m²K. Thus, the switching range of $U_{Loss,stg}$ in the solar simulator is even higher than indicated by the tests with the dark method which can be attributed to the lower wind speeds in the latter method.

The electrical efficiency curve is not affected by switching from inflated to deflated mode. Figure 5.14 indicates the steady-state test points of the electrical efficiency of both operation modes and a single, linear efficiency curve is observed. At $\Delta T = 0$ K, i.e. $T_m = T_a = 29$ °C, an electrical efficiency of $\eta_{el,0} = 11.5$ % was registered. By contrast, an electrical efficiency under standard test conditions $\eta_{el,STC} = 13.9$ % was measured in the flasher. The operation mode, however, strongly affects cell temperatures and hence the electrical efficiency during stagnation. The electrical efficiency during stagnation amounts to $\eta_{el,stg} = 5.9$ % in the inflated mode, but to $\eta_{el,stg} = 9.6$ % in the deflated mode on account of reducing stagnation temperatures from 154.0 °C to 94.5 °C. An intelligent control of the ETFE cushion can therefore lead to a gain of electrical yields by managing the collector temperatures.

5.4.2.5 Dynamic operation of the overheating protection

Two test sequences were conducted on the full-size PVT collector in the indoor solar simulator with the objective to analyze the dynamic operation of the OHP and its effect on absorber temperatures and the thermal efficiency.

Maximum absorber temperatures were measured during stagnation at no-flow conditions while the collector was deflated to avoid destruction. PT100 sensors measured the temperatures on the back side of the PVT absorber at two thirds height.

The dynamic sequence for three different operating conditions revealed the following maximum absorber temperatures (Figure 5.15, left):

- OC Mode, no wind: $T_{abs,max}$ = 94.3 °C
- MPP-Mode, no wind: $T_{abs,max}$ = 90.1 °C
- MPP-Mode, u_{wind} = 3 m/s: $T_{abs,max}$ = 68.0 °C

Accordingly, the maximum absorber temperatures during worst-case stagnation conditions amount to $T_{abs,max}$ = 94.3 °C, which is uncritical for all employed materials. The measured temperature on the absorber in MPP mode $T_{abs,max}$ = 90.1 °C is slightly lower than the standard stagnation temperature (T_{stg} = 94.5 °C) where a security margin of 20 K is assumed.

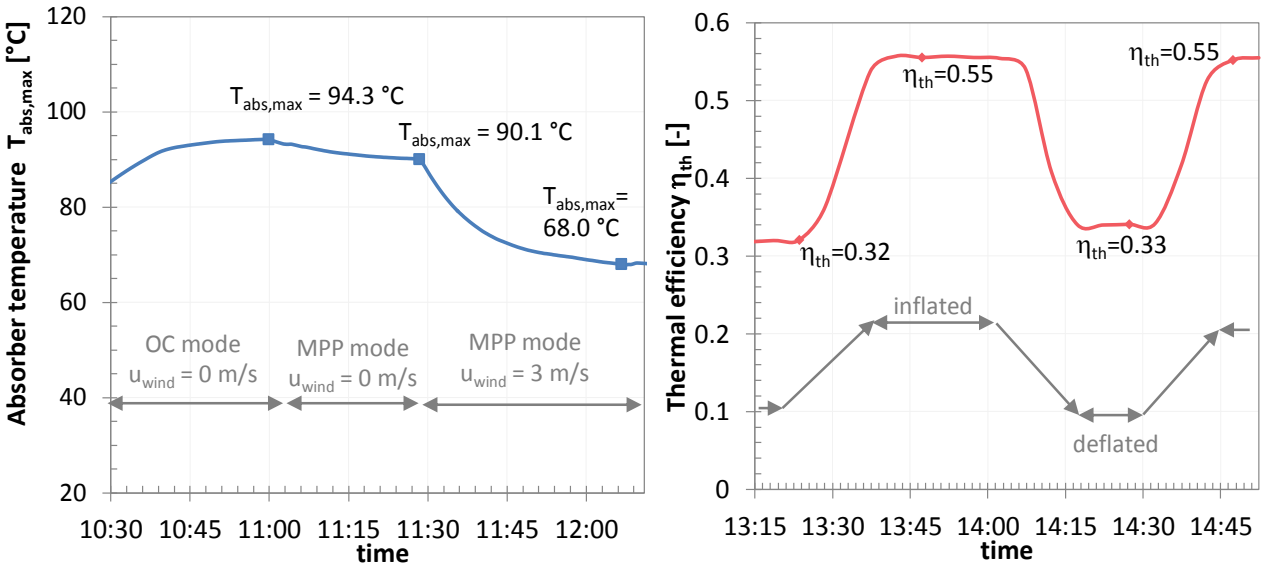

Figure 5.15: Dynamic operation of the overheating protection. Left: maximum absorber temperature during stagnation in deflated mode with varying boundary conditions. Right: Sequence of inflating and deflating at $T_{fl,in}$ = 45 °C and T_a = 28 °C.

In a second test sequence (Figure 5.15, right), the dynamic behavior and reaction time of the switchable film insulation was analyzed. For this purpose, the cushion was inflated and deflated in the solar simulator while the thermal efficiency was monitored. The operating conditions were kept at a constant level of G = 992.5 W/m², $T_{fl,in}$ = 45 °C, and u_{wind} = 3 m/s. A small air blower with a rated power of 20 W and maximum pressure of p = 0.05 bar was used for inflating and deflating the cushion, which took 16 minutes each.

The thermal efficiency directly reacts on changes of the filling level of the cushion. Only during deflation, it requires a short starting time until a minimum air volume is evacuated and an effect on the thermal efficiency is registered. Moreover, it is an important observation that the initial efficiency of η_{th} = 55 % is reached again after a full deflation and inflation cycle.

5.4.2.6 Discussion and outlook

The first PVT collector prototype with switchable film insulation achieved remarkable experimental results with a good overall performance during normal operation and a high switching range of the heat losses by deflating the cushion.

Despite the already good results, there is still potential for optimization. Due to the curvature shape of the cushion, partial shading from the collector frame is no issue in this collector concept. This allows higher packing factors of the PV cells and thus higher electrical yields. The optical efficiency of the PVT collector can be improved by using FEP instead of ETFE films and by an optimized production process of the low-e coating with less reflection losses. As shown in section 5.4.2.3, an Argon filling is capable to further reduce convective heat losses by 16 $\%_{rel}$. Finally, a full-size PVT collector of larger dimensions might achieve lower heat losses, especially at the edges of the cushion.

Further research is required to bring the collector concept from the current prototype stage to a commercial product. The durability of the ETFE film needs to be tested at combined temperature and UV radiation ageing and outdoor exposure. Passive and fail-safe methods have to be tested to deflate the collector reliably during system failures. Possible approaches are valves that open passively at high temperatures or during power failure. Additionally, the parasitic electricity consumption for running the air blower needs to be weighed against potential electrical yield gains through a cooling of the collector. The low-e coating can be also applied on the interior surface of the ETFE film (Siefert et al. 2016; Georg et al. 2017). With such a low-e-coated ETFE film, an unglazed PVT collector can be retrofitted to boost the thermal performance and achieve the characteristics of a glazed PVT collector with low-e coating.

Finally, the switchable insulation enables novel applications such as night cooling (Eicker and Dalibard 2011) or the application in a heat pump system with excellent performance in a parallel integration mode with inflated collectors and in a serial integration mode with deflated collectors. Beyond the application in PVT collectors, the switchable film insulation is also a promising overheating protection for flat plate collectors or other applications, where a large switching range of the heat loss coefficient is required.

5.4.3 PVT collector with sorption-based switchable insulation

5.4.3.1 Description of collector concept

The sorption-based overheating protection utilizes the principle of adsorption in vacuum to switch its U-value: at low temperatures, the working medium is adsorbed at an adsorbent material located inside a vacuum flat-plate collector. With increasing absorber temperatures, the adsorbed medium evaporates and thus increases the gas pressure. The increasing gas pressure switches the heat losses from an unconducting to a conducting state. Different combinations of working media (e.g. water, ethanol) and adsorbent materials (e.g. silica gel, zeolite, SAPO) can be used for this application.

The switchable insulation requires neither mechanical, movable actuators, nor external energy for the operation of the OHP, but is entirely passive. Furthermore, the switchable insulation is also applicable for conventional solar thermal collectors, windows, or building elements.

The collector design is mainly inspired by the principle of vacuum flat plate collectors. There are some commercial products for vacuum flat plate collectors available, e.g. by SRB Energy (CH), Thermosolar (DE), and TVP Solar (CH). The air tightness was tested for one commercial vacuum flat plate collector product and a high leakage rate of 1.2 mbar/ls was detected. This is most probably due to the intrusion of air into the evacuated vacuum chamber, necessitating a frequent reevacuation of the collector.

The development of a permanent vacuum-tight edge compound is also a challenge for the research of vacuum insulation glass VIG. VIG is a double-pane isolation glass separated by a vacuum gap. Small spacers inside the vacuum gap deliver the required mechanical stability and prevent a collapse of the glass panes. Soldered glass-metal-glass compounds are a promising approach for the hermetical edge sealing which is currently under research (Glaser et al. 2016).

The feasibility of an active, switchable vacuum insulation for PVT collectors was jointly demonstrated by Fraunhofer ISE and Solvis in the project PVTmax (Wendker et al. 2012). An external vacuum pump actively regulates the vacuum pressure inside this PVT collector. A pressure below $p < 0.01$ mbar gave a good thermal insulation during regular operation, while a pressure above $p > 1$ mbar resulted in a significant reduction of thermal losses.

Pailthorpe et al. (1987) report on a passive sorption based overheating protection for vacuum tube collectors. The vacuum tube is filled with a desorbable gas, which specifically adsorbs on the absorber surface. With increasing temperature of the absorber, the pressure inside the vacuum tube increases, resulting in a higher heat transfer coefficient.

Henning et al. (2011) filed a patent for a sorption-based overheating protection. The working medium and the sorbents have to be matched to achieve a relevant increase of gas pressure to switch the heat losses from unconducting to a highly conducting state. The principle functionality of this patent will be investigated in the following section by experimental and numerical analysis.

However, the available VIG and vacuum flat plate collector technology are unable to permanently maintain the low gas pressure inside the vacuum chamber. The development and construction of a fully functional, full-sized, vacuum-tight PVT collector with sorption-based switchable insulation is therefore out of the scope for this thesis. Instead, a feasibility study based on experimental results combined with the numerical PVT collector model will be presented in the following section.

Figure 5.16 depicts a possible construction design of a PVT collector with sorption-based switchable vacuum insulation. The low-e-coated PVT absorber is located inside an evacuated vacuum chamber with a transparent front glazing. The rear side of the vacuum chamber can be carried out as either a deep-drawn steel casing or also made of glass. In both cases, a vacuum-tight edge compound is required, which must be flexible enough to withstand the different thermal elongation of the front glazing and steel casing. Moreover, spacers inside the vacuum gap are required to absorb and distribute the mechanical load of the atmospheric pressure.

The adsorbent is thermally coupled to the rear side of the PVT absorber, so that adsorbent and absorber are at similar temperatures. For the suggested collector design, an adsorbent coating is applied at the

back of the PVT absorber so that the vapor pressure has to propagate to the front gap to switch thermal losses at both the front and back side.

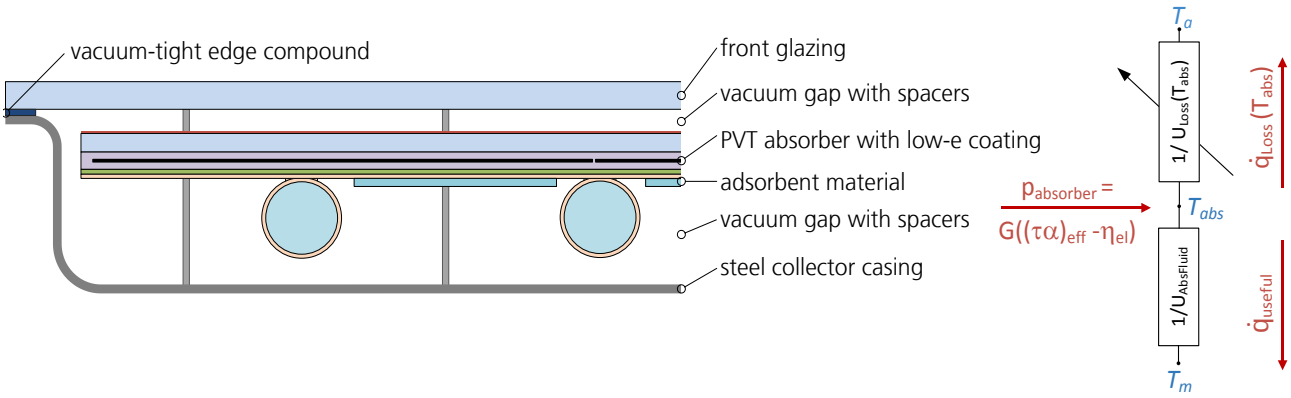

Figure 5.16: Schematic collector construction of the PVT collector with sorption-based switchable vacuum insulation.

5.4.3.2 Gas pressure dependence of heat losses

The heat losses by gas conduction in a vacuum regime are a function of the gas pressure. Natural convection occurs at gas pressures between p = 0.1 - 1 bar, resulting in relatively high thermal losses. Lowering the gas pressure to p = 1 - 100 mbar suppresses natural convection, but gas heat conduction still takes place. A further reduction of the gas pressure below p = 0.1 mbar finally suppresses also gas heat conduction losses, rendering the lowest heat loss rates (Benz and Beikircher 1999).

Beikircher et al. (1996) derived empirical correlations for the dependency of gas heat conduction losses from the gas pressure. The Knudsen number as quotient of mean free length l_{free}, and the distance in the vacuum gap d_{gap} is given by:

$$Kn = \frac{l_{free}}{d_{gap}} = \frac{1}{d_{gap}\, p} \cdot \frac{0.008313\, m}{1 + \frac{116\, K}{T}} \tag{5.8}$$

Then, the heat loss coefficient for gas heat conduction in vacuum is expressed as:

$$h_{vac} = \frac{\lambda}{d_{gap}} \frac{1}{1 + \frac{19}{4} Kn} \tag{5.9}$$

Figure 5.17 shows the dependence of the heat loss coefficient h_{vac} from pressure and gap distance, evaluated with Eq. (5.8) and Eq. (5.9). Accordingly, the gas pressure has to be maintained below p = 0.1 mbar to achieve low heat losses. Above p = 0.1 mbar the heat loss coefficient increases continuously until reaching a plateau around p = 5 mbar. Thereby, the gap distance functions as a lever. With a smaller gap distance d_{gap}, the heat losses h_{vac} increase almost proportionally.

To achieve a high switching range for the heat losses, the pressure should be varied between 0.1 and 1 mbar. In this pressure range, the heat losses can be increased by a factor of 3 from $h_{vac,0.1mbar}$ = 6.5 W/m²K to $h_{vac,1mbar}$ = 20.0 W/m²K, at a gap distance of 1 mm.

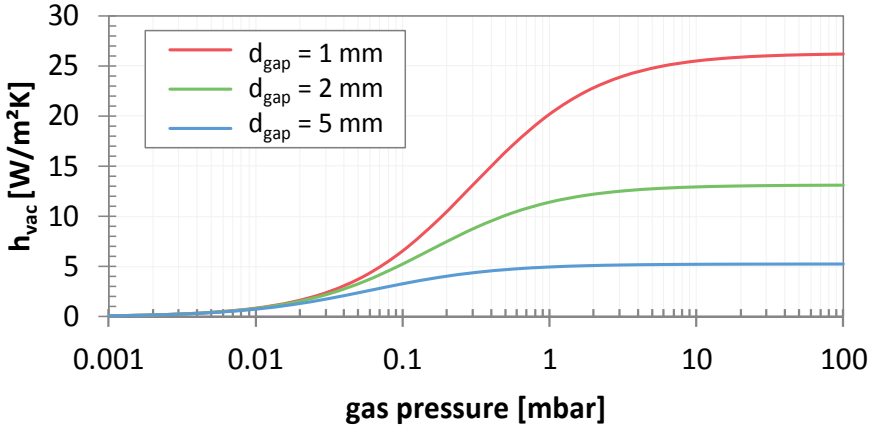

Figure 5.17: Theoretical dependence of the convective heat transfer coefficient h_{vac} from the gas pressure.

To confirm this theoretical model with experimental results, performance measurements on the vacuum PVT collector, which was developed and tested within the project PVTmax (Wendker et al. 2012), were reevaluated.

This PVT collector features a vacuum insulation glass (VIG) on the front side that is made up by the PV module glass and the front glazing, with a viton and rubber sealing edge compound. The gap distance amounts to d_{gap} = 3 mm and round stainless steel pins with a diameter of 4 mm are equally spaced in a distance of 80 mm between the front glazing and the PVT absorber. As this VIG edge compound is not entirely vacuum-tight, the vacuum PVT collector is connected to a vacuum pump stand and the VIG has to be evacuated at regular intervals.

The thermal performance η_{th} was measured at different gas pressures in the solar simulator at otherwise constant operating conditions (fluid inlet temperature $T_{fl,in}$ = 76 °C, irradiance G = 991 W/m², and ambient temperature T_a = 33 °C). To mathematically derive the overall heat loss coefficient U_{Loss} from the thermal efficiency η_{th}, the definition of F′ as a function of $U_{AbsFluid}$ in Eq. (3.19) is employed into the following notation of η_{th}:

$$\eta_{th} = F'[(\tau\alpha)_{eff} - \eta_{el} - U_{Loss}\frac{\Delta T}{G}] \tag{5.10}$$

Solving Eq. (5.10) and Eq. (3.19) for U_{Loss} leads to:

$$U_{Loss} = \frac{(\tau\alpha)_{eff} - \eta_{th} - \eta_{el}}{\frac{\eta_{th}}{U_{AbsFluid}} + \frac{T_m - T_{amb}}{G}} \tag{5.11}$$

where the collector parameters $(\tau\alpha)_{eff}$ = 0.832 and $U_{AbsFluid}$ = 61.2 W/m²K are assumed constant.

The blue markers in Figure 5.18 show resulting steady-state heat loss coefficient U_{Loss} for varying gas pressures. Switching the gas pressure from p = 0.004 mbar to p = 1 mbar effectuates an increase of U_{Loss} from 6.4 W/m²K to 11.5 W/m²K. These two values of U_{Loss} correspond to stagnation temperatures of T_{stg} = 125 °C, and T_{stg} = 180 °C according to Eq. (5.6).

Numerical simulations of the collector heat losses were carried out with the PVT collector model. The thermal circuit for U_{Loss} in the vacuum gap is solved using a parallel connection of the three thermal re-

sistances for gas heat conduction in vacuum regime $1/h_{vac}$, radiative heat losses $1/h_{rad}$, and heat conduction through the pins $h_{cond,Gap}$. The resulting overall heat loss coefficient U_{Loss} and its breakdown into the individual heat transfer mechanisms is also plotted in Figure 5.18.

Good agreement between the experiment and numerical model can be stated. Only above p = 0.5 mbar, the numerical models underestimate the experimental results of U_{Loss}. Nonetheless, the numerical model for the pressure dependence of heat losses in a vacuum regime can be used for further analysis.

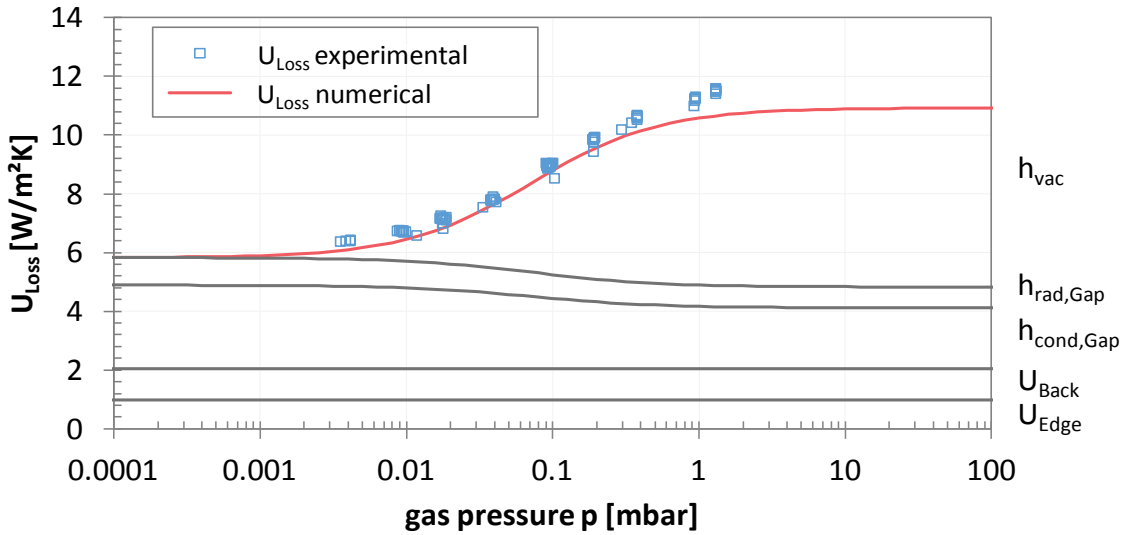

Figure 5.18: Experimental (blue markers) and numerical analysis (lines) of the gas pressure dependence of thermal losses. Measurements were conducted at G = 991 W/m², $T_{fl,in}$ = 76 °C, and T_a = 33 °C.

5.4.3.3 Temperature dependence of gas pressure

The next relevant relationship concerns the dependence of the gas pressure on the temperature. This relationship is described numerically with the established thermodynamic theory of absorption and adsorption processes. For the present analysis, we focus on adsorption processes with water as working medium. Utilizing other working media or applying absorption processes to switch the gas pressure might also be feasible and yield similar results.

The water uptake X describes the state of the adsorbate and is defined as the ratio of the dry mass of the adsorbed medium to the mass of the adsorbate. The equilibrium conditions depend on material properties, temperature and pressure and follow a characteristic curve with X(p,T). Different models are available to describe the dynamic equilibrium of adsorption processes, e.g. empirically-determined characteristic curves based on the Dubinin potential theory, which can be parametrized for different materials by measurement of the thermodynamic properties (Nunez 2001).

The closed adsorption process in the PVT collector is characterized by a constant mass content of adsorbate and water which is either in the adsorbed or gaseous state. An increase of the temperature T leads to desorption of water and thus a reduction of water uptake X and an increase of pressure p.

Assuming a sufficiently high adsorbate mass in relation to the vacuum volume, the water uptake X is reduced only insignificantly by the desorption of water. Only a small number of desorbed water molecules are needed to achieve the desired changes in the relevant pressure ranges. The small quantities of desorbed water do not significantly alter the adsorbents water uptake X, as sufficient adsorbent is pre-

sent and the vacuum volume is comparably small. With the simplification of a constant X, the equilibrium can be described by an isosteric change of state. The pressure p is then given by (Nunez 2001):

$$p = p_0 e^{-\frac{h_{ad}}{RT}+C} \tag{5.12}$$

with the initial pressure p_0, the adsorbent temperature T, the adsorbent enthalpy h_{ad}, the gas constant R, and a characteristic offset C.

Experiments which reproduce the situation inside the vacuum gap of the PVT collector were conducted to verify the described numerical correlations and the assumptions of isosteric change of state. For this purpose, a saturated adsorbent was placed inside a vacuum chamber, which was then evacuated until a specified initial pressure p_0 was reached. Afterwards, the temperature in the insulated vacuum chamber was increased by an external heat supply. During the cool-down phase, a Pirani pressure sensor measured the distribution of the internal gas pressure.

Figure 5.19 shows the measured pressure curves of silica gel and zeolite at two different initial pressures p_0 = 0.01 mbar and p_0 = 0.1 mbar. These experimental pressure curves are compared with numerical results for the isosteric pressure curve according to Eq. (5.12). The exponents for this equation are obtained with empirical characteristic curve fits on basis of the Dubinin potential theory for the silica gel and zeolite adsorbents (Nunez 2001).

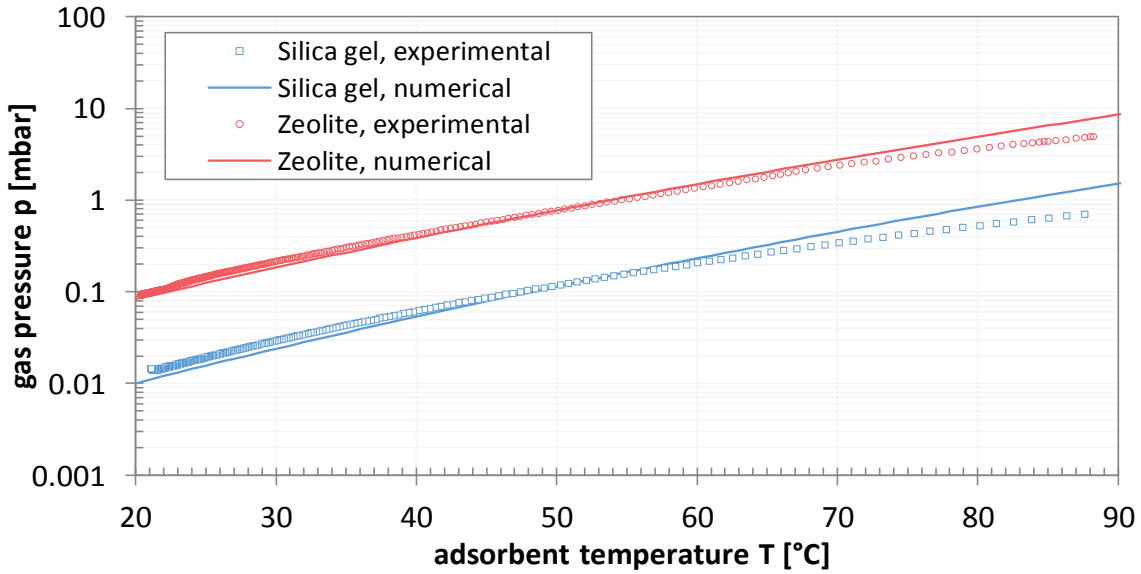

Figure 5.19: Experimental and numerical pressure curve of silica gel and zeolite in a vacuum chamber as function of the adsorbent temperature.

A relatively good agreement over a wide temperature range can be observed. Yet, the numerical model overestimates the gas pressure at temperatures above T = 70 °C. This might be related to the fact that at higher temperatures the change of the water uptake X begins to influence the equilibrium state with the consequence of lower gas pressures. Another possibility for the differences might be experimental uncertainty for the temperature and gas measurement. Nonetheless, the assumption of an isosteric change of state seems reasonable and consequently pressure curves according to Eq. (5.12) describe the temperature-dependent pressure variance with sufficient accuracy.

5.4.3.4 Numerical simulation of the efficiency curve

The two experimentally confirmed correlations for the gas pressure dependence of heat losses in Eq. (5.9) and for the temperature-dependence of the gas pressure in Eq. (5.12) are implemented in the numerical PVT collector model. Using these validated correlations, the efficiency curves and collector temperatures for the PVT collector with sorption-based switchable insulation are obtained numerically.

The design of the vacuum flat plate PVT collectors leaves open several free parameters for optimizing the performance and the switching range for the overheating protection open.

Firstly, the gap distance d_{gap} between the front glazing and the PVT absorber is an important lever for high heat losses during stagnation. According to Figure 5.17, a gap distance of d_{gap} = 1 mm is selected for the simulations to achieve sufficiently high gas heat conduction losses. The conductive heat losses through the spacer pins increase proportionally to the smaller gap distance. To reduce these heat losses to an acceptable level, the simulation assumes a reduction of the pins' thermal conductivity λ_{pin} by a factor of five compared to the PVT collector in PVTmax.

Secondly, the adsorbent material only has a minor influence on the desorption characteristics. The offset between the two pressure curves in Figure 5.19 originates from different initial pressures p_0. As indicated by numerical simulations and experimental measurements, the choice of the adsorbent material has only a minor influence on the characteristics of the curves. A commercial silica gel product with well-known parametrization for the equilibrium is used for the simulations. Thereby, the adsorbent mass relative to the vacuum volume is sufficiently large to allow the assumption of isosteric change of state.

Thirdly, the initial pressure p_0 at T_{abs} = 25 °C has to be adjusted to fine-tune the switching temperature of heat losses. With a too low initial pressure, the heat losses are triggered at too high absorber temperatures. With a too high initial gas pressure, high heat losses already occur at low absorber temperatures and thus reduce the thermal efficiency during regular operation. Therefore, the initial pressure p_0 has an important influence on the functionality of the overheating protection. Figure 5.20 (left) shows the efficiency curve obtained from the numerical PVT collector model with three values of the initial pressure p_0. For a well-balanced operation, p_0 = 0.01 mbar is too high and achieves high heat losses during normal operation, and p_0 = 0.0001 mbar is too low resulting in critical stagnation temperatures.

The overheating protection in the PVT collector should preferably feature low heat losses below T_{abs} = 60 °C, and a sharp increase of heat losses above that temperature. Heat losses increase strongly above p = 0.01 mbar as shown in Figure 5.18. Hence, setting the pressure to p = 0.01 mbar at T_{abs} = 60 °C triggers heat losses above this temperature. According to Eq. (5.12), an initial pressure of p_0 = 0.0005 mbar at T_{abs} = 25 °C is required to set the trigger point described above.

This initial pressure is very low and difficult to maintain in practice. The initial pressure can be set via an initial evacuation of the vacuum chamber combined with heating up the PVT absorber. During operation, outgazing of components inside the vacuum chamber might alter the pressure conditions and thus shift the trigger temperature. Nonetheless, the low operating pressures impose a high challenge for the vacuum tightness of the edge compound, allowing only a minimal leakage rate.

Finally, the construction of the vacuum chamber also influences performance and stagnation temperatures. The vacuum gap can be situated at the front between PVT absorber and front glazing, at the back, between PVT absorber and collector casing, or both back and front, as illustrated in Figure 5.16. Numeri-

cal simulations for these three cases were conducted with the PVT collector model and the resulting efficiency curves are plotted in Figure 5.20 (right).

Vacuum at both back and front achieves the lowest stagnation temperatures of $T_{abs,max}$ = 113 °C followed by vacuum at the front with $T_{abs,max}$ = 118 °C. Vacuum insulation at the back yields a stagnation temperature of $T_{abs,max}$ = 147 °C, which is an insufficient temperature reduction for the materials employed in PVT collectors. The limited potential of switchable insulation at the collector back can be attributed to the relatively large vacuum gap distance d_{gap}, and the difficulty to activate the heat loss path on the backside of the collector with its specific on-roof or in-roof mounting situation. Therefore, the switchable vacuum insulation has to be located at the front side in any case, and optionally at the backside, too.

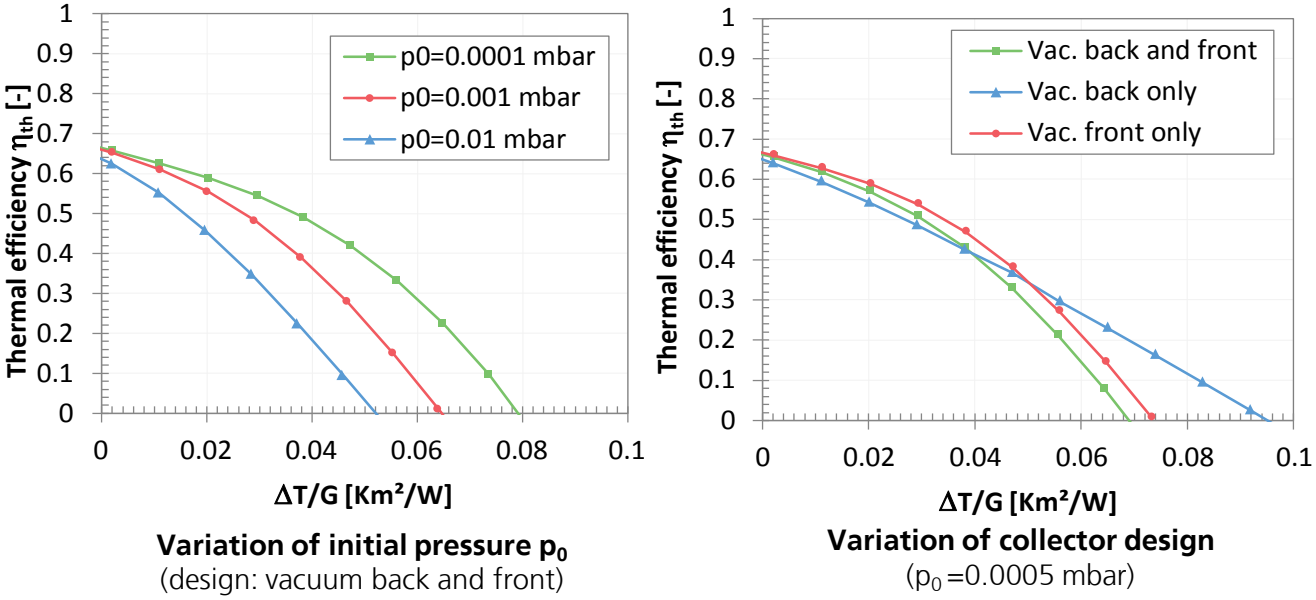

Figure 5.20: Thermal efficiency curves of the PVT collectors with sorption-based OHP with variation of initial pressure (left) and collector design (right). Results obtained from numerical PVT collector model at G = 1000 W/m², T_a = 25 °C, and u_{wind} = 3 m/s, MPP mode.

Simulations for a proposed PVT collector design with an initial gas pressure of p_0 = 0.0005 mbar were carried out on the basis of these considerations. The collector features vacuum at the front and back of the absorber with a gap spacing of d_{gap} = 1 mm at the front and d_{gap} = 15 mm at the back. For comparison purposes, a PVT collector with identical design parameters, yet without collector-integrated adsorbents, was also assessed numerically. Both resulting thermal efficiency curves η_{th} with the corresponding collector heat losses U_{Loss} are plotted in Figure 5.21.

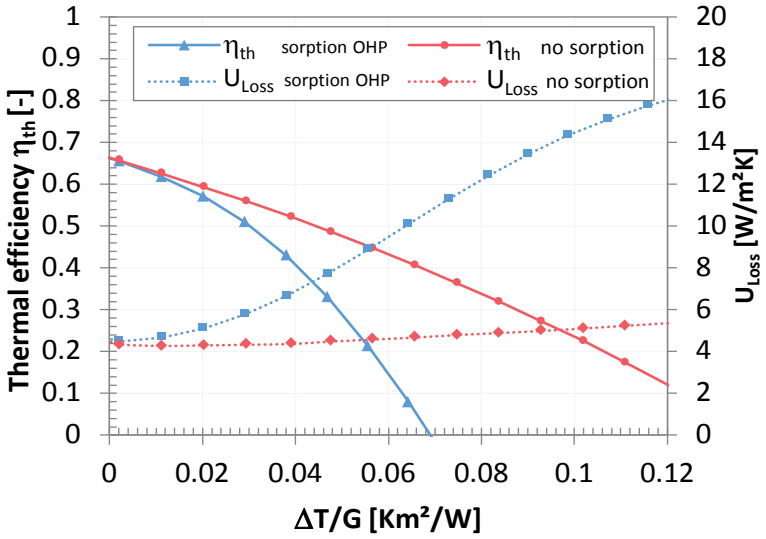

	sorption OHP	no sorption
$\eta_{th,0}$	0.671	0.678
c_1 W/m²K]	3.35	2.47
c_2 [W/m²K²]	0.09	0.007
$T_{abs,max}$ [°C]	112.7	186.2
$U_{loss,stg}$ [W/m²K]	11.3	5.5
$\eta_{el,stg}$	9.0 %	4.9 %

Figure 5.21: Thermal efficiency curves of a PVT collector with sorption-based overheating protection compared to a vacuum PVT collector without sorption. Results obtained from numerical PVT collector model at G = 1000 W/m², T_a = 25 °C, and u_{wind} = 3 m/s, MPP mode.

Numerical simulations were also carried out for the stagnation case to determine the maximum absorber temperatures, applying boundary conditions of u_{wind} = 0 m/s, G = 1000 W/m², T_a = 30 °C, OC mode. The resulting maximum absorber temperature of the PVT collector with sorption OHP amounts to $T_{abs,max}$ = 112.7 °C, which corresponds to $U_{Loss,stg}$ = 11.3 W/m²K. Thus, the sorption-based OHP achieves a total switching range of ΔU_{Loss} = 6.0 W/m²K compared to the initial $U_{Loss,0}$ = 4.3 W/m²K.

Without adsorbent, the vacuum PVT collector would achieve a maximum absorber temperature of $T_{abs,max}$ = 186.2 °C, which corresponds to $U_{Loss,stg}$ = 5.5 W/m²K. Hence, the sorption based overheating protection increases the collector heat loss coefficient by $\Delta U_{Loss,stg}$ = 5.8 W/m²K and thus reduces the stagnation temperature by 73 K.

The major difference to the previously discussed OHP is the absence of a discrete switching point with an unsteady jump of U_{Loss}. Instead, U_{Loss} experiences a continuous transition from low to high thermal losses as a function of the absorber temperature. Unfortunately, this also affects the thermal efficiency in the operating range. At an absorber temperature of T_{abs} = 60 °C, which corresponds to a typical operating temperature of glazed PVT collectors, U_{Loss} is already slightly elevated at 5.6 W/m²K. Afterwards, the heat loss coefficient increases on average by 0.17 W/m²K per Kelvin of increased absorber temperature. This affects the operation of the PVT collector during normal operation, when technically no OHP would be required.

Consequently, the parametrization of the efficiency curve is not as straight-forward as for the previous PVT collectors, where two separate efficiency curves describe the two different OHP states. For the sorption-based PVT collector, the heat losses U_{Loss} and thus the thermal efficiency η_{th} are a function of the absolute value of the absorber temperature. This contrasts to conventional collector theory, where the efficiency curve is described as a function of the relative temperature difference ΔT and the irradiance G.

However, a parametrization of the efficiency curve with the additional parameter T_{abs} is complex and difficult to integrate into standardized performance models in system simulation software. Instead, the efficiency curve is separated into one segment below T_{abs} = 60 °C and one segment above T_{abs} = 60 °C

and parameterized for the respective segments, despite the continuous transition of heat losses. This method was also applied by Föste et al. (2016) for collectors with thermochromic absorber coatings and allows a sufficient modelling accuracy. Table 5.4 shows the parametrized efficiency curve parameters of the two segments.

Table 5.4: Parametrization of the PVT collector with sorption-based OHP in two segments.

Parameter	Segment T_{abs} < 60 °C	Segment T_{abs} > 60 °C
$\eta_{th,0}$	0.663	0.674
c_1	3.61 W/m²K	2.27 W/m²K
c_2	0.05 W/m²K²	0.11 W/m²K²

5.4.3.5 Discussion and outlook

A feasibility study on a sorption-based overheating protection was presented which utilizes the temperature-dependent desorption properties of adsorbents to increase the gas pressure and thus increase heat losses at high absorber temperatures. The overheating protection is entirely passive and free of movable parts enabling a fail-safe operation and potentially high customer acceptance. Owing to the vacuum insulation, the PVT collector concept achieves a high thermal efficiency in the operating range at low absorber temperatures.

Low initial pressures below p_0 = 0.001 mbar are required to adjust the trigger temperature for the OHP to T_{abs} = 60 °C. These low pressures impose a high constructive challenge for the design of the vacuum chamber and its hermetical edge sealant. Currently, the technology for these edge sealants is still under research and not commercially available for the application in PVT collectors. An alternative application are vacuum tubes, where the sealing technology is further evolved. Moreover, vacuum insulation panels can be transformed into a switchable insulation in the same manner. However, a switchable vacuum insulation at the rear side of the collector alone is insufficient to avoid critical temperatures.

Within this thesis, the theory for heat transfer and desorption characteristics was derived from small-scale experimental measurements. The next step for further development is an experimental proof-of-concept at a full-sized collector. Once hermetical VIG edge sealants are commercially available, the sorption-based OHP concept can be implemented into a vacuum insulation glass or a PVT collector of similar construction.

5.4.4 Comparison and evaluation of novel PVT collectors with overheating protection

The novel, experimentally investigated PVT collectors are now compared with regards to their accomplished efficiency, and each OHP approach is evaluated with the previously defined evaluation criteria.

The electrical efficiency of all three PVT collectors is very similar with an efficiency at standard test conditions of $\eta_{el,STC}$ = 13.9 %. Only the vented PVT collector achieves a slightly lower electrical efficiency ($\eta_{el,STC}$ = 13.7 %), as a front glazing without anti-reflective coating was used.

Figure 5.22 compares the thermal efficiency curves of the three PVT collectors. The OHP concepts with ventilation and film insulation are characterized by two efficiency curves, one for the normal operation mode and one with activated OHP. These PVT collectors can dynamically switch between the two states.

In contrast to this, the sorption-based OHP approach has a continuous efficiency curve with a high quadratic heat loss coefficient $c_{2,}$ which indicates the increase of thermal losses at high absorber temperatures. As the heat losses in this OHP approach are a function of the absolute absorber temperature, the efficiency curve is only valid for the specific boundary test conditions.

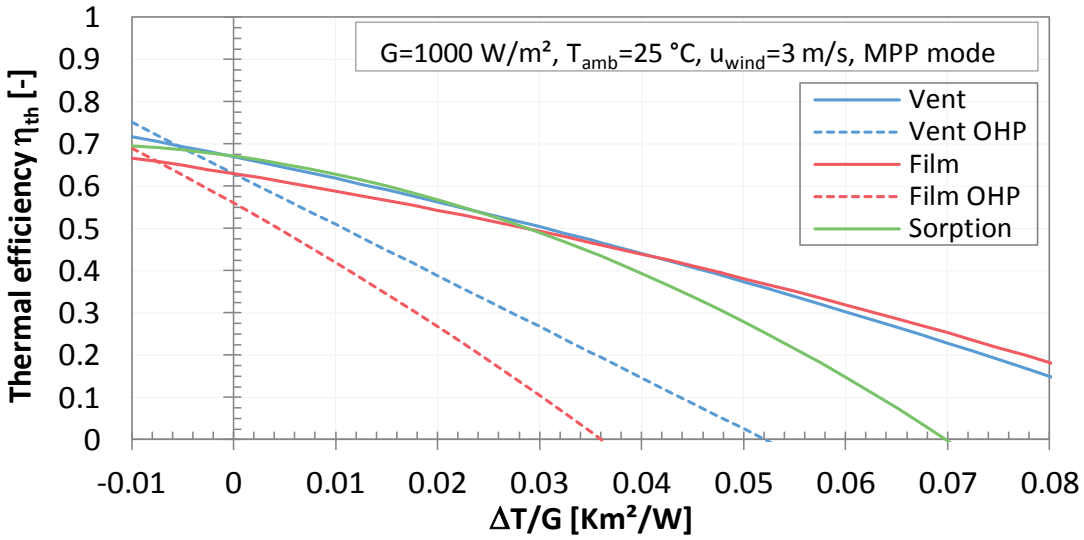

Figure 5.22: Efficiency curves of novel PVT collectors with overheating protection.

Comparing the efficiency curve of the three PVT collectors during regular operation, the sorption-based PVT collector achieves the highest thermal efficiency up to absorber temperatures of T_{abs} = 50 °C. Above these temperatures, the thermal efficiency decreases continuously. The PVT collector with ventilation has slightly higher heat losses than the collector with film insulation, owing to the emissivity of the low-e coating of $\varepsilon_{373K,vent}$ = 0.30 compared to $\varepsilon_{373K,film}$ = 0.14.

The intersection of the OHP efficiency curves with the x-axis indicates the stagnation temperature. Accordingly, the switchable film insulation achieves the lowest stagnation temperature, followed by the ventilation and the sorption-based OHP.

A consistent comparison of the suitability of the overheating protection can be carried out with the previously defined evaluation criteria. The novel OHP concepts are assessed in Table 5.5 on a scale from 1 to 3 with respect to the five evaluation criteria of temperature reduction, intrinsic safety, efficiency reduction, production and operational costs and potential synergies. The effect of efficiency reduction on annual yields is analyzed in more detail in chapter 5.5.2, and the results are already included in the evaluation.

Table 5.5: Evaluation of novel PVT collectors concepts with overheating protection on a scale from one to three.

Evaluation Criteria	Ventilation	Switchable film insulation	Sorption-based OHP
1. Temperature reduction	**3** T_{stg} = 101.8 °C ΔU_{Loss} = 6.5 W/m²K	**3** T_{stg} = 94.5 °C ΔU_{Loss} = 16.0 W/m²K	**2** T_{stg} = 112.7 °C ΔU_{Loss} = 5.8 W/m²K
2. Intrinsic safety	**2** Possible, with thermal actuators	**2** Possible, with thermally controlled valve	**3** Intrinsically fail-safe
3. Efficiency reduction	**3** None	**3** None	**2** higher η at $T_{abs} < 50$ °C lower η at $T_{abs} > 50$ °C
4. Additional costs	**1** High production costs for fins and flaps	**2** Medium production costs as glazing is substituted by film	**1** High production costs for vacuum insulation glazing and edge sealant
5. Potential synergies	**2** - Suitable as source for heat pump with opened flaps with enhanced air-to-water heat exchange	**2** - Flexible operation modes, e.g. very effective for night cooling or as source for heat pump - No edge shading	**2** - Slim and light collector construction - Concept usable for switchable VIG windows
	- Lower temperature load reduces degradation and ageing - Lower material requirements in collector and system - Higher electrical yields through flexible, demand-oriented operation		

Each OHP concept has its specific strengths and weaknesses, which are summarized by the radar chart in Figure 5.23. All three OHP concepts have a high temperature reduction potential and a low efficiency reduction in common. However, the additional production and operation costs have to be considered a major limitation for a wider market success of PVT collectors with overheating protection.

Regarding the evaluation criteria of costs, the additional material costs of the ventilated PVT collector amount to approximately 10 €/m² for glue and the fins, and 7 €/m² for the thermal actuators. The PVT collector with switchable film insulation employs an ETFE film of 100 µm thickness at costs of 10 €/m², but costs of a double-sided AR front cover in the range of 25 €/m² can be saved. Additionally, the pressure supply requires 20 € for the pump, which is sufficient for ca. 10 m² of collectors, plus additional materials for the hydraulics and valves. The operational energy amounts to ca. 10 Wh/m² per sequence of inflating and deflating. For the sorption-based OHP, high development, material, and production costs are required for the vacuum insulation and especially the hermetical edge sealant. These additional costs have to be weighed against the cost reduction potential of collector and system due to lower material requirements and the possibility to use standard PV components.

To conclude, three novel OHP concepts were investigated and compared. The OHP by ventilation is a state-of-the-art approach, which is already widely discussed in the scientific literature for solar thermal collectors, and now applied for PVT collectors. The switchable film insulation is a novel OHP which was specifically designed and developed for PVT collectors. It features the highest switching range of thermal losses as the film triggers both convective and radiative heat losses. The passive sorption based overheating protection is intrinsically fail-safe and especially interesting for this reason.

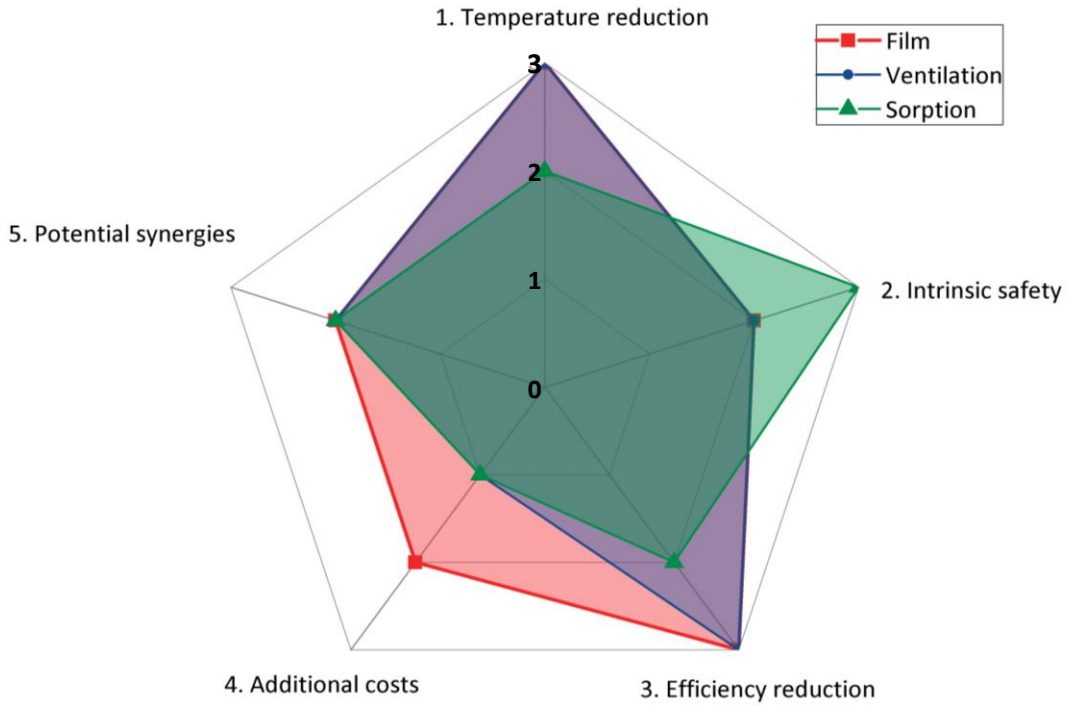

Figure 5.23: Radar chart for the novel OHP concepts evaluated with the five OHP criteria on a scale from 1 to 3.

5.5 Yield assessment for PVT collectors with overheating protection

The operation of a PVT collector with overheating protection differs from a collector with inflexible, fixed efficiency curve. Activating the overheating protection reduces the collector temperatures and thus increases the instantaneous electrical efficiency but also reduces the instantaneous thermal efficiency. Therefore, an adequate control of the overheating protection, either active or passive, is required. In the following section we investigate how an overheating protection affects temperatures and yields by means of annual system simulations. Firstly, control strategies, which avoid excessive collector temperatures and allow for a flexible, demand-driven operation, are presented and analyzed. Then, the useful electrical and thermal yields of the novel PVT demonstrators with overheating protection are assessed applying suitable control strategies.

5.5.1 Development and optimization of control strategies for PVT collectors with overheating protection

5.5.1.1 Concept of flexible, demand-driven operation of PVT collectors with OHP

The main objective of the overheating protection concerns the limitation of the maximum collector temperatures. The OHP can be controlled either passively or actively. Passive control includes, for example, temperature controlled valves or actuators that activate the OHP in case of power outage or fluid standstill. An active OHP control requires an active controller with input parameters and control settings. Although active control strategies typically require electricity, the OHP concept can still be carried out in a fail-safe manner if the OHP is activated passively in case of power outage or control failure.

Reducing the collector temperature by an overheating protection does not necessarily imply a reduction of yields, as observed for conventional solar thermal collectors (Reiter 2014; Föste et al. 2016). On the contrary, if intelligently controlled, the overheating protection can be used to achieve a flexible, demand-driven operation. Controlling the collector temperature is the key to a flexible operation: as is known, the cell and fluid temperatures in PVT collectors are thermally coupled. PV cells prefer low cell temperatures, but the fluid temperatures are dictated by the temperature level in the storage. High fluid temperatures are not required by solar thermal systems, and thermal yields are generated below T_m = 90 °C, as was shown in section 4.6.

The novel approach for a flexible, demand-driven operation for PVT collectors with OHP is illustrated in Figure 5.24. By controlling the OHP, the PVT collector is able to switch between the heat-driven or electricity-driven operation. The terminology is obviously inspired by combined heat and power plants, where also a distinction is made between heat-driven and electricity-driven operation.

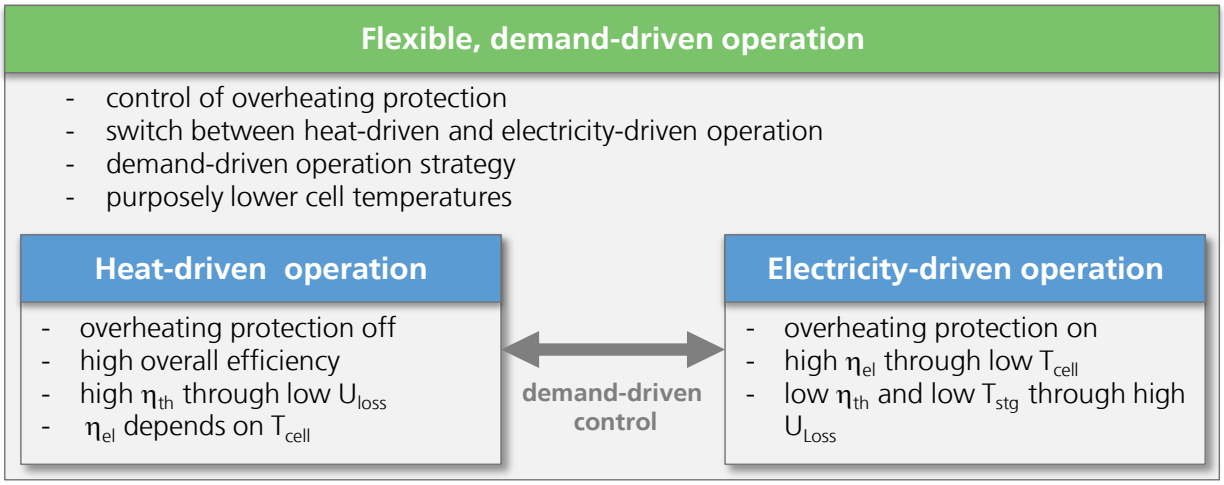

Figure 5.24: Flexible operation of PVT collectors through a demand-driven switch of the overheating protection.

A demand-oriented control strategy of the OHP achieves a flexible generation of heat and electricity. Depending on the current demand for either electricity or heat, the PVT collector can turn the overheating protection on and off. For instance, at periods of a low heat demand during summer or holidays, the PVT collector is switched to electricity-driven mode to lower the cell temperatures and thus increase electrical efficiency. This measure is most effective during stagnation, when the highest reduction of cell temperatures is achieved. However, also during regular operation a purposeful reduction of the thermal efficiency reduces storage temperatures on the long run and thus reduces the fluid temperatures in the collector. Nonetheless, the heat-driven operation mode with deactivated OHP has the highest overall efficiency and is therefore the standard operation mode.

5.5.1.2 Simulation methodology

Annual system simulations based on the simulation framework defined in section 4.2 are used to analyze control strategies and their effect on collector temperatures, yields, and primary energy savings on a system level.

The glazed PVT collector with switchable film insulation is used as a reference collector with its corresponding efficiency parameters in Figure 5.14. This collector is selected because of its high switching

range of the overheating protection, allowing an analysis of the potential of the demand-driven operation. The effect of different OHP concepts on yields and primary energy savings, however, might differ from the results obtained with this collector.

The TRNSYS collector model was modified to allow a flexible switch between two sets of efficiency curve parameters. In the original version of the collector model, the efficiency parameters have to be provided as fixed parameters that cannot be changed during a simulation run. Therefore, we modified the collector model, so that the efficiency parameters are provided as input variables that can be changed during any simulation time step. The functionality of the implementation was verified by comparing the measured test sequence in Figure 5.8 with corresponding simulations.

The combi system (d) with a PVT collector array of A_{ap} = 20.4 m² is used as a reference system (compare Figure 4.22). Combi systems typically achieve considerable heat surpluses in summer when the heat demand is low and solar heat gains are high. Therefore, it is expected that the flexible control strategies achieve the highest benefit in these system types. Similar results can be expected in the domestic hot water system (c), although the mismatch between supply and demand is smaller there. The heat demand in the solar heat pump system (a) and domestic hot water system (b) in multi-family homes is relatively constant. In systems (a) and (b), a demand-oriented control of the OHP will most likely not increase primary energy yields, but the function of the OHP concerns the limitation of collector temperatures for the event of system failures.

5.5.1.3 Definition of an optimization function

For the comparison and optimization of control strategies, an optimization function was defined. The primary objective of the optimization is to avoid excessive absorber temperatures above 120 °C. If the absorber temperature during any simulation time step of the annual simulation exceeds this defined maximum temperature, the simulation is deemed invalid. For this case, a penalty function is added to the optimization function to numerically express the invalidity of the simulation run.

The secondary objective concerns the optimization of useful solar energy gains. The collector yields E_{PV} and Q_{coll} are unsuitable indicators as they do not differentiate between useful and excess yields. Excess electricity feeds into the grid and excess heat dissipates as heat losses from storage and pipes. Thus, both excess electricity and heat are not used to cover the local electricity and heat demand.

For demand-driven control strategies it is however essential that the supply matches the demand, i.e. yields are harvested to locally cover the electricity and heat demand, either directly or via the storage. Therefore, primary energy savings from electricity and heat savings on the system level are used as optimization variable.

The electricity savings E_{sav} are defined analogously to electrical coverage rate f_{cov} in Eq. (4.25) as:

$$E_{sav} = f_{cov} \cdot E_{demand} = E_{selfcon} \tag{5.13}$$

The thermal savings Q_{sav} are defined analogously to the fractional energy savings f_{sav} in Eq. (4.28) as:

$$Q_{sav} = f_{sav} \cdot Q_{conv} = Q_{conv} - Q_{Aux} \tag{5.14}$$

The complete optimization function is given by:

$$cf = f_{p,el}E_{sav} + f_{p,gas}Q_{sav} - IF\left(T_{Absorber,t} > 120\,°C\right) THEN\ 9999, ELSE\ 0, END\ IF \quad (5.15)$$

with the primary energy factors for electricity and gas $f_{p,el}$ = 2.0 and $f_{p,gas}$ = 1.1. The implemented penalty function, here in pseudo code notation, adds the arbitrary high value of 9999 in case of a violation of the temperature limit.

5.5.1.4 Description of the analyzed control strategies

An apt control strategy for the overheating protection avoids excessive temperatures, can be carried out both passively or actively, preferably requires a limited amount of additional sensors, and also considers the demand side in a certain way. From these requirements, the following basic control strategies were elaborated:

- **Absorber temperature control:** The absorber temperature is the most obvious control parameter concerning the avoidance of excessive temperatures in the absorber and PV cells. The OHP is activated when the absorber temperature exceeds a specified threshold temperature $T_{abs,thresh}$. While active OHP approaches require an additional temperature sensor at the absorber, passive OHP approaches activate the OHP autonomously depending on the absorber temperature. The absorber threshold temperature $T_{abs,thresh}$, above which the OHP is activated and below which the OHP is deactivated, is subject to optimization in the following section.
- **Fluid temperature control:** The OHP is activated when the fluid temperature at the collector array outlet exceeds a specified temperature threshold $T_{fl,thresh}$. Most actively pumped solar thermal systems already use a temperature sensor at the collector outlet for the differential control of the collector circuit. Hence, this sensor can be used for an active OHP control strategy. Also passive OHP concepts with temperature-controlled valves use the fluid outlet temperature as control parameter for the activation of the OHP (e.g. Konetsu and Torrens (2004) and Thür and Hintringer (2013)).
- **Storage temperature control:** The OHP is activated when the temperature in the upper segment of the water storage exceeds a specified threshold temperature $T_{stor,thresh}$. As the water in the storage heats up during periods of low heat demand, the storage temperature is a suitable parameter for the charging state, and thus also for the heat demand. The storage temperature sensor is also already present in solar thermal systems for the differential control.
- **Seasonal operation:** As overheating occurs in summer when the heat demand is low, one possible approach is the seasonal operation. The OHP is switched on at the end of the heating period and switched off again at the beginning of the heating period. Therefore, only one switch per year is required, which opens the possibility for manual or energy-intensive OHP concepts. The optimization parameter in this control strategy is the period during which the OHP is active. The seasonal operation strategy has to be viewed critically concerning the real implementation, as the optimization is highly dependent on the weather and climate data, and therefore only valid for the analyzed weather data set.

- **Pump control:** The overheating protection is activated when the pump fails or is turned off, i.e. the flow rate in the collector comes to a halt. For safety reasons, most collector controllers switch off the pump if the storage temperature exceeds 90 °C (Scheuren 2008), which is one reason for stagnation and collector overheating. Although the pump control of the OHP is capable of avoiding excessive collector temperatures, it also negatively affects the collector control. When the pump is off, the OHP is always active and thus fluid outlet temperatures are naturally lower. Consequently, the collector control does not reactivate the collector circuit even when the temperatures might be sufficient for a regular operation with deactivated OHP, as the collector control only registers the lower fluid outlet temperatures in OHP mode. Ultimately, this results in a significant reduction of operation hours.
- **OHP always off** (heat-driven operation) and
- **OHP always on** (electricity-driven operation) are also assessed to analyze the general potential for a flexible operation and represent the benchmark for maximum heat and maximum electricity generation.

These control strategies were implemented in TRNSYS to assess passive and active control strategies. Other control strategies have also been tested but did not yield better results. For instance, the state of charge of the battery storage is a good indicator for the electricity demand, but is not suitable to avoid overheating. More complex control algorithms such as a model-predictive control on basis of weather forecasts (Oldewurtel et al. 2012) or artificial neural networks (Kramer et al. 2017) might realize higher primary energy savings, but also require more research and development efforts.

5.5.1.5 Optimization results

The optimization was carried out by coupling TRNSYS with the generic optimizer GenOpt (Wetter 2011) using the Hooke Jeeves algorithm for maximizing the optimization function in Eq. (5.15). The optimum control parameters $T_{abs,thresh}$, $T_{fl,thresh}$, $T_{stor,thresh}$ were each identified by the optimization procedure. For the seasonal control strategy, the optimum period with active OHP was identified in the same manner. Table 5.6 summarizes the resulting temperatures and energy savings of the optimized control strategies.

All control strategies, except the reference case "OHP always off", achieve the primary objective of limiting the absorber temperatures to T_{abs} = 120 °C. This demonstrates the general capability of the OHP control strategies to reduce stagnation temperatures effectively. However, the optimized control strategies achieve only an insignificant increase of primary energy savings in the range of 0.1 - 0.5 %. This contrasts to the expectations of the demand-driven operation described in chapter 5.5.1.1.

Nonetheless, as indicated by the characteristic temperature T_{char}, the energy yields are shifted towards a lower temperature level. Hence, the PVT collector operates with lower fluid temperatures but still generates the same or higher primary energy savings. A detailed analysis of the effect of the OHP control strategy on collector temperatures and yields will be given in the two following sections.

Table 5.6: Controller parameters, temperatures and energy savings of the optimized control strategies. Simulation results for combi system (d), PVT collector with switchable film insulation, location of Würzburg.

Description	Optimized control parameter	Duration of T_{abs} > 120°C [h]	$T_{abs,max}$ [°C]	E_{sav} [kWh/m² a]	Q_{sav} [kWh/m²a]	Q_{PES} [kWh/m² a]	T_{char} [°C]
OHP always off		17	140	99	171	287	53
Absorber temperature control	$T_{abs,thresh}$ = 77.5 °C	0	84	100	170	287	50
Fluid temperature control	$T_{fl,thresh}$ = 75.5 °C	0	82	100	170	287	49
Storage temperature control	$T_{stor,thresh}$ = 72.2 °C	0	82	101	170	288	44
Seasonal control	period with active OHP: 20.05-07.09	0	118	102	162	280	41
Pump Control		0	98	103	148	266	39
OHP always on		0	64	105	81	194	30

As the load and generation profile of the domestic hot water system (c) differs from the previously investigated combi system (d), also the primary energy gains and the optimum parameter settings differ from the values presented in Table 5.6. To study the effect of optimized OHP control strategies in a domestic hot water system, simulations were conducted analogously for system (c). The optimized control parameter settings lie slightly above the parameters for the combi system and amount to $T_{abs,thresh}$ = 85° C, $T_{fl,thresh}$ = 80 °C, and $T_{stor,thresh}$ = 75 °C. With these specifically optimized control parameters, the PVT collectors achieve a small increase of the primary energy savings of 0.1 % for both the fluid and absorber temperature control strategy and 0.6 % for the storage temperature control strategy. These results are in line with the results obtained for combi system (d).

5.5.1.6 Effect of the OHP control strategy on collector temperatures

Figure 5.25 compares the annual distribution of absorber temperatures for different OHP control strategies in combi system (d). The benchmark cases "OHP always off" and "OHP always on" represent the maximum and minimum temperature load scenarios.

All analyzed control strategies reduce the temperature load of the absorber. The storage temperature control strategy achieves the most effective temperature reduction, followed by the fluid and absorber temperature control. It is interesting to observe that the maximum absorber temperatures in these three temperature-controlled strategies remain below 85 °C and thus below the certification temperature of PV modules. Also the seasonal and the pump control avoid critical temperatures. However, singular temperature peaks between T_{abs} = 100 – 120 °C occur, as no explicit temperature signal is used for these control strategies.

In general, the OHP control strategies shift the absorber temperatures to a lower level and thus also reduce T_{char}. Next to the increased electrical performance, this leads to a reduction of temperature-induced ageing effects. According to the Arrhenius kinetics theory, it is not only important to avoid temperature peaks, but the durability benefits in any case from a reduced temperature load, enabling a more reliable operation of the PVT collector over the entire expected lifetime.

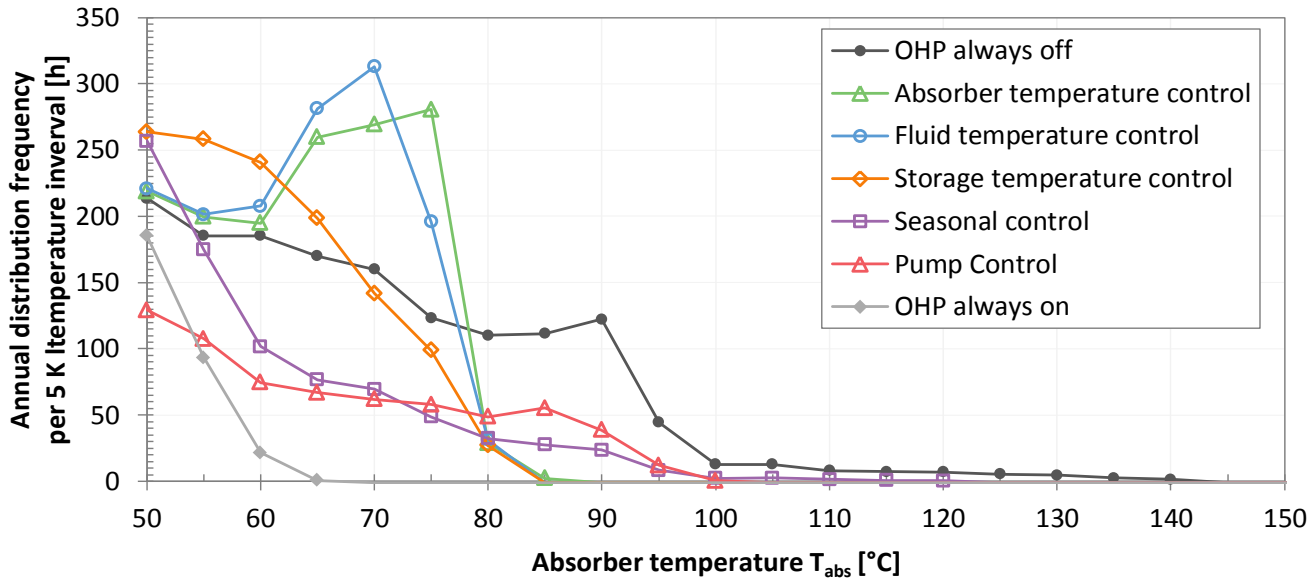

Figure 5.25: Annual distribution frequency of the absorber temperatures for the glazed PVT collector with switchable film insulation with different control strategies in system (d), Würzburg.

5.5.1.7 Effect of the OHP control strategy on primary energy savings

Figure 5.26 shows the electrical and thermal collector yields E_{PV} and Q_{coll}, each divided into useful energy savings E_{sav} and Q_{sav} and unused energy. The unused energy yields do not contribute to the electrical or thermal energy savings of the decentral PV battery and heating system. On the electrical side, the unused collector yield consists of feed-in electricity to the grid as well as inverter and cable losses. On the thermal side, the unused collector yield comprises heat losses of storage and piping.

It has to be noted that the electrical and thermal yields also depend on simulation assumptions and boundary conditions. Particularly the system type, dimensions of the collector array and the storage volume have a strong influence on the simulated yields and primary energy savings. The presented results are therefore only representative for the investigated system (d), with an aperture area of A_{ap} = 20.4 m² of glazed PVT collectors with low-e, and a storage volume of V_{stor} = 0.9 m³.

With smart control strategies of the overheating protection, the thermal yields Q_{coll} decrease due to the temporary reduction of the thermal efficiency. At the same time, the electrical yields E_{PV} increase due to lower characteristic temperatures T_{char}. However, the benefit on the system level with respect to useful energy savings is considerably smaller in relation to the additional collector yields. Although the reduced thermal yield affects the useful heat savings only minimally, the gain of electricity savings due to the increased electrical yield is also only small.

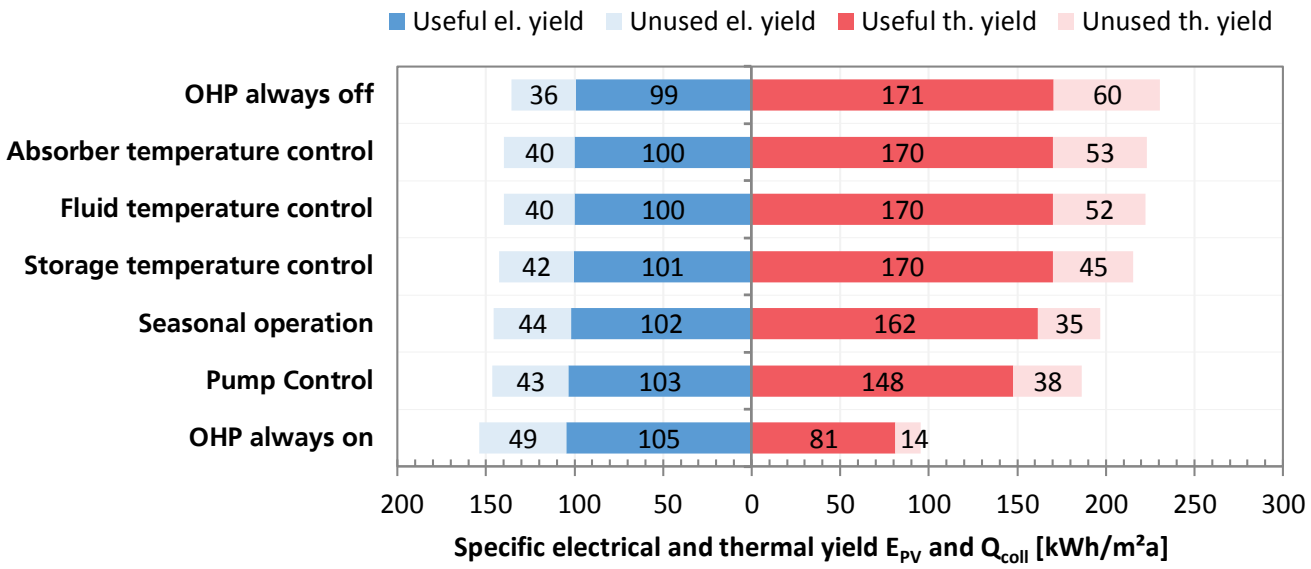

Figure 5.26: Electrical and thermal yields E_{PV} and Q_{coll} of optimized OHP control strategies divided into useful system savings E_{sav} and Q_{sav} and unused yields in system (d), Würzburg.

Comparing the reference case "OHP always off" with the "storage temperature control" operation strategy, the thermal collector yield Q_{coll} decreases by 6.6 %, while the useful heat savings Q_{sav} decrease by only 0.2 %. This is due to the fact that the thermal yields are reduced in periods of low thermal demand, i.e. high storage temperatures, and therefore the thermal energy savings are only minimally affected. The objective of the demand-driven reduction of thermal efficiency, and thus absorber temperatures, is therefore fulfilled.

Comparing the electrical yields of the two aforementioned simulation cases, the increase of the electrical collector yield E_{PV} by 5.2 % only leads to a 1.3 % increase of useful electricity savings E_{sav}. Thus, only a small fraction of the additional electrical yield also contributes to the overall performance of the electrical home battery system. The larger fraction of the additional electrical yield feeds into the grid and is not used locally.

The comparison of the cases "OHP always off" and "OHP always on" demonstrates the overall potential for a flexible operation of PVT collectors with OHP control. The yields of any operational strategy lie between these two benchmark cases. Accordingly, it is indeed possible to trade thermal yields for electrical yields by activating the OHP. Yet, the overall effect on the useful electricity savings E_{sav} is relatively small. Therefore, the OHP is only capable to a limited extent to match the supply of PVT generated heat and electricity to the current heat and electricity demand.

Figure 5.27 shows the sensitivity of control parameters on primary energy savings. The threshold control parameters for the different control strategies are varied and shown on the x-axis. The OHP is activated when the absorber, fluid, or storage temperature exceed the specified threshold value. The grey-dotted lines refer to the benchmark cases "OHP always on" and "OHP always of". For none of the control strategies, a distinct optimum can be found, but rather a flat optimum plateau. From this follows that there is no strong dependency of the primary energy savings on the control parameters.

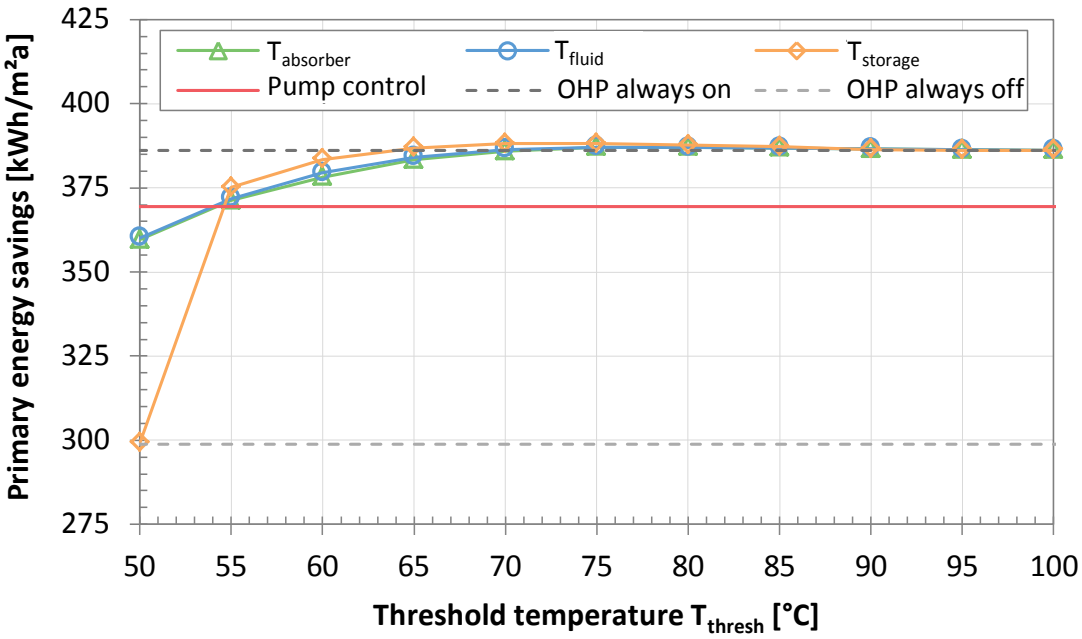

Figure 5.27: Sensitivity analysis of threshold control parameter settings of the OHP on primary energy savings in system (d), Würzburg.

If the threshold temperature is set too low, the OHP is frequently active and thermal yields decrease. If the threshold temperature is set too high, high collector temperatures are more frequent, resulting in lower electrical yields. Moreover, the risk of overheating increases.

5.5.1.8 Discussion of results

Different control strategies were analyzed regarding to their capability to resolve the basic conflict of PVT collectors "low vs. high temperatures requirements" or "electricity vs. heat priority". All three temperature-controlled OHP strategies effectively reduce collector temperatures without significantly reducing the heat savings. These control strategies with the optimized parameter settings are therefore recommended for future application. The "pump control" strategy, although avoiding high temperatures, requires a modification of the collector control to avoid a reduction of operating hours. The seasonal control strategy neither reliably avoids critical temperatures, nor achieves high primary energy yields.

The potential for a flexible, demand-driven operation is relatively small and the increase of primary energy savings is lower than originally expected. First simulations results, which are published by Lämmle and Hermann (2015), suggested an increase of the electrical yield E_{PV} by 8 %. However, these simulations only regard overall electrical yields and disregard E_{sav} in a decentral battery home PVT system. Moreover, the simulations were conducted with an older, unvalidated version of the PVT collector model. For these reasons, primary energy savings are lower than originally expected and the hypothesis of increasing primary energy savings through a demand-driven control of the OHP as postulated in section 5.4.1.1 could only be partially confirmed.

Alternatively, control-based possibilities to reduce the fluid and absorber temperatures are also applicable for PVT collectors without OHP. The night cooling strategy circulates hot water from the storage through the collector during night when the storage temperature is too high. Thus, the storage gets rid of excess

heat and increases its heat capacity for the following day. This effect can be enhanced when combined with mixing the stratified water in the storage (Lustig 2002; Scheuren 2008; Frank et al. 2014).

System simulations with an implemented night cooling strategy combined with mixing of the storage for reference system (d) show similar results in the range of the storage-temperature-controlled OHP strategy. Both simulation cases avoid absorber temperatures above 120 °C and achieve identical heat savings of Q_{sav} = 170 kWh/m²a. The OHP strategy achieves slightly higher electricity savings of E_{sav} = 101 kWh/m²a compared to E_{sav} = 100 kWh/m²a of the night cooling strategy. Therefore, the night cooling combined with storage mixing is an alternative strategy which is also capable of reducing collector temperatures. However, night cooling alone is insufficient to guarantee a fail-safe operation during power outage and system failures.

5.5.2 Yield assessment of novel PVT collectors with overheating protection

The objective of the final section concerns the assessment of PVT systems with the novel PVT collectors with overheating protection. For this purpose, we analyze the annual yields in the reference systems and compare the collector yields with the glazed PVT collector "PVT01-low-e" without overheating protection.

The performance coefficients for the PVT collectors are taken from experimental data, except for the sorption-based OHP, where numerical simulation results are used. The performance parameters for both regular operation mode and overheating protection mode are given in Table 5.7.

Table 5.7: Performance coefficients and OHP control strategy for the assessment of yields of overheating-protected PVT collectors.

		PVT glazed low-e	PVT OHP vented	PVT OHP film	PVT OHP sorption
Regular operation					
$\eta_{th,0}$		0.67	0.67	0.63	0.66
c_1	W/m²K	3.98	4.973	3.92	3.61
c_2	W/m²K²	0.025	0.019	0.021	0.048
$\eta_{el,STC}$		0.139	0.137	0.139	0.139
Overheating protection					
OHP control strategy		No OHP	Absorber temperature $T_{abs,thresh}$ = 77.5 °C	Storage temperature $T_{stor,thresh}$ = 72.3 °C	Absorber temperature $T_{abs,thresh}$ = 60 °C
$\eta_{th,0}$		-	0.63	0.56	0.67
c_1	W/m²K	-	12.09	13.5	2.3
c_2	W/m²K²	-	0	0.056	0.108

System simulations were carried out for the four reference systems with system dimensions according to Table 4.7. For each PVT collector, a suitable OHP control strategy is implemented. The vented PVT collector uses a passive absorber temperature control which opens the collector flaps at $T_{abs,thresh}$ = 77.5 °C. The switchable film is controlled actively and deflates the cushion when the storage temperature exceeds $T_{stor,thresh}$ = 72.3 °C. The passive, sorption-based OHP control changes the efficiency curve parameters ac-

cording to the absorber temperature based on the parametrization of the efficiency curve for the two segments above and below T_{abs} = 60 °C.

Figure 5.28 shows the resulting electrical and thermal collector yields separated into useful and unused system yields. Comparing the four system types, the application of an overheating protection is most effective for high operating temperatures, where the OHP reduces the characteristic temperature by up to ΔT_{char} = 10 K. The main objective of limiting absorber temperatures is achieved by all assessed collectors with overheating-protected collectors.

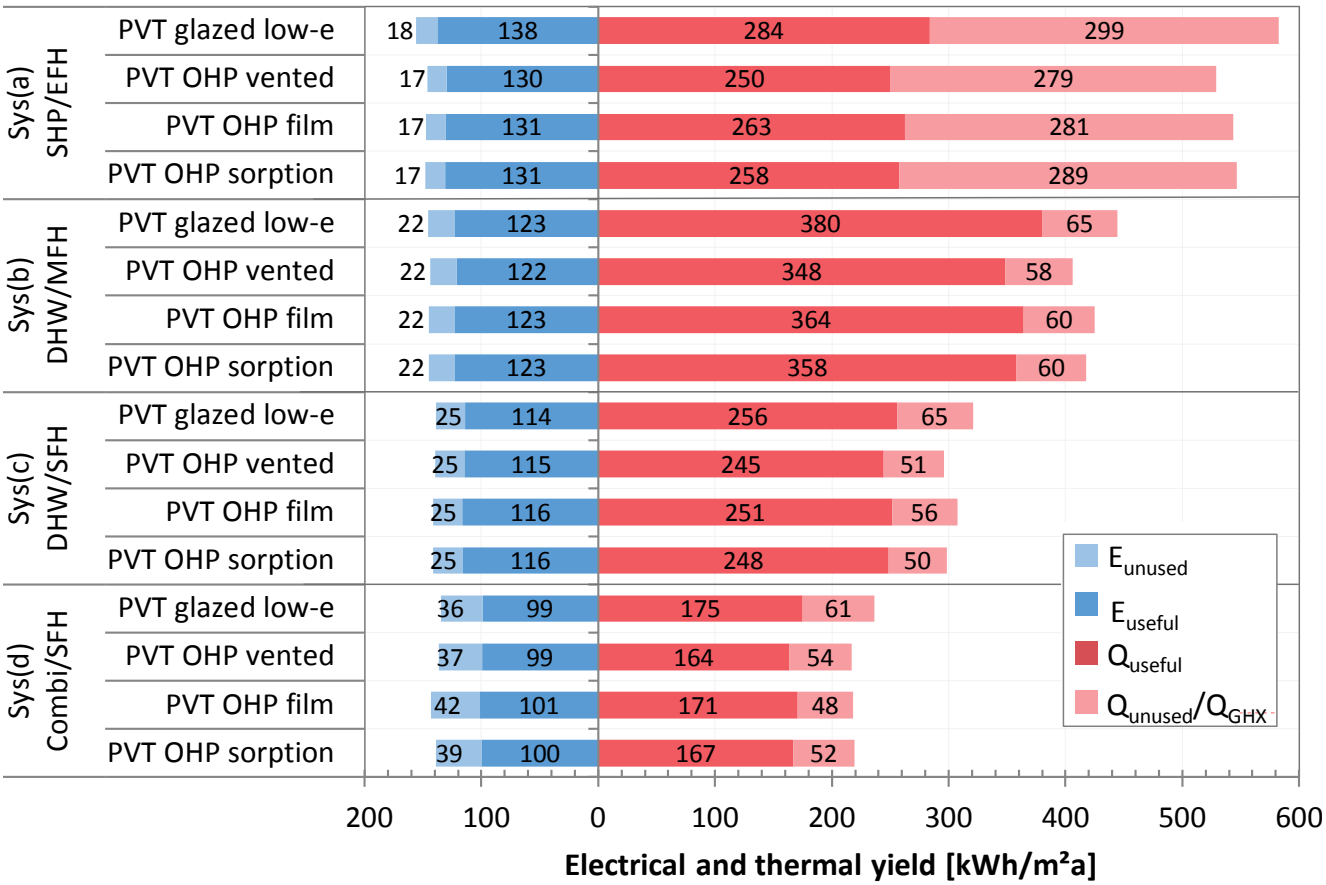

Figure 5.28: Assessment of electrical and thermal yields for systems (a) – (d) with PVT collectors with OHP.

The effect of the OHP on the electrical yields are marginal and hardly any differences between the four PVT collectors can be found. A slightly lower electrical yield is registered in system (a), which is most likely due to the complex system control with two heat sinks. Almost no effect of the OHP can be found in system (b), while a positive effect is found in system (c) and (d) where the useful electrical yield increases between 0.3 % up to 2.5 %.

All PVT collectors with OHP have a small reduction of the useful thermal yields. In total, the reduction of useful thermal yield amounts to 2 % - 8 % in systems (b), (c) and (d). As shown in the previous section, the control of the OHP is only partly responsible for this effect. The major share of the useful thermal yield reduction is attributable to the slightly reduced thermal efficiency of the PVT collectors with OHP.

Hereby it is important to differentiate between two reasons for the reduction of thermal yields: either due to a technologically immanent lower thermal efficiency in normal operation, or due to the reduced

thermal efficiency of the specific prototype with non-ideal design. For the vented OHP, the reduction of the thermal yields compared to the PVT collector without OHP is attributable to the specific, non-ideal design with a front glazing without AR coating and the slightly higher emissivity of the applied low-e coating. The integrated ventilation channels have no observable effect on the thermal efficiency.

For the film and sorption OHP, on the contrary, the reduction of thermal yields is directly attributable to the application of the OHP. The PVT collector with switchable film has a slightly reduced optical efficiency due to the technologically immanent lower transmittance of the ETFE film compared to AR glass. In a similar way, the sorption-based OHP has a reduced thermal efficiency above absorber temperatures of T_{abs} = 50 °C due higher heat loss rates at medium absorber temperatures. These considerations are responsible for the differences between the evaluation of the three OHP concepts in Figure 5.23 and the assessment of yields in Figure 6.28.

In summary, the overheating protection causes only a minor increase of the useful electrical yields of 0.3 % - 2.5 % and a minor decrease of the useful thermal yields of 2 % - 8 %. Consequently, the simulation results from chapter 4 can be transferred in good approximation also to the PVT collectors with low-e and overheating protection and the major findings from chapter 4 are also valid for PVT collectors with overheating protection.

6 CONCLUSION AND OUTLOOK

6.1 Conclusion on highly efficient PVT collectors with low-e coatings

Highly efficient PVT collectors with low-e coatings were analyzed in chapter 3 by means of experimental and numerical methods. The major findings concerning the initially stated research questions are summarized as follows:

- *What is the effect of low-e coatings on the thermal and electrical efficiency?*

  Two PVT collectors of identical design, one with and one without low-e coating, were tested and their efficiency was compared. At $\Delta T/G = 0.05$ Km²/W, the silver-based low-e coating improves the thermal efficiency by 57 $\%_{rel}$, while the electrical efficiency drops by 4 $\%_{rel}$. The numerical PVT collector model allows an in-depth analysis of the effect of low-e coatings on thermal and electrical performance. Accordingly, low-e coatings suppress radiative heat losses and thus reduce U_{Loss} by 38 %. However, a small drop of the optical efficiency has to be accepted due to a small reduction of the glass transmittance of 4.4 %.

- *Which low-e coatings are suitable for application in PVT collectors?*

  Suitable low-e coatings for the application in PVT collectors require a proper balance between a high transmittance and a low emissivity. A specifically developed rating figure can be used to evaluate optical parameters. Few suitable highly transparent low-e coatings are available commercially, which might limit a wider deployment of low-e coatings in PVT collectors. The application of low-e directly on the PVT absorber is favorable under energetic considerations, but the application is also possible on the internal side of the front cover.

- *How can low-e coatings realize an optimum overall efficiency?*

  The objective of applying low-e coatings in PVT collectors is to optimize the overall efficiency for highest overall energy yields. To achieve this, a high thermal efficiency of the PVT collector is required for operating in challenging weather conditions with low levels of irradiance and low ambient temperatures. Due to their reduced heat losses, low-e coatings enable a good overall performance in Central European climate at medium temperatures.

  Evaluating the gross energy yields on an annual basis, the thermal yield in Würzburg increases by 68 %, while the electrical yield drops by 4 % at a mean fluid temperature of $T_m = 50$ °C, compared to a PVT prototype without low-e coating. At medium temperature levels, PVT collectors with low-e achieve highest primary energy yields of available PVT collector technologies.

The presented collector development focused primarily on the improvement of the thermal characteristics, while the electrical efficiency was not subject of the research. To demonstrate the full potential of PVT collectors, future work should therefore also address optimization of the electrical efficiency.

Firstly, an optimized coating layout and modified production processes can reduce reflectance and absorptance losses in the coating and thus increase the optical efficiency. Secondly, the employed PV cells of the PVT prototype, which were produced in 2012, are slightly outdated and the cell efficiency has increased significantly since then. Using current PV technologies with a higher rated power and a lower temperature coefficient might increase the electrical performance significantly. Suitable candidates are heterojunction PV cells, e.g. TopCon from Fraunhofer ISE or HIT from Panasonic. Thirdly, a simple but effective measure concerns the reduction of the electrical efficiency due to inactive area without PV cells. New PVT designs should include this aspect to achieve a high electrical output per collector area.

Noble gas fillings can further improve the thermal efficiency. This effective measure reduces convective heat losses without affecting the optical and electrical efficiency and is therefore ideal for the combination with low-e coatings.

Overheating is an issue aggravated by low-e coatings. Stagnation temperatures of the presented prototype exceed T_{stg} = 150 °C. Standard materials of PV modules are not designed for these temperatures, which is why PVT collectors with temperature-resistant materials need to be developed or overheating protection has to be applied.

6.2 Conclusion on the assessment of PVT Systems

Collector yields and system performance were assessed in chapter 4 with the novel characteristic temperature approach. The systematic assessment of different collector technologies, system configurations, and locations gives a good overview of the capability of available PVT technologies and their suitability in PVT systems with varying operating temperatures. The key findings are summarized as follows:

- *Which factors influence the electrical and thermal yields?*

  The PVT collector technology, whether unglazed, glazed, or glazed with low-e, determines pivotally if the focus lies on electricity or heat generation. Originating from the trade-off between a high optical efficiency versus low thermal losses, PVT collectors either achieve high electrical or high thermal yields.

  Electrical and thermal yields per collector technology show a strong correlation with the mean operating temperature which is quantified by the newly defined characteristic temperature T_{char}. This indicator reduces the multiple factors that influence the energy yields to a single value. In general, high operating temperatures are unfavorable for PVT systems, as they reduce both electrical and thermal yields.

- *Which PVT technology is suitable for which application, especially concerning PVT collectors with low-e?*

  Given the central importance of T_{char}, suitable PVT collector technologies should be selected according to the mean operating temperature level of the system. Lowering $T_{char,}$ particularly through an adequate sizing of PVT collector array and components, achieves a significant optimization of the system performance.

  PVT collectors with low-e coatings are suitable for a wide temperature range. In all analyzed systems, they achieve the highest primary energy yields. On the other hand, PVT collectors with a low thermal efficiency suffer from a low utilization factor and low thermal yields. Consequently, larger collector ar-

rays cannot compensate a lower thermal efficiency, in contrast to PV modules. An improved thermal efficiency is therefore essential for medium temperature levels.

- *What are the energetic benefits and the economic expenses of PVT systems?*

  A comparison with a side-by-side installation of conventional flat plate collectors and PV modules shows the central energetic benefit of PVT collectors. By co-generating electricity and heat in the same component, PVT collectors enable an increase of the electricity generation of up to 250 % with an equal collector area and equal overall heat output.

  However, the higher energy output is connected with 21 % higher levelized costs of energy, which is primarily caused by the high costs of the PVT collectors. Yet, the potential to reduce costs through large-scale collector manufacturing or through lower system costs by lower temperature requirements has not yet been included in the economic assessment.

Field installations of systems with glazed PVT collectors with low-e coatings are the next stage in the development process. The simulation results for this PVT technology were particularly promising, but experimental confirmation from in-situ measurements is pending. In the best case, PVT collectors are monitored in parallel to a side-by-side installation, allowing robust experimental results and a transparent comparison of yields. Thus, the energetic benefit of the PVT technology can be confirmed experimentally. Moreover, the evaluation of monitoring data from a PVT system can underpin the currently simulation-based characteristic temperature approach by an experimental validation.

Future research on the system integration of PVT collectors should concern the design of integral PVT systems that are specifically developed to fully exploit the benefits of PVT collectors. These systems have low to medium temperature levels facilitating high electrical and thermal yields. Moreover, the new systems should have an integral energy concept, where the coupling of heat and electricity does not only concern the generation of energy in the PVT collectors, but is also implemented on the demand side, for example by heat pumps. Under these circumstances, PVT collectors are a competitive technological option, whenever high primary energy yields on limited areas are desired.

6.3 Conclusion on PVT collectors with overheating protection

The application of overheating protection for PVT collectors with low-e coatings was demonstrated in chapter 5. Two innovative PVT prototypes were built and tested: venting as a state-of-the-art OHP approach, and an innovative switchable film insulation, where a polymer film regulates convective and radiative heat losses. These prototypes prove that a targeted switch of the thermal losses avoids excessive temperatures, while maintaining a high efficiency during regular operation. The key findings are summarized as follows:

- *What are the thermal requirements of the materials employed in PVT collectors?*

  Based on material tests, no explicit temperature limit can be identified for the materials. However, high temperatures are seen particularly critical for the polymer encapsulant EVA where yellowing, browning or delamination might occur. In addition, thermo-mechanic stress resulting from the thermal expansion of different materials, can lead to breakage of cell connectors or damage to the PVT absorber.

As a general rule, elevated temperatures accelerate ageing and degradation. Therefore, low material temperatures are favorable in any case. A maximum temperature of 120 °C can nonetheless serve as an indicative guideline which the absorber should not exceed permanently.

- *How does the overheating protection influence temperatures and yields?*

The effect of the overheating protection on performance and stagnation temperatures was studied at the two PVT prototypes. Venting reduces stagnation temperatures from T_{stg} = 149 °C to T_{stg} = 102 °C and the switchable film insulation limits absorber temperature to $T_{abs,max}$ = 95 °C. Thus, the overheating protection effectively avoids critical temperatures and reduces ageing and degradation effects.

The targeted reduction of the collector temperatures by the OHP also affects the electrical efficiency through lower cell temperatures and thus higher electrical yields. Annual system simulations for the PVT collector with switchable film insulation show that the application of the OHP increases electrical collector yields by E_{PV} = 3 - 7 %, depending on the control strategy of the OHP. However, the thermal collector yields decrease by Q_{Coll} = 3 - 14 %, on account of temporarily increased thermal losses.

Hence, the overheating protection enables a small range of flexibility for the operation with a priority on either electricity or heat generation. In this regard, a differentiation between useful and unused energy yields has to be made, as the OHP mainly reduces unusable heat yields during periods with a low heat demand. Nonetheless, the potential for a flexible, demand-oriented operation of the PVT collector by an overheating protection is smaller than originally expected.

- *Which overheating protection concepts are suitable for the application in PVT collectors?*

After an extensive screening, classification, and evaluation of available OHP concepts, the conclusion is reached that there is no perfect overheating protection approach, but each concept has its strengths and weaknesses. A closer look at the specific characteristics of each individual OHP approach is therefore essential. However, all concepts have in common that additional costs for the OHP arise, which need to be weighted against the potentially lower costs in collector and system, due to less demanding material requirements and the possibility to use standard PV components.

The investigated OHP concepts are very promising and achieve good overall results. Venting is a state-of-the-art OHP for flat plate collectors and was now successfully applied to PVT collectors for the first time. The novel switchable film insulation rendered an unprecedented switching range for U_{Loss} with uncritical temperatures in the deflated mode similar to an unglazed PVT collector. The innovative sorption-based OHP concept functions without movable parts and is entirely passive and fail-safe. However, heat losses increase continuously without a discrete switching point affecting the thermal performance already at uncritical absorber temperatures.

Further research is still required prior to a commercialization of the novel PVT collectors with OHP. Solutions for a fail-safe activation of the overheating protection need to be developed. Moreover, reliability issues have to be analyzed and solved, for instance concerning the weathering stability of the polymer film at elevated temperatures.

The alternative approach of intrinsically temperature-resistant PVT collectors does not require an OHP mechanism. Consequently, there are no costs for the OHP and no movable parts prone to failure, which may lead to a higher user acceptance. Such PVT collectors only employ materials that are suitable for temperatures up to 160 °C, for example encapsulants and glues made of silicone, which also might involve elevated component costs. Additionally, an absorber design with reduced thermo-mechanic stress

has to be developed. Absorber elements made of steel (e.g. Koch et al. (2015)) are particularly interesting, given the similar temperature expansion coefficient of steel and glass. These collectors can also achieve an increase of electrical yields by the application of suitable system control approaches, e.g. night cooling and storage mixing.

6.4 General conclusions

The framework of thermal management was applied on three levels with varying degrees of success. On the collector level, the low-e coatings are a door opener to reduce heat losses and thus enable an optimized overall performance. Also, the approach on system level to consider the mean operating temperatures as central parameter to evaluate and optimize yields is expedient. During operation, overheating protection is able to avoid excessive temperatures. However, the objective of a flexible operation with optimized primary energy yields by lowering the collector temperature was only achieved to a limited extent. Overall, it can be stated that the collector temperatures are indeed the key to a better overall collector performance, but it is difficult to uncouple the electrical and thermal operation.

These three large thematic complexes were discussed extensively by simulation and experiment, allowing a multifaceted consideration of the PVT technology on multiple levels. The system-oriented development approach is especially important for PVT collectors due to the diverging temperature requirements of PV and solar thermal. Unfortunately, the wide scope did not always allow an analysis of specific aspects in the desired depth. Consequently, some topics were only touched upon and must be considered in future research work.

Nonetheless, this thesis has demonstrated that PVT collectors are an interesting and promising technological option: they are almost free from carbon emissions during operation and offer a high energy efficiency and maximum overall solar yields on a given area. On the basis of glazed PVT collectors with low-e coatings, the potential of PVT technology was illustrated and hopefully a valuable contribution was made to its technological development.

The success of PVT collectors – and glazed PVT collectors with low-e coatings in particular – will ultimately depend on various factors. Next to energy efficiency, the durability and reliability are important aspects for the collector development. Furthermore, the economic attractiveness concerning manufacturing and indirect costs has to be improved to be competitive with alternative technologies. Complete PVT solutions with pre-configured packages of PVT collectors and heating systems facilitate the decision-making for end customers. Finally, the soft aspects of architectonic integration of the PVT collectors into the building envelope in an aesthetic way should not be underestimated, as PVT collectors offer a two-in-one solution with a homogeneous appearance.

In the future, PVT collectors will have to prove themselves in comparison with competing technologies such as conventional PV and solar thermal, heat pumps, PV in combination with heating rods, and emerging heating technologies. In this context, the advantage of PVT collectors lies in its high overall efficiency and thus high primary energy yields. PVT collectors can exploit this technological advantage especially in urban areas where the conflict of utilizing suitable areas is expected to increase.

Finally, the success of PVT collectors will also depend on the further development of the solar thermal industry. Particularly glazed PVT collectors can be regarded as an extension to the conventional collector technology aiming at classical solar thermal applications. However, the current political focus of the

global transformation of the energy system from fossil fuels to renewable energy lies primarily on power generation. Nonetheless, the heat sector with its high share of greenhouse gas emissions is just as important and a decarbonization of this sector by a balanced technology mix is essential to achieve the goals of the Paris Agreement.

Appendix A SPECIFICATIONS OF PVT PROTOTYPES

PVT01 - low-e

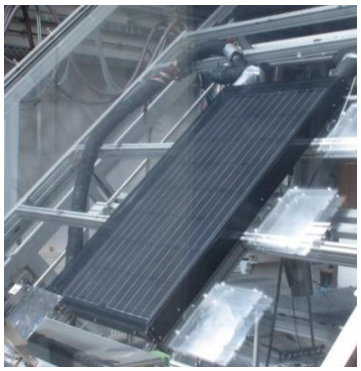

PVT02 - no low-e

PVT03 - vented

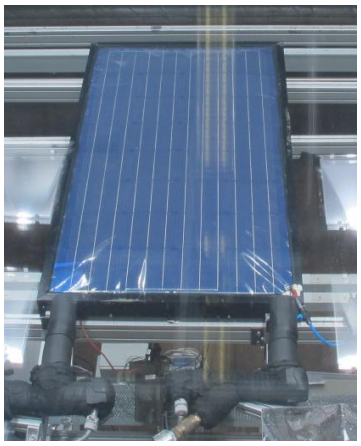

PVT04 - film

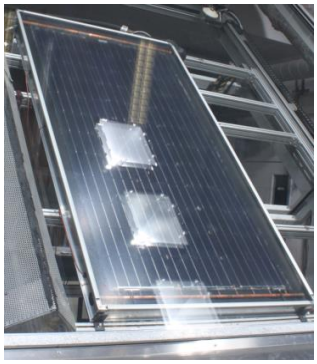

PVT05 - glued1

PVT06 - glued2

Figure A.1: Photos of PVT collectors PVT01 – PVT06 during testing.

Table A.1: Characteristics of PVT collector prototypes (part 1).

	PVT01 low-e	**PVT02 no low-e**	**PVT03 vented**		**PVT04 film**		**PVT05 glued1**	**PVT06 glued2**
Collector design								
Front cover	2 AR, τ = 0.97	2 AR, τ = 0.97	low iron glass, τ = 0.92		ETFE 100 µm, τ = 0.92		2 AR, τ = 0.97	2 AR, τ = 0.97
low-e coating	ISE low-e, ε = 0.14	none, ε = 0.91	Euroglas, ε = 0.30		ISE low-e ε = 0.14		none, ε = 0.91	none, ε = 0.91
PVT absorber	Direct lamination, sheet-tube absorber	Direct lamination, sheet-tube absorber	Direct lamination, sheet-tube absorber		Direct lamination, sheet-tube absorber		Glued, sheet-tube-absorber	Glued, sheet-tube-absorber
PV cell / module technology	Bosch 3BB 32 cells, m-Si cells	Bosch 3BB 32 cells, m-Si cells	Bosch 3BB 32 cells, m-Si cells		Bosch 3BB 32 cells, m-Si cells		Almaden SEAM72-300, p-Si cells	Almaden SEAM72-300, p-Si cells
Tube spacing	77 mm	77 mm	77 mm		77 mm		100 mm	100 mm
Overheating protection	none	none	yes		yes		none	none
Solar thermal tests								
Test in MPP/OC	✓ / ✓	✓ / ✗	✓ / ✓		✓ / ✗		✓ / ✗	✓ / ✓
Steady-State (SS) / Quasi-dynamic Method (QDM)	SS	SS	QDM		SS		SS	QDM
Indoor/ Outdoor	Indoor	Indoor	Outdoor		Indoor		Indoor	Outdoor
			Normal	**OHP**	**Normal**	**OHP**		
$\eta_{th,0}$	0.669	0.63	0.67	0.63	0.63	0.56	0.47 [9]	0.62 [6]
c_1	3.979	6.37	4.973	12.09	3.92	13.5	3.61	5.54
c_2	0.025	0.023	0.019	0.00	0.021	0.056	0.0226	0.012
b_0			0.167					0.15
$K_{\theta,d}$			0.944					0.98
$\eta_{el,0}$ [7]	0.112	0.115			0.115			
b_1	0.52	0.54			0.54			
date of tests	11.09. 2011	27.11.2014	01.09.2016		30.10.2015		24.08.2015	01.09.2016

[6] Relative to absorber area $A_{absorber}$

[7] Relative to the aperture area $A_{aperture}$

Table A.2: Characteristics of PVT collector prototypes (part 2).

	PVT01 low-e	**PVT02 no low-e**	**PVT03 vented**		**PVT04 film**		**PVT05 glued1**	**PVT06 glued2**
PV module test								
$\eta_{el,STC}$ [8]			13.7%		13.9%		14.6%	14.3%
P_{MPP}			111.2 W		112.7 W		286.6 W	280.1 W
FF			75.4 %		75.6 %		76.0 %	75.9 %
U_{OC}			19.47 V		19.78 V		45.23 V	45.33 V
I_{SC}			7.58 A		7.54 A		8.29 A	8.15 A
date of tests			08.11.2016		02.12.2015		19.08.2016	08.11.2016
Geometric parameters								
Gross area A_g	1.04 m²	1.04 m²	1.08 m²		1.04 m²		2.56 m²	2.56 m²
Aperture area A_{ap}	0.92 m²	0.92 m²	0.97 m²		0.92 m²		2.34 m²	2.34 m²
Absorber area A_{abs}	0.92 m²	0.92 m²	0.97 m²		0.92 m²		1.96 m²	1.96 m²
PV Module area A_{PV}	0.81 m²	0.81 m²	0.81 m²		0.81 m²		1.96 m²	1.96 m²
Derived parameters			***Normal***	***OHP***	***Normal***	***OHP***		
$(\tau\alpha)_{eff}$ [-]	0.832	0.87	0.83	0.83	0.82	0.82	0.88	0.88
F' [-]	0.93	0.88	0.94	0.87	0.92	0.87	0.64	0.83
$U_{Loss,\Delta T=0\ K}$ [W/m²K]	5.0	7.9	5.8	13.9	4.8	17.1	6.5	7.0
$U_{AbsFluid}$ [W/m²K]	61.2	62.1	61.2	61.2	61.2	61.2	9.9	34.6
T_{stg} [°C]	152.3	127.3	148.0	102.1	148.9	86.1	135.0	143.1
$U_{Loss,stg}$ [W/m²K]	7.0	9.8	8.5	15.9	6.8	22.7	10.4	9.4

[8] Relative to PV module area A_{PV}

Appendix B COLLECTOR SIMULATIONS

B.1 Numerical calculation of the Nusselt number Nu

The approach for the calculation of the Nusselt number and thus the heat transfer coefficient between pipe and fluid is based on the empirical correlations for fluid flow in the VDI Heat Atlas (2010). Hydrodynamically developed flow and a constant heat flux from wall to fluid can be assumed according to Matuska and Zmrhal (2009). For these assumptions, the Nusselt number can be calculated with the following correlations.

The Nusselt number for laminar flow regimes, i.e. Re < 2300, is given by:

$$Nu_{lam} = \sqrt[3]{4.364^3 + 0.6^3 + \left[1.953\left(RePr\frac{d_i}{l}\right)^{\frac{1}{3}} - 0.6\right]^3} \tag{B.1}$$

The Nusselt number for turbulent flow regimes, i.e. Re > 10000, is given by:

$$Nu_{turb} = \frac{\frac{\xi}{8}RePr}{1 + 12.7\sqrt{\frac{\xi}{8}}(\mathrm{Pr}^{2/3} - 1)}\left[1 + \left(\frac{d_i}{l}\right)^{2/3}\right] \tag{B.2}$$

with:

$$\xi = (1.8\log_{10}Re - 1.5)^{-2} \tag{B.3}$$

In the laminar-turbulent transition flow regime between Re = 2300 and 10000, the Nusselt number is given by:

$$Nu_{\gamma} = (1-\gamma)Nu_{lam}(Re = 2300) + \gamma Nu_{turb}(Re = 10000) \tag{B.4}$$

with the intermittence factor γ:

$$\gamma = \frac{Re - 2300}{1000 - 2300} \tag{B.5}$$

The mean logarithmic temperature difference ΔT_{LM} is defined as:

$$\Delta T_{LM} = \frac{T_{fluid,out} - T_{fluid,in}}{ln(\frac{T_{pipe,mean} - T_{fluid,in}}{T_{pipe,mean} - T_{fluid,out}})} \tag{B.6}$$

with the collector fluid inlet and outlet temperatures $T_{fluid,in}$ and $T_{fluid,out}$, and the mean pipe wall temperature $T_{pipe,mean}$.

B.2 Implementation of the numerical PVT collector model in Modelica

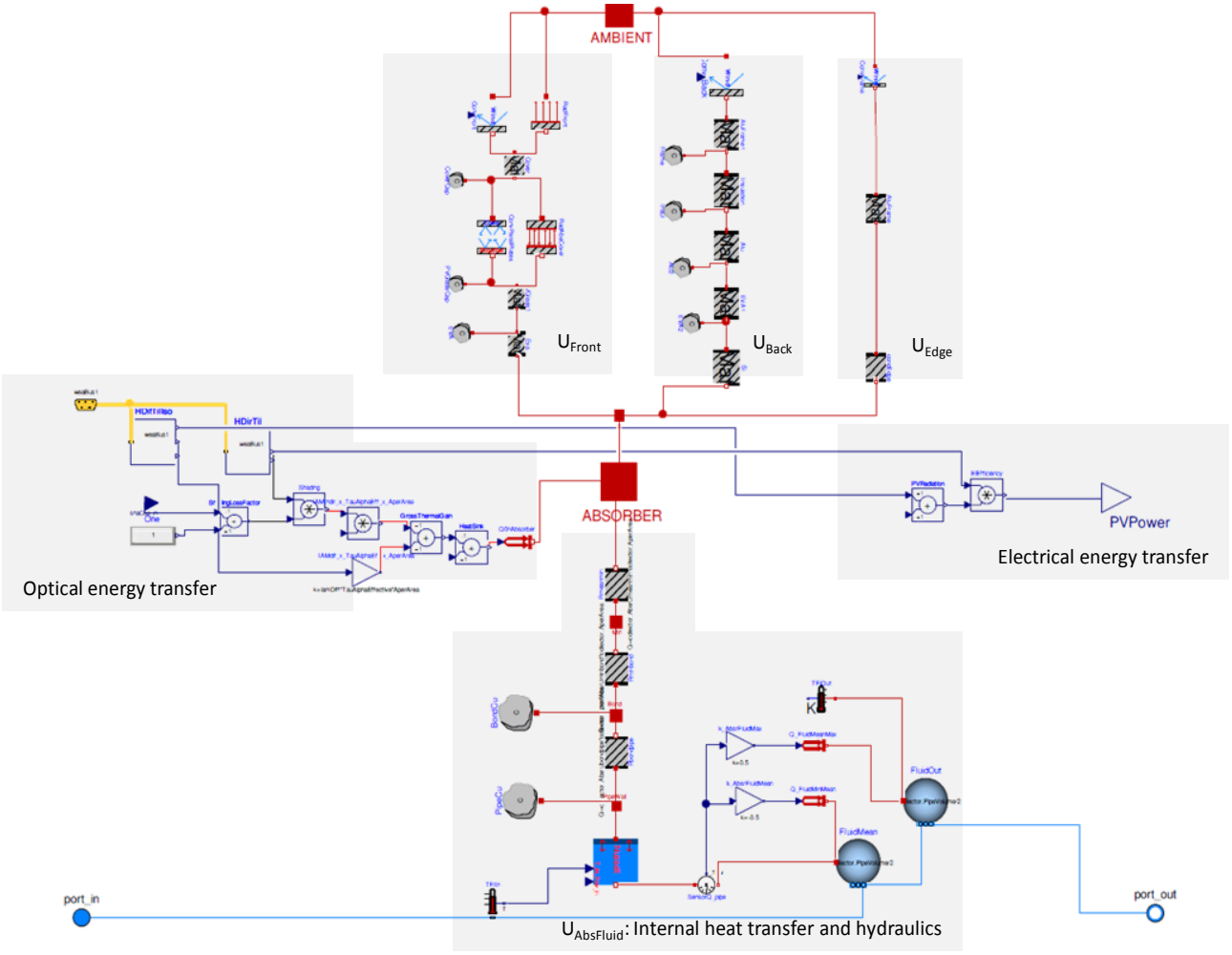

Figure B.1: Visualization of the nodal network of the numerical model implemented in Dymola/Modelica including lumped thermal capacitances and hydraulics.

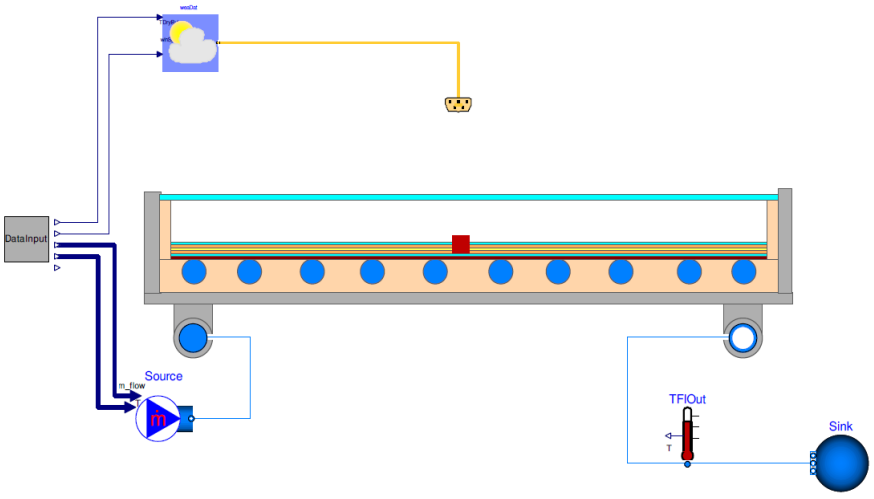

Figure B.2: Modelling environment for emulating a test environment for collectors (courtesy Böhm 2015).

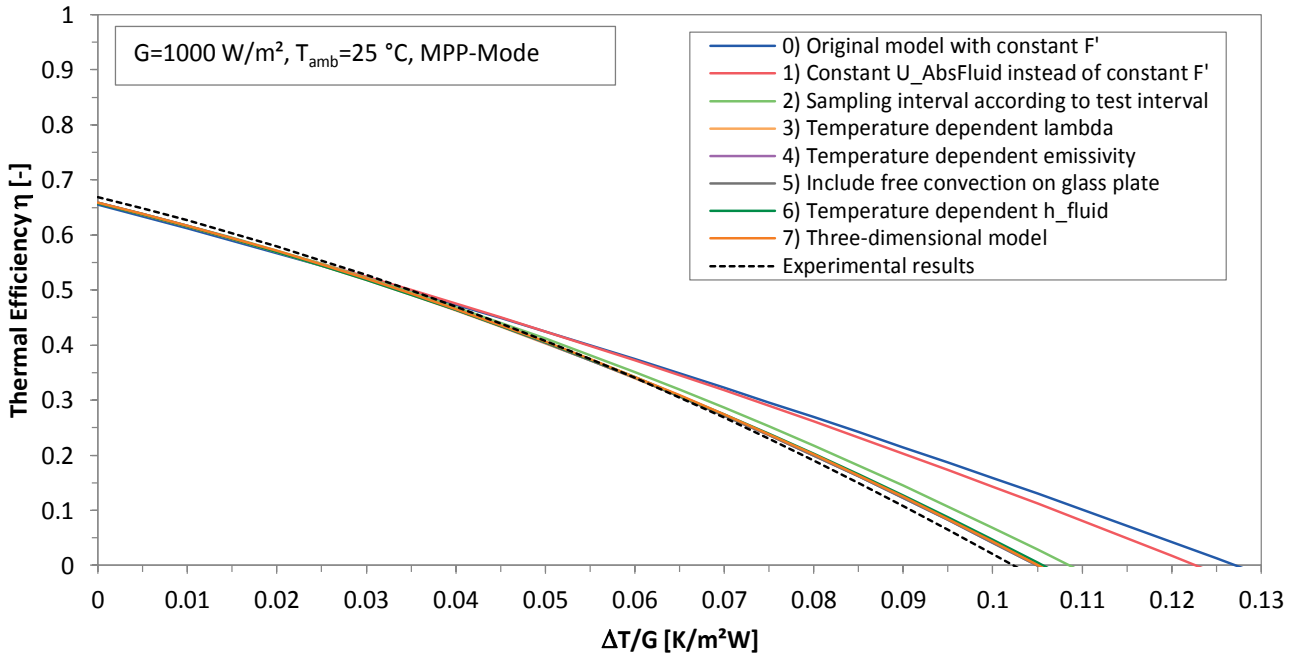

Figure B.3: Evolution of thermal efficiency of the numerical model with increasing level of detail.

B.3 Simulation of PVT collectors with varying low-e coatings on Position 3

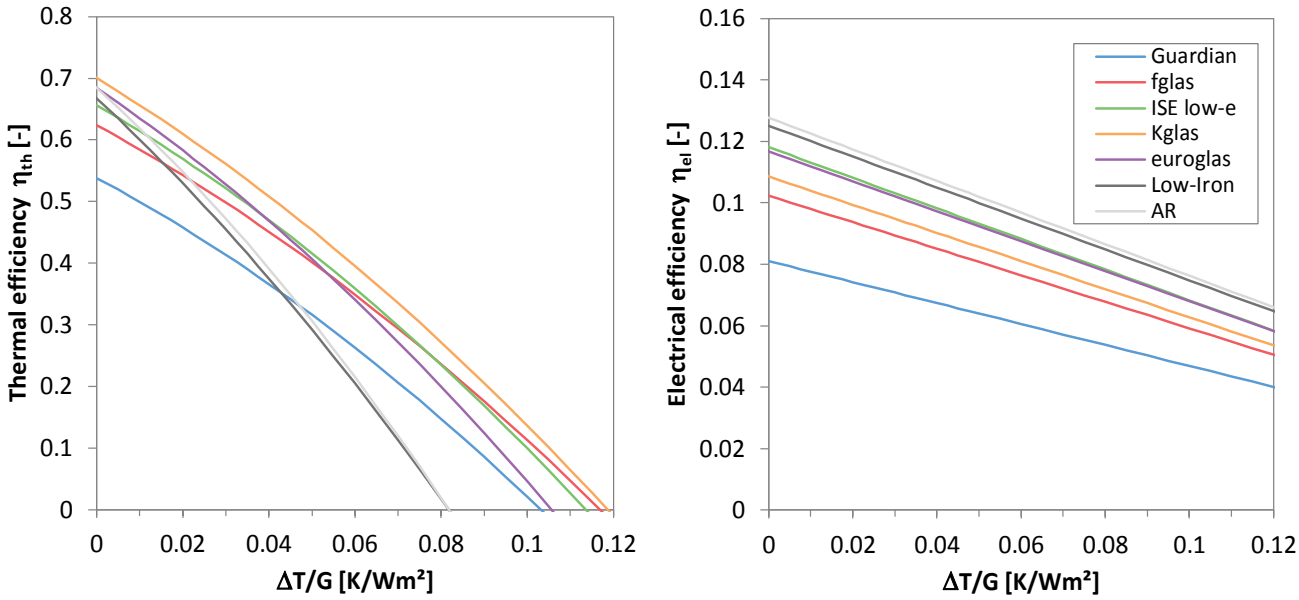

Figure B.4: Evaluation of seven different low-e coatings of a glazed PVT collector with low-e on Position 3.

Table B.1: Evaluation of seven different low-e coatings of a glazed PVT collector with low-e on Position 3.

coating Pos. 3	$\eta_{el,STC}$	$(\tau\alpha)_{eff}$	ε_{Pos3}	$\eta_{th,0}$	c_1 [W/m²K]	c_2 [W/m²K²]	$\eta_{el,0}$	b_1	U_{Loss}
Guardian	8.6%	66.3%	4.0%	0.54	3.72	0.01	0.08	0.34	5.10
fglas	11.0%	77.7%	8.0%	0.62	3.78	0.01	0.10	0.43	5.36
ISE low-e	11.5%	83.3%	10.0%	0.66	4.04	0.02	0.12	0.50	5.67
K-Glas	11.7%	87.1%	15.0%	0.70	4.24	0.01	0.11	0.46	5.77
Euroglas	12.6%	87.1%	30.0%	0.68	4.72	0.02	0.12	0.49	6.56
Low-Iron	13.4%	89.0%	92.0%	0.67	6.48	0.02	0.13	0.50	9.08
AR	13.7%	90.9%	92.0%	0.68	6.34	0.02	0.13	0.51	9.08

B.4 ScenoCalc simulations for different PVT technologies at varying locations

Table B.2: ScenoCalc simulations for different technologies at different locations.

		Athens			Zürich			Würzburg			Stockholm		
Total irradiance I_{tot} [kWh/m²a]		1765			1714			1244			1166		
T_{mean} [°C]		25	50	75	25	50	75	25	50	75	25	50	75
Thermal yield [kWh/m²a]	PV module	0	0	0	0	0	0	0	0	0	0	0	0
	PVT unglazed	634	55	0	284	20	0	277	20	0	229	12	0
	PVT glazed	985	469	148	652	262	60	529	208	50	475	191	44
	PVT glazed low-e	1072	678	346	816	469	204	632	347	152	573	319	141
	CPC PVT	627	352	174	427	217	97	336	157	65	374	200	92
	Flat plate collector	1308	928	609	1054	720	447	796	514	306	728	472	285
Electrical yield [kWh/m²a]	PV module	252	252	252	255	255	255	183	183	183	173	173	173
	PVT unglazed	255	231	203	248	223	196	181	163	143	169	152	134
	PVT glazed	240	217	192	232	209	186	171	154	136	159	144	127
	PVT glazed low-e	229	205	182	220	198	176	162	146	129	152	136	121
	CPC PVT	108	98	88	105	95	85	76	69	62	73	66	59
	Flat plate collector	0	0	0	0	0	0	0	0	0	0	0	0

Appendix C SYSTEM SIMULATIONS

C.1 Calculation of $U_{AbsFluid}$ from test results

The recent standards for testing PVT collectors ((ISO 9806 2013; SKN 2015) do not include test procedures to determine the thermal coupling between PV cells and fluid, which is an important, collector-specific parameter describing the quality of internal heat transfer. Recent research (Helmers and Kramer 2013; Fritzsche et al. 2014; Zenhäusern et al. 2015; Adam et al. 2014a) present and discuss different approaches. Up to date, the scientific community has not decided on a shared standard for an electrical and thermal performance model. Therefore, the openly available test data do not provide information on the internal heat transfer coefficient $U_{AbsFluid}$ which is however required as simulation input.

Stegmann et al. (2012) developed a procedure for the calculation of the internal heat transfer coefficient for unglazed PVT collectors. The input for the calculation is based on available test data in OC mode. The following approach extends the validity of the procedure for glazed collectors with test data in MPP mode. Figure C.1 shows the four steps necessary for the calculation of $U_{AbsFluid}$.

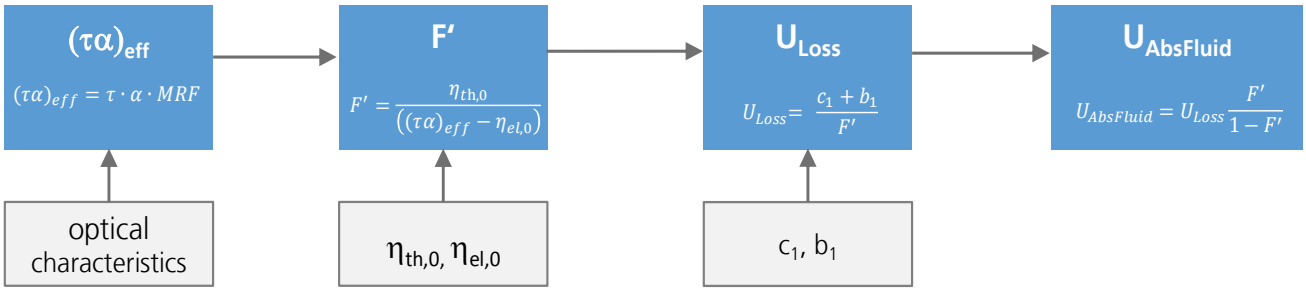

Figure C.1 Procedure for the calculation of $U_{AbsFluid}$ based on test results.

Firstly, the effective transmittance-absorptance product $(\tau\alpha)_{eff}$ is derived from optical characteristics, i.e. transmittance and reflectance of the glazing and absorptance of the PVT laminate (compare Eq. (3.1)). Table C.1 gives an overview of $(\tau\alpha)_{eff}$ for typical PVT collector configurations.

Table C.1: Effective transmittance-absorptance product $(\tau\alpha)_{eff}$ for typical PVT collector configurations.

PVT collector configuration	τ_{cover}	$\alpha_{laminate}$	Multi reflection factor MRF	$(\tau\alpha)_{eff}$
unglazed	1	0.901	1	0.901
glazed AR	0.96	0.901	1.001	0.87
glazed AR, low-e	0.96	0.86	1.002	0.83
glazed	0.93	0.901	1.004	0.84
glazed, low-e	0.93	0.86	1.006	0.80

Secondly, the collector efficiency factor F' is calculated from the conversion factor $\eta_{th,0}$ (compare Eq. (3.16)):

$$F' = \frac{\eta_{th,0}}{\left((\tau\alpha)_{eff} - \eta_{el,0}\right)} \quad \text{(C.1)}$$

Thirdly, the overall collector heat loss coefficient U_{Loss} is extracted from the linear thermal heat loss coefficient c_1 (Fischer et al. 2004). The temperature dependence of U_{Loss} is neglected, so that U_{Loss} is only valid

at $\Delta T = 0$ K. In the same manner the temperature dependence of electrical efficiency b_1 has to be taken into account:

$$U_{Loss,\Delta T=0K} = \frac{c_1 + b_1}{F'} \tag{C.2}$$

Finally, $U_{AbsFluid}$ is derived from the definition of F′ (compare Eq. (3.19)):

$$U_{AbsFluid} = U_{Loss,\Delta T=0\ K} \frac{F'}{1 - F'} \tag{C.3}$$

The described procedure strongly depends on an accurate determination of F′ and U_{Loss} on the basis of the performance coefficients. Hence, the procedure is sensitive towards small changes of measured performance data. One also has to keep in mind that $\eta_{th,0}$, $\eta_{el,0}$, c_1, and b_1 result from multiple-linear regression and are consequently interdependent and have a high uncertainty in itself.

To conclude, this approach allows a standardized procedure for the calculation of $U_{AbsFluid}$. Owing to the high uncertainty of $U_{AbsFluid}$ on small variations of input data, the approach has to be considered as a makeshift solution. In the future, a PVT performance model needs to be developed and agreed on which includes a standardized procedure to determine the coefficient for coupling the electrical and thermal efficiencies, either in the form of $U_{AbsFluid}$ or in a different form.

C.2 Conversion of thermal efficiency parameters between MPP and OC mode

According to ISO 9806 (2013) it is possible to measure the thermal efficiency in both maximum power point (MPP) and open circuit (OC) mode. However, the thermal efficiency is strongly affected by the modes of operation (Hofmann et al. 2010). In any case, the simulation model requires thermal performance parameters as model input in MPP. If a PVT collector is tested in OC, in contrast to recent SKN regulations, a conversion to MPP is necessary in order to be able to enter the collector data in MPP to the collector model.

For this purpose, a practical formalism for the conversion is derived theoretically and validated with experimental data. This approach is mainly based on the energy balance (Figure 3.2) and the corresponding equations in Helmers and Kramer (2013).

The basis for the conversion formalism is formed by the following equation from Helmers and Kramer (2013):

$$\eta_{th,OC} = \eta_{th,MPP} + \Delta\eta_{th,OC-MPP} = \eta_{th,MPP} + \eta_{el} - \Delta\eta_{th,Loss} \tag{C.4}$$

The thermal efficiency in open circuit mode $\eta_{th,OC}$ is always higher than the thermal efficiency in MPP $\eta_{th,MPP}$ where $\Delta\eta_{th,OC\text{-}MPP}$ is the difference of thermal efficiency between MPP and OC Mode. $\Delta\eta_{th,OC\text{-}MPP}$ consists of two parts: electrical energy extracted in PV cells η_{el}, and the difference of thermal losses owing to lower absorber temperatures $\Delta\eta_{th,Loss}$. The latter originates from the fact that the PV cells serve as energy sink reducing the absorber temperature and thus thermal losses.

The electrical efficiency during measurements with a constant irradiance G can be expressed as a function of cell temperature and the temperature coefficient γ (compare Eq. (2.1)). At this point the notation as a function of the reduced temperature is more useful:

$$\eta_{el} = \eta_{el,0} - b_1 \frac{\Delta T}{G} \tag{C.5}$$

Both parameters $\eta_{el,0}$ and b_1 can be expressed solely as a function of known parameters, after employing the temperature dependence of the electrical efficiency in Eq. (2.1) and the explicit notation of T_{cell} as a function of the thermal efficiency in Eq. (C.5):

$$\eta_{el,0} = \eta_{el,STC} \frac{1 - \gamma \left(\frac{GF'(\tau\alpha)_{eff}}{U_{AbsFluid}} + T_{amb} \right)}{1 - \gamma \left(\frac{GF'}{U_{AbsFluid}} \right)} \tag{C.6}$$

$$b_1 = \eta_{el,STC} \frac{\gamma G (U_{AbsFluid} - a_{1,OC})}{U_{AbsFluid} - \eta_{el,STC} \gamma G} \tag{C.7}$$

Helmers and Kramer (2013) derived an expression which quantifies the difference of thermal losses $\Delta\eta_{th,Loss}$ by a present electrical power output. Assuming equal mean fluid temperatures $\Delta\eta_{th,Loss}$ is given by the following term:

$$\Delta\eta_{th,Loss} = (1 - F')\, \eta_{el} \tag{C.8}$$

Insertion of Eq. (C.5) and Eq. (C.8) in Eq. (C.4) results in:

$$\eta_{th,OC} = \eta_{th,MPP} + F' \eta_{el,0} - F' b_1 \frac{\Delta T}{G} \tag{C.9}$$

For glazed PVT collectors Eq. (C.9) can be expressed as:

$$\eta_{th,0,OC} - c_{1,OC} \frac{\Delta T}{G} - c_{2,OC} \frac{\Delta T^2}{G} = \eta_{th,0,MPP} - c_{1,MPP} \frac{\Delta T}{G} - c_{2,MPP} \frac{\Delta T^2}{G} + F' \eta_{el,0} - F' b_1 \frac{\Delta T}{G} \tag{C.10}$$

Finally, η_{th0}, c_1, and c_2 can be calculated by equating coefficients:

$$\eta_{th0,OC} = \eta_{th0,MP} + F' \eta_{el,0} \tag{C.11}$$

$$c_{1,OC} = c_{1,MPP} + F' b_1 \tag{C.12}$$

$$c_{2,MPP} = c_{2,OC} \tag{C.13}$$

The conversion formalism works in both directions, either to calculate MPP values from OC values or the other way round.

For the validation of the conversion formalism, five PVT collectors were tested in both conditions, in MPP and OC mode. Then, the conversion formalism was applied to calculate the MPP efficiency based on the tested OC efficiency curve. Comparing the tested with the converted MPP curve, ideally identical curves should be obtained.

In all five cases, the comparison shows very good agreement between the tested and converted MPP curves. A maximum difference between tested and converted efficiency of $\Delta\eta_{th,max} = |\eta_{th,MPP,tested} - \eta_{th,MPP,converted}| = 0.02$ is observed. This lies well below the uncertainty range for collector tests. The root mean square error RMSE of the five tested and converted efficiency curves equals RMSE = 0.008. The efficiency curves for two exemplary PVT collectors are shown in Figure C.2.

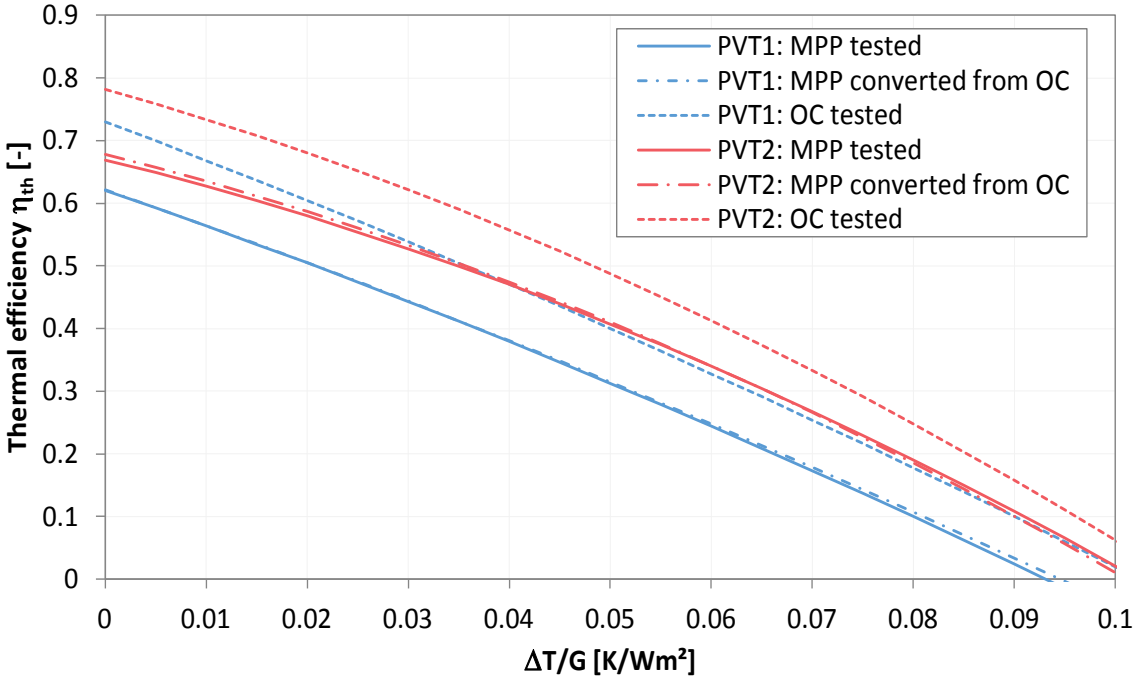

Figure C.2: Conversion between MPP and OC mode: the calculated thermal efficiency curve in MPP mode is derived from the measured OC curve applying the conversion formalism and compared to the measured MPP curve.

Table C.2: Performance coefficients from five tested PVT collectors in MPP and OC mode together with converted MPP performance coefficients.

		PVT collector 1	PVT collector 2	PVT collector 3	PVT collector 4	PVT collector 5
MPP tested	$\eta_{th,MPP}$	0.62	0.66	0.67	0.72	0.69
	$c_{1,MPP}$	5.54	4.792	3.979	6.14	3.499
	$c_{2,MPP}$	0.012	0.018	0.025	0.024	0.0164
	$\eta_{el,o}$	0.130	0.113	0.115	0.100	0.117
	b_1	0.52	0.52	0.51	0.51	0.51
OC tested	$\eta_{th,OC}$	0.73	0.75	0.78	0.82	0.80
	$c_{1,OC}$	6.10	5.82	4.56	6.50	4.21
	$c_{2,OC}$	0.010	0.006	0.026	0.026	0.013
MPP converted	$\eta_{th,MPP}$	0.62	0.65	0.68	0.73	0.69
	$c_{1,MPP}$	5.63	5.34	4.04	6.03	3.65
	$c_{2,MPP}$	0.010	0.006	0.026	0.026	0.013

C.3 Assessment of annual thermal and electrical yields at various European locations

Table C.3: Summary of annual thermal and electrical yields with varying collector technology for systems (a) – (d) at different locations

	Collector technology	Irradiance	System (a) SHP / SFH			System (b) DHW / MFH		System (c) DHW / SFH		System (d) Combi / SFH	
	[kWh/m²a]	I_{tot}	E_{PV}	$Q_{Storage}$	Q_{Regen}	E_{PV}	Q_{Coll}	E_{PV}	Q_{Coll}	E_{PV}	Q_{Coll}
Athens	PV module	1823	244			244		244		244	
	PVT unglazed	1823	251	180	745	248	401	246	308	243	212
	PVT glazed	1823	220	318	693	218	637	213	508	206	344
	PVT glazed low-e	1823	203	369	713	203	751	195	595	185	403
	Flat plate collector	1823		444	807		969		709		461
Davos	PV module	1732	232			232		232		232	
	PVT unglazed	1732	251	185	189	240	358	237	254	235	185
	PVT glazed	1732	194	321	182	195	535	191	423	187	330
	PVT glazed low-e	1732	176	391	192	179	627	174	511	169	409
	Flat plate collector	1732		549	242		852		685		560
Würzburg	PV module	1293	179			179		179		179	
	PVT unglazed	1293	182	121	255	182	248	180	176	179	126
	PVT glazed	1293	159	258	266	159	445	156	359	153	272
	PVT glazed low-e	1293	148	310	278	148	525	145	432	140	330
	Flat plate collector	1293		398	304		672		544		408
Stockholm	PV module	1177	162			162		162		162	
	PVT unglazed	1177	165	117	189	165	235	163	167	162	120
	PVT glazed	1177	145	226	196	145	393	143	315	139	235
	PVT glazed low-e	1177	134	273	210	135	467	132	383	127	286
	Flat plate collector	1177		349	248		603		489		357

C.4 Optimization of PVT systems with the characteristic temperature approach

The characteristic temperature has a significant influence on the energy yields: the lower the operating temperature of the PVT collector, the higher are its electrical and thermal output. Hence, an appropriate objective for optimizing PVT systems is the reduction of T_{char}. The following section discusses exemplarily four case studies and demonstrates how these strategies reduce the characteristic temperature and influence energy yields.

C.4.1 Case study #1: Collector operation mode in system (a) SHP / SFH

PVT heat pump systems with borehole or ground heat exchangers can be operated in different operation modes. In the parallel mode (P), the PVT collector directly feeds into the storage. In the regeneration mode, the solar heat regenerates the borehole, i.e. compensates for the heat extracted by the heat pump. Apparently, the operation mode and its underlying control strategy affect the characteristic temperature and yields.

For case study #1, two operation modes are compared in system (a) SHP/SFH with unglazed PVT collectors. The reference case is given by the P/R operation mode as in chapter 4.2.2.1 and the optimized case is given by the regeneration mode excluding the option of parallel operation.

Switching the operation mode from P/R to R effectuates a reduction of T_{char} from 21.3 to 19.3 °C. At the same time, the thermal yield of the PVT array increases by + 87 %. This sharp increase of the heat gain results mostly from the control strategy. The collector circuit is switched on when the temperature difference between collector outlet and borehole heat exchanger outlet exceeds 6 K. Due to the lower temperature level of the ground compared to the storage tank, the collector circuit is operational for much longer periods and even in states without irradiance, when the collector acts more as an ambient heat exchanger than a solar collector. Despite the reduction of T_{char} by 2.0 °C, the electrical yields are constant in both the reference and optimized case. This is caused by similar levels of the PV cell temperatures, which are hardly affected by the operation mode.

It has to be mentioned that it is critical to compare the mere value of the thermal yields of both cases. The value of heat directly delivered to the storage in parallel mode (P) is higher than heat used for the borehole regeneration. Firstly, an additional conversion step of the heat pump is required until the heat can be utilized, which entails additional electricity consumption. Secondly, the thermal losses of the ground storage are higher due to lateral heat exchange to neighboring sediments. Under system performance considerations, one kWh of heat to the storage is therefore more valuable than one kWh heat for regeneration.

C.4.2 Case study #2: Reduction of hot water temperatures in system (b) DHW / MFH

The minimum draw-off temperature of hot water systems in multi-family houses is subject to legal regulations. To avoid the formation of harmful legionella, the water temperature in large hot water systems has to be maintained above 60 °C at any location in the piping system according to DVGW (2004).

Under mere efficiency considerations, in contrast, low temperature (low exergy) systems are favorable. A reduction of system temperatures reduces heat distribution and circulation losses and increases the efficiency of renewable heat generation by solar thermal or heat pumps. For instance this reduction can be

achieved by a two-pipe system with decentralized heat exchanger stations for each apartment or a four-pipe system with membrane ultra-filtration (Helbig and Mercker 2017).

For case study #2, the effect of reducing hot water draw-off temperatures on PVT yields is studied in system (b) DHW / MFH with glazed PVT collectors (section 0). For this purpose the set temperature of hot water is reduced from T_{tap}= 60 °C to T_{tap} = 45 °C. For a consistent comparison, the total heat load is kept at constant levels by adjusting the draw-off volumes accordingly considering that hot water is mixed with cold water to achieve a constant tap temperature of T_{tap} = 45 °C.

The reduction of the system temperatures effectuates a drop of T_{char} from 44.4 °C to 42.8 °C. This increases the thermal collector yields by 9.5 % and the electrical yield by 0.7 %. In addition to that, the heat distribution losses are reduced by 50.4 %.

C.4.3 Case study #3: Increase storage volumes in system (c) DHW / SFH

Thermal storages play an important role in efficient solar thermal systems. They accumulate solar heat from short periods up to several months and thus enable a better match between the solar radiation and the heat demand. Moreover, larger storage volumes may lead to lower storage and thus collector temperatures and reduce the periods of stagnation by larger buffer volumes.

For case study #3, the effect of increasing the storage volume is studied in system (c) DHW/SFH with glazed PVT collectors with low-e (chapter C.6.3). For this purpose, the storage volume is increased by 50 % from V = 0.35 m³ to V = 0.525 m³. The larger storage volume effectuates a reduction of T_{char} from 49.1 °C to 48.2 °C, which increases the thermal yield by 5.0 % and the electrical yield by 0.7 %.

C.4.4 Case study #4: Storage stratification in system (d) Combi / SFH

Due to the different density of cold and hot water, thermal storages have a natural stratification with hot water in the upper layer and cold water in the lower layer. Efficient storages in solar thermal systems avoid mixing of hot and cold water by using special stratifying devices. These devices reduce the fluid impulse during charging and discharging, so that less mixing of cold and hot water occurs (Streicher 2012). Thus, lower temperatures in the lower storage layers allow for low collector inlet temperatures, and higher temperatures in the upper storage layer reduce the auxiliary heating demand.

In case study #4, the influence of stratification is studied in system (d) combi/SFH with glazed PVT collectors with low-e (chapter C.6.4). In general, stratification in thermal storages is difficult to model numerically. Nonetheless, the importance of stratification in efficient solar thermal systems and especially PVT systems is known. In the first case, stratification effects are disregarded by discretizing the thermal storage with 2 nodes in the vertical direction. The optimized case is modeled by a storage with 25 nodes, which represents a fairly good stratification behavior (Drück 2006).

The thermal stratification in the storage effectuates a reduction of T_{char} from 53.9 °C to 53.4 °C. This results in an increase of 0.4 % of the electrical yield and an increase of 6.5 % of the thermal yield.

C.4.5 Summary and Outlook

Reducing the operation temperatures should be an integral part of system optimizations to boost thermal and electrical yields. The presented case studies show four exemplary optimization measures and their effect on T_{char} and energy yields. This demonstrates that the characteristic temperature T_{char} is an appropriate indicator to quantify the effect of temperature reductions. Figure C.3 gives a qualitative

overview of the optimization measures and shows the four case studies in bold symbols together with the characteristic collector curve.

Although T_{char} is in general suitable to quantify temperature reductions and optimization potential, the applicability of the characteristic temperature approach for optimizing PVT systems also has its limitations.

Case study #1 demonstrates that the correlation between T_{char} and electrical and thermal yields is not strongly linear. Despite reducing T_{char} by 2.0 K, the electrical yield is hardly affected due to nearly constant PV cell temperatures. On the other hand, the thermal yield increases by 87 $\%_{rel}$ because of the change of operation mode and the corresponding collector control.

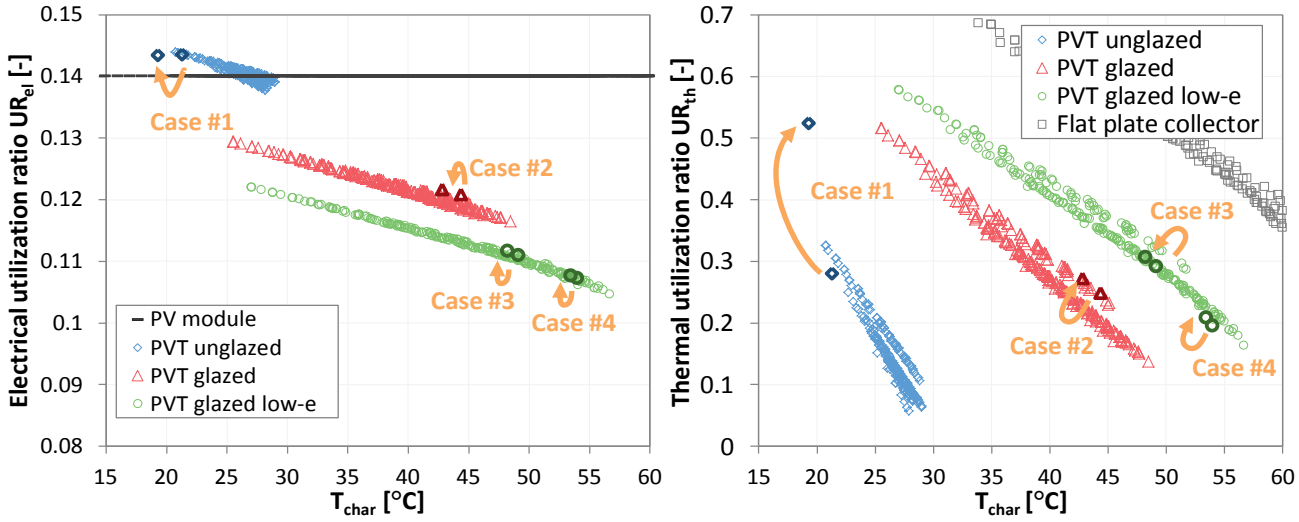

Figure C.3: Optimization of PVT systems with the characteristic temperature approach highlighting four case studies.

Façade integration is an effective measure for optimizing the tilt angle of collectors to better match the solar irradiance in the collector plane to the heat demand, which mainly occurs during winter in combi systems. The reorientation further reduces thermal loads and stagnation periods in summer, when there is an excess of the solar resource available. Therefore, a steeper inclination angle reduces collector temperatures and has its advantages despite the lower overall irradiance in the collector plane. However, changing the tilt angle is not covered by the characteristic temperature approach since the characteristic curve is only valid for one specific collector orientation. In this case, it is insufficient to use only T_{char} for quantifying the optimization measure, but a more detailed approach is required.

From these four case studies, it also becomes clear that small modifications of the system design have a relatively small effect on T_{char} compared to the wide temperature ranges in Figure C.3, which mainly result from the size of the collector array. Therefore, the most important optimization parameter remains the size of the PVT collector array in relation to the heat demand. The smaller a PVT array, the lower the solar fraction, the lower is T_{char} and the higher are the specific yields. Consequently, a PVT array should be rather under- than oversized to achieve low characteristic temperatures and high yields.

Table C.4: Case studies for the optimization of PVT systems highlighting the reduction of T_{char} and the increased yields.

	Case #1	Case #2	Case #3	Case #4
Optimization measure	Operation mode from P/R to R	Reduction of draw-off temperature	Increase of storage Volume	Stratification
System	Sys (a) SFH/SFH	Sys (b) DHW/MFH	Sys (c) DHW/SFH	Sys (d) Combi/SFH
Collector type	Unglazed PVT	Glazed PVT	Glazed PVT low-e	Glazed PVT low-e
T_{char} before optimization	21.3 °C	44.4 °C	49.1 °C	53.9 °C
T_{char} after optimization	19.3 °C	42.8 °C	48.2 °C	53.4 °C
Relative increase of el. yield	0.0 %	0.7 %	0.7 %	0.4%
Relative increase of th. yield	87.0 %	9.5 %	5.0 %	6.5 %

C.5 Comparison of system performance indicators of PVT systems with FPC and PV systems

Table C.5: Detailed assessment of system performance of PV modules. Array sized for identical electrical yield as PVT.

Description	Parameter	Unit	System (a) SHP/SFH	System (b) DHW/MFH	System (c) DHW/SFH	System (d) Combi/SFH
System dimensions						
Collector Technology			PV module	PV module	PV module	PV module
PV module area	A_{PV}	m²	18.8	29.3	6.1	14.1
Electrical peak power	$P_{peak,el}$	kW_P	2.8	4.4	0.9	2.1
Collector performance						
Irradiance in collector plane	I_{tot}	kWh/m²	1293	1293	1293	1293
Specific electrical yield	E_{coll}	kWh/m²	179	179	179	179
Primary energy yield	Q_{PES}	kWh/m²	358	358	358	358
Electrical utilization ratio	UR_{el}	-	0.138	0.138	0.138	0.138
Electrical system performance						
Electricity demand	E_{demand}	MWh	4.56	36.80	4.56	4.56
Total electrical yield	$E_{Coll,tot}$	MWh	3.36	5.24	1.09	2.52
Battery losses	$E_{loss,battery}$	MWh	0.11	0.01	0.03	0.09
Inverter and cable losses	$E_{loss,inverter}$	MWh	0.27	0.42	0.09	0.20
Electrical coverage rate	f_{cov}	-	0.51	0.13	0.21	0.44
Self-consumption rate	$f_{selfcon}$	-	0.75	1.00	0.97	0.86

Table C.6: Detailed assessment of system performance of solar thermal system with flat plate collectors. Array sized for identical thermal yields as PVT systems.

Description	Parameter	Unit	System (a) SHP/SFH	System (b) DHW/MFH	System (c) DHW/SFH	System (d) Combi/SFH
System dimensions						
Collector Technology			FPC	FPC	FPC	FPC
Gross collector area	A_{gross}	m²	8.7	16.4	5.5	13.1
Collector aperture area	A_{aper}	m²	8.0	15.0	5.0	12.0
Heat storage volume	V_{store}	m³	0.6	0.9	0.4	0.9
Thermal peak power	$P_{peak,th}$	kW_P	6.3	11.9	4.0	9.5
Collector performance						
Irradiance in collector plane	I_{tot}	kWh/m²	1293	1293	1293	1293
Specific thermal yield	Q_{coll}	kWh/m²	711	672	544	408
Primary energy yield	Q_{PES}	kWh/m²	782	739	599	448
Thermal utilization ratio	UR_{th}	-	0.55	0.52	0.42	0.32
Thermal system performance						
Heat demand hot water demand	$Q_{demand,DHW}$	MWh	2.6	26.6	2.6	2.6
Heat demand space heating	$Q_{demand,SpH}$	MWh	8.5	0.0	0.0	8.5
Overall thermal collector yield	$Q_{usefulgain}$	MWh	5.7	10.1	2.7	4.9
Heat losses piping and heat exchanger	$Q_{loss,pipesHX}$	MWh	0.1	1.3	0.6	0.8
Collector heat to storage	$Q_{Coll2store}$	MWh	3.1	8.8	2.2	4.1
Collector heat to ground heat exchanger	$Q_{Coll2GHX}$	MWh	2.4	0	0	0
Heat loss storage	$Q_{loss,store}$	MWh	0.8	0.8	0.6	1.1
Auxiliary heat to storage	Q_{aux}	MWh	8.7	18.4	0.9	8.0
Heat losses conventional heating system	$Q_{l,conv}$	MWh	0.5	1.7	0.5	0.5
Solar fraction	f_{sol}	-	0.22	0.31	0.65	0.28
Fractional energy savings	f_{sav}	-	0.25	0.35	0.70	0.31

Table C.7: Detailed assessment of system performance of PVT system (a) – (d).

Description	**Parameter**	**Unit**	**System (a) SHP/SFH**	**System (b) DHW/MFH**	**System (c) DHW/SFH**	**System (d) Combi/SFH**
System dimensions						
Collector Technology			PVT unglazed	PVT glazed	PVT glazed low-e	PVT glazed low-e
Gross collector area	A_{gross}	m²	18.5	41.0	9.3	22.2
Collector aperture area	A_{aper}	m²	18.5	37.6	8.5	20.4
PV module area	A_{PV}	m²	18.5	34.5	7.8	18.7
Heat storage volume	V_{store}	m³	0.6	0.9	0.4	0.9
Electrical peak power	$P_{peak,el}$	kW_P	2.8	5.5	1.2	2.8
Thermal peak power	$P_{peak,th}$	kW_P	10.7	23.7	5.7	13.7
Collector performance						
Irradiance in collector plane	I_{tot}	kWh/m²	1293	1293	1293	1293
Specific electrical yield	E_{coll}	kWh/m²	182	152	139	135
Specific thermal yield	Q_{coll}	kWh/m²	307	273	321	237
Primary energy yield	Q_{PES}	kWh/m²	702	603	631	530
Electrical utilization ratio	UR_{el}	-	0.141	0.117	0.107	0.104
Thermal utilization ratio	UR_{th}	-	0.238	0.211	0.248	0.183
Electrical system performance						
Electricity demand	E_{demand}	MWh	4.6	36.8	4.6	4.6
Total electrical yield (considering cable and inverter losses)	E_{tot}	MWh	3.1	4.4	0.9	2.1
Battery losses	$E_{loss,battery}$	MWh	0.11	0.02	0.03	0.10
Inverter and cable losses	$E_{loss,inverter}$	MWh	0.21	0.33	0.07	0.16
Electrical coverage rate	f_{cov}	-	0.50	0.14	0.23	0.47
Self-consumption rate	$f_{selfcon}$	-	0.39	0.96	0.68	0.44
Thermal system performance						
Heat demand hot water demand	$Q_{demand,DHW}$	MWh	2.6	26.6	2.6	2.6
Heat demand space heating	$Q_{demand,SpH}$	MWh	8.5	0.0	0.0	8.5
Overall thermal collector yield	$Q_{usefulqain}$	MWh	5.7	10.3	2.7	4.8
Heat losses piping and heat exchanger	$Q_{loss,pipesHX}$	MWh	0.0	1.5	0.6	0.8
Collector heat to storage	$Q_{Coll2store}$	MWh	1.0	8.8	2.2	4.1
Collector heat to ground heat exchanger	$Q_{Coll2GHX}$	MWh	4.6	0	0	0
Heat loss storage	$Q_{loss,store}$	MWh	0.6	2.3	1.2	1.8
Auxiliary heat to storage	Q_{aux}	MWh	10.6	18.5	0.9	8.0
Heat losses conventional heating system	$Q_{l,conv}$	MWh	0.5	1.7	0.5	0.5
Solar fraction	f_{sol}	-	0.05	0.31	0.65	0.28
Fractional energy savings	f_{sav}	-	0.09	0.35	0.70	0.31
PVT specific indicators						
Characteristic temperature	T_{char}	°C	21.3	44.4	49.1	54.2
Area requirement factor	f_{area}	-	2.3	2.5	1.7	1.7
Surplus electricity rate	$f_{surplus}$	-	1.8	1.2	1.6	1.6

C.6 Scorecards of PVT systems

C.6.1 Scorecard of system (a) – SHP / SFH with unglazed PVT collectors

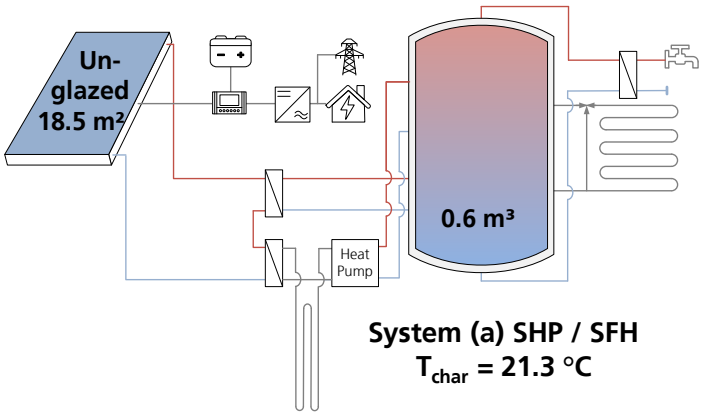

Figure C.4: Electrical and hydraulic layout of the PVT system (a) including PVT technology, collector area $A_{collector}$, and storage volume $V_{Storage}$.

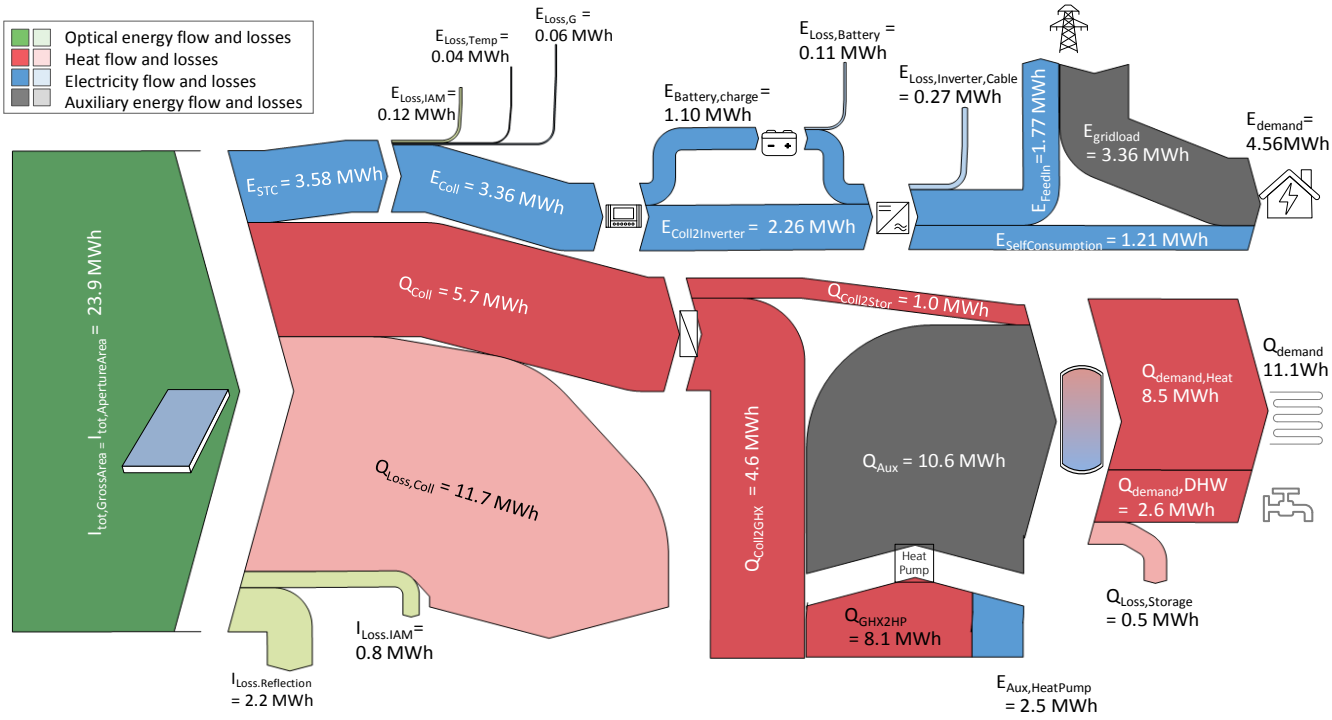

Figure C.5: Visualization of optical (green), thermal (red), and electrical (blue) energy flows of PVT system (a) in a Sankey diagram.

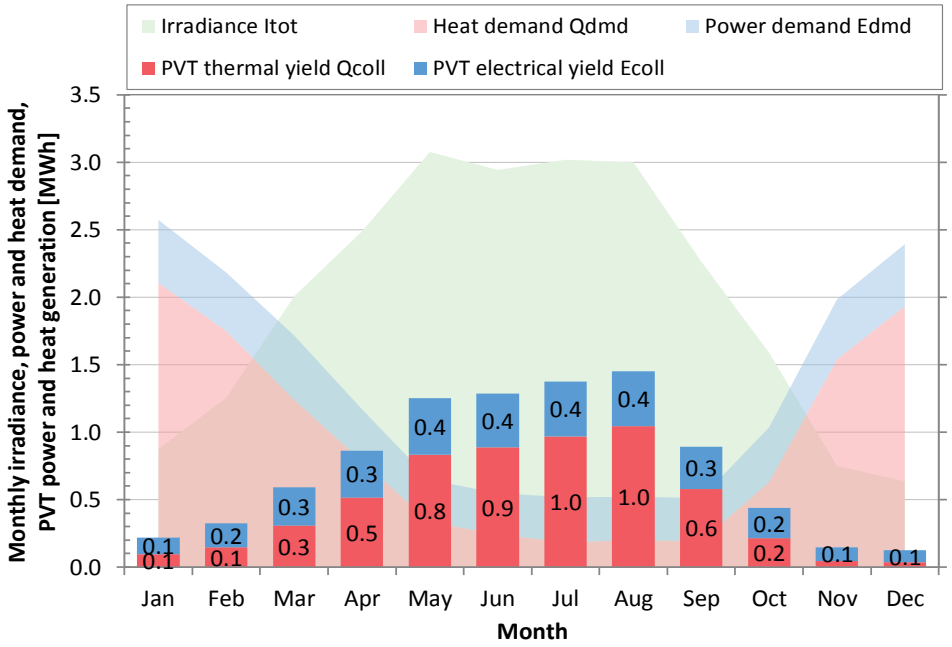

Figure C.6: Monthly irradiance, electricity and heat demand, electrical and thermal yield.

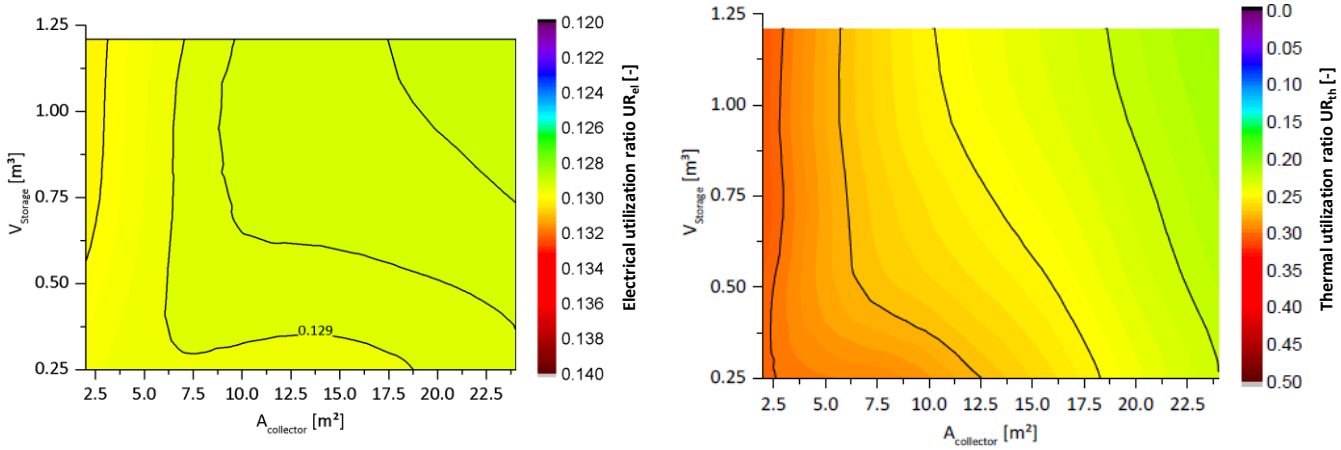

Figure C.7: Sensitivity analysis of electrical utilization ratio (left) and thermal utilization ratio (right) with regards to collector aperture area $A_{collector}$ and storage volume $V_{Storage}$.

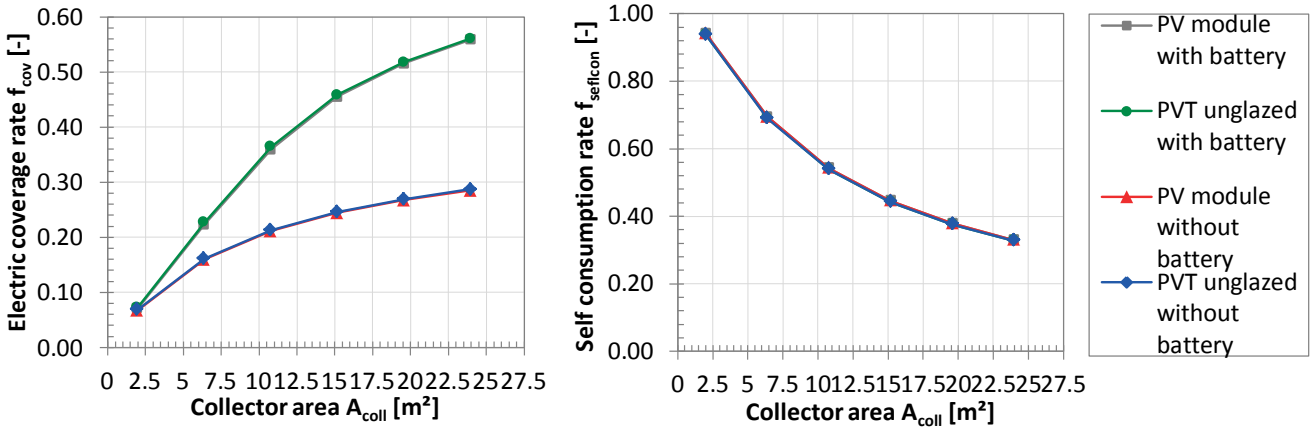

Figure C.8: Electrical coverage rate f_{cov} and self-consumption rate $f_{selfcon}$ for PV modules and unglazed PVT collectors in system (a).

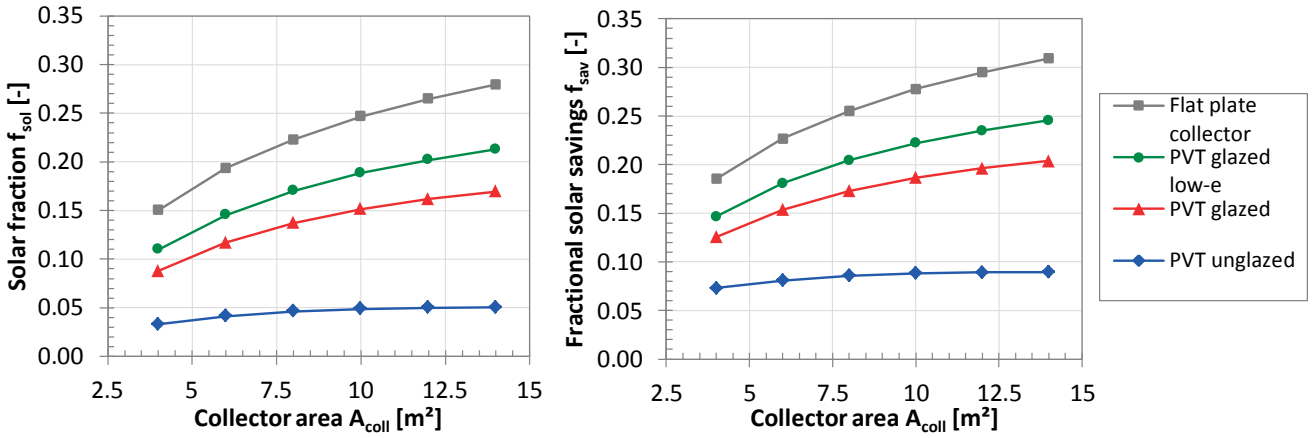

Figure C.9: Solar fraction f_{sol} and fractional solar savings f_{sav} as a function of the collector area A_{coll} in system (a).

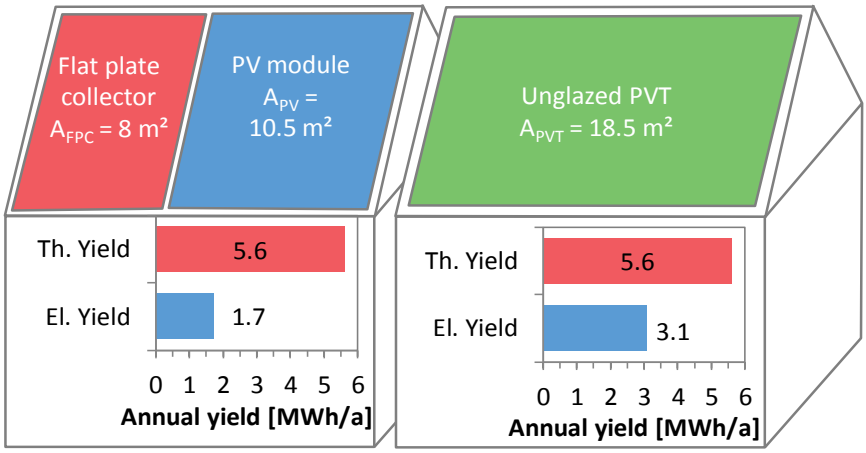

Figure C.10: Limited area assessment of PVT system (a). Comparison of a side-by-side installation of flat plate collectors and PV modules with a PVT installation of same overall thermal yield on the same roof area.

C.6.2 Scorecard of system (b) – DHW / MFH with glazed PVT collectors

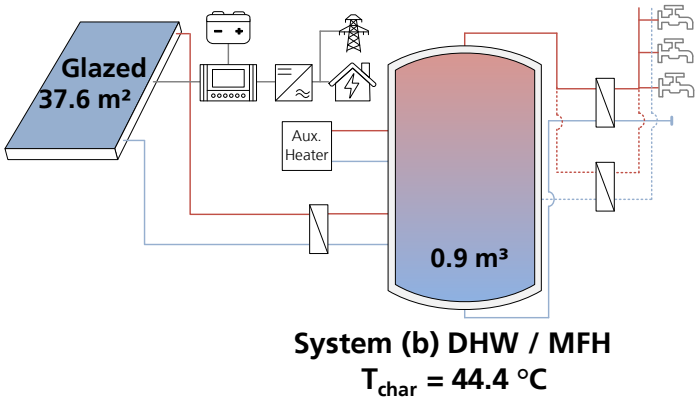

Figure C.11: Electrical and hydraulic layout of PVT system (b) including PVT technology, collector area A_{coll}, and storage volume $V_{Storage}$.

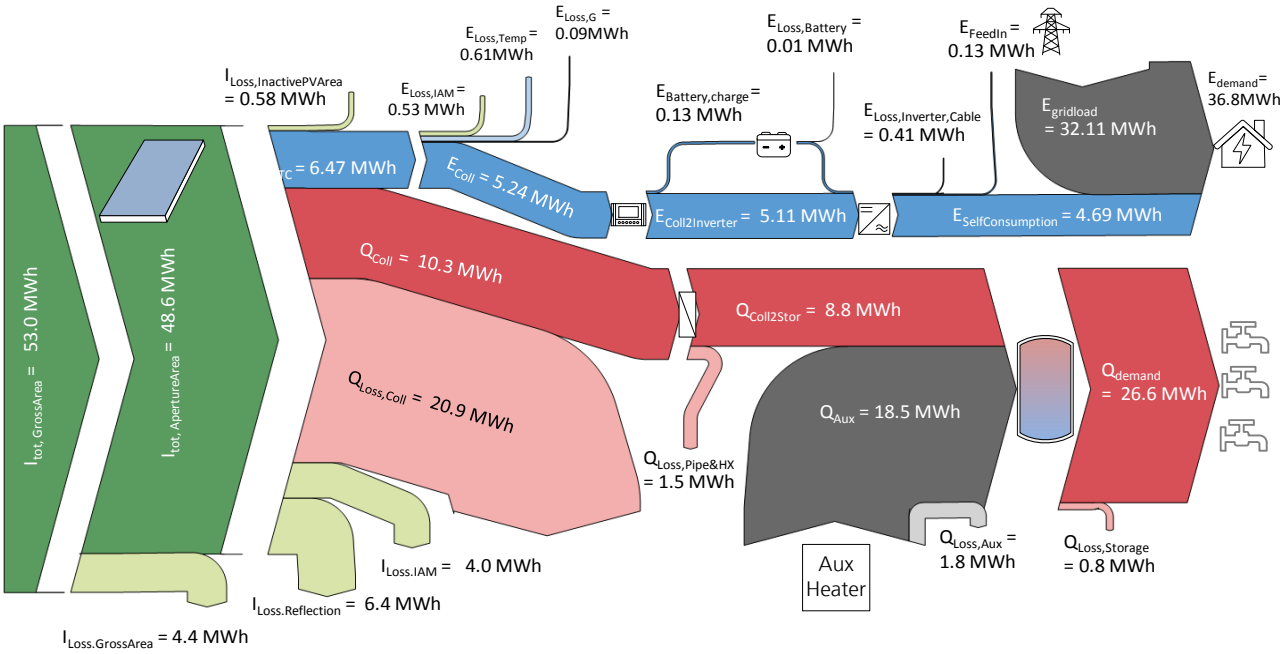

Figure C.12: Visualization of optical (green), thermal (red), and electrical (blue) energy flows of PVT system (b) in a Sankey diagram.

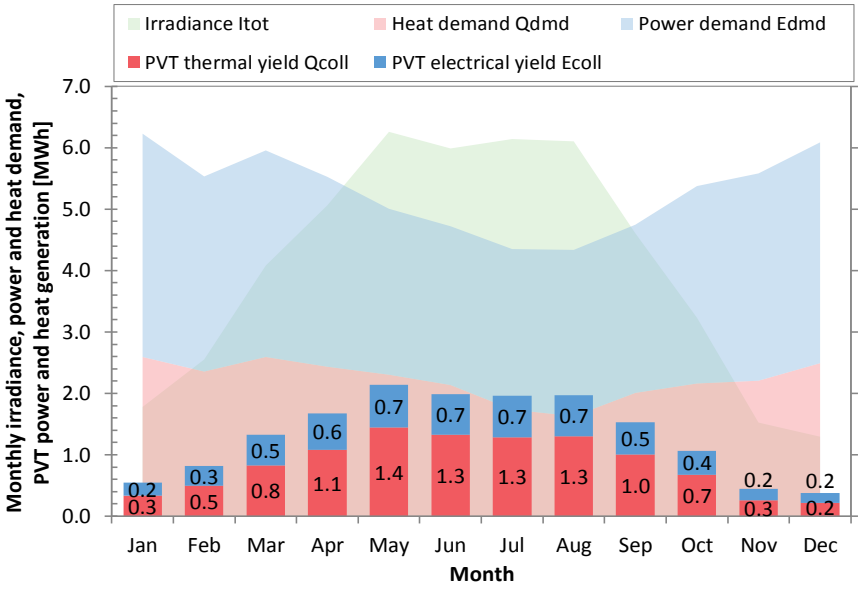

Figure C.13: Monthly irradiance, electricity and heat demand, electrical and thermal yield.

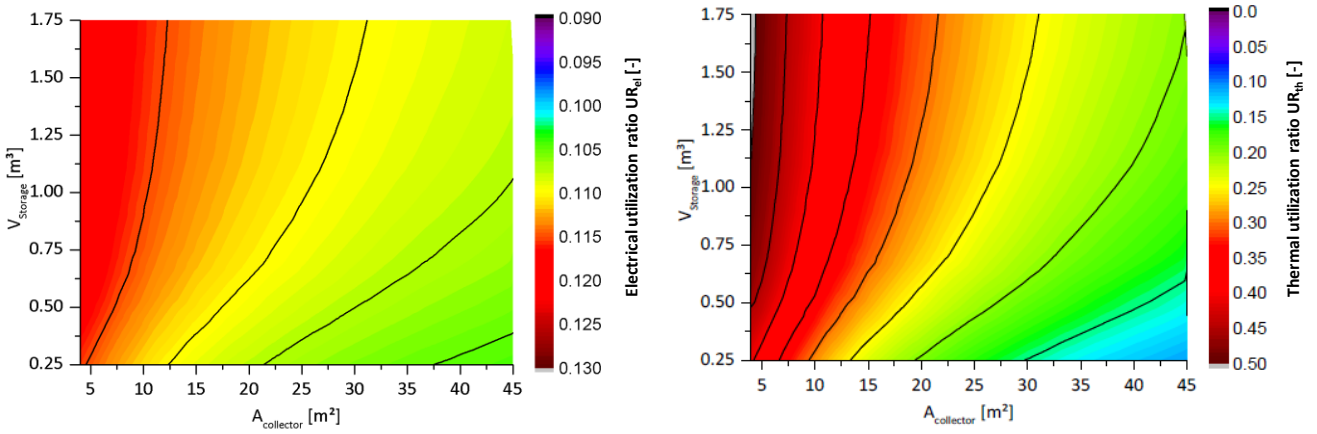

Figure C.14: Sensitivity analysis of electrical utilization ratio (left) and thermal utilization ratio (right) with regards to collector aperture area A_{coll} and storage volume $V_{Storage}$.

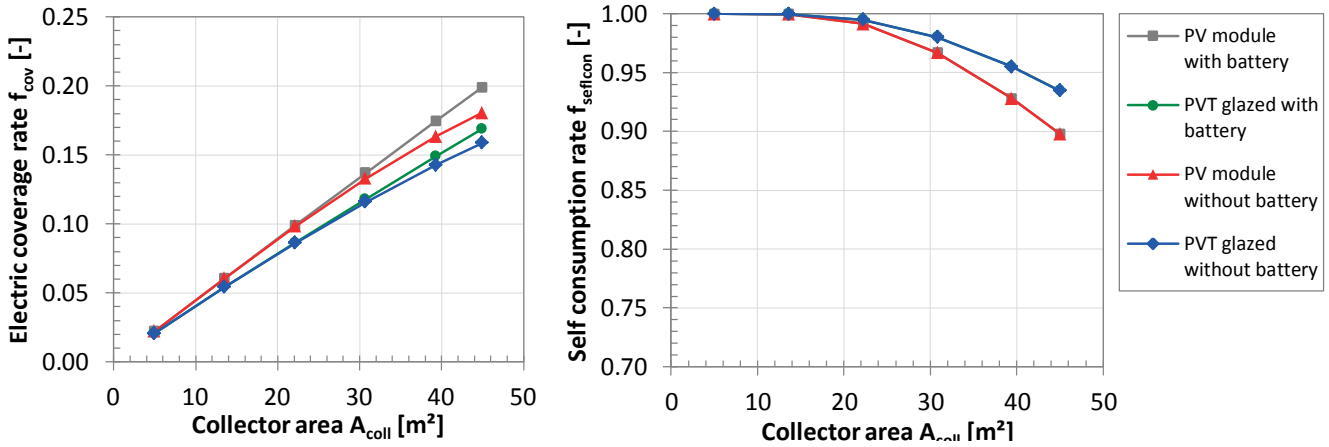

Figure C.15: Electrical coverage rate f_{cov} and self-consumption rate $f_{selfcon}$ for PV modules and glazed PVT collectors in system (b).

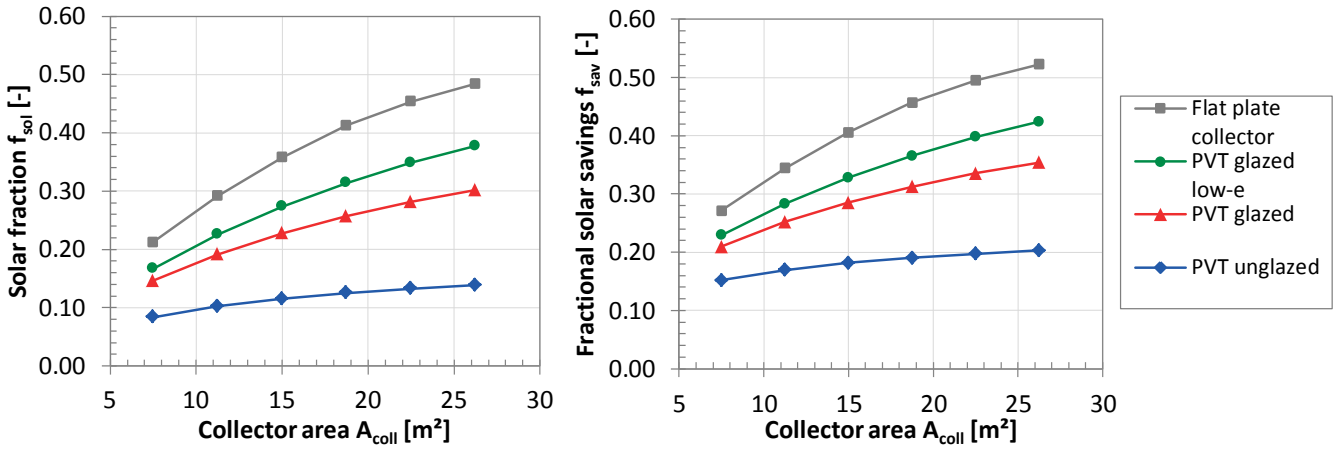

Figure C.16: Solar fraction f_{sol} and fractional solar savings f_{sav} as a function of the collector area A_{coll} in system (b).

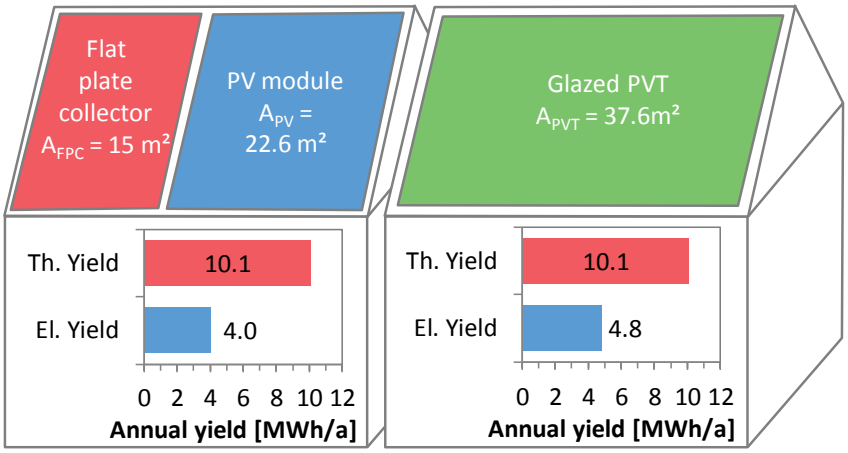

Figure C.17: Limited area assessment of PVT system (b). Comparison of a side-by-side installation of flat plate collectors and PV modules with a PVT installation of same overall thermal yield on the same roof area.

C.6.3 Scorecard of system (c) – DHW / SFH with glazed PVT collectors with low-e

Chapter 4.5.2 covers system (c) in full detail. At this point, only the missing sensitivity analysis is presented in Figure C.18.

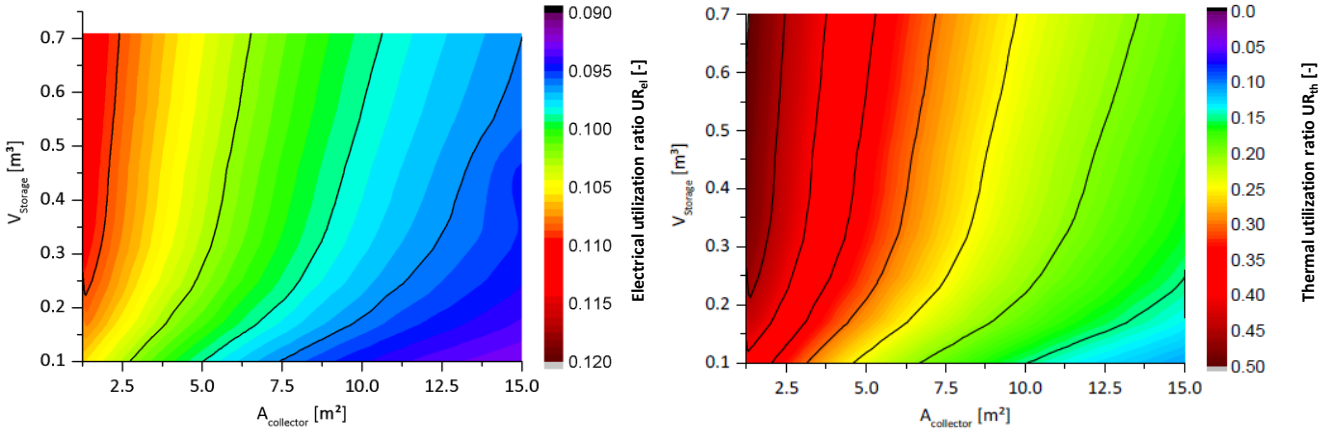

Figure C.18: Sensitivity analysis of electrical utilization ratio (left) and thermal utilization ratio (right) with regards to collector aperture area A_{coll} and storage volume $V_{Storage}$.

C.6.4 Scorecard of system (d) – Combi / SFH with glazed PVT collectors with low-e

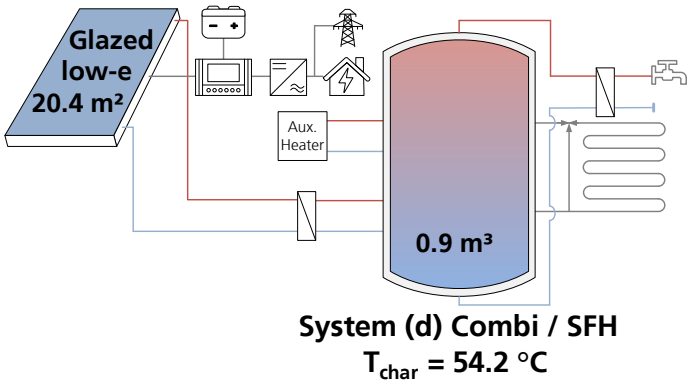

Figure C.19: Electrical and hydraulic layout of PVT system (d) including PVT technology, collector area A_{coll}, and storage volume $V_{Storage}$.

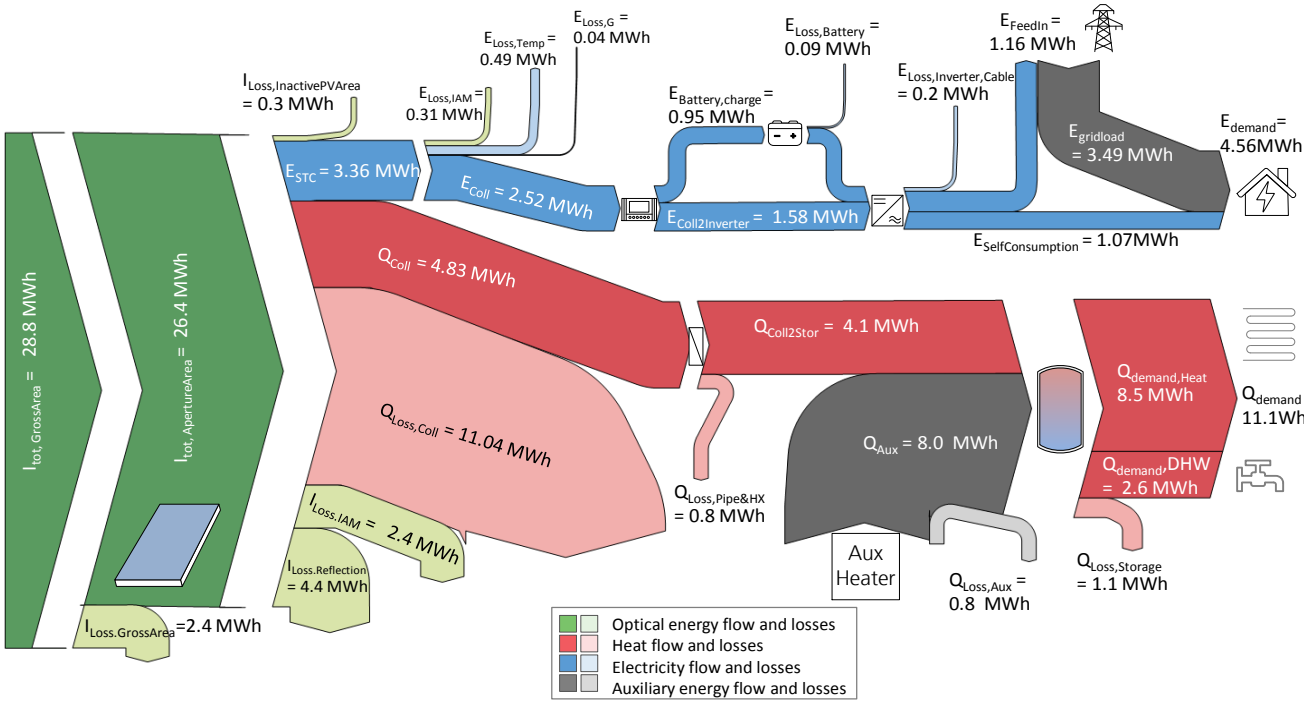

Figure C.20: Visualization of optical (green), thermal (red), and electrical (blue) energy flows of PVT system (d) in a Sankey diagram.

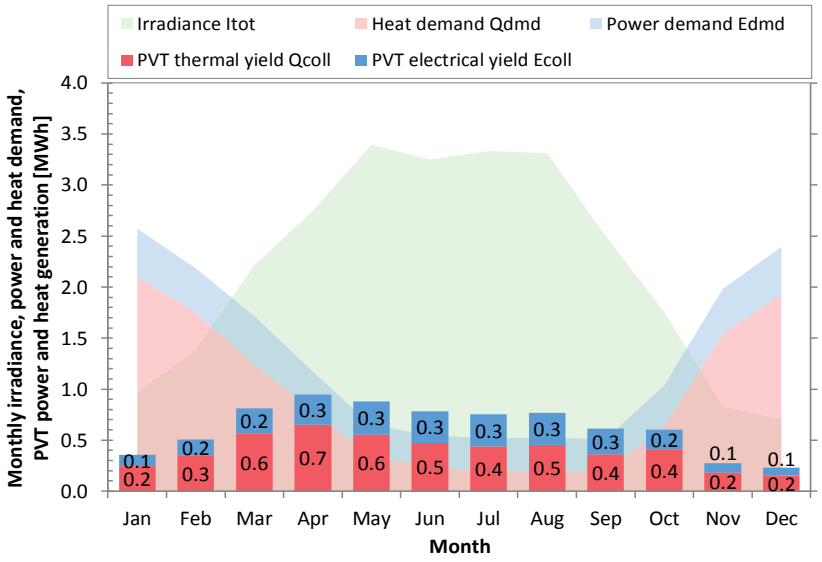

Figure C.21: Monthly irradiance, electricity and heat demand, electrical and thermal yield.

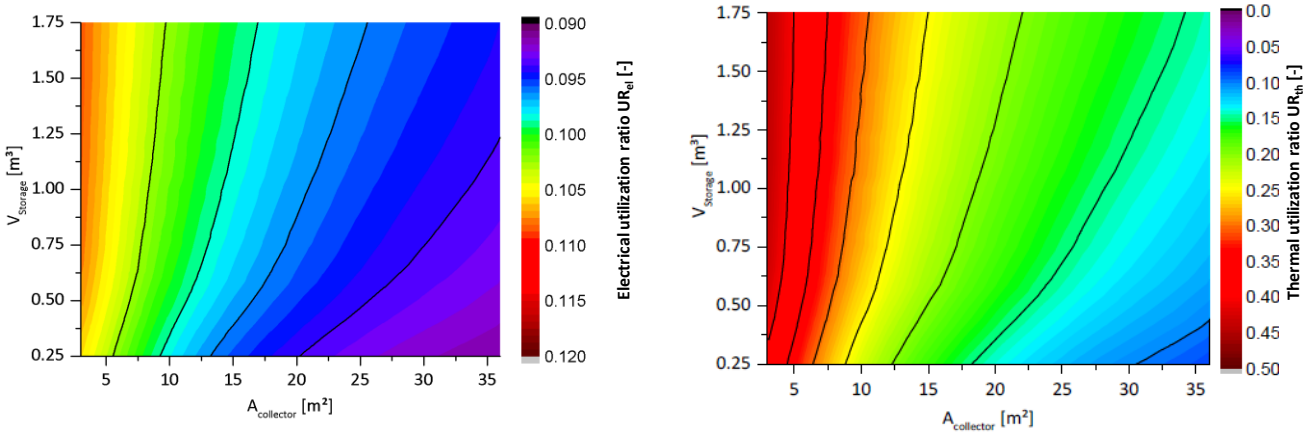

Figure C.22: Sensitivity analysis of electrical utilization ratio (left) and thermal utilization ratio (right) with regards to collector aperture area A_{coll} and storage volume $V_{Storage}$.

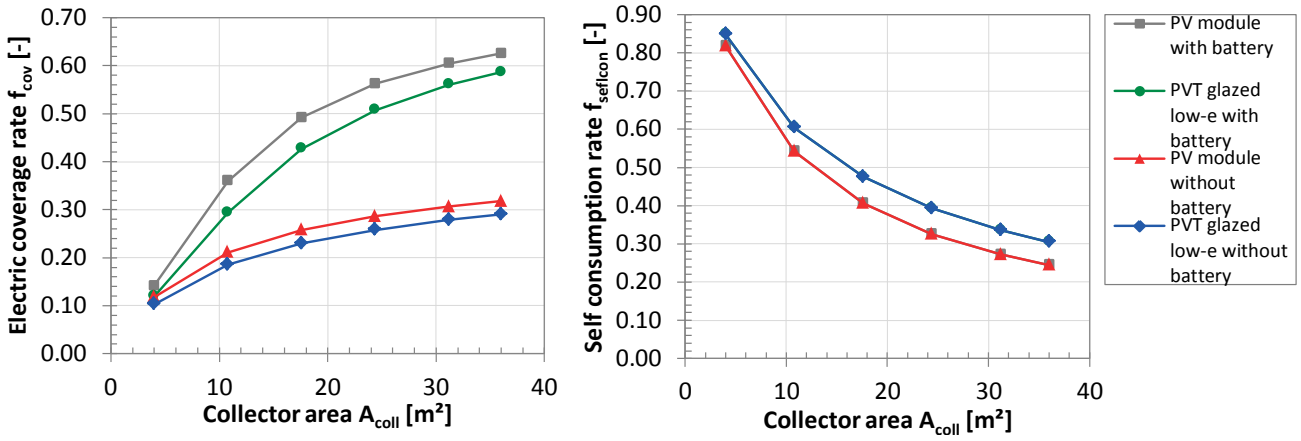

Figure C.23: Electrical coverage rate f_{cov} and self-consumption rate $f_{selfcon}$ for PV modules and glazed PVT collectors with low- e in system (d).

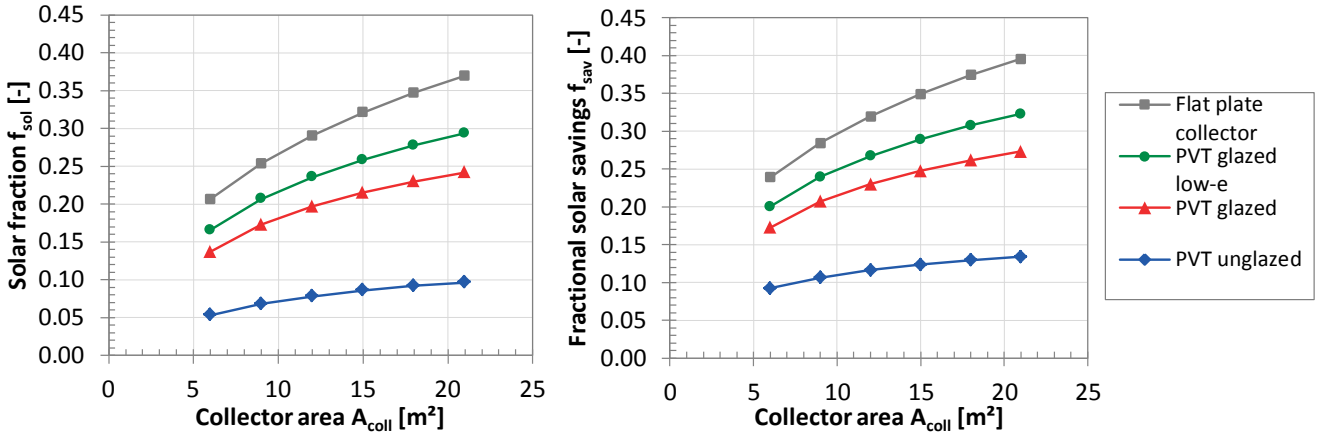

Figure C.24: Solar fraction f_{sol} and fractional solar savings fsav as a function of the collector area A_{coll} in system (d).

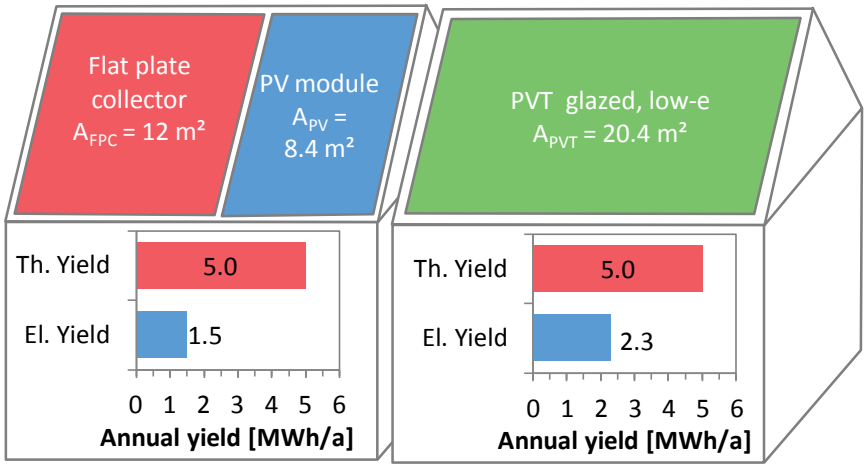

Figure C.25: Limited area assessment of PVT system (a). Comparison of a side-by-side installation of flat plate collectors and PV modules with a PVT installation of same overall thermal yield on the same roof area.

Appendix D OVERHEATING PROTECTION

D.1 Temperature reduction nomograms for dimensioning OHP concepts

The temperature reduction is a central evaluation criterion and design parameter for OHP concepts. In the following section, tools and nomograms for preliminarily assessing and dimensioning OHP approaches are presented. A detailed design of the OHP and collector construction can be carried out based on detailed numerical models as presented in chapter 3.1. Nonetheless, it is essential to understand the fundamental relationship between the OHP design parameters, the efficiency and temperature reduction potential of the four defined OHP categories. The energy balance of the two-node PVT collector model as in Figure D.1 forms the basis for the following discussions.

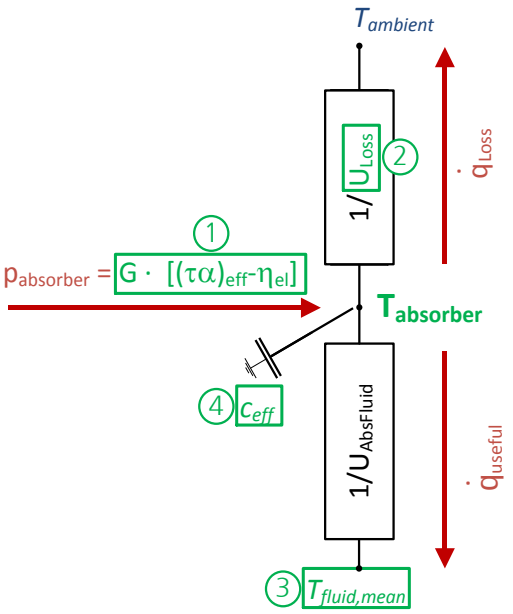

Figure D.1: Energy balance of the two-node PVT collector model including four OHP design parameters.

D.1.1 Reduce $(\tau\alpha)_{eff}$

OHP category 1 aims at switching to low a $(\tau\alpha)_{eff}$ during stagnation. This reduces the energy flux on the absorber p_{el} and thus limits stagnation temperatures.

The impact of reducing $(\tau\alpha)_{eff}$ on the thermal efficiency curve is illustrated in Figure D.2. The efficiency curves are simulated with the detailed numerical collector model for the glazed PVT collector with low-e. The electrical efficiency η_{el} can be considered as an additional heat sink, which reduces $(\tau\alpha)_{eff}$. The efficiency curves are hence given as function of $(\tau\alpha)_{eff}$ - η_{el}.

The overheating protection is activated by switching from high to low $(\tau\alpha)_{eff}$ - η_{el} .This corresponds to switching from an efficiency curve with high to low optical and thermal efficiency. The stagnation temperature can be roughly estimated from the x-intersect of the efficiency curves.

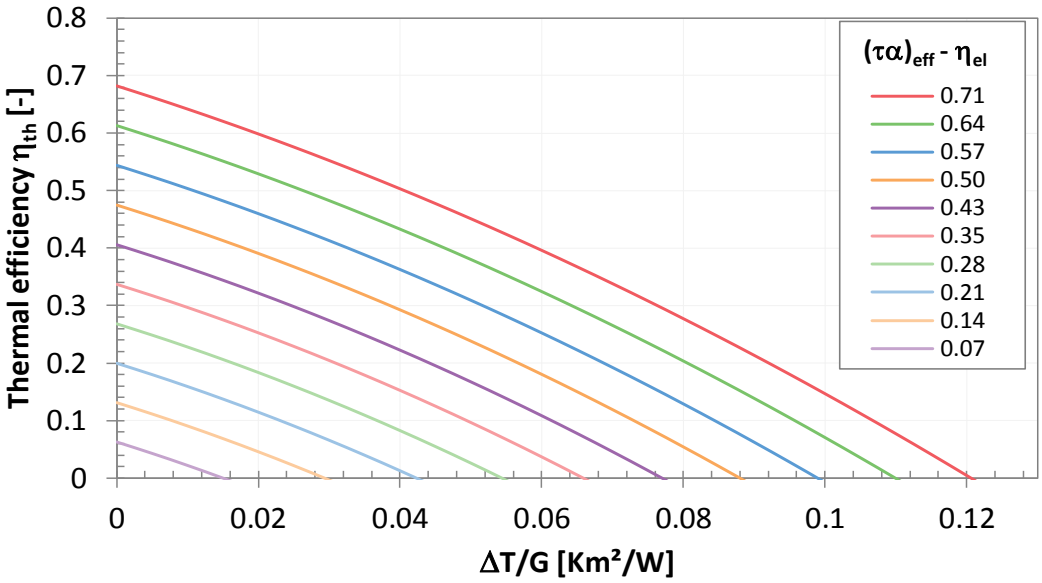

Figure D.2: Impact of a variation of $(\tau\alpha)_{eff} - \eta_{el}$ on the thermal efficiency curve, simulated for glazed PVT collector with low-e coating at G=1000 W/m², T_a = 30 °C, and MPP mode.

To assess the stagnation temperatures of different types of PVT collectors, i.e. with different values of U_{Loss}, a more generalized approach is required. Instead of using the detailed two-node collector model, the mean absorber temperature during steady-state stagnation is derived from the two-node PVT model as in Figure D.1. Accordingly, the energy balance is expressed as:

$$\dot{q}_{useful} = G(\tau\alpha)_{eff} - G\eta_{el} - U_{Loss}\,(T_{abs} - T_a) \tag{D.1}$$

During stagnation in no-flow conditions, no useful heat is generated and consequently $\dot{q}_{useful} = 0$. Furthermore, we neglect the heterogeneous temperature distribution and the local temperature maximum. ISO 9806 recommends adding a margin of 20 K to compensate for this effect. Moreover, we assume that both U_{Loss} and η_{el} are constant and thus neglect their temperature dependence. This assumption is reasonably accurate, as we only consider stagnation conditions and thus a limited temperature range. Considering these simplifications and solving to the absorber temperature T_{abs}, Eq. (D.1) can be expressed as:

$$T_{abs} = T_a + G\frac{(\tau\alpha)_{eff} - \eta_{el}}{U_{Loss}} \tag{D.2}$$

Evaluating Eq. (D.2) for varying values of U_{Loss} leads to the nomogram in Figure D.3. Each collector type is characterized by its U_{Loss} value. This means that every curve stands for one specific collector type. The reduction of the absorber temperature can be read from the y-axis for a given combination of $(\tau\alpha)_{eff} - \eta_{el}$ in normal operation and during stagnation.

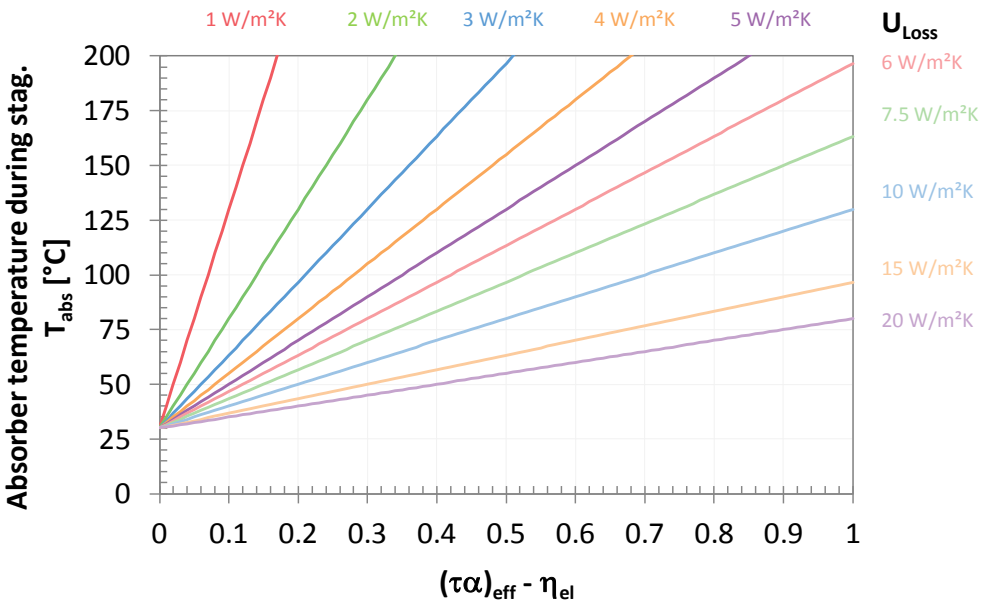

Figure D.3: Nomogram for preliminary dimensioning of an overheating protection by reducing $(\tau\alpha)_{eff}$. Absorber temperatures are evaluated for G = 1000 W/m², T_a = 30 °C without considering a security margin for T_{abs}.

D.1.2 Increase U_{Loss}

OHP category 2 aims at switching to high heat losses U_{Loss} during stagnation. This increases the heat loss flux to ambient $\dot{q}_{Loss}$ and thus lowers stagnation temperatures.

The influence of U_{Loss} on the thermal efficiency curve is illustrated in Figure D.4. The efficiency curves are simulated with the detailed numerical collector model for the glazed PVT collector with low-e with $(\tau\alpha)_{eff}$ = 0.83 and $\eta_{el,STC}$ = 0.13.

The overheating protection is activated by switching from a low to a high value of U_{Loss}. This corresponds to switching from an efficiency curve with high to low optical efficiency. The stagnation temperature can be roughly estimated from the x-intersect of the efficiency curves.

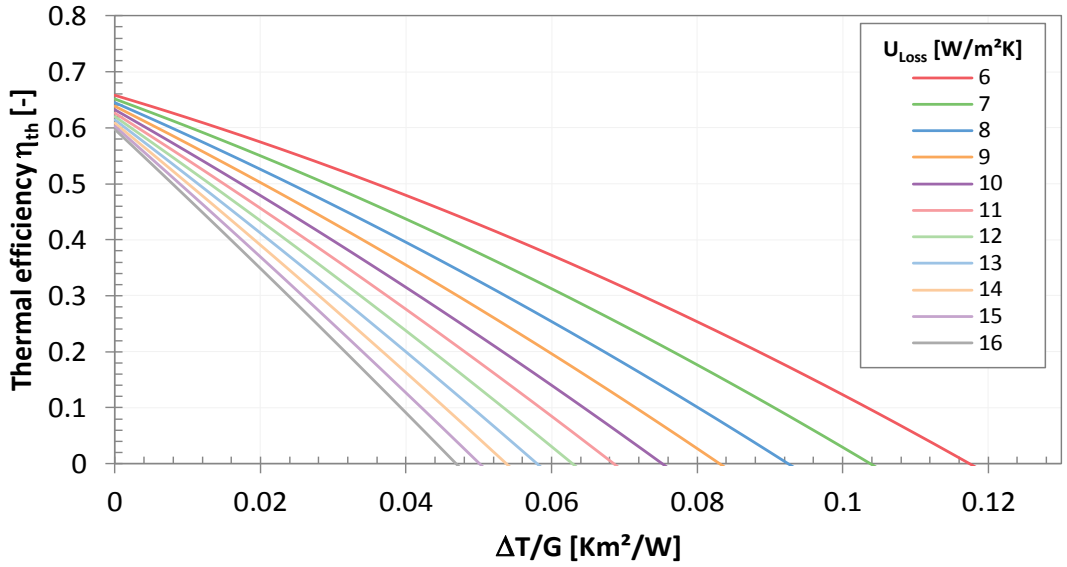

Figure D.4: Effect of U_{Loss} on the thermal efficiency curve, simulated for a glazed PVT collector with low-e.

The same energy balance applies as for reducing $(\tau\alpha)_{eff}$ in OHP category 1. Hence, Eq. (D.2) is also valid with the mentioned simplifications. Evaluating Eq. (D.2) for varying values of $(\tau\alpha)_{eff} - \eta_{el}$ leads to the nomogram in Figure D.5. Every curve stands for one collector type with a specific value of $(\tau\alpha)_{eff} - \eta_{el.}$ The reduction of the absorber temperature can be read from the y-axis for the respective values of U_{Loss} in normal operation and in stagnation.

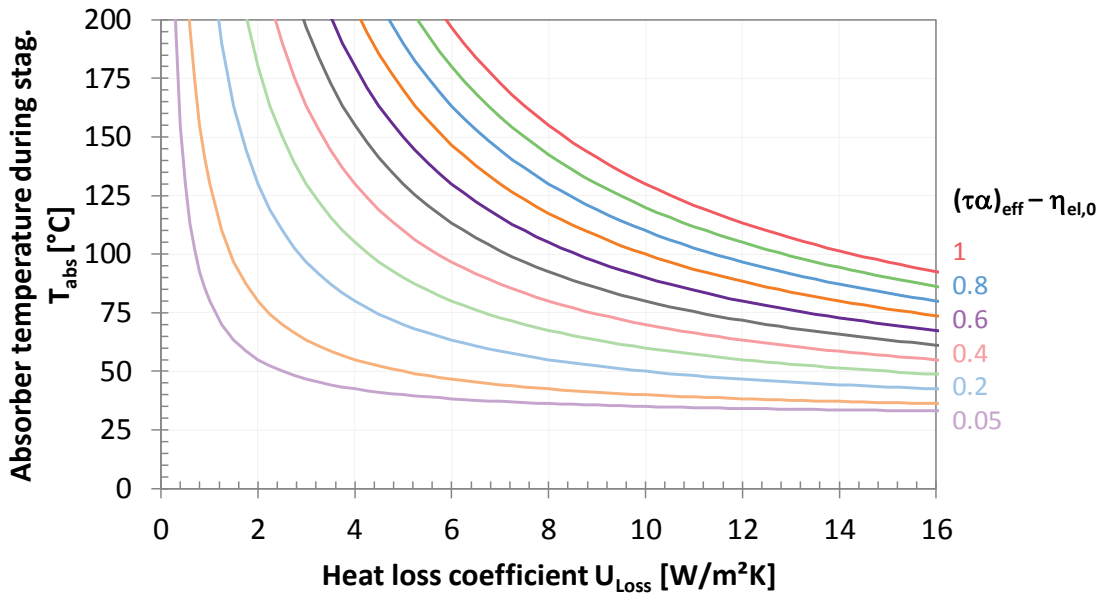

Figure D.5: Nomogram for preliminary dimensioning an overheating protection by increasing U_{Loss}. Absorber temperatures are given for G = 1000 W/m², T_a = 30 °C without considering a security margin for T_{abs}.

D.1.3 Reduction of the mean fluid temperature T_m

OHP category 3 aims at reducing the mean fluid temperature T_m during stagnation. This lowers absorber temperatures by maintaining low fluid temperatures at all time and getting rid of the remaining heat gain $\dot{q}_{useful}$, which also occurs during stagnation. The heat gain then has to be dissipated to the environment by internal or external heat dissipators. Therefore, the central design criterion of OHP category is the overall heat transfer coefficient which is characterized by $(UA)_{external}$. $(\tau\alpha)_{eff}$, η_{el}, and U_{Loss} remain constant, which is why the efficiency curves are not changed.

For dimensioning $(UA)_{external}$, the following assumptions are made. Firstly, we assume that the absorber temperature equals the fluid temperature. Thus, the influence of internal heat transfer coefficient $U_{AbsFluid}$ on the absorber temperature is neglected, although the heat gain $\dot{q}_{useful}$ results in small temperature difference between fluid and absorber temperatures, depending on the internal thermal heat transfer coefficient $U_{AbsFluid}$. Secondly, we neglect the temperature increase of the fluid temperature in direction of fluid flow.

The overall heat transfer coefficient of the heat dissipator $(UA)_{external}$ has to be dimensioned, so that the collector heat gain $Q_{gain,Coll}$ is reliably dissipated to the environment. During steady-state conditions, the collector heat gain $Q_{gain,coll}$ equals the dissipated heat of the heat dissipator $Q_{external}$:

$$Q_{gain,coll} = Q_{external} \tag{D.3}$$

The collector heat gain is influenced significantly by the total collector area A_{coll} and the thermal efficiency at the maximum fluid temperature $\eta_{th}(T_{m,max})$, while the dissipated heat $Q_{external}$ is a function of the temperature difference and the UA-value of the heat dissipator:

$$G\ A_{coll}\ \eta_{th}(T_{m,max}) = (UA)_{external}(T_m - T_a) \tag{D.4}$$

Solving Eq. (D.4) to the mean fluid temperature T_m leads to:

$$T_m = T_a + G\ \eta_{th}(T_{m,max})\frac{A_{coll}}{(UA)_{external}} \tag{D.5}$$

Evaluating Eq. (D.5) for varying values of $\eta_{th,Stag}$ leads to the nomogram in Figure D.6. Every curve stands for one collector type with a specific thermal efficiency during stagnation $\eta_{th,Stag.}$ The reduction of the mean fluid temperature can be read from the y-axis from the difference between the respective values of $(UA)_{external}/A_{coll}$ in normal operation and in stagnation.

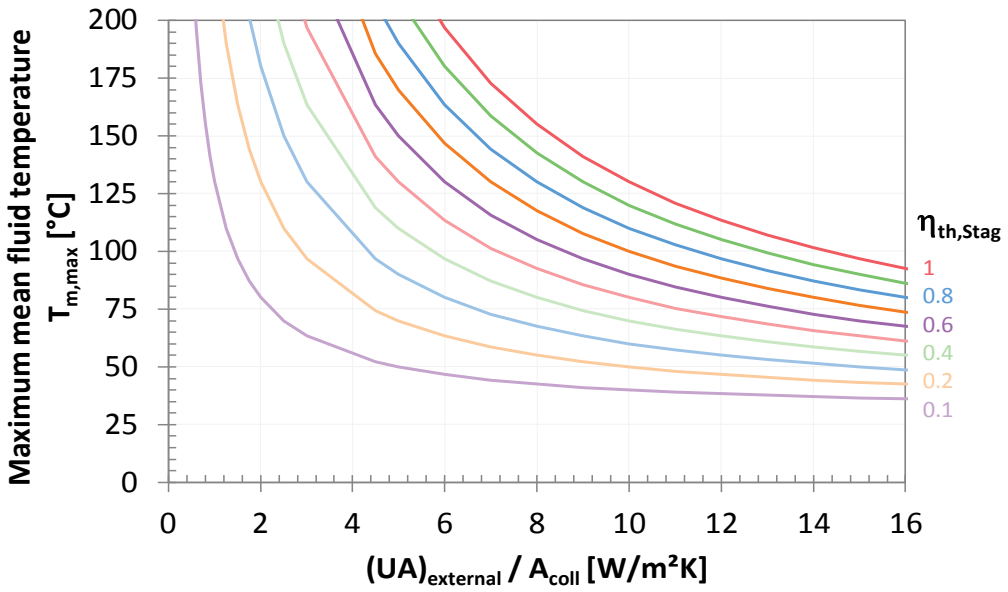

Figure D.6: Nomogram for preliminary dimensioning an overheating protection by reducing $T_{fluid,mean}$. Maximum mean fluid temperatures are given for G = 1000 W/m², T_a = 30 °C without considering a security margin for T_{abs} with respect to difference between absorber and fluid temperature and temperature increase in direction of fluid flow.

D.1.4 Increase of c_{eff}

OHP category 4 aims at buffering high absorber temperatures by increasing the effective capacity c_{eff}. For this purpose, heat is stored in thermal masses coupled to the collector, e.g. phase change materials or integrated collector storage. The effective capacity c_{eff} comprises the central design parameter of OHP category 4.

The steady-state efficiency curve is not altered by an increase of thermal capacity. Instead, the collector dynamics have to be considered. The dynamic energy balance of the two-node model according to Figure D.1 is expressed as:

$$c_{eff}\frac{dT_{abs}}{dt} = G[(\tau\alpha)_{eff} - \eta_{el}] - U_{Loss}(T_{abs} - T_a) \qquad (D.6)$$

This differential equation describes the dynamic temperature variation. The maximum absorber temperatures $T_{abs,max}$ cannot be solved explicitly, but have to be calculated from the temporal distribution of G and T_a of a characteristic day. We now look at a hot and high-irradiance summer day for the location of Würzburg. In fact, this is the worst-case scenario day with the highest annual absorber temperatures of a collector in permanent stagnation.

shows the resulting absorber temperatures in permanent stagnation of three PVT collectors with varying effective capacities c_{eff}. For the example, we assume constant values of U_{Loss} = 6 W/m²K and $(\tau\alpha)_{eff} - \eta_{el}$ = 0.72, corresponding to a glazed PVT collector with low-e.

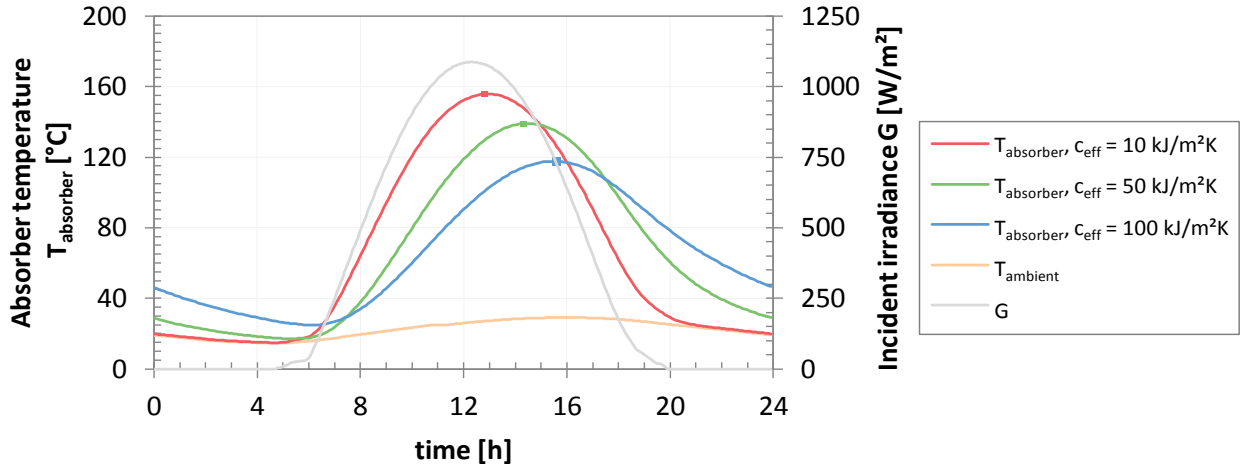

Figure D.7: Temperature distribution of three types of PVT collectors with varying c_{eff} during permanent stagnation on a hot summer day in Würzburg. The maximum absorber temperatures for each c_{eff} are indicated by the colored data point.

Evaluating the maximum absorber temperatures in the same way for varying effective capacity c_{eff} leads to the nomogram in Figure D.8. We varied the collector technology by a parameter variation of U_{Loss}. Thus, every curve stands for one collector type with a specific heat loss coefficient $U_{Loss.}$ The maximum absorber temperatures as function of c_{eff} and U_{Loss} can be read from the y-axis.

To give an example, a typical value of the effective capacity of a PVT collector without PCM amounts to c_{eff} = 10 kJ/m²K. This collector reaches a maximum absorber temperature of T_{abs} = 160 °C. An effective capacity of c_{eff} = 50 kJ/m²K would be required to limit absorber temperatures below T_{abs} < 140 °C. The thermal characteristics of a typical, paraffin-based PCM features a thermal capacity of c_p = 2 kJ/kgK and a heat storage capacity of h_{stor} = 200 kJ/kg. To achieve the required effective capacity of 50 kJ/m²K, approximately 10 kg/m² of PCMs would be required.

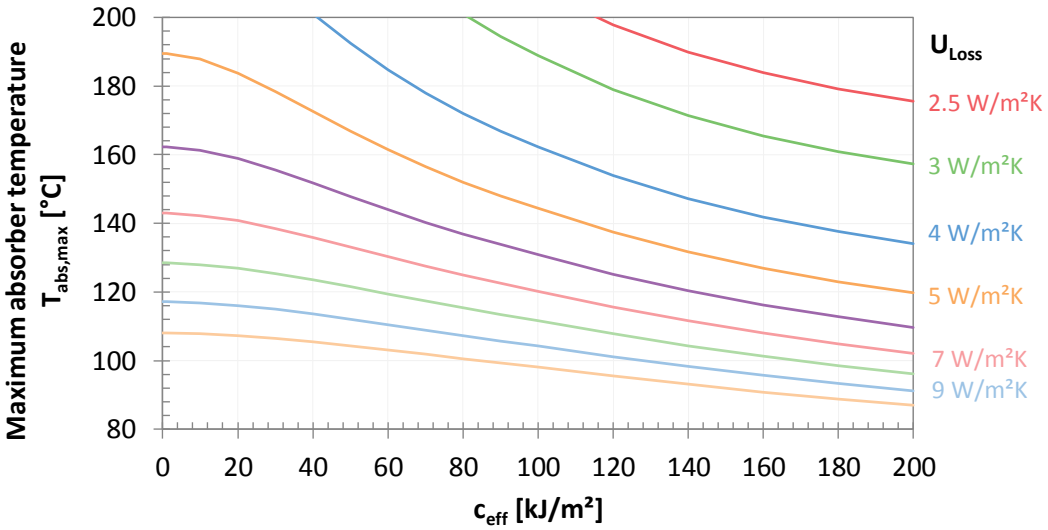

Figure D.8: Nomogram for preliminary dimensioning an overheating protection by increasing the effective capacity c_{eff}. Maximum absorber temperatures are given for a worst-case day in Würzburg without considering a security margin for T_{abs} with respect to a non-uniform temperature distribution.

BIBLIOGRAPHY

Abu Bakar, Mohd Nazari; Othman, Mahmod; Hj Din, Mahadzir; Manaf, Norain A.; Jarimi, Hasila (2014): Design concept and mathematical model of a bi-fluid photovoltaic/thermal (PV/T) solar collector. Renewable Energy 67, pp. 153–164. DOI: 10.1016/j.renene.2013.11.052.

Adam, Mario; Kramer, Korbinian; Fritzsche, Ulrich; Hamberger, Stephan (2014a): Abschlussbericht PVT-Norm. Förderkennzeichen 01FS12035 -„Verbundprojekt: Standardisierung und Normung von multifunktionalen PVT Solarkollektoren (PVT-Norm), Teilvorhaben Betrachtung Normentwurf und Systemintegration aus Herstellersicht, Information über Notwendigkeit der Norm".

Adam, Mario; Wirth, Hans Peter; Radosavljevic, Rada (2014b): Verbundprojekt: Standardisierung und Normung von multifunktionalen PVT Solarkollektoren (PVT-Norm). Projektbericht der FH Düsseldorf.

Affolter (2000): New Generation of Hybrid Solar PV_T Collectors. LESO_PB/EPFL, Lausanne.

Assoa, Y. B.; Menezo, C.; Fraisse, G.; Yezou, R.; Brau, J. (2007): Study of a new concept of photovoltaic–thermal hybrid collector. Solar Energy 81 (9), pp. 1132–1143. DOI: 10.1016/j.solener.2007.04.001.

Aste, Niccolò; del Pero, Claudio; Leonforte, Fabrizio (2014): Water flat plate PV–thermal collectors: A review. Solar Energy 102, pp. 98–115. DOI: 10.1016/j.solener.2014.01.025.

ASTM (2008): ASTM G173-03 - Tables for Reference Solar Spectral Irradiances: Direct Normal and Hemispherical on 37 Tilted Surface. DOI: 10.1520/G0173-03R08.

Baer, Stephen (1984): Thermal Control System For Solar Collector - US4528976.

BAFA (2015): Richtlinien zur Förderung von Maßnahmen zur Nutzung erneuerbarer Energien im Wärmemarkt. Fassung vom 11. März 2015. Bundesamt für Wirtschaft und Ausfuhrkontrolle.

Bakker, M.; Zondag, H. A.; Elswijk, M. J.; Strootman, K. J.; Jong, M.J.M. (2005): Performance and costs of a roof-sized PV/thermal array combined with a ground coupled heat pump. Solar Energy 78 (2), pp. 331–339. DOI: 10.1016/j.solener.2004.09.019.

BDEW (2017a): BDEW-Heizkostenvergleich Altbau 2017 - Ein Vergleich der Gesamtkosten verschiedener Systeme zur Heizung und Warmwasserbereitung in Altbauten. Bundesverband der Energie- und Wasserwirtschaft e.V.

BDEW (2017b): BDEW-Strompreisanalyse Mai 2017 - Haushalte und Industrie - Berlin 31. Mai 2017. Bundesverband der Energie- und Wasserwirtschaft e.V.

Becker, Rainer; Rommel, Matthias; Wittwer, Christof (2006): Regelungstechnische Untersuchungen zur Vermeidung von Stillstanddssituationen bei großen solarthermischen Anlagen. Tagungsband 16. Symposium Thermische Solarenergie 2006. Bad Staffelsein: OTTI-Kolleg.

Beikircher, T.; Goldemund, G.; Benz, N. (1996): Gas heat conduction in an evacuated tube solar collector. Solar Energy 58 (4-6), pp. 213–217. DOI: 10.1016/S0038-092X(96)00065-5.

Beikircher, Th.; Osgyan, P.; Fischer, S.; Drück, H. (2014): Short-term efficiency test procedure for solar thermal collectors based on heat loss measurements without insolation and a novel conversion towards daytime conditions. Solar Energy 107, pp. 653–659. DOI: 10.1016/j.solener.2014.06.009.

Benson, D. K.; Potter, T. F.; Tracy, C. E. (1994): Design of a Variable-Conductance Vacuum Insulation. NREL/TP-452-5814. Proceedings of the SAE 1994 Annual Meeting.

Benz, N.; Beikircher, T. (1999): High efficiency evacuated flat-plate solar collector for process steam production. Solar Energy 65 (2), pp. 111–118. DOI: 10.1016/S0038-092X(98)00122-4.

Bertram, Erik; Glembin, Jens; Rockendorf, Gunter (2012): Unglazed PVT collectors as additional heat source in heat pump systems with borehole heat exchanger. Energy Procedia 30, pp. 414–423. DOI: 10.1016/j.egypro.2012.11.049.

Bilbao, J. I.; Sproul, A. B. (2015): Detailed PVT-water model for transient analysis using RC networks. Solar Energy 115, pp. 680–693. DOI: 10.1016/j.solener.2015.03.003.

Böhm, Frederik Gero (2015): Modellierung und dynamische Simulation eines abgedeckten PVT-Kollektors in Dymola/Modelica. Masterarbeit, RWTH Aachen, E.ON Energy Research Center, Fraunhofer ISE.

Bouzoukas, Asterios (2008): New Approaches for Cooling Photovoltaic/Thermal (PV/T) Systems. Dissertation at University of Nottingham.

Boyle, Richard; Williams, Christophe; Cottington, Norman (2012): Hybrid solar collector - US 20120318328 A1. United States Patent.

Butler, Barry Lynn (2002): US7913684 - Solar heat transfer system high temperature pressurized loop - US patent.

Cadafalch, J. (2002): An overheating protection system for flat plat solar collectors with transparent insulation. Proceedings of Eurosun, Lisbon, Portugal.

Cartmell, B.P; Shankland, N.J; Fiala, D.; Hanby, V. (2004): A multi-operational ventilated photovoltaic and solar air collector: application, simulation and initial monitoring feedback. Solar Energy 76 (1-3), pp. 45–53. DOI: 10.1016/j.solener.2003.08.037.

Çengel, Yunus A.; Ghajar, Afshin J. (2015): Heat and mass transfer. Fundamentals & applications. Fifth edition. New York, N.Y.: McGraw-Hill Education.

Charalambous, P. G.; Maidment, G. G.; Kalogirou, S. A.; Yiakoumetti, K. (2007): Photovoltaic thermal (PV/T) collectors: A review. Applied Thermal Engineering 27 (2-3), pp. 275–286. DOI: 10.1016/j.applthermaleng.2006.06.007.

Chow, T. T. (2003): Performance analysis of photovoltaic-thermal collector by explicit dynamic model. Solar Energy 75 (2), pp. 143–152. DOI: 10.1016/j.solener.2003.07.001.

Chow, T. T. (2010): A review on photovoltaic/thermal hybrid solar technology. Applied Energy 87 (2), pp. 365–379. DOI: 10.1016/j.apenergy.2009.06.037.

Collins, Mike; Zondag, H. A. (2008): Recommended Standard for Characterization and Monitoring of PV/Thermal Systems. A technical teport of IEA SHC - Task 35 PV/Thermal Solar Systems Report DB2. IEA SHC Task 35.

Coventry, Joseph Sydney (2004): A solar concentrating photovoltaic / thermal collector. Australian National University.

Cox, C. H.; Raghuraman, P. (1985): Design considerations for flat-plate-photovoltaic/thermal collectors. Solar Energy 35 (3), pp. 227–241. DOI: 10.1016/0038-092X(85)90102-1.

Cummings, R. D. (1977): Temperature control in solar-to-thermal energy converters - US 4102325 A. United States Patent.

da Silva, R. M.; Fernandes, J.L.M. (2010): Hybrid photovoltaic/thermal (PV/T) solar systems simulation with Simulink/Matlab. Solar Energy 84 (12), pp. 1985–1996. DOI: 10.1016/j.solener.2010.10.004.

Delisle, Véronique; Kummert, Michaël (2014): A novel approach to compare building-integrated photovoltaics/thermal air collectors to side-by-side PV modules and solar thermal collectors. Solar Energy 100, pp. 50–65. DOI: 10.1016/j.solener.2013.09.040.

Di Su; Jia, Yuting; Alva, Guruprasad; Liu, Lingkun; Fang, Guiyin (2017): Comparative analyses on dynamic performances of photovoltaic–thermal solar collectors integrated with phase change materials. Energy Conversion and Management 131, pp. 79–89. DOI: 10.1016/j.enconman.2016.11.002.

DIN (1982): DIN 4757-4:1982-07 - Solarthermische Anlagen - Teil 4: Sonnenkollektoren; Bestimmung von Wirkungsgrad, Wärmekapazität und Druckabfall.

DIN EN (2012): DIN EN 12977-2:2012-06. Thermische Solaranlagen und ihre Bauteile - Kundenspezifisch gefertigte Anlagen - Teil 2: Prüfverfahren für solar betriebene Warmwasserbereiter und Kombinationssysteme.

DIN V 18599-1, 2013: DIN V 18599-1 Berichtigung 1:2013-05 Titel (deutsch): Energetische Bewertung von Gebäuden - Berechnung des Nutz-, End- und Primärenergiebedarfs für Heizung, Kühlung, Lüftung, Trinkwarmwasser und Beleuchtung - Teil 1: Allgemeine Bilanzierungsverfahren, Begriffe, Zonierung und Bewertung der Energieträger, Berichtigung zu DIN V 18599-1:2011-12.

Dittmann, Sebastian; Friesen, Thomas; Frontin, Francesco; Bohren, Andreas; Zenhäusern, Daniel; Rommel, Matthias (2014): Indoor and Outdoor Testing of an Unglazed PVT Collector.

Drück, Harald (2006): Multiport Store - Model for TRNSYS - Type 340. Institut für Thermodynamik und Wärmetechnik (ITW), Universität Stuttgart.

Du, Dengfeng; Darkwa, Jo; Kokogiannakis, Georgios (2013): Thermal management systems for Photovoltaics (PV) installations: A critical review. Solar Energy 97, pp. 238–254. DOI: 10.1016/j.solener.2013.08.018.

Duffie, John A.; Beckman, William A. (2013): Solar engineering of thermal processes. Fourth Edition: John Wiley & Sons.

Dupeyrat, P.; Hermann, Michael; Graf, Wolfgang; Wilson, Helen Rose; Kuhn, Tilmann E. (2011a): Investigation of the effective transmittance-absorptance product of solar thermal collectors regarding recent improvements of glazing and absorber spectral properties. Proceedings of ISES Solar World Congress, Kassel.

Dupeyrat, P.; Ménézo, C.; Fortuin, S. (2014): Study of the thermal and electrical performances of PVT solar hot water system. Energy and Buildings 68, pp. 751–755. DOI: 10.1016/j.enbuild.2012.09.032.

Dupeyrat, Patrick (2011a): Experimental development and simulation investigation of a Photovoltaic-Thermal hybrid solar collector. INSA de Lyon, France. L'Institut National des Sciences Appliquées de Lyon.

Dupeyrat, Patrick (2011b): Thermal collector and PVT collector - Patent EP 2565554 A1 on 9/2/2011.

Dupeyrat, Patrick; Ménézo, Christophe; Rommel, Matthias; Henning, Hans-Martin (2011b): Efficient single glazed flat plate photovoltaic–thermal hybrid collector for domestic hot water system. Solar Energy 85 (7), pp. 1457–1468. DOI: 10.1016/j.solener.2011.04.002.

Dupeyrat, Patrick; Ménézo, Christophe; Wirth, Harry; Rommel, Matthias (2011c): Improvement of PV module optical properties for PV-thermal hybrid collector application. Solar Energy Materials and Solar Cells 95 (8), pp. 2028–2036. DOI: 10.1016/j.solmat.2011.04.036.

Dursun, Aylin; Rekstad, J.; Meir, M. (2014): Partly Glazed Solar Collectors as a new method for preventing overheating. Proceedings of Gleisdorf Solar 2014.

DVGW (2004): Arbeitsblatt W 551 2004-4 - Trinkwassererwärmungs- und Trinkwasserleitungsanlagen; Technische Maßnahmen zur Verminderung des Legionellenwachstums; Planung, Errichtung, Betrieb und Sanierung von Trinkwasser-Installationen. Deutscher Verein des Gas- und Wasserfaches.

Eicker, Ursula (2012): Solare Technologien für Gebäude. Grundlagen und Praxisbeispiele. 2., vollständig überarbeitete Auflage. Wiesbaden: Vieweg+Teubner Verlag / Springer Fachmedien Wiesbaden GmbH, Wiesbaden.

Eicker, Ursula; Dalibard, Antoine (2011): Photovoltaic–thermal collectors for night radiative cooling of buildings. Solar Energy 85 (7), pp. 1322–1335. DOI: 10.1016/j.solener.2011.03.015.

Eltermann, Fabian; Roeder, Kerstin; Wiesenfarth, Maike; Wilde, Juergen; Bett, Andreas W. (2012): Degradation study on optical materials for concentrator photovoltaics. AIP Conference Proceedings, pp. 276–280. DOI: 10.1063/1.4753885.

EN ISO 9488 (1999): EN ISO 9488:1999 - Solar energy - Vocabulary.

EPA, Council (2010): Directive 2010/31/EU of the European Parliament and of the Council of 19 May 2010 on the energy performance of buildings. Official Journal of the European Union.

Faiman, David (2008): Assessing the outdoor operating temperature of photovoltaic modules. Prog. Photovolt: Res. Appl. 16 (4), pp. 307–315. DOI: 10.1002/pip.813.

Fischer, David; Härtl, Andreas; Wille-Haussmann, Bernhard (2015): Model for electric load profiles with high time resolution for German households. Energy and Buildings 92, pp. 170–179. DOI: 10.1016/j.enbuild.2015.01.058.

Fischer, S.; Heidemann, W.; Müller-Steinhagen, H.; Perers, B.; Bergquist, P.; Hellström, B. (2004): Collector test method under quasi-dynamic conditions according to the European Standard EN 12975-2. Solar Energy 76 (1-3), pp. 117–123. DOI: 10.1016/j.solener.2003.07.021.

Fischer, Stephan (2011): Dynamische Prüfung von Sonnenkollektoren unter besonderer Berücksichtigung der Einfallswinkelkorrektur und der Reduzierung der Prüfdauer. Universität Stuttgart. Institut für Thermodynamik und Wärmetechnik (ITW).

Fischer, Stephan; Müller-Steinhagen, H. (2009): Collector efficiency testing - the 2-node collector model ready for implementation in European Standard EN 12975. Proceedings ISES Solar World Congress.

Fischer, Stephan; Sommer, K.; Drück, H.; Gillmann, Steffen (2016): Innovativer PVT-Kollektor mit variabel steuerbarer elektrischer und thermischer Leistung. Tagungsband 26. Symposium Thermische Solarenergie 2016. Bad Staffelsein: OTTI-Kolleg.

Florschuetz, L. W. (1979): Extension of the Hottel-Whillier model to the analysis of combined photovoltaic/thermal flat plate collectors. Solar Energy 22 (4), pp. 361–366. DOI: 10.1016/0038-092X(79)90190-7.

Fortuin, Stefan; Hermann, Michael; Stryi-Hipp, Gerhard; Nitz, Peter; Platzer, Werner (2014): Hybrid PV-thermal Collector Development: Concepts, Experiences, Results and Research Needs. Energy Procedia 48, pp. 37–47. DOI: 10.1016/j.egypro.2014.02.006.

Föste, S.; Giovannetti, F.; Reineke-Koch, R. (2013): Hocheffiziente Flachkollektoren mit selektiv beschichteten Zweischeibenverglasungen. Abschlussbericht - Kurzbezeichnung: „HFK Low-e". Institut für Solarenergieforschung GmbH Hameln / Emmerthal.

Föste, Sebastian; Pazidis, Alexandra; Reineke-Koch, Rolf; Hafner, Bernd; Mercs, David; Delord, Christine (2016): Flat Plate Collectors with Thermochromic Absorber Coatings to Reduce Loads During Stagnation. Energy Procedia 91, pp. 42–48. DOI: 10.1016/j.egypro.2016.06.169.

Fraisse, G.; Ménézo, C.; Johannes, K. (2007): Energy performance of water hybrid PV/T collectors applied to combisystems of Direct Solar Floor type. Solar Energy 81 (11), pp. 1426–1438. DOI: 10.1016/j.solener.2006.11.017.

Frank, Elimar; Mauthner, Franz; Fischer, Stephan (2014): Overheating prevention and stagnation handling in solar process heat applications. Technical Report A.1.2. IEA SHC Task 49.

Frick, Steffen (2014): Kostenanalyse und Fertigungsoptimierung von Polymerkollektoren für den globalen Markt. Proceedings of Gleisdorf Solar 2014.

Fritzsche, Ulrich; Althaus, Jörg; Bott, Matthias (2014): Qualification of PVT Collectors - Current Status. Proceedings of Eurosun 2014, Aix-Les-Bains.

Georg, Andreas; Graf, Wolfgang; Schweiger, Dietmar; Wittwer, Volker; Nitz, Peter; Wilson, Helen Rose (1998): Switchable glazing with a large dynamic range in total solar energy transmittance (TSET). Solar Energy 62 (3), pp. 215–228. DOI: 10.1016/S0038-092X(98)00014-0.

Georg, Andreas; Siefert, Wolfgang; Heintze, Moritz; Belardi, Jacobi (2017): Verbundprojekt follow-e: Energiesparende funktionelle Beschichtungen von Polymermaterialien für die Folienarchitektur-Abschlussbericht Fraunhofer ISE, Trumpf Hüttinger, Rowo Coating, Dunmore Europe.

Gillmann, Steffen (2010): DE102010019158A1 - Solarkollektor. Deutsches Patent.

Giovannetti, F.; Föste, S.; Ehrmann, N.; Rockendorf, G. (2014): High transmittance, low emissivity glass covers for flat plate collectors: Applications and performance. Solar Energy 104, pp. 52–59. DOI: 10.1016/j.solener.2013.10.006.

Glaser, Siegfrid; Kübler, Rainer; Graf, Wolfgang; Weinläder, Helmut (2016): Abschlussbericht zum Verbundprojekt "Flexibler Randverbund für Vakuumisolierglas-Systeme (VIG-S). Förderkennzeichen 03ET1147.

Goetzberger, A.; Hoffmann, Volker U. (2005): Photovoltaic solar energy generation. Berlin, New York: Springer.

Gomes, João; Bastos, Silvio; Henriques, Mafalda; Diwan, Linkesh; Olsson, Olle (2015): Evaluation of the Impact of Stagnation Temperatures in Different Prototypes of Low Concentration PVT Solar Panels. Proceedings of ISES Solar World Congress 2015, Daegu.

Góngora-Gallardo, G.; Castro-Gil, M.; Colmenar-Santos, A.; Tawfik, Mohamed (2013): Efficiency factors of solar collectors of parallel plates for water. Solar Energy 94, pp. 335–343. DOI: 10.1016/j.solener.2013.05.014.

Good, Clara; Andresen, Inger; Hestnes, Anne Grete (2015): Solar energy for net zero energy buildings – A comparison between solar thermal, PV and photovoltaic–thermal (PV/T) systems. Solar Energy 122, pp. 986–996. DOI: 10.1016/j.solener.2015.10.013.

Greppi, Matteo (2013): Numerical optimization,modeling and system evaluation of a thermophotovoltaic hybrid panel. Dissertation at university of Bologa.

Grote, Karl-Heinrich; Feldhusen, Jörg (2011): Dubbel. Berlin, Heidelberg: Springer Berlin Heidelberg.

Haedrich, Ingrid; Eitner, Ulrich; Wiese, Martin; Wirth, Harry (2014): Unified methodology for determining CTM ratios: Systematic prediction of module power. Solar Energy Materials and Solar Cells 131, pp. 14–23. DOI: 10.1016/j.solmat.2014.06.025.

Haller, Michael; Perers, Bengt; Bale, Chris; Paavilainen, Janne; Dalibard, Antoine; Fischer, Stefan; Bertram, Erik (2012): TRNSYS Type 832 v5. 00 „Dynamic Collector Model by Bengt Perers": Updated Input-Output Reference.

Harrison, S. J.; Lin, Q.; Mesquita, L. C.; Valletta, D. A. (2004): Method and apparatus for solar collector with integral stagnation temperature control - WO 2004070289 A1. Patent.

Harrison, Stephen; Cruickshank, Cynthia A. (2012): A review of strategies for the control of high temperature stagnation in solar collectors and systems. Energy Procedia 30, pp. 793–804. DOI: 10.1016/j.egypro.2012.11.090.

Haurant, Pierrick; Ménézo, Christophe; Gaillard, Leon; Dupeyrat, Patrick (2015): Dynamic numerical model of a high efficiency PV–T collector integrated into a domestic hot water system. Solar Energy 111, pp. 68–81. DOI: 10.1016/j.solener.2014.10.031.

Hausner, Robert; Fink, Christian; Wagner, Waldemar; Riva, Richard; Hillerns, Frank (2003): Entwicklung von thermischen Solarsystemen mit unproblemantischen Stagnationsverhalten. Abschlussbericht. AEE INTEC, Institut für Nachhaltive Technologien.

Heimrath, Richard; Haller, Michel (2007): The reference heating system, the template solar system of Task 32. A report of IEA Solar Heating and Cooling programme–Task 32.

Helbig, Sonja; Mercker, Oliver (2017): Wärmeversorgungssysteme im Mehrfamilienhaus. Tagungsband 27. Symposium Thermische Solarenergie 2017. Bad Staffelsein: OTTI-Kolleg.

Helmers, Henning; Bett, Andreas W.; Parisi, Jürgen; Agert, Carsten (2012): Modeling of concentrating photovoltaic and thermal systems. Progress in Photovoltaics: Research and Applications, pp. n/a. DOI: 10.1002/pip.2287.

Helmers, Henning; Kramer, Korbinian (2013): Multi-linear performance model for hybrid (C)PVT solar collectors. Solar Energy 92, pp. 313–322. DOI: 10.1016/j.solener.2013.03.003.

Helmers, Henning; Thor, Wei Yi; Schmidt, Thomas; van Rooyen, De Wet; Bett, Andreas W. (2013): Optical analysis of deviations in a concentrating photovoltaics central receiver system with a flux homogenizer. Applied optics 52 (13), pp. 2974–2984. DOI: 10.1364/AO.52.002974.

Helminger, Franz (2012): Summary report on stagnation temperature determination (R2:19). Qaist - Quality Assurance in solar thermal heating and cooling technology. ESTIF.

Hengstberger, Florian; Zauner, Christoph; Resch, Katharina; Holper, Stefan; Grobbauer, Michael (2016): High temperature phase change materials for the overheating protection of facade integrated solar thermal collectors. Energy and Buildings 124, pp. 1–6. DOI: 10.1016/j.enbuild.2016.04.020.

Henning, Hans-Martin; Nunez, Tomas; Dupeyrat, Patrick; Henninger, Stefan (2011): Solarthermischer Kollektor - Patent DE102011112974 B3.

Hermann, Michael (2005): Bionische Ansätze zur Entwicklung energieeffizienter Fluidsysteme für den Wärmetransport. Universität Karlsruhe. Fachgebiet Strömungsmaschinen.

Heß, Stefan (2014): Low-Concentrating, Stationary Solar Thermal Collectors for Process Heat Generation. Dissertation. De Montfort University Leicester, Freiburg. Institute of Energy and Sustainable Development IESD.

Heydenreich, Wolfgang; Müller, Björn; Reise, Christian (2008): Describing the world with three parameters: a new approach to PV module power modelling. Proceedings of the 23rd European Photovoltaic Solar Energy Conference and Exhibition, September 1–5, 2008, Valencia, Spain.

Hofmann, P.; Dupeyrat, P.; Kramer, K.; Hermann, M.; Stryi-Hipp, G. (2010): Measurements and benchmark of PV-T collectors according to EN 12975 and development of a standardized measurement procedure. Proceedings of EuroSun, Graz, Austria.

Hollands, K. G. T.; Konicek, L.; Raithby, G. D.; Unny, T. E. (1976): Free Convective Heat Transfer Across Inclined Air Layers. J. Heat Transfer 98 (2), p. 189. DOI: 10.1115/1.3450517.

Hussain, Shafqat; Harrison, Stephen J. (2015): Experimental and numerical investigations of passive air cooling of a residential flat-plate solar collector under stagnation conditions. Solar Energy 122, pp. 1023–1036. DOI: 10.1016/j.solener.2015.10.029.

IEA (2012): Technology Roadmap Solar Heating and Cooling. International Energy Agency.

IEC 60812 (2006): IEC 60812:2006(E) - Analysis techniques for system reliability - Procedure for failure-mode and effects analysis (FMEA). International Electrotechnical Commission.

IEC 60904 (2006): IEC 60904-1:2006 - Photovoltaic devices - Part 1: Measurement of photovoltaic current-voltage characteristics. International Electrotechnical Commission.

IEC 61853 (2011): IEC 61853-1:2011 Photovoltaic (PV) module performance testing and energy rating - Part 1: Irradiance and temperature performance measurements and power rating. International Standard.

Ille, Fabian; Adam, Mario; Radosavljevic, Radojka; Wirth, Hans Peter (2014): Market and simulation analysis of PVT applications for the determination of new PVT test procedures. EuroSun 2014, ISES Conference Proceedings. DOI: 10.18086/eurosun.2014.16.09.

IPCC (2014): Climate change 2014: Synthesis Report. Contribution of Working Groups I, II and III to the Fifth Assessment Report of the Intergovernmental Panel on Climate Change. With assistance of R. K. Pachuari, L. Meyer. Geneva, Switzerland: Intergovernmental Panel on Climate Change.

IPCC (2015): Climate change 2014 : Mitigation of climate change. Summary for Policymakers and Technical summary. With assistance of O. Edenhofer, R. Richs-Madruga, Sokona Y. Geneva: Intergovernmental Panel on Climate Change.

ISO 9806 (2013): ISO 9806:2013 Solar energy - Solar thermal collectors - Test methods.

ISO 9806 (2017): ISO 9806:2017 Solar energy - Solar thermal collectors - Test methods.

ISO/FDIS 22975-2 (2014): Solar energy - Collector components and materials - Part 3: Absorber surface durability.

ITRPV (2017): International Technology Roadmap for Photovoltaic - Eight Edition, March 2017.

Jack, Steffen; Parzefall, Johannes; Luttmann, Thomas; Janßen, Philipp; Giovannetti, Federico (2014): Flat Plate Aluminum Heat Pipe Collector with Inherently Limited Stagnation Temperature. Energy Procedia 48, pp. 105–113. DOI: 10.1016/j.egypro.2014.02.013.

Jack, Steffen; Rockendorf, G. (2013): Wärmerohre in Sonnenkollektoren - Wärmetechnische Grundlagen und Bewertung sowie neue Ansätze zur Integration. Abschlussbericht zum Vorhaben Kurzbezeichnung: HP-Opt. Institut für Solarenergieforschung GmbH Hameln / Emmerthal.

Jelle, Bjørn Petter; Kalnæs, Edsjø; Gao, Tao (2015): Low-Emissivity Materials for Building Applications: A State-of-the-Art Review and Future Research Perspectives. Energy and Buildings.

Jordan, Ulrike; Vajen, Klaus (2005): DHWcalc: Program to generate domestic hot water profiles with statistical means for user defined conditions. Proceedings of the ISES Solar 2005, pp. 8–12.

Kalogirou, S. A.; Tripanagnostopoulos, Y. (2006): Hybrid PV/T solar systems for domestic hot water and electricity production. Energy Conversion and Management 47 (18-19), pp. 3368–3382. DOI: 10.1016/j.enconman.2006.01.012.

Karrer, Hanne; Pröll, Markus (2015): Thermische Anbindung von PV Zellen in einem CPC PVT Kollektor. Tagungsband 25. Symposium Thermische Solarenergie 2015. Bad Staffelsein: OTTI-Kolleg.

Kearney, Meghan; Davidson, Jane; Mantell, Susan (2005): Polymeric Absorbers for Flat-Plate Collectors: Can Venting Provide Adequate Overheat Protection? Journal of Solar Energy Engineering 127 (3), pp. 421–424.

Kessentini, Hamdi (2014): Numerical and experimental study of a flat plate collector with honeycomb transparent insulation and overheating protection system. Doctoral Thesis. Universitat Politècnica de Catalunya, Barcelona, checked on 5/19/2015.

King, D.L; Boyson, W. E.; Kratochvilll, J.A (2004): Photovoltaic Array Performance Model. Report SAND2004-3535. Sandia National Laboratories.

King, David L.; Kratochvil, Jay A.; Boyson, William E. (1997): Temperature coefficients for PV modules and arrays: measurement methods, difficulties and results. Proceedings of the 26 th IEEE PVSC, pp. 1183–1186.

Klein, S.A.; Beckman, W.A.; Mitchell, J.W.; Duffie, John A. (2015): TRNSYS, a transient system simulation program, version 17.02.

Klier, S. (2013): Overheat protection mechanism for solar thermal collector - WO 2012110916 A3. Patent.

Koch, Lotta; Hermann, Michael; Bauch, Maximilian (2012): Investigation of new integrated solar thermal absorbers by means of a 2-D model. Proceedings of Eurosun 2012, Rijeka, Croatia.

Koch, Lotta; Hermann, Michael; Jerg, Carmen; Kennemann, Franziska (2015): SAPRES - Herstellung von Solarabsorbern im Hohlpräge-Steckziehverfahren. Förderkennzeichen 0325989A/B.

Koehl, Michael; Heck, Markus; Wiesmeier, Stefan; Wirth, Jochen (2011): Modeling of the nominal operating cell temperature based on outdoor weathering. Solar Energy Materials and Solar Cells 95 (7), pp. 1638–1646. DOI: 10.1016/j.solmat.2011.01.020.

Köhl, M. (2015): Exkoll - Konzeption von extrudierten Polymerkollektoren und Komponenten. Abschlussbericht, Fraunhofer ISE.

Koke, Johannes; Clement, Uwe (2016): Software in a loop - Polysun und Matlab zur Optimierung solarthermischer Systeme. 1. Internationale Konferenz zur Simulation gebäudetechnischer Energiesyste, SIGES 2016.

Konetsu, S. L.; Torrens, Rasal (2004): Sistema de colectores solares planos - WO 2004092660 A1 - US Patent.

Konstantin, Panos (2009): Praxisbuch Energiewirtschaft. Berlin, Heidelberg: Springer Berlin Heidelberg.

Köntges, Marc; Kurtz, Sarah; Packard, Corinne; Jahn, Ulrike; Berger, Karl A.; Kato, Kazuhiko (2014): Performance and reliability of photovoltaic systems. Subtask 3.2: Review of failures of photovoltaic modules : IEA PVPS task 13 : external final report IEA-PVPS. Sankt Ursen: International Energy Agency Photovoltaic Power Systems Programme.

Kramer, Korbinian; Helmers, Henning (2013): The interaction of standards and innovation: Hybrid photovoltaic–thermal collectors. Solar Energy 98, Part C, pp. 434–439. DOI: 10.1016/j.solener.2013.08.042.

Kramer, Wolfgang; Bohrer, Jan; Bitterling, Moritz (2017): Künstliche neuronale Netzwerke für die Anwendung in der Solarthermie. Tagungsband 27. Symposium Thermische Solarenergie 2017. Bad Staffelsein: OTTI-Kolleg.

Kurtz, Sarah; Whitfield, Kent; TamizhMani, G.; Koehl, Michael; Miller, David; Joyce, James et al. (2011): Evaluation of high-temperature exposure of photovoltaic modules. Prog. Photovolt: Res. Appl. 19 (8), pp. 954–965. DOI: 10.1002/pip.1103.

Kusyy, O.; Vajen, K. (2011): Theoretical investigation on a control-based approach to avoid stagnation of solar heating systems. Proceedings of ISES Solar World Congress, Kassel.

Lämmle, Manuel; Hermann, Michael (2015): Thermisches Management von PVT-Kollektoren - Ergebnisse aus Systemsimulationen. Tagungsband 25. Symposium Thermische Solarenergie 2015. Bad Staffelsein: OTTI-Kolleg.

Lämmle, Manuel; Jäger, Helmut; Hermann, Michael; Thoma, Christoph; Mülhöfer, Georg; Wiese, Martin et al. (2017a): PVTgen2 - Entwicklung und Pilotfertigung eines abgedeckten Photovoltaisch-thermischen Hybrid-Kollektors der zweiten Generation mit verbesserter thermischer Leistungsfähigkeit. Abschlussbericht - Teilprojekt Fraunhofer ISE. Fraunhofer Institut für Solare Energiesysteme ISE.

Lämmle, Manuel; Kroyer, Thomas; Fortuin, Stefan; Wiese, Martin; Hermann, Michael (2016a): Development and modelling of highly-efficient PVT collectors with low-emissivity coatings. Solar Energy (130), pp. 161–173. DOI: 10.1016/j.solener.2016.02.007.

Lämmle, Manuel; Oliva, Axel; Hermann, Michael; Kramer, Korbinian (2017b): PVT collector technologies in solar thermal systems: a systematic assessment of electrical and thermal yields with the novel characteristic temperature approach. Solar Energy (155), pp. 867–879. DOI: 10.1016/j.solener.2017.07.015.

Lämmle, Manuel; Thoma, Christoph; Hermann, Michael (2016b): A PVT Collector Concept with Variable Film Insulation and Low-emissivity Coating. Energy Procedia 91, pp. 72–77. DOI: 10.1016/j.egypro.2016.06.174.

Lampert, C. (1998): Smart switchable glazing for solar energy and daylight control. Solar Energy Materials and Solar Cells 52 (3-4), pp. 207–221. DOI: 10.1016/S0927-0248(97)00279-1.

Lang, Reinhold; Wallner, Gernot M.; Fischer, Jörg (2013): Solarthermische Systeme aus Polymerwerkstoffen: das Großforschungsvorhaben SolPro. Erneuerbare Energie 2013-01.

Letz, Thomas; Bales, Chris; Perers, Bengt (2009): A new concept for combisystems characterization: The FSC method. Solar Energy 83 (9), pp. 1540–1549. DOI: 10.1016/j.solener.2009.05.002.

Louvet, Yoann; Fischer, Stephan; Furbo, Simon; Giovannetti, F.; Mauthner, Franz; Mugnier, Daniel; Philippen, Daniel (2017): Guideline for levelized cost of heat (LCOH) alculations for solar thermal applications - Info Sheet A.2. IEA SHC Task 54, Price Reduction of Solar Thermal Systems.

Lustig, Konrad (2002): Experimentelle Untersuchungen zum Stillstandsverhalten von thermischer Solaranlagen. Universität Karlsruhe.

Magalhães, Pedro M.L.P.; Martins, João F.A.; Joyce, António L.M. (2016): Comparative Analysis of Overheating Prevention and Stagnation Handling Measures for Photovoltaic-thermal (PV-T) Systems. Energy Procedia 91, pp. 346–355. DOI: 10.1016/j.egypro.2016.06.282.

Mahdjuri, F. (1999): Solar collector with temperature limitation using shape memory metal. Renewable Energy 16 (1-4), pp. 611–617. DOI: 10.1016/S0960-1481(98)00236-5.

Mahjouri, Fariborz (2004): Vacuum Tube Liquid-Vapor (Heat-Pipe) Collectors. Proceedings of the Solar Conference - American Institute of Architects.

Makki, Adham; Omer, Siddig; Sabir, Hisham (2015): Advancements in hybrid photovoltaic systems for enhanced solar cells performance. Renewable and Sustainable Energy Reviews 41, pp. 658–684. DOI: 10.1016/j.rser.2014.08.069.

Mangold, Dirk (1996): Kostenanalyse der Herstllung von Solarkollektoren und mögliche Kostenreduktionen durch Massenfertigung. Tagungsband 6. Symposium Thermische Solarenergie 1996. Bad Staffelsein: OTTI-Kolleg.

Martínez, A.; Astrain, D.; Rodríguez, A.; Aranguren, P. (2014): Thermoelectric Self-Cooling System to Protect Solar Collectors from Overheating. Journal of Elec Materi 43 (6), pp. 1480–1486. DOI: 10.1007/s11664-013-2743-4.

Matuska, Tomas; Sourek, Borivoj; Jirka, Vladimir; Pokorny, Nikola (2015): Glazed PVT Collector with Polysiloxane Encapsulation of PV Cells: Performance and Economic Analysis. International Journal of Photoenergy 2015, pp. 1–7. DOI: 10.1155/2015/718316.

Matuska, Tomas; Zmrhal, Vladimir (2009): KOLEKTOR 2.2 - A mathematical model and design tool - reference handbook (3rd draft, 01-2009). Czech Technical University in Prague, Faculty of Mechanical Engineering, Dept. of Environmental Engineering.

Mause, Elmar; Golovatai-Schmidt, Eduard; Popp, Markus; Hurst, Sebastian (2010): Thermomanagement bei Schaeffler: Wie viel Wasser braucht ein Motor? Schaeffler Kolloquim 2010.

Mauthner, Franz; Weiss, Werner; Spörk-Dür, Monika (2016): Solar Heat Worldwide. Markets and Contribution to the Energy Supply 2014.

Max, Johannes F.J.; Reisinger, Gerhard; Hofmann, Thomas; Hinken, Josef; Tantau, Hans-Jürgen; Ulbrich, Andreas et al. (2012): Glass–film-combination: Opto-physical properties and energy saving potential of a novel greenhouse glazing system. Energy and Buildings 50, pp. 298–307. DOI: 10.1016/j.enbuild.2012.03.051.

McAdams, William H. (1954): Heat transmission. 3. ed., internat. student ed. New York: McGraw-Hill.

Meteonorm (2016): Meteonorm - global meteorological databae, Version7.

Michael, Jee Joe; S, Iniyan; Goic, Ranko (2015): Flat plate solar photovoltaic–thermal (PV/T) systems: A reference guide. Renewable and Sustainable Energy Reviews 51, pp. 62–88. DOI: 10.1016/j.rser.2015.06.022.

Mickiewicz, Rafal; Li, Biao; Doble, Dan; Christian, Theresa (2011): Effect of encapsulation modulus on the response of PV modules to mechanical stress. Proceedings of 26th EUPVSEC.

Mittag, Max; Haedrich, Ingrid; Neff, Tobias; Hoffmann, Stephan; Eitner, Ulrich; Wirth, Harry (2015): TPEdge: Qualification of a gas-filled, encapsulation-free glas-glas photovoltaic module. Proceedings of 31st European PV Solar Energy Conference and Exhibition.

Modelica (2012): Modelica - A Unified Object-Oriented Language for Systems Modeling Version 3.3.

Mojiri, Ahmad; Taylor, Robert; Thomsen, Elizabeth; Rosengarten, Gary (2013): Spectral beam splitting for efficient conversion of solar energy—A review. Renewable and Sustainable Energy Reviews 28, pp. 654–663. DOI: 10.1016/j.rser.2013.08.026.

Moore, S. W. (1983): Solar collector apparatus having increased energy rejection during stagnation - US 4392481 A. US Patent.

Morris, Jesse; Calhoun, Koben; Goodman, Joseph; Seif, Daniel (2013): Reducing Solar PV Soft Costs - A Focus On Installation Labor Rocky Mountain Institute.

Mueller, Dirk; Wemhoener, Carsten (2013): Solar Panel with Variable Heat Dissipation - United States Patent US 20130306133 A1.

Nitz, P. M. (1999): Optische Modellierung und Vermessung thermotroper Systeme. Dissertation. Universität Freiburg, Freiburg, Germany. Fakultät für Physik.

Norton, Brian (2014): Harnessing solar heat.

Nunez, Tomas (2001): Charakterisierung und Bewertung von Adsorbentien für Wärmetransformationsanwendungen. Dissertation an der Albert-Ludwigs-Universität in Freiburg im Breisgau.

Ochs, F.; Heidemann, W.; Müller-Steinhagen, H. (2008): Effective thermal conductivity of moistened insulation materials as a function of temperature. International Journal of Heat and Mass Transfer 51 (3-4), pp. 539–552. DOI: 10.1016/j.ijheatmasstransfer.2007.05.005.

Oldewurtel, Frauke; Parisio, Alessandra; Jones, Colin N.; Gyalistras, Dimitrios; Gwerder, Markus; Stauch, Vanessa et al. (2012): Use of model predictive control and weather forecasts for energy efficient building climate control. Energy and Buildings 45, pp. 15–27. DOI: 10.1016/j.enbuild.2011.09.022.

Pailthorpe, B. A.; Collins, R. E.; O'Shea, S. (1987): Temperature Limitation in Evacuated Solar Collector Tubes. Australian Journal of Physics 40, 643–658.

Panzer, Clemens (2016): Experimentelle Untersuchungen neuartiger Konzepte für photovoltaisch-thermische Kollektoren. Masterarbeit, Karlsruhe Institute of Technology (KIT), Fraunhofer ISE.

Perers, Bengt; Kovacs, Peter; Olsson, Marcus; Pettersson, Martin Perssonb Ulrik (2012): A Tool for Standardized Collector Performance Calculations Including PVT. Energy Procedia 30, pp. 1354–1364. DOI: 10.1016/j.egypro.2012.11.149.

Pfänder, Katja (2015): Techno-ökonomische Bewertung von PVT-Kollektoren. Masterarbeit, Hochschule für Technik, Stuttgart, Hochschule für Forstwirtschaft Rottenburg, Fraunhofer ISE.

Philipps, Simon; Warmuth, Werner (2017): Photovoltaics Report, updated: 12. July 2017. Fraunhofer ISE, PSE AG.

Proell, M.; Karrer, H.; Brabec, C. J.; Hauer, A. (2016): The influence of CPC reflectors on the electrical incidence angle modifier of c-Si cells in a PVT hybrid collector. Solar Energy 126, pp. 220–230. DOI: 10.1016/j.solener.2016.01.012.

Proell, M.; Osgyan, P.; Karrer, H.; Brabec, C. J. (2017): Experimental efficiency of a low concentrating CPC PVT flat plate collector. Solar Energy 147, pp. 463–469. DOI: 10.1016/j.solener.2017.03.055.

Pröll, Markus; Karrer, Hanne; Osgyan, P. (2016): Schwach konzentrierender PV-T Kollektor für hohe Gesamteffizienz. Forschungsbericht Abschlussbericht FKZ 0325993A.

Raetz, Karl-Heinz (1998): Sonnenkollektor mit Temperaturbegrenzung - DE19847195. Deutsches Patentamt.

Ramschak, T.; Hausner, R.; Fink, Christian (2016): Temperaturbegrenzung für Kunststoffkollektoren durch Durchlüftung - Zusammenfassung. Tagungsband 26. Symposium Thermische Solarenergie 2016. Bad Staffelsein: OTTI-Kolleg.

Reiter, C. (2014): Polymeric Solar-Thermal Flat-Plate Collectors. PhD thesis. De Montfort University Leicester. Institute of Energy and Sustainable Development, checked on 5/11/2015.

Reiter, C.; Ehrenwirth, M.; Brandmayr, Sebastian; Trinkl, C.; Zörner, W. (2014): Simulationsgestützte Leistungsanpassung von Kunststoffkollektoren. Tagungsband 24. Symposium Thermische Solarenergie 2014. Bad Staffelsein: OTTI-Kolleg.

Resch, Katharina; Wallner, Gernot M. (2009): Thermotropic layers for flat-plate collectors—A review of various concepts for overheating protection with polymeric materials. Solar Energy Materials and Solar Cells 93 (1), pp. 119–128. DOI: 10.1016/j.solmat.2008.09.004.

RHC (2012): Strategic Research Priorities for Solar Thermal Technology. European Technology Platform on Renewable Heating and Cooling.

Robinson-Gayle, S.; Kolokotroni, M.; Cripps, A.; Tanno, S. (2001): ETFE foil cushions in roofs and atria. Construction and Building Materials 15 (7), pp. 323–327. DOI: 10.1016/S0950-0618(01)00013-7.

Rockendorf, G.; Schreitmüller, K. R.; Wetzel, W. (1993): Thermal collector thest methods - a comparison of the heat loss measurement and a measurement under radiation. Proceedings ISES Solar World Congress, Budapest.

Rommel, Matthias; Siems, Thorsten; Schüle, Kurt; Mehnert, Stefan (2007): Systemuntersuchungen großer solarthermischer Kombianlagen. Schlussbericht zum Teilprojekt: Entwicklung von Techniken zur Beherrschung des Stillstandsbetriebs. Kurzbezeichnung "StagSim". Fraunhofer Institut für Solare Energiesysteme ISE.

Rommel, Matthias; Zenhäusern, Daniel; Baggenstos, Aleksis; Türk, Ozan; Brunold, Stefan (2015): Development of Glazed and Unglazed PVT Collectors and First Results of their Application in Different Projects. Energy Procedia 70, pp. 318–323. DOI: 10.1016/j.egypro.2015.02.129.

Rommel, Matthias; Zenhäusern, Daniel; Baggenstos, Alexis; Türk, Ozan; Brunold, Stefan (2014): Application of Unglazed PVT Collectors for Domestic Hot Water Pre-heating in a Development and Testing System. Energy Procedia 48, pp. 638–644. DOI: 10.1016/j.egypro.2014.02.074.

Rummler, Nele (2008): Bericht über die Ermittlung des internen thermischen Leitwerts von Absorberstreifen. ISFH Hameln.

Ruschenburg, Jörn; Herkel, Sebastian; Henning, Hans-Martin (2013): A statistical analysis on market-available solar thermal heat pump systems. Solar Energy 95, pp. 79–89. DOI: 10.1016/j.solener.2013.06.005.

Santbergen, R.; Rindt, C.C.M.; Zondag; van Zolingen, R.J.Ch. (2010): Detailed analysis of the energy yield of systems with covered sheet-and-tube PVT collectors. Solar Energy 84 (5), pp. 867–878. DOI: 10.1016/j.solener.2010.02.014.

Scheuren, Jörn (2008): Untersuchungen zum Stagnationsverhalten solarthermischer Kollektorfelder. Dissertation. University, Kassel.

Schmidt, Christian; Lämmle, Manuel; Kramer, Korbinian (2017): Quellenseitig in Wärmepumpe-Heizsysteme integrierte Kollektoren – Definition von Anforderungen und Bewertung von Rechenmodellen und Messverfahren zur Modellkalibrierung und Versuch einer objektiven Bewertung. Tagungsband 27. Symposium Thermische Solarenergie 2017. Bad Staffelsein: OTTI-Kolleg.

Schmidt, H.; Sauer, D. U. (1996): Wechselrichter-Wirkungsgrade - Praxisgerechte Modellierung und Abschätzung. Sonnenenergie, ISSN: 0172-3278 (4), pp. 43–47.

Serale, Gianluca; Baronetto, Sara; Goia, Francesco; Perino, Marco (2014): Characterization and Energy Performance of a Slurry PCM-based Solar Thermal Collector. A Numerical Analysis. Energy Procedia 48, pp. 223–232. DOI: 10.1016/j.egypro.2014.02.027.

Sharpe, Timhothy E. (1984): Solar Heat Collector System - US4485804. United States Patent.

Siefert, Wolfgang; Kindle-Hasse, B.; Hildbrand, C.; Georg, Andreas; Kroyer, Thomas; Graf, Wolfgang et al. (2016): Low-e coatings on ETFE films for membrane architecture. 1. Internationale Konferenz zur Simulation gebäudetechnischer Energiesyste, SIGES 2016.

SKN (2011): Scenocalc v3.07 - Description of the Energy Output Calculator, a program for calculation of annual solar collector energy output. Available online at: http://www.estif.org/fileadmin/estif/content/projects/QAiST/QAiST_results/Energy%20Output%20Calculator%20v3.07. Solar Keymark Network.

SKN (2015): Solar Keymark Network - Annex J - Specific requirements for PVT collector Certification. SKN_N0106_AnnexJ_R2.

SKN (2016): ScenoCalc v5.01. Description of ScenoCalc (Solar Collector Energy Output Calculator), a program for calculation of annual solar collector energy output. Solar Keymark Network.

Skoplaki, E.; Palyvos, J.A. (2009): On the temperature dependence of photovoltaic module electrical performance: A review of efficiency/power correlations. Solar Energy 83 (5), pp. 614–624. DOI: 10.1016/j.solener.2008.10.008.

Slaman, M.; Griessen, R. (2009): Solar collector overheating protection. Solar Energy 83 (7), pp. 982–987. DOI: 10.1016/j.solener.2009.01.001.

Smyth, M.; Eames, P. C.; Norton, B. (2006): Integrated collector storage solar water heaters. Renewable and Sustainable Energy Reviews 10 (6), pp. 503–538. DOI: 10.1016/j.rser.2004.11.001.

Solarus (2017): Technical Brochure of C-PVT "Power Collector" (http://solarus.com/wp-content/uploads/2017/08/Solarus-Technische-Brochure-web-v1.pdf) and Personal Communication.

Staudacher, Thomas; Eller, Sebastian (2012): Dezentrale Stromversorgung eines Einfamilienhauses - Stromversorgung mit Photovoltaik, Batterie und Netzanschluss. BWK Bd. 64 (2012), Nr. 6.

Staudacher, Thomas; Eller, Sebastian (2015): Simulationsmodell Dezentrale Stromversorgung. https://www.ffe.de/themen-und-methoden/modelle-und-tools/405-simulationsmodell-dezentrale-stromversorgung.

Stazi, F.; Giampaoli, M.; Tittarelli, F.; Di Perna, C.; Munafò, P. (2016): Durability of different glass coatings in humid and saline environments, ageing impact on heat-light transmission and thermal comfort. Building and Environment 105, pp. 210–224. DOI: 10.1016/j.buildenv.2016.05.029.

Stegmann, Martin; Bertram, Erik; Rockendorf, G.; Janßen, Stefan (2012): Modell eines unverglasten photovoltaisch-thermischen Kollektors basierend auf genormten Prüfverfahren. OTTI Symposium SolarthermieTagungsband 22.

Stephens, R. B. (1981): Fluid optical switch for a solar collector - US4270517.

Stieglitz, Heinzel (2012): Thermische Solarenergie. Grundlagen, Technologie, Anwendungen. Berlin, Heidelberg: Springer Berlin Heidelberg.

Streicher, Wolfgang (2012): Solar Thermal Heating Systems. Lecture script, Division Energy Efficient Buildings, University of Innsbruck.

Swinbank, W. C. (1963): Long-wave radiation from clear skies. Quarterly Journal of the Royal Meteorological Society (Volume 89, Issue 381, pages 339–348).

61215, 2016: Terrestrial Photovoltaic (PV) Modules - Design qualification and type approval - Edition 1.0.

Thür, A.; Hintringer, C. (2013): Status Quo der Entwicklungen eines überhitzungsgeschützten Kunststoffkollektors. Erneuerbare Energie (01).

Tripanagnostopoulos, Y. (2007): Aspects and improvements of hybrid photovoltaic/thermal solar energy systems. Solar Energy 81 (9), pp. 1117–1131. DOI: 10.1016/j.solener.2007.04.002.

UNFCCC (2015): Adoption of the Paris Agreement. Proposal by the President. FCCC/CP/2015/L.9/Rev1. Conference of the parties (COP). United Nations Office at Geneva (Switzerland).

UniKoll (2015): Beschreibung UNIKoll. Available online at http://www.unikoll.eu/beschreibung-unikoll.html, checked on 3/10/2015.

Vasiliev, L. L. (2004): The sorption heat pipe—a new device for thermal control and active cooling. Superlattices and Microstructures 35 (3-6), pp. 485–495. DOI: 10.1016/j.spmi.2003.09.010.

VDI (2010): VDI Heat Atlas. Second Edition: Springer-Verlag Berlin Heidelberg, Verein Deutscher Ingenieure.

VDI (2014): VDI 6002 - VDI-Richtilinie Solare Trinkwassererwärmung Allgemeine Grundlagen Systemtechnik und Anwendung im Wohnungsbau. Verein Deutscher Ingenieure.

Vela Solaris (2013): Polysun Simulation Software - User Manual.

Weißmüller, C.; Frenz, H.; Krämer, E. (2012): Proficiency Test - QAiST testing of solar collectors and solar systems 2010 - 2011. Final report.

Wendker, Kai; Jäger, Helmut; Dolezal, Adam; Stryi-Hipp, Gerhard; Fortuin, S.; Hädrich, Ingrid et al. (2012): Photovoltaisch-thermische Kollektorsysteme mit maximiertem Gesamtertrag. Projekt gefördert durch Deutsche Bundesstiftung Umwelt (DBU) Förderzeichen: 28569. Fraunhofer_Institut für Solare Energiesysteme ISE.

Wetter, Michael (1997): Vertical Borehole Heat Exchanger EWS Model - TRNSYS Type 451 - Version 2.4.

Wetter, Michael (2011): GenOpt (R) - Generic Optimization Program. User Manual, Version 3.1.0. Lawrence Berkeley National Laboratory - http://SimulationResearch.lbl.gov.

Wirth, Harry (2017): Aktuelle Fakten zur Photovoltaik in Deutschland - Fassung vom 24.1.2017. Fraunhofer ISE.

Witt, J. D.; Mesquite, Tex. (1984): Overheat emergency outfocus mechanism for solar energy collector - Patent US4484568.

Wittwer, Christof; Rommel, Matthias (1996): Implementierung des 2x4 Knotenmodells eines Kollektors und die Validierung anhand von Meßdaten bei Normal- und Low-Flowbetrieb. Tagungsband Symposium Thermische Solarenergie 1996. Bad Staffelsein: OTTI-Kolleg.

Würfel, Peter; Würfel, Uli (2008): Physics of Solar Cells. From Principles to New Concepts. 2., aktualis. u. erg. Aufl. Weinheim, Bergstr: WILEY-VCH.

Yedidi, K.; Tatapudi, S.; Mallineni, J.; Knisely, B.; Kutiche, J.; TamizhMani, G. (2014): Failure and degradation modes and rates of PV modules in a hot-dry climate: Results after 16 years of field exposure. Proc. of IEEE 40th Photovoltaic Specialist Conference (PVSC), 2014, pp. 3245–3247. DOI: 10.1109/PVSC.2014.6925626.

Zahoransky, Richard A.; Allelein, Hans-Josef; Bollin, Elmar; Oehler, Helmut; Schelling, Udo (2010): Energietechnik - Systeme zur Energieumwandlung. Kompaktwissen für Studium und Beruf. Wiesbaden: Vieweg+Teubner Verlag.

Zenhäusern, Daniel; Bamberger, Everlyn; Baggenstos, Aleksis (2017): PVT Wrap-Up - Energiesysteme mit Photovoltaisch-Thermischen Solarkollektoren. Project report of Institut für Solartechnik SPF.

Zenhäusern, Daniel; Bohren, Andreas; Rommel, Matthias; Dittmann, Sebastian (2015): Thermische und elektrische Charakterisierung von unabgedeckten PVT-Kollektoren. Tagungsband 25. Symposium Thermische Solarenergie 2015. Bad Staffelsein: OTTI-Kolleg.

Zondag; Vries, D. W. de; van Helden, W.G.J.; van Zolingen, R.J.C.; van Steenhoven, A. A. (2002a): The thermal and electrical yield of a PV-thermal collector. Solar Energy 72 (2), pp. 113–128. DOI: 10.1016/S0038-092X(01)00094-9.

Zondag, H. A.; Bakker, M.; van Helden, W. G. J. (2006): PVT Roadmap - A European guide for the development and market introduction of PV-Thermal technology.

Zondag, H. A.; de Vries, D. W.; van Helden, W. G. J.; van Zolingen, R. J. C.; van Steenhoven, A. A. (2002b): The thermal and electrical yield of a PV-thermal collector. Solar Energy 72 (2), pp. 113–128. DOI: 10.1016/S0038-092X(01)00094-9.

Zondag, H. A.; Jong, M.J.M.; van Helden, W.G.J. (2001): Development and applications for PV thermal. Proceedings of the 17th European Photovoltaic Solar Energy Conference, Munich, Germany.

Zondag, H.A. (2008): Flat-plate PV-Thermal collectors and systems: A review. Renewable and Sustainable Energy Reviews 12 (4), pp. 891–959.

Zondag, Herbert A.; van Helden, W.G.J.; Elswijk, M. J.; Backker, M. (2004): PV-Thermal collector development - an overview of the lessons learnt. 19th European PV Solar Energy Conference and Exhibition 7-11 June 2004, Paris France.

PUBLICATION LIST

Journals:

- Lämmle, Manuel; Kroyer, Thomas; Fortuin, Stefan; Wiese, Martin; Hermann, Michael (2016): Development and modelling of highly-efficient PVT collectors with low-emissivity coatings. Solar Energy (130), pp. 161–173. DOI: 10.1016/j.solener.2016.02.007.
- Lämmle, Manuel; Thoma, Christoph; Hermann, Michael (2016): A PVT Collector Concept with Variable Film Insulation and Low-emissivity Coating. Energy Procedia 91, pp. 72–77. DOI: 10.1016/j.egypro.2016.06.174.
- Lämmle, Manuel; Oliva, Axel; Hermann, Michael; Kramer, Korbinian (2017): PVT collector technologies in solar thermal systems: a systematic assessment of electrical and thermal yields with the novel characteristic temperature approach. Solar Energy (155), pp. 867–879. DOI: 10.1016/j.solener.2017.07.015.
- Lämmle, Manuel; Hermann, Michael; Kramer, Korbinian; Panzer, Clemens; Piekarczyk, Andreas; Thoma, Christoph; Fahr, Sven (2018): Development of highly efficient, glazed PVT collectors with overheating protection to increase reliability and enhance energy yields. Submitted to *Solar Energy*.

Conferences:

- Lämmle, Manuel; Kroyer, Thomas; Fortuin, Stefan; Hermann, Michael (2014): Modelling Results of Covered PVT Collectors Regarding Low-e Coatings and F'. Eurosun2014 - ISES Proceedings, pp. 1–10. DOI: 10.18086/eurosun.2014.16.14.
- Lämmle, Manuel; Hermann, Michael (2015): Thermisches Management von PVT-Kollektoren - Ergebnisse aus Systemsimulationen. Tagungsband 25. Symposium Thermische Solarenergie 2015. Bad Staffelsein: OTTI-Kolleg.
- Lämmle, Manuel; Panzer, Clemens; Hermann, Michael (2017): Abgedeckter PVT-Kollektor mit Low-e-Beschichtung und Belüftung als Überhitzungsschutz. Tagungsband 27. Symposium Thermische Solarenergie 2017. Bad Staffelsein: OTTI-Kolleg.
- Lämmle, Manuel; Hermann, Michael (2017): Charakteristischer Temperaturansatz für die Auslegung und Optimierung von PVT- und Solarthermie-Systemen. Tagungsband 27. Symposium Thermische Solarenergie 2017. Bad Staffelsein: OTTI-Kolleg.
- Lämmle, Manuel; Kramer, Korbinian; Hermann, Michael (2017): Assessing suitable fields of application for PVT collectors with the characteristic temperature approach. Proceedings ISES Solar World Congress and Solar Heating and Cooling (SHC) Conference, Abu Dhabi, 2017.

Publications as co-author:

- Maurer, C., Sprenger, W., Lämmle, M., Kuhn, T.E., 2015. Simple models for architecture with BIPVT or BIST. Conference Proceedings of the 10th Energy Forum on Advanced Building Skins.
- Schmidt, Christian; Lämmle, Manuel; Kramer, Korbinian (2017): Quellenseitig in Wärmepumpe-Heizsysteme integrierte Kollektoren – Definition von Anforderungen und Bewertung von Rechenmodellen und Messverfahren zur Modellkalibrierung und Versuch einer objektiven Bewertung. Tagungsband 27. Symposium Thermische Solarenergie 2017. Bad Staffelsein: OTTI-Kolleg.
- Schmidt, Christian; Schäfer, Arim; Thoma, Christoph; Rajkiran Jayachandran, Ezekiel; Lämmle, Manuel; Geimer, Konstantin; Korbinian Kramer (2018): Quellenseitig in Wärmepumpen-Heizsystem integrierte PVT-Kollektoren – Experimentelle Messungen am Einzelmodul und am Gesamtsystem. Tagungsband Symposium Solarthermie - Technik für die Wärmewende.

Other publications:

- Lämmle, Manuel (2016): PVT-Kollektoren - die solare Kraft-Wärme-Kopplung. Ingenieurspiegel 1/2016.
- Lämmle, Manuel (2016): Vergleich von PVT-Kollektortechnologien - Wirkungsgradkennwerte, Bruttoerträge, Systemsimulationen. Posterbeitrag zum PVT-Workshop im Vorfeld des OTTI Symposiums Thermische Solarenergie am 19.04.2016.
- Lämmle, Manuel; Jäger, Helmut; Hermann, Michael; Thoma, Christoph; Mülhöfer, Georg; Wiese, Martin et al. (2017): PVTgen2 - Entwicklung und Pilotfertigung eines abgedeckten Photovoltaisch-thermischen Hybrid-Kollektors der zweiten Generation mit verbesserter thermischer Leistungsfähigkeit. Abschlussbericht - Teilprojekt Fraunhofer ISE.

LIST OF FIGURES

LIST OF TABLES

NOMENCLATURE

Symbol	Unit	Definition
A	m^2	area
A_{ap}	m^2	aperture area
A_{gross}	m^2	gross collector area
A_{PV}	m^2	PV module area
b_0	-	incident angle modifier
b_1	W/m^2K	temperature coefficient of PV efficiency relative to $\Delta T/G$
c_1	W/m^2K	linear heat loss coefficient of thermal efficiency
c_2	W/m^2K^2	quadratic heat loss coefficient of thermal efficiency
c_3 - c_6	-	thermal performance coefficients
c_{eff}	kJ/m^2	effective thermal collector capacity
c_p	J/kgK	specific heat capacity
d	m	thickness, diameter, distance
E_L	W/m^2	long wave irradiance > 3µm
E_{PV}	kWh/m^2	specific electrical output
E_λ	$W/m^2µm$	spectral irradiance, spectral emissive power
F´	-	collector efficiency factor
f	-	rating figure
f_{area}	-	area requirement factor
f_{cov}	-	electrical coverage rate
f_p	-	primary energy factor
f_{sav}	-	fractional energy savings
f_{sol}	-	solar thermal fraction
$f_{surplus}$	-	electrical surplus yield rate
G	W/m^2	hemispherical solar irradiance
h	W/m^2K	heat transfer coefficient
I_{tot}	kWh/m^2a	annual irradiation in the collector plane
K_θ	-	incident angle modifier
Kn	-	Knudsen number
$\dot{m}$	kg/h	mass flow rate of heat transfer fluid
Nu	-	Nusselt number
P	W	power
p	W/m^2	specific power
p	Pa	pressure
PR	-	performance ratio
Pr	-	Prandtl number
$\dot{q}$	W/m^2	specific heat flux
Q_{coll}	kWh/m^2a	specific thermal collector yield
Ra	-	Rayleigh number
RMSE	-	root mean square error
T	K	temperature
T_a	°C	ambient temperature

T_m	°C	mean fluid temperature
T_{char}	°C	characteristic temperature
U	W/m²K	U-value
UR	-	utilization ratio
u_{wind}	m/s	wind speed
V	m³	volume

Symbol	Unit	Definition
α	-	absorptance
γ	%/K	temperature coefficient of PV power
δ	-	elongation
ε	-	emissivity
ε_{373K}	-	emissivity at T = 373 K
η	-	efficiency
λ	m	wavelength
ρ	-	reflectance
σ	W/m²K⁴	Stefan-Boltzmann constant
τ	-	transmittance
$(\tau\alpha)_{eff}$	-	effective transmittance-absorptance product

Subscript	Definition
0	related to $\Delta T = T_m - T_a = 0$ K
abs	absorber, absolute percentage
ad	adsorbent
aux	auxiliary
AM1.5	weighted with AM1.5 spectrum
c-Si	weighted with spectral response of crystalline silicon cells
coll	collector
cond	conductive
conv	convective, conventional
eff	effective
el	electrical
lam	laminar flow regime
MAP	weighed with the MAP function
PE	primary energy
rad	radiative
regen	regeneration of borehole
rel	relative percentage
sat	saturation
selfcon	self-consumption
stg	stagnation
th	thermal
tot	total
turb	turbulent flow regime
vac	vacuum

Abbreviation	Definition
COP	coefficient of performance
DHW	domestic hot water
FPC	flat plate collector
IAM	incidence angle modifier
MFH	multi family home
MPP	maximum power point
OC	open circuit
OHP	overheating protection
PV	photovoltaic
PVT	photovoltaic thermal
SFH	single family home
SHP	solar heat pump
STC	standard test conditions

Danksagung

An dieser Stelle möchte ich die Gelegenheit wahrnehmen, mich bei all denjenigen zu bedanken, die aktiv oder passiv, inhaltlich oder emotional, dazu beigetragen haben, die Doktorarbeit erfolgreich und mit Spaß an der Sache fertigzustellen:

- Bei Prof. Hans-Martin Henning für die Betreuung der Doktorarbeit, der sich trotz vielfältiger Verpflichtungen intensiv mit der Arbeit auseinandersetzte und durch eine beeindruckende Auffassungsgabe stets wertvolle Hilfestellungen gab.
- Bei Prof. Andreas Wagner für die freundliche Übernahme des Korreferats.
- Bei Michael Hermann für die fachliche Betreuung der Doktorarbeit. Die vielzähligen Diskussionen und die sprudelnden Ideen trugen maßgeblich zur letztendlichen Form der Doktorarbeit bei. Außerdem weiß ich Zeit und Fleiß, die in das Korrekturlesen flossen, zu schätzen.
- Bei meinen Masteranden, Praktikanten und Hiwis für ihre wertgeschätzten Beiträge zur Doktorarbeit: Hugo, Ezekiel, Clemens, Katja, Fredi, Marc, und nicht zu vergessen Philipp. Es war stets eine bereichernde Freude mit euch zusammenzuarbeiten.
- Bei Stefan Fortuin, der mich in die PVT-Welt einführte und auf dessen Vorarbeiten ich aufbauen durfte.
- Bei Christoph Thoma, Sven Fahr und Korbinian Kramer vom TestLabs Solar Thermal Systems für die Unterstützung bei den Messungen. Was bin ich froh, dass ich auf eure Teststände und euer Know-How zurückgreifen konnte und die Messungen nicht selbstständig durchführen musste.
- Bei Thomas Kroyer für die Nachhilfe im Bereich der Beschichtungstechnologien und low-e-Schichten.
- Beim TRNSYS-Crack Axel Oliva für die Tipps und Tricks im Umgang mit einer Software aus der gefühlten Steinzeit.
- Bei Helmut Jäger der Fa. Solvis für die fruchtbare Zusammenarbeit und die wegweisenden Diskussionen innerhalb des Verbundprojekts PVTgen2.
- Bei Portia, Jan und Ida, die mir im Lektorat die schlimmsten englischen Böcke ausgetrieben haben.
- Bei meinen Bürobuddies Axel und Mehmet. Auch wenn die Arbeitsatmosphäre nicht unbedingt der einer Bibliothek entsprach, so war die Bürogemeinschaft stets willkommene Ablenkung und Motivation.
- Bei den inspirierenden Kollegen vom Fraunhofer ISE, allen voran meiner Mittagspausen-, Espressopausen-, Dienstags-Fußballgruppen-, Feierabend- und Wochenend-Crew, die für mich weit mehr als nur Kollegen geworden sind.
- Und zu guter Letzt bei meinen wundervollen Freunden und beim gesamten Lämmle- und Leonhardt-Clan für jegliche Unterstützung in vielfältiger Form <3.

Para ser grande, sê inteiro: nada
Teu exagera ou exclui.

Sê todo em cada coisa. Põe quanto és
No mínimo que fazes.

Assim em cada lago a lua toda
Brilha, porque alta vive

Ricardo Reis / Fernando Pessoa
Odes